UNIVERSITY OF CALIFORNIA, SAN DIEGO

Chemistry of Atmospheric Aerosol Particles and their resulting Warm Cloud-Nucleation Properties

A dissertation submitted in partial satisfaction of the requirements for the degree

Doctor of Philosophy

in

Chemistry

by

Meagan Julia Kerry Moore

Committee in charge:

Professor Kimberly Prather, Chair
Professor Judy Kim
Professor Katja Lindenberg
Professor Tadeusz Molinski
Professor Lynn Russell

2011

The dissertation of Meagan Julia Kerry Moore is approved, and it is acceptable in quality and form for publication on microfilm and electronically:

Chair

University of California, San Diego
2011

DEDICATION

In loving memory of Morna Paige Marolda (1982-2008)

There are good ships
and there are wood ships
and there are ships that sail the sea…
But the best ships are friendships
and may they always be.

EPIGRAPH

We cannot solve our problems
with the same thinking
when we created them.

Albert Einstein

TABLE OF CONTENTS

LIST OF ABBREVIATIONS

AIM aerosol inorganic model

APS aerodynamic particle sizer

ART-2a adaptive resonance theory-2a

ATOFMS aerosol time-of-flight mass spectrometer

CCN cloud condensation nuclei

CCNc cloud condensation nuclei counter

CIFEX Cloud Indirect Forcing Experiment

CN condensation nuclei

CPC condensation particle counter

DCA dicarboxylic acid

DMA differential mobility analyzer

EC elemental carbon

LDI laser desorption/ionization

OC organic carbon

OPC optical particle counter

PMT photomultiplier tube

PSL polystyrene latex sphere

RH relative humidity

RSF relative sensitivity factor

SMPS scanning mobility particle sizer

SPMS single-particle mass spectrometer

SOA secondary organic aerosol

WSOC water soluble organic carbon

LIST OF SYMBOLS

a_w	activity of water
b_{ext}	extinction coefficient
C_c	Cunningham slip correction
D	particle diameter
D_a	aerodynamic diameter
D_{act}	activation diameter
D_{dry}	dry particle diameter
D_g	geometric diameter
D_m	mobility diameter
dT	temperature gradient
e	elementary charge
e	vapor pressure of water
e_s	saturation vapor pressure of water
H	Henry's law coefficient
I	transmitted light intensity
I_o	incident light intensity
L	path length
M	molecular weight
m_s	solute mass
n	refractive index
n_{re}	real refractive index (scattering)
n_{im}	imaginary refractive index (absorption)
n	number of elementary charges

N_d	cloud droplet concentration
p	partial pressure/vapor pressure
q_{sh}	sheath flow rate
R	universal gas constant
r	particle radius
r_c	critical radius
S	water saturation ratio (e/e_s)
S_c	critical supersaturation
T	temperature
V	DMA rod voltage
V_s	volume of the dry particle
V_w	volume of water
v_w	partial molar volume of water
ε	component volume fraction
κ	hygroscopicity parameter
μ	gas viscosity
$\sigma_{s/a}$	surface tension
ρ	density
ν	number of dissociated ions per molecule (Van't Hoff factor)
χ	dynamic shape factor
λ	wavelength

LIST OF FIGURES

LIST OF TABLES

.

ACKNOWLEDGEMENTS

First and foremost I would like to thank Professor Kimberly Prather for supporting and guiding my research over the past five years. I am also appreciative for the frequent occasions to present my research at scientific conferences and be exposed to the newest research in our field. I have benefited greatly from her initiation of collaborations with Greg Roberts at the Scripps Institution of Oceanography (SIO), and Sonia Kreidenweis at Colorado State University.

I am very grateful to the many past and present members of the Prather research group for their hard work in progressing aerosol time-of-flight mass spectrometry into a constructive and important research tool, and also for all the help they provided to me and my research. I am particularly indebted to Hiroshi Furutani, Ryan Sullivan and Melanie Zauscher. Hiroshi Furutani helped initiate the bubble bursting project in the lab which I became a part of, and was a constant source of valuable advice and help when I was beginning my laboratory experiments, and I have learned to have great respect for his unwavering attention to detail. Ryan Sullivan's dedicated assistance with laboratory experiments, data analysis and valuable advice was key to my successful research progress. Melanie Zauscher's regular and committed support of my field work, data analysis, and writing; in addition to her friendship, was central to many of my accomplishments. I am very grateful to Ying Wang, Elizabeth Fitzgerald, and Matthew Spencer for their feedback and review of the manuscripts that are contained in this dissertation. I would like to thank Lindsay Hatch for her help editing Chapter 1 of this dissertation. Jessica Charrier's regular and dedicated assistance with the bubbling experiments described in Chapter 2 and Appendix 1 was invaluable and greatly appreciated. Andrew Ault and Cassandra Gaston's assistance with the fires 2007 experiment described in Chapter 3 was greatly appreciated. Manuel Ruidiaz, Satoshi Takahama and Alberto Cazorla's assistance with

the optimizing the data analysis method to work with the new scanning CCN data presented in Chapter 4 was tremendously appreciated. I am grateful to John Holecek for his help with data collection and analysis with the CIFEX data set described in Chapters 5 & 6. Finally, I would like to thank Dr. Bob Moision and Joe Mayer for their help manufacturing many of the pieces of equipment used in this research and their assistance in instrumental troubleshooting.

I wish to thank the members of my Ph.D. committee for their thoughtful advice and comments regarding my research: Profs. Lynn Russell, Judy Kim, Katja Lindenberg, and Tadeusz Molinski. Graduate courses on atmospheric thermodynamics and aerosols taught by Prof. Lynn Russell gave me a valuable background that I regularly use in my research.

Most of the work described here would not have been feasible without the generosity of Greg Roberts, who lent our group many of his cloud condensation nuclei counters, helped us operate and repair the instruments, design experiments, and interpret the results.

I would like to thank the Lihini Aluware laboratory, SIO, for use of their oven for combustion of glassware for the bubbling experiments, and Drs. Grant Deane and Dale Stokes, at SIO, for their assistance in validation of the bubbling technique via picture imaging used in the bubbling experiments. I am very grateful to the Great Basin Unified Air Pollution Control District, especially Daniel Johnson, for their assistance during the Owens Lake field campaign. Odelle Hadley and Craig Corrigan's assistance with the CIFEX data set described in Chapters 5 & 6 was greatly appreciated.

I am also indebted to Prof. Mary Beth Williams at The Pennsylvania State University. The three years I spent in her research group as an undergraduate student exposed me to the field of materials research and provided me with a solid foundation understanding the research process, which I continued to apply during in my dissertation research. Finally, I would like to thank my high school A.P. chemistry teacher, Marsha Folger, for inspiring and continued

support of my interest in chemistry, which led me to study it in undergraduate and graduate school.

The National Science Foundation's funding of the majority of this research is greatly appreciated. The NSF supported the Prather group's participation in the Owens Lake campaign. I am also grateful for the UCSD's Chancellor Interdisciplinary Collaboratories Fellowship, Pacific Northwest National Laboratory Aerosol Chemistry and Climate Institute Fellowship and the San Diego Fellowship which supported me during my research. I would like to thank the National Oceanic and Atmospheric Administration (NOAA), grant NOAA/NA17RJ1231, and V. Ramanathan (UCSD) for the support of the CIFEX research, especially John Ogren and Betsy Andrews at NOAA/ESRL/GMD.

I am very grateful to all my family back in the northeast for their support and help with my move to California and during my graduate studies. I am lucky and fortunate to have had the support of good friends back in the northeast, and to have made new friends in San Diego, both at UCSD and outside of grad school. All of my friends made my move to California easier, greatly improving my graduate school experience. I am especially thankful to all the friends and colleagues I met at UCSD for their regular advice and support.

The text and figures of Chapter 2 of a submitted manuscript: Moore, M.J.K., Furutani, H.; Roberts, G.; Moffet, R.; Gilles, M.; Palenik, B.; Prather, K.A., Effect of Organic Matter on Sea Spray Aerosol Production by Bubble Bursting and its Cloud Condensation Nuclei (CCN) Activity, submitted to Atmospheric Environment. The dissertation author was the primary investigator and author of this paper.

The contents of Chapter 3 are part of a manuscript in preparation, Moore, M.J.K., Sullivan, R.C., Roberts, G.C., Wang, Y., Zauscher, M.D., Prather, K.A., A comparison of

single particle mixing state and CCN activity during the 2007 and 2008 San Diego Wildfires, to be submitted to Atmospheric Environment. The dissertation author was the primary investigator and author of this paper.

The contents of Chapter 4 are part of a manuscript in preparation, Moore, M.J.K., Fitzgerald, E.M.M., Zauscher, M.D., Roberts, G.C., Prather, K.A., Real-time Single Particle Composition and Cloud Condensation Nuclei (CCN) Activity at Owens (dry) Lake Bed, to be submitted to Journal of Geophysical Research. The dissertation author was the primary investigator and author of this paper.

The contents of Chapter 5 are part of a manuscript in preparation, Moore, M.J.K., Spencer, M.T., Roberts, G.C., Corrigan, C., Prather, K.A., Real-time Single Particle Composition, Absorption, Scattering and Cloud Condensation Nuclei (CCN) Activity at Trinidad Head, CA during Cloud Indirect Forcing Experiment (CIFEX), to be submitted to Journal of Geophysical Research. The dissertation author was the primary investigator and author of this paper.

The contents of Chapter 6 are part of a manuscript in preparation, Moore, M.J.K., Spencer, M.T., Prather, K.A., Evidence for two distinct sources of oxalate during the Cloud Indirect Forcing Experiment (CIFEX), to be submitted to Environmental Science and Technology. The dissertation author was the primary investigator and author of this paper.

VITA AND PUBLICATIONS

May 2005	B.S. Chemistry, Pennsylvania State University
2002-2005	Research Assistant, Department of Chemistry, Pennsylvania State University
2005-2006	Teaching Assistant, Department of Chemistry & Biochemistry, University of California, San Diego
March 2007	M.S. Chemistry, Department of Chemistry & Biochemistry, University of California, San Diego
2005-2011	Graduate Student Researcher, Department of Chemistry & Biochemistry, University of California, San Diego
March 2011	Ph.D. Chemistry, Department of Chemistry & Biochemistry, University of California, San Diego

M. J. K. Moore, H. Furutani, G. Roberts, R.C. Moffet, M. Giles, B. Palenik, K.A. Prather, Effect of Organic Matter on Sea Spray Aerosol Production by Bubble Bursting and its Cloud Condensation Nuclei (CCN) Activity, submitted to *Atmospheric Environment*, 2010.

R. C. Sullivan, M. J. K. Moore, M. D. Petters, S. M. Kreidenweis, G. C. Roberts, K. A. Prather, Increased hygroscopicity of atomized insoluble mineral particles due to metastable hydrate formation, *Aerosol Science and Technology*, 2010, 44(10), 830-846.

R. C. Sullivan, M. J. K. Moore, M. D. Petters, S. M. Kreidenweis, G. C. Roberts, K. A. Prather, Effect of chemical mixing state on the hygroscopicity and cloud nucleation properties of calcium mineral dust particles. *Atmospheric Chemistry and Physics*, 2009, 9, 3306-3316.

A. P. Ault, M. J. K. Moore, H. Furutani, G. Dominguez, M. Thiemens, K. A. Prather, Impact of Emissions from the Los Angeles Port Region on San Diego Air Quality during Regional Transport Events, *Environmental Science and Technology*, 2009, 43(10), 3500-3506.

R. C. Sullivan, M. J. K. Moore, M. D.Petters, S. M. Kreidenweis, G. C. Roberts, K. A. Prather, Timescale for hygroscopic conversion of calcite mineral particles through heterogeneous reaction with nitric acid, *Phys. Chem. Chem. Phys*., 2009, 11, 7826.

ABSTRACT OF THE DISSERTATION

Chemistry of Atmospheric Aerosol Particles and their resulting Warm Cloud-Nucleation Properties

by

Meagan Julia Kerry Moore

Doctor of Philosophy in Chemistry

University of California, San Diego, 2011

Professor Kimberly Prather, Chair

Atmospheric aerosol particles are a major component of the troposphere and affect regional and global atmospheric chemistry and climate. The size and chemistry of these particles influences the warm and cold cloud nucleation ability and optical properties of the aerosol particles. This dissertation investigates the atmospheric chemistry of aerosol particles and their role in warm cloud nucleation through a combination of laboratory experiments and field measurements. The effect of organics on the cloud condensation nuclei (CCN) activity of sea spray aerosols is described in Chapter 2. Sea spray aerosol produced by bubbling solutions composed of simplistic mixtures of NaCl and oleic acid or SDS had a significant effect on CCN activity, even in very small amounts; while artificial seawater solutions containing microorganisms, the common cyanobacteria (Synechococcus) and DMS-producing green algae (Ostreococcus), produced particles containing ~34 times more carbon than the particles produced from pure ASW, with no significant change observed in the overall CCN activity. During the fall of 2007 and 2008, over 300,000 acres burned in San Diego County wildfires. The resulting particle chemistry and estimated hygroscopicity during these wildfire events are explored in Chapter 3. The contribution of wildfire emissions were much larger and played a more significant role in affecting cloud condensation nuclei and total particle concentrations in 2007 than in 2008. The overall particle hygroscopicity during the biomass

burning dominated periods was very similar; however in 2008, the particle hygroscopicity was dominated by local sources rather than biomass burning, due to the much smaller particle size mode. Owens Lake is one of the largest sources of $PM_{2.5}$ in the Western Hemisphere, producing highly soluble dust plumes, and therefore there is great potential for those particles to impact cloud formation and possibly precipitation in the region. Chapter 4 explores particle chemistry and estimated hygroscopicity at Owens Lake. No significant change in particle hygroscopicity or CCN activity occurred concurrently with the change in mixing of particle classes during two different dust events at Owens Lake; indicating that the large dust particles were most likely completely CCN active and the smaller particles are likely dictating the hygroscopicity, as most of the dust particles are large enough and would activate to become CCN regardless of their hygroscopicity. The Cloud Indirect Forcing Experiment (CIFEX) took place to study the influence of aerosols on cloud properties at Trinidad Head, a coastal site in northern California representing clean marine air with periodic long-range transport. Chapters 5 & 6 explore particle chemistry, mixing state, optical properties and estimated hygroscopicity during CIFEX. Our measurements demonstrate how changes in hygroscopicity and optical properties evolve over time in the atmosphere as a function of particle chemistry and the mixing state of the aerosol. Two distinct oxalate events with enrichment of oxalate on different particle types and sizes suggest two separate sources of oxalate.

Chapter 1

Introduction

1.1 Atmospheric aerosol particles

Atmospheric aerosol are solid or liquid particles suspended in a gas and typically ranges in diameter from ~0.002 to ~10 μm [*Finlayson-Pitts and Pitts*, 2000; *Hinds*, 1999; *Seinfeld and Pandis*, 1998]. Aerosol particles can be directly emitted into the atmosphere (primary), such as dust, sea-salt, pollen, or formed in the atmosphere by chemical reactions (secondary), such as combustion by-products [*Finlayson-Pitts and Pitts*, 2000; *Seinfeld and Pandis*, 1998]. Concentrations of aerosol particles in the atmosphere range from 10^2 to 10^5 cm^{-3} or higher, depending on the location [*Curry and Webster*, 1999; *Hinds*, 1999]. The concentration, mass, size, chemical composition, density, surface area, and optical properties of particles determine their role in atmospheric processes [*Finlayson-Pitts and Pitts*, 2000; *Seinfeld and Pandis*, 1998]. Aerosol particles will be referred to interchangeably by the terms, aerosol and particle, for the remainder of this dissertation.

Particles affect Earth's climate in many different ways. Particles both absorb and scatter incoming solar radiation and absorb outgoing terrestrial radiation [*Charlson and Pilat*, 1969; *Haywood and Boucher*, 2000; *McCormick and Ludwig*, 1967]. Aerosol particles also nucleate cloud drops, or act as cloud condensation nuclei (CCN) [*Lohmann and Feichter*, 2005; *McFiggans et al.*, 2006; *Seinfeld and Pandis*, 1998]. By acting as CCN, aerosol particles cause changes in cloud droplet number and size, affecting the radiative properties and lifetime of clouds and also affect precipitation, known as the indirect effect [*Albrecht*, 1989; *Liou and Ou*, 1989; *Lohmann and Feichter*, 2005; *Twomey*, 1974; *Warner*, 1968].

While clouds cover ~60% of the Earth's surface [*Seinfeld and Pandis*, 1998], the global mean radiative forcing estimate of aerosol indirect effect represents the highest uncertainty and one of the lowest levels of scientific understanding regarding future climate change [*Ramaswamy et al.*, 2001; *Solomon et al.*, 2007].

1.1.1 Optical properties

The interaction of gases, particles, and clouds with electromagnetic radiation is essential for the energy balance of the Earth. The intensity of radiation reaching the Earth's surface is expressed by the Beer-Lambert Law:

$$\frac{I}{I_o} = e^{-b_{ext}L} \qquad (1.1)$$

where I_o and I are the incident and transmitted light intensities, respectively, L is the path length, and b_{ext} is the extinction coefficient [*Curry and Webster*, 1999; *Finlayson-Pitts and Pitts*, 2000; *Hinds*, 1999; *Seinfeld and Pandis*, 1998]. The extinction coefficient represents the total reduction in light intensity from both scattering and absorption which is expressed as:

$$b_{ext} = b_{ag} + b_{sg} + b_{ap} + b_{sp} \qquad (1.2)$$

where b_{ag} and b_{sg} are the absorption and scattering by gases and b_{ap} and b_{sp} are the absorption and scattering by particles [*Curry and Webster*, 1999; *Finlayson-Pitts and Pitts*, 2000; *Hinds*, 1999; *Seinfeld and Pandis*, 1998]. Light absorption by gases, mainly NO_2, is much less than total light scattering and absorption by particles [*Finlayson-Pitts and Pitts*, 2000]. The ability of a particle to both scatter or absorb electromagnetic radiation is strongly linked to both its size and composition [*Finlayson-Pitts and Pitts*, 2000; *Seinfeld and Pandis*, 1998]. The refractive index of a material, n, is defined as the ratio of the speed of light in a vacuum to that

of the material. The index of refraction for materials that both absorb and scatter light, *n*, is expressed as a complex number that depends on wavelength:

$$n = n_{\text{re}} + in_{\text{im}} \qquad (1.3)$$

where $i = \sqrt{-1}$, n_{re} is the real refractive index and corresponds to the scattering, while n_{im} is the imaginary refractive index and corresponds to the absorption [*Curry and Webster*, 1999; *Finlayson-Pitts and Pitts*, 2000; *Hinds*, 1999; *Seinfeld and Pandis*, 1998]. Water and ice both exhibit $n_{im} \sim 0$ across the visible spectrum (λ = 0.4-0.8 μm), leading to no absorption of visible radiation by clouds [*Curry and Webster*, 1999]. However, liquid water and ice can absorb significant infrared radiation (λ > 1μm) [*Curry and Webster*, 1999].

1.1.2 Aerosol size distributions

Particle size depends on the aerosol source and formation mechanism. The source and size affects the particle's impact on health, visibility, and climate [*Finlayson-Pitts and Pitts*, 2000; *Hinds*, 1999; *Seinfeld and Pandis*, 1998]. Several size metrics have been utilized to describe particle diameter since many particles have irregular shapes that cannot be accurately described by a simple geometric diameter (D_g). Aerodynamic diameter, D_a, is the most common way to describe effective particle size and is defined as the diameter of a sphere of unit density (ρ_o, 1 g cm^{-3}) that has the same terminal falling speed in air as the particle in question [*Finlayson-Pitts and Pitts*, 2000; *Hinds*, 1999]:

$$D_a = D_g \chi \sqrt{\frac{\rho_p}{\rho_o}} \qquad (1.4)$$

where ρ_p is the density of the particle and χ is the dynamic shape factor; χ = 1 for spheres [*Finlayson-Pitts and Pitts*, 2000; *Hinds*, 1999]. A spherical particle of higher than unit density will have a larger aerodynamic diameter than its geometric diameter.

Size distributions of particles are plotted as the number of particles normalized to the width of the particle diameter size range interval. The number of particles per unit size interval is plotted on the y-axis (vertical) versus log of the diameter on the x-axis (horizontal). Examples of different particle size distributions and modes are shown in Figure 1.1. Particle number, mass, volume, and surface area display different size distributions and are important for different applications; for example, health standards of particles are defined in terms of mass, whereas surface and volume considerations are important in controlling reactions of gases with particles [*Finlayson-Pitts and Pitts*, 2000]. As shown in Figure 1.1, particle number is dominated by small particles, while particle volume, and hence mass, becomes more important at larger sizes.

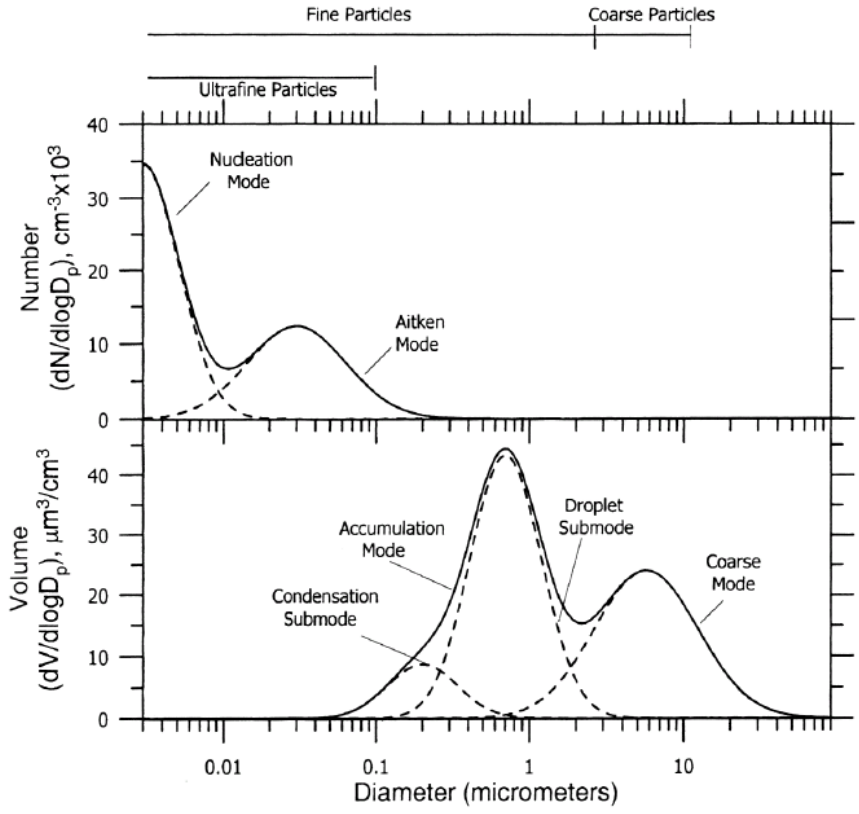

Figure 1.1. Typical aerosol size distributions by particle number (top) and particle mass (bottom). (Figure taken from Seinfeld & Pandis (2006), © 2006 by John Wiley & Sons, Inc.)

Coarse particles (~1 to ~10 μm) are usually produced by mechanical processes such as grinding, wind, or erosion and settle out of the atmosphere by sedimentation [*Finlayson-Pitts and Pitts*, 2000; *Hinds*, 1999; *Seinfeld and Pandis*, 1998]. They are usually composed of mineral dust and sea salt [*Finlayson-Pitts and Pitts*, 2000; *Hinds*, 1999; *Turpin and Lim*, 2001]. Particles in the accumulation mode (~0.08 to ~2 μm) are predominantly from the condensation of low-volatility vapors and coagulation of multiple small particles [*Finlayson-Pitts and Pitts*, 2000; *Hinds*, 1999; *Turpin and Lim*, 2001]. Accumulation mode particles are generally composed of more organics than larger coarse-mode particles due to the different sources of these particles such as combustion, however they can also contain soluble inorganic compounds such as ammonium, sulfate and nitrate [*Finlayson-Pitts and Pitts*, 2000; *Hinds*, 1999; *Turpin and Lim*, 2001]. Accumulation-mode particles are typically removed by cloud activation and precipitation processes, as they are too small for sedimentation [*Finlayson-Pitts and Pitts*, 2000]. Aitken nuclei (~0.01 to ~0.2 μm) arise from ambient-temperature gas-to-particle conversion and combustion processes involving hot supersaturated vapors that condense [*Finlayson-Pitts and Pitts*, 2000; *Hinds*, 1999]. Aitken-mode particles typically have short lifetimes by acting as nuclei for condensation of low-vapor-pressure gases and growing into the accumulation mode, and/or undergoing rapid coagulation processes [*Finlayson-Pitts and Pitts*, 2000]. Nucleation particles (< 0.01 μm) are formed exclusively from gas-to-particle conversion. For reference, threshold particle sizes for cloud droplet activation are typically in the 40-200 nm size range [*McFiggans et al.*, 2006] and will be discussed further in sections 1.2.1 and 1.4.1.

1.1.3 Chemical composition

The chemical composition of aerosol particles is wide-ranging, complex, and varies with location and atmospheric conditions. Particles are made up of many different inorganic

and organic compounds that vary widely in solubility, density and surface tension. Mixing state is used to describe whether two or more species are found together in one particle- "internally mixed"- or instead as separate particles in the same sample- "externally mixed." Tropospheric particles are typically internally mixed in both organic and inorganic materials [*Lee et al.*, 2002; *McFiggans et al.*, 2006; *Middlebrook et al.*, 1998]. The mixing of different species in a particle is very important in dictating their role in atmospheric processes. Particle mixing state dictates the reactivity, ability to scatter and absorb radiation, CCN activity, and therefore atmospheric lifetime of the aerosol.

1.1.3.1 Inorganic aerosol particles

Primary inorganic particles are generally formed from mechanical processes, such as mineral dust particles lofted by winds and sea salt particles from breaking waves. Because of the mechanical processes involved, these particles are predominantly in the supermicron ($D > 1$ μm) size range, however both mineral dust and sea salt aerosol also have significant, but less abundant, modes in the submicron (< 1 μm) size range.

Secondary inorganic aerosol mass is dominated by nitric and sulfuric acids which involve heterogeneous and/or multiphase reactions with trace gases including NO_x ($NO + NO_2$), HNO_3, NO_3, N_2O_5, SO_2 and H_2SO_4 with preexisting aerosol particles. Gaseous basic ammonia (NH_3) can then partially or fully neutralize the acidic particles, forming ammonium nitrate and ammonium sulfate. The uptake of sulfuric acid is diffusion-limited and controlled by particle surface area [*Bassett and Seinfeld*, 1984], therefore ammonium sulfate salts (NH_4HSO_4 and $(NH_4)_2SO_4$) are predominantly in the submicron size range. Ammonium nitrate is sensitive to ambient relative humidity (RH) and temperature, and therefore partitions between the gas and particle phases, with equilibrium ratios dependent on atmospheric conditions. Inorganic nitrate-containing compounds tend to take over the larger submicron and supermicron size ranges due to nitric acid being a weaker acid than sulfuric and the semi-

volatile nature of ammonium nitrate salts [*Bassett and Seinfeld*, 1984; *Song and Carmichael*, 1999].

1.1.3.2 Organic aerosol particles

Organic matter makes up an important fraction of aerosol mass in a variety of atmospheric environments. The composition of organic species in the atmosphere is complex, even in remote environments with little or no contribution from combustion emissions. Typical organic compounds found in ambient aerosol include alkanes, alkenes, aromatics, fatty acids, alcohols and organic bases [*Finlayson-Pitts and Pitts*, 2000; *Jacobson et al.*, 2000; *Seinfeld and Pandis*, 1998]. Regional organic aerosols are typically from biomass burning, vegetative detritus, bacteria, viruses, fungal spores and sources, while urban organic aerosol emissions are mainly from fossil fuel combustion [*Jacobson et al.*, 2000]. Elemental carbon (EC) and polycyclic aromatic hydrocarbons (PAHs) are primarily produced from combustion sources, such as fossil fuel and biomass, however, depending on combustion conditions, organic carbon (OC) can also be co-emitted and mix with EC [*Jacobson et al.*, 2000]. Water soluble organic carbon (WSOC) is a subgroup of OC and is made up of hundreds or more individual compounds, such as oxalate and other organic acids [*Chebbi and Carlier*, 1996; *Mochida et al.*, 2003] that each contribute only a very small portion to the overall aerosol mass [*Hamilton et al.*, 2004; *Kanakidou et al.*, 2005; *Maria et al.*, 2004; *Murphy*, 2005; *Saxena*, 1996].

Oxidation of organics leads to condensed-phase multifunctional organic products known as secondary organic aerosol (SOA) [*Finlayson-Pitts and Pitts*, 2000; *Grosjean*, 1992; *Grosjean and Seinfeld*, 1989; *Jacobson et al.*, 2000; *Seinfeld and Pandis*, 1998]. A variety of organics in particles should be primary in nature, however the complexity of organics found in particles and the many different sources of organics in the atmosphere, both primary and secondary, make it very difficult to identify distinct sources of organics [*Finlayson-Pitts and*

Pitts, 2000; *Jacobson et al.*, 2000; *Seinfeld and Pandis*, 1998]. Once oxidized, these aerosols can be transported significant distances [*Finlayson-Pitts and Pitts*, 2000; *Jacobson et al.*, 2000; *Sempere and Kawamura*, 1996]. The relative importance of secondary organic aerosol to the organic particulate carbon is varied by conditions, but generally ranges from ~5-50% [*Gray et al.*, 1986; *Hildemann et al.*, 1994a; *Hildemann et al.*, 1994b; *Pandis et al.*, 1992; *Turpin and Huntzicker*, 1995; *Turpin et al.*, 1991].

Organic aerosol is typically internally mixed with inorganic components. A common source of internally mixed inorganic and organic aerosol is biomass burning. Fine particle potassium with carbonaceous signatures such as levoglucosan are known to be markers for biomass combustion [*Andreae*, 1983; *Engling et al.*, 2006b; *Fabbri et al.*, 2008; *Fine et al.*, 2004; *Li et al.*, 2003; *Pekney et al.*, 2006; *Reid et al.*, 2005]. An additional source of internally mixed organic and inorganic aerosol is marine aerosol. Surface-active compounds (surfactants) are present in the ocean surface microlayer and become incorporated in marine aerosol when bubbles burst from breaking waves [*Lewis and Schwartz*, 2004]. Up to 60% of the mass of marine aerosol particles can be organic, with the organic mass fraction typically being larger for smaller particles than larger particles [*Middlebrook et al.*, 1998; *O'Dowd et al.*, 2004].

1.2 Hygroscopic and cloud nucleating properties of aerosols

Water vapor makes up ~0-4% of the atmospheric concentration of gases and varies greatly with time and location [*Curry and Webster*, 1999]. The amount of water vapor in the atmosphere is controlled by evaporation/sublimation, how it is transported in the atmosphere, and the amount that is removed by precipitation [*Pruppacher and Klett*, 1997]. The cooling by adiabatic expansion of humid air as it ascends in the atmosphere can cause a supersaturation of water vapor, which typically results in the formation of a cloud or fog. The supersaturation

reached in a cloud or fog will depend on the moisture content of the atmosphere and the thermodynamic state of the atmosphere that controls the development of updrafts [*Pruppacher and Klett*, 1997]. Typical cloud supersaturations in the atmosphere are ~0.2 – 2%, while fog supersaturations are lower, around ~0.02-0.2% [*Pruppacher and Klett*, 1997]. Fog drops typically have radii from a few μm to ~30-40 μm and clouds usually have drops from 5 μm to ~100 μm [*Pruppacher and Klett*, 1997].

1.2.1 Aerosol particles and cloud formation

Aerosol particles that are capable of initiating drop formation under atmospheric supersaturations are called cloud condensation nuclei (CCN). Early work by Köhler provided the basis for describing the equilibrium size of a droplet with water saturation ratio [*Koehler*, 1936]. The conditions for water equilibrium between the gas and aqueous phases are influenced by the curvature of the particles and the presence of solutes. The vapor pressure over a curved surface always exceeds that of the same substance over a flat surface. Known as the Kelvin effect, the curvature of a particle surface reduces the attractive forces between surface water molecules, making it increasingly easier for water molecules to leave the droplet surface as the droplet size decreases [*Curry and Webster*, 1999; *Hinds*, 1999; *Seinfeld and Pandis*, 1998]. The Raoult effect is due to the presence of a solute which lowers the equilibrium vapor pressure above the droplet surface, thereby allowing growth by condensation to occur at a lower supersaturation than for pure water [*Curry and Webster*, 1999; *Hinds*, 1999; *Seinfeld and Pandis*, 1998]. The balance between the Kelvin and Raoult effects is described by Köhler Theory and can be derived from an energy balance at phase equilibrium to yield a general equilibrium relation between an aqueous salt solution droplet and water vapor:

$$\frac{e}{e_s} = a_w \exp\left(\frac{2\nu_w \sigma_{s/a}}{RTr}\right) \qquad (1.5)$$

where e is the vapor pressure of water, e_s is the saturation vapor pressure of water, a_w is the water activity, v_w is the partial molar volume of water, $\sigma_{s/a}$ is the surface tension of the droplet, R is the universal gas constant, T is the droplet temperature and r is the particle radius [*McFiggans et al.*, 2006; *Pruppacher and Klett*, 1997; *Seinfeld and Pandis*, 1998]. However, since this form of the Köhler equation is complicated, a simplified form of the Köhler equation has been derived [*Pruppacher and Klett*, 1997; *Seinfeld and Pandis*, 1998]:

$$S = \frac{e}{e_s} \approx 1 + \frac{A}{D} - \frac{B}{D^3} \tag{1.6}$$

where

$$A = \frac{2M_w\sigma_{s/a}}{RT\rho_w} \tag{1.6a}$$

and

$$B = \frac{\nu m_s M_w}{M_s\left(\frac{4}{3\pi\rho_w}\right)} \tag{1.6b}$$

where ν is the Van't Hoff Factor, or number of dissociated ions per solute molecule, m_s is the solute mass, M_w is the molecular weight of water, M_s is the molecular weight of the solute, and ρ_w is the density of water. Term A is known as the Kelvin term, while term B is known as the Raoult term. A Taylor series expansion of Eq. (1.6), also demonstrated in Figure 1.2, shows a single characteristic maximum in supersaturation for a given dry particle composition and size, known as the critical supersaturation, S_c, associated with a unique size, known as the activation diameter, D_{act}, or critical radius, r_c, where $r_c=D_{act}/2$. The analytical solutions for Eq. (1.6) are as follows:

$$D_{act} = 2\left(\frac{3B}{A}\right)^{1/2} \tag{1.7}$$

$$S_c = \left(\frac{4A^3}{27B} \right)^{1/2} \qquad (1.8)$$

Once the droplet grows above its critical size, D_{act}, the droplet will continue to grow as the surrounding S increases above S_c, until S decreases below the equilibrium value of S at the corresponding value of D [*McFiggans et al.*, 2006; *Pruppacher and Klett*, 1997]. Figure 1.2 illustrates the contribution of the curvature/Kelvin term and the solute/Raoult term to the Köhler equation.

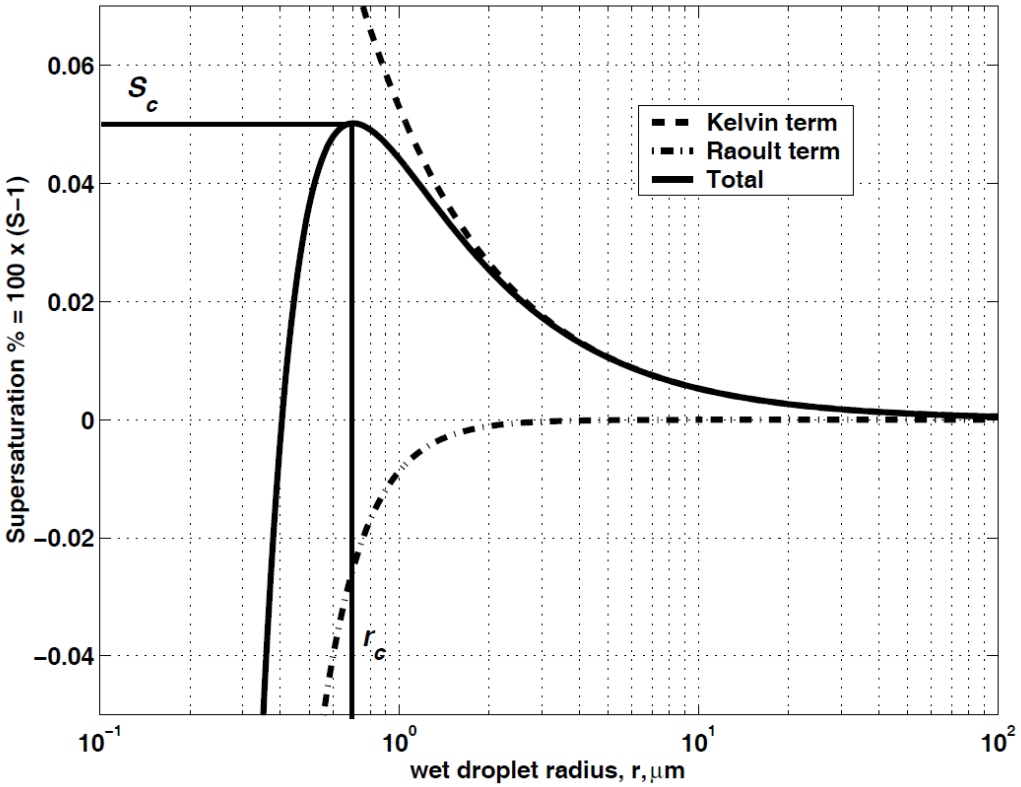

Figure 1.2. The Köhler equation illustrated as a competition between the curvature (Kelvin) and solute (Raoult) terms. (Figure used under the Creative Commons License)

Particles that consist of soluble substances are the most likely to act as CCN and ultimately form cloud droplets. However, combustion particles, which can be water insoluble,

can also serve as CCN [*Petters et al.*, 2009; *Weingartner et al.*, 1997] and contribute a significant fraction of CCN in areas with large combustion sources. For a given composition and supersaturation, the determining factor whether a particle activates or not is its dry size. The sensitivity of droplet activation to particle size, particle composition and supersaturation can vary depending on atmospheric conditions. The concentration of cloud droplets (N_d) is more sensitive to the size of the particles, especially in polluted environments, where there are high concentrations of particles, some of which can contribute to the number fraction of CCN [*Feingold*, 2003; *McFiggans et al.*, 2006; *Rissman et al.*, 2004]. The number of activated droplets depends on the number distribution of particles of a given type and not particle mass, however, the activation of individual particles depends on the fraction of soluble mass [*McFiggans et al.*, 2006]. Particles smaller than ~ 40 nm are not likely to become CCN regardless of their composition, while larger particles ~ ≥ 200 nm almost always have enough soluble material to become CCN, therefore particles 40-200 nm represent the activation threshold size range [*McFiggans et al.*, 2006]. To directly probe if an aerosol is likely to act as a CCN, measurements report potential CCN concentrations at specific supersaturations or as a supersaturation-dependent spectrum.

1.2.2 Hygroscopicity parameter (κ)

To describe the relationship between dry particle diameter and CCN activity, a single hygroscopicity parameter (κ) is used to quantify the water uptake characteristics [*Petters and Kreidenweis*, 2007]. The saturation ratio over a droplet has been described previously in Eqs. 1.5 and 1.6. The parameterization of κ is defined through its effect on the water activity (a_w) of the solution:

$$\frac{1}{a_w} = 1 + \kappa \frac{v_s}{v_w} \qquad (1.9)$$

where V_s is the volume of the dry particle and V_w is the volume of the water present in the particle. Assuming the sum of water associated with individual solutes is the total volume of water, and converting to volume equivalent diameter, the relationship between supersaturation and particle diameter is defined as:

$$S(D) = \frac{D^3 - D_{dry}^3}{D^3 - D_{dry}^3(1-\kappa)} \exp\left(\frac{A}{D}\right) \qquad (1.10)$$

where D is the diameter of the droplet, D_{dry} is the diameter of the dry particle, $A = 2.1\text{x}10^{-9}$ m is a constant presuming a surface tension of 0.072 J m^{-2} (pure water) and temperature of 298.15 K [*Petters and Kreidenweis*, 2007].

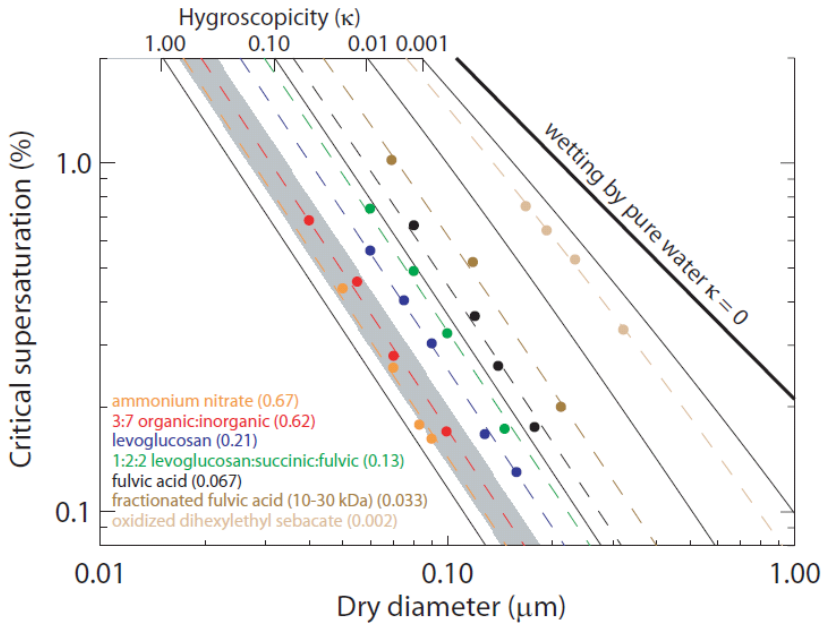

Figure 1.3. Single hygroscopicity parameter (*κ)* shown as isolines in critical supersaturation-dry diameter space. Overlaid are data points from standards illustrating typical *κ* values. (Figure used under the Creative Commons License)

Typical atmospheric values of *κ* range from 0 to 1.4. Highly soluble inorganic salts have *κ* values from 0.5-1.4, while slightly to very hygroscopic organics have *κ* values from 0.01-0.5 and non-hygroscopic particles have values of zero [*Petters and Kreidenweis*, 2007]. For

complex ambient experimental data, a κ value can be obtained from fitting CCN activity data assuming a $\sigma_{s/a}$ of 0.072 J/m^{-2} (that of pure water) and T = 298.15 K [*Petters and Kreidenweis*, 2007]. An example of specific compounds and their hygroscopicities is shown in Figure 1.3.

1.2.3 In-cloud processing of CCN-active aerosol particles

While clouds cover ~60% of the earth's surface, the presence of clouds is varies significantly with geographical location [*Seinfeld and Pandis*, 1998]. Clouds form and evaporate repeatedly with only ~ 10% of all clouds generating precipitation [*Pruppacher and Klett*, 1997; *Seinfeld and Pandis*, 1998]. Therefore, aerosol particles that activate to form CCN are most likely activated and deactivated ~10 times before finally being removed from the atmosphere [*Hoppel et al.*, 1990]. When particles activate into CCN, they become a dilute water droplet. Trace gas phase atmospheric species will then partition to the dilute water solution in the droplet to reestablish gas-particle equilibrium. For species A, the equilibrium between the gas and aqueous phase can be described as:

$$A(g) \leftrightarrow A(aq) \qquad (1.11)$$

The equilibrium between the gaseous and dissolved A is expressed by the Henry's Law coefficient H_A:

$$[A(aq)] = H_A p_A \qquad (1.12)$$

where p_A is the partial pressure of A in the gas phase and [A(aq)] is the aqueous phase concentration of A [*Seinfeld and Pandis*, 1998]. Soluble gases such as NO_3, HNO_3, and H_2O_2 have very large Henry's Law coefficients implying that these species are predominantly found in the aqueous phase, while other gas phase species such as O_2, NO and NO_2 have low Henry's Law coefficients and are predominantly found in the gas phase [*Seinfeld and Pandis*, 1998]. Once many species are dissolved, they can react with water and undergo acid-base equilibrium reactions. As the pH of the cloud or fog droplet changes, the Henry's law constant can change dramatically [*Seinfeld and Pandis*, 1998]. Many reactions that occur slowly in the

gas phase can occur quite rapidly in the aqueous phase, including oxidation reactions that yield water-soluble organics [*Ervens et al.*, 2004b; *Seinfeld and Pandis*, 1998]. The more oxidized products formed in these reactions have a lower vapor pressure than their precursors, and typically remain in the particulate phase after the droplet has evaporated. In-cloud processing is one of the main pathways for particulate sulfate production [*Ervens et al.*, 2004b; *Sorooshian et al.*, 2006; *Yu et al.*, 2005], and can lead to a high degree of internal mixing of sulfate due to scavenging of non-activated interstitial particles by cloud droplets within clouds. Scavenging during cloud processing is responsible for internal mixtures of sea salt and mineral dust [*Andreae et al.*, 1986; *Niimura et al.*, 1998] as well as sea salt and elemental carbon [*Holecek et al.*, 2007; *Spencer et al.*, 2008]. As particles become cloud processed and accumulate sulfate and other lower vapor pressure reaction products, their physical and chemical properties change; making them both larger and more soluble, thereby increasing the likelihood of activating as a CCN again.

1.3 Major instrumentation

As atmospheric aerosol particles range in size over four orders of magnitude and vary in composition with size, time and location, they present a significant analytical challenge [*McMurry*, 2000]. While there is a wide range of different analytical and sampling methods to measure aerosol particle composition, characterizing the chemical composition of aerosol particles as a function of size is still only partially complete [*Putaud et al.*, 2004]. Studying the link between the size-resolved particle chemistry of ambient aerosols and their CCN properties is crucial for developing suitable models for the effect of aerosols on cloud formation and radiative forcing as well as in-cloud chemical processing [*McMurry*, 2000]. The main instruments used for the research conducted in this thesis are discussed below.

1.3.1 Aerosol time-of-flight mass spectrometry (ATOFMS)

Single particle mass spectrometry (SPMS) is used to study online individual particle composition [*Murphy*, 2007; *Murphy et al.*, 2006; *Noble and Prather*, 2000; *Sullivan and Prather*, 2005; *Ziemann*, 1998]. These techniques measure real-time changes in the size and chemical composition of individual particles. The SPMS instrument used for this thesis research is an aerosol time-of-flight mass spectrometer (ATOFMS) [*Gard et al.*, 1997]. Aerosols are pulled into the vacuum of the instrument. A converging nozzle inlet is used for analyzing particles D_a ~0.2-3 μm with maximum transmission efficiency at ~1.7 μm, while an aerodynamic lens is used on a separate instrument to efficiently analyze submicron aerosols ~80- 1000 nm [*Su et al.*, 2004].

A schematic of the ATOFMS is shown in Figure 1.4. After each particle enters the inlet, it is accelerated to its size- and shape-dependent terminal velocity. The particle then passes through two 532 nm continuous-wave diode-pumped Nd:YAG laser beams. Two elliptical mirrors collect the back-scattered laser light from the two separate laser beams and focus it onto a photomultiplier tube (PMT) and calculate the time-of-flight of the particle between the laser beams. Particle velocity is calculated using the time-of-flight measurement and the distance between the two laser beams. Through a calibration of particle velocity versus dry diameter using polystyrene latex spheres (PSLs) of known size, the aerodynamic diameters of atmospheric particles can be determined from the time-of-flight measurement. Below the two continuous wave lasers, a timing circuit uses the calculated time-of-flight to determine when to trigger the firing of a Q-switched Nd:YAG laser (4^{th} harmonic, 266 nm). The UV laser pulse rapidly desorbs and ionizes the particle constituents in the source region of a time-of-flight mass spectrometer. Positive and negative ions are passed into two separate ion flight tubes in the dual-polarity mass spectrometer where they enter a reflectron to increase the mass resolution before being deflected back 180° towards the ion source. A microchannel

plate detector facing the reflectron detects the ions and sends a signal to a data acquisition board. In this way, particle aerodynamic size, and composition with positive and negative mass spectra are acquired for each individual particle in real-time.

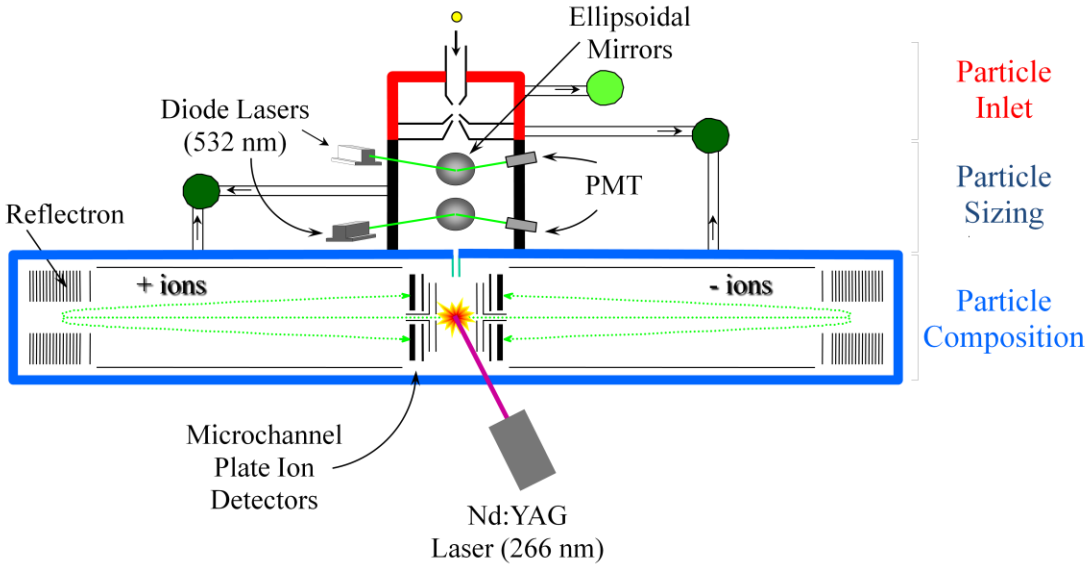

Figure 1.4. Schematic of the current nozzle ATOFMS instrument for on-line individual particle analysis.

The laser desorption ionization (LDI) method used here can detect both the refractory and non-refractory aerosol species. While quantification of specific chemical components has been demonstrated [*Bhave et al.*, 2002], it remains a challenge due to the highly variable signals produced by LDI [*Wenzel and Prather*, 2004], and significant matrix effects from the different particle types. The ion signals can be quantified by characterizing relative sensitivity factors (RSFs) for specific chemical species in model aerosol standards [*Gross et al.*, 2000]. RSFs have been used to quantify various cations and anions in sea salt as well as measure the relative amount of organic carbon (OC) associated with elemental carbon (EC) [*Gross et al.*, 2000; *Spencer and Prather*, 2006]. In this dissertation, ATOFMS is used to observe particle

chemical composition in the ambient atmosphere, mainly focusing on biomass burning and mineral dust particles.

1.3.1.1 ATOFMS data analysis

The ATOFMS data acquisition system allows rapid collection of single-particle data, allowing for the analysis of changes in particle chemistry with high size (0.010-0.10 μm) and time resolution. Due to the high volume of data collected using this on-line technique, modern data analysis tools are required. YAADA (Yet Another ATOFMS Data Analyzer, http://www.yaada.org/) is a software toolkit used within Matlab to analyze the single particle data. The ART-2a classification algorithm is used to sort ATOFMS single-particle mass spectra into clusters of particles with similar mass spectral features [*Rebotier and Prather*, 2007; *Song et al.*, 1999]. The algorithm functions by randomly selecting particles from the dataset and comparing the dot product of the mass spectra from two individual particles. If the dot product is greater than or equal to the defined vigilance factor, then both particles are put into the same cluster. This grouping method continues with the remaining particle mass spectra, until each particle is either put into a matching particle cluster, or a new particle cluster is created to which additional particles can be added. The clusters are then regrouped by testing the dot product of each cluster with one another to decrease the number of total particle clusters. A vigilance factor of 0.80 or greater is commonly used to appropriately differentiate between similar mass spectra that are from different particle sources. Generally, the top 50 most populated ART-2a clusters that usually represent 90% or more of the total particles are then manually inspected and classified into particle types (sea salt, mineral dust, elemental carbon, metals, organic carbon, biomass burning, others) based on the mass spectral fingerprints observed in prior ATOFMS ambient and source characterization studies [*Ault et al.*, 2010; *Moffet et al.*, 2008; *Pratt et al.*, 2010; *Qin and Prather*, 2006; *Silva*, 2000; *Silva et al.*, 1999; *Sodeman et al.*, 2005; *Spencer et al.*, 2008; *Toner et al.*, 2006].

Further analysis of ATOFMS data is determined by the specific questions to be addressed. Generally, the fractions of various particle types are plotted versus time and particle size to study changes in aerosol properties due to meteorological changes, diurnal cycles, and any other specific atmospheric events. Searches for specific chemical markers in individual particles or particle classes are also performed. Examples of specific biomass burning chemical markers are shown in Chapters 3, aromatic chemical markers are discussed in Chapter 5, and oxalate, secondary, and in-cloud/aqueous processing markers are analyzed in Chapter 6. Relative changes in the amounts of specific chemical compounds can be inferred upon careful analysis of the ion peak area signals from the ATOFMS data by searching on the same particle matrix.

1.3.2 Size distribution and particle counting instruments

Particle behavior and source in the atmosphere is largely determined by size. As stated previously, typical particle size ranges in the atmosphere are ~0.001-10 μm. There are many instruments that measure concentrations of particles in size bins, known as particle size distributions. Each instrument typically covers around one order of magnitude of particle size ranges and there are no instruments that cover the entire range.

1.3.2.1 Aerodynamic particle sizer (APS)

An aerodynamic particle sizer (APS) is used to determine the aerodynamic diameter of individual particles ~0.5-20 μm from their time-of-flight between two continuous wave lasers once the particle has been accelerated to its terminal velocity. This is the same principle of operation as used in the sizing region of the ATOFMS, however, the continuous wave laser beams on the APS are slightly overlapping, and therefore much smaller than on the ATOFMS, which reduces coincidence errors from overlapping particles traversing the laser beam(s), while reducing the sizing accuracy [*Hinds*, 1999]. The APS used in this research is a TSI, Inc. model 3221 APS [*Volckens and Peters*, 2005] as shown in Figure 1.5. The APS has a total

sample flow of 5.0 lpm; 4.0 lpm is filtered and used as a sheath flow to surround the 1.0 lpm of aerosol sample flow through the detection region, as shown in the top of Figure 1.5. The stated resolution of the TSI, Inc. Model 3221 APS is ± 0.02 μm at 1.0 μm. The measured particle diameters are grouped into distinct size bins ranging from 0.523 to 20 μm by combining the signals from the different size-resolved channels. Any measured particles smaller than 0.523 μm are placed in one large unresolved bin. Typically, we obtain a complete APS size distribution in 1 minute by averaging the size-resolved channel signals over the time period.

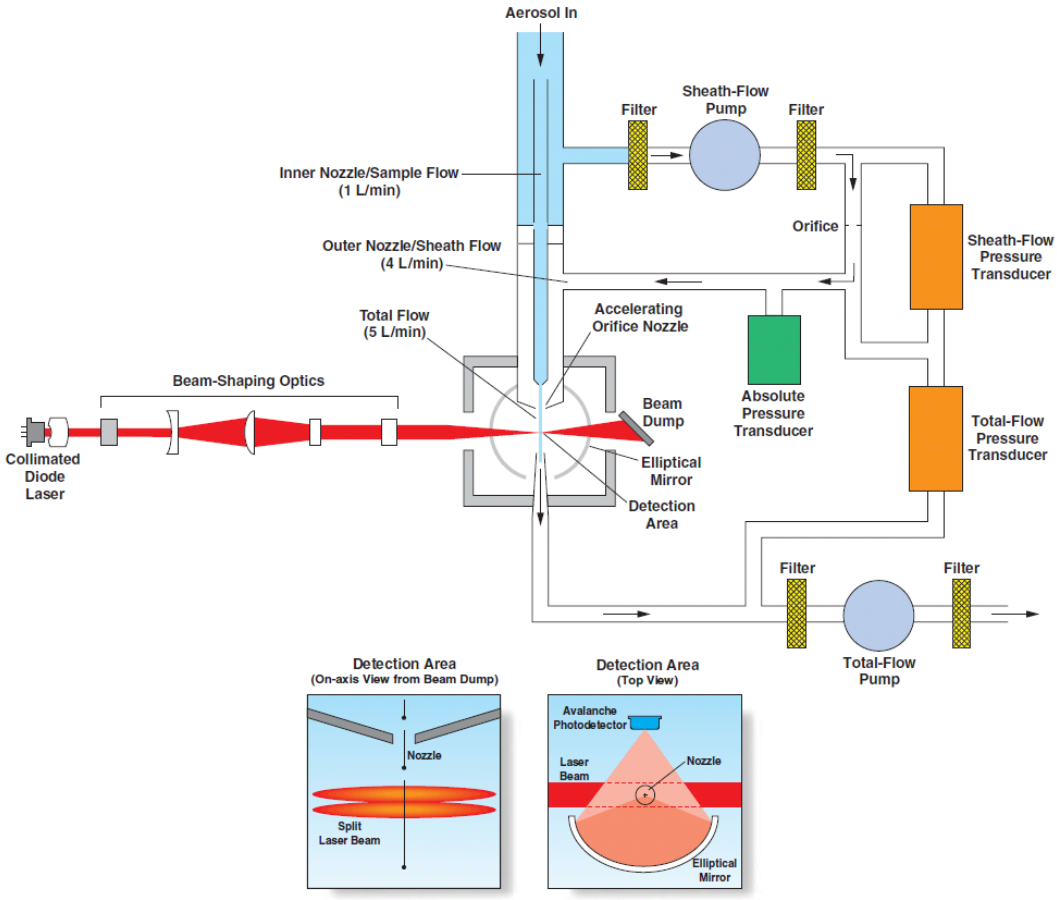

Figure 1.5. Schematic of the Aerodynamic Particle Sizer (APS, TSI Model 3321) that measures the size of particles between 0.5 and 20 μm. (Diagram courtesy of TSI, Inc.)

1.3.2.2 Differential Mobility Analyzer (DMA)

A differential mobility analyzer (DMA) transmits a discrete mobility particle size through the instrument. Mobility size is based on the size and shape of a particle, but not its density. Therefore, particles of different densities will have similar mobility size if they have similar shape. In the inlet of the instrument, charge equilibrium is established using a bipolar aerosol neutralizer that exposes the aerosol particles to a high concentration of positive and negative ions. The distribution of electrical charges across the aerosol size distribution can be described using the Wiedensohler approximation to the corrected Fuchs charge distribution [*Wiedensohler*, 1988]. The proportion of particles containing an electrical charge and the number of charges per particle increase exponentially with particle size, therefore particles greater than ~200 nm will have multiple charges, while particles less than ~100 nm will only have ~10% of particles with multiple charges and the charge distribution is centered around +1 [*Flagan*, 2001].

After the aerosols reach charge equilibrium, they enter the cylindrical DMA tube. A part of the aerosol flow is filtered into a recirculation loop where it is used as the sheath flow into the DMA, as shown in Figure 1.6. A large, variable negative voltage is applied to the center rod of the DMA tube, forming an electric field that attracts positively charged particles flowing through the DMA towards the center of the cylinder [*Hinds*, 1999]. There is a small opening at the bottom of the DMA that a narrow portion of the aerosol, those with the correct mobility size, exit the cylinder; the remaining aerosol with mobility sizes above and below impact on the surface of the cylinder or rod and do not exit the electrode [*Hinds*, 1999]. The particle mobility diameter that exits the DMA is a function of the particle's physical size, shape, and number of charges as described by:

$$\frac{D_m}{C_c} = \frac{2neVL\chi}{3\mu q_{sh} \ln\left(\frac{r_2}{r_1}\right)} \tag{1.13}$$

where D_m is the mobility diameter, C_c is the Cunningham slip correction, n is the number of elementary charges, e, V is the rod voltage, L is the rod's length, χ is the particle's dynamic shape factor, μ is the gas viscosity, q_{sh} is the sheath flow rate, and r_1 and r_2 are the inner and outer radii of the DMA cylinder. Non-spherical particles ($\chi > 1$) have larger mobility diameters than volume-equivalent spherical particles due to the extra drag force experienced by non-spherical particles as they move towards the DMA rod [*DeCarlo et al.*, 2005].

The DMA used in this work is a TSI, Inc. model 3081, long DMA, which is used to measure a particle size range of ~20 to 1000 nm, depending on particular instrumental settings [*Flagan*, 2001; *Knutson and Whitby*, 1975]. A schematic is shown in Figure 1.6. Below 20 nm diffusional broadening can seriously degrade the size resolution, and supermicron particles cannot be effectively transmitted because the voltages needed cannot be safely applied. An optimal sheath-to-aerosol flow ratio of 10:1 should be used for the greatest size resolution. Typical sheath and aerosol flow rates used in this work are 10.0 and 1.0 lpm. The DMA can be operated in two modes; the first is used to continuously select one mobility diameter by leaving the rod voltage, V, fixed so that a known particle size can be transmitted. This mode is used to provide a monodisperse aerosol population. In the second mode, the voltage is continuously scanned across the particle size range. If the scanning mode is used, the DMA is typically coupled in series to a condensation particle counter (CPC), described below, to measure the submicron size distribution.

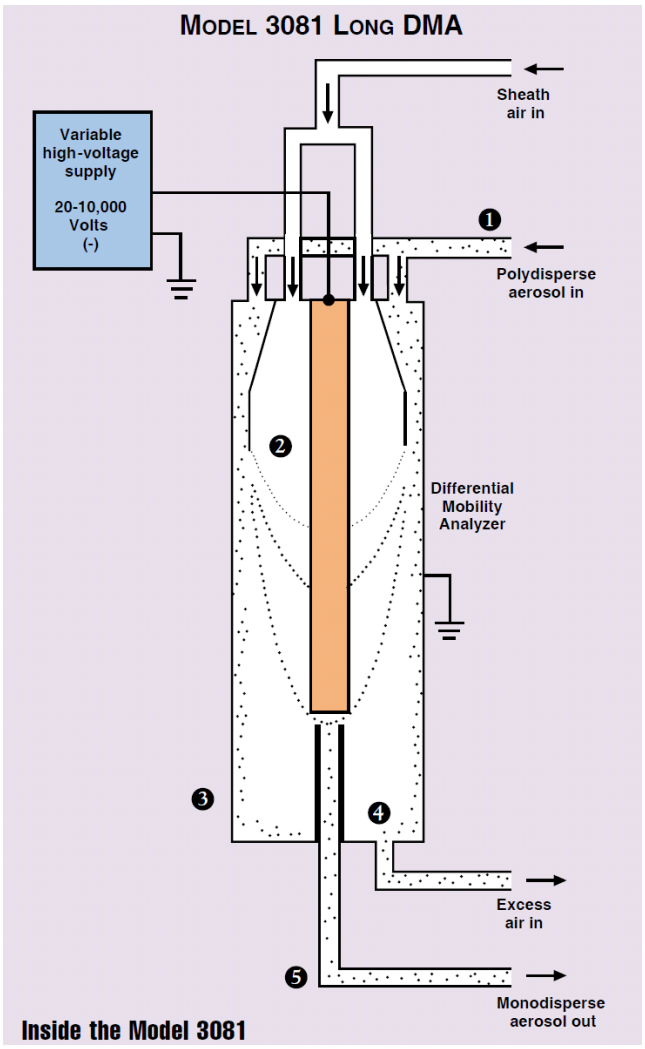

Figure 1.6. Schematic of the Differential Mobility Analyzer electrode (DMA, TSI Model 3081) that measures the size of particles between 0.0025 and 0.6 μm. (Diagram courtesy of TSI, Inc.)

1.3.2.3 Condensation particle counter (CPC)

The condensation particle counter (CPC) can count all particles, or condensation nuclei (CN) regardless of their size, composition, or shape, if they are above a certain nanoparticle size threshold (~10 nm). The CPC forces all particles to grow by exposing them to a hot saturated vapor stream of butanol. An optical particle counter (OPC) counts each grown particle by detecting the scattered light from the aerosol particle as it traverses a

continuous laser beam [*Hinds*, 1999]. The CPC used in this work is a Model 3010 (TSI, Inc.) [*Mertes et al.*, 1995]. A schematic of the CPC is shown in Figure 1.7. While this CPC model uses butanol, more recent models now operate with water [*Hering et al.*, 2005]. The 3010 CPC can count all particles greater than 10 nm, up to 10,000 particles/cm^3, with an aerosol sample flow of 1.0 lpm. The CPC can be coupled with a DMA (described previously) to measure submicron aerosol size distributions.

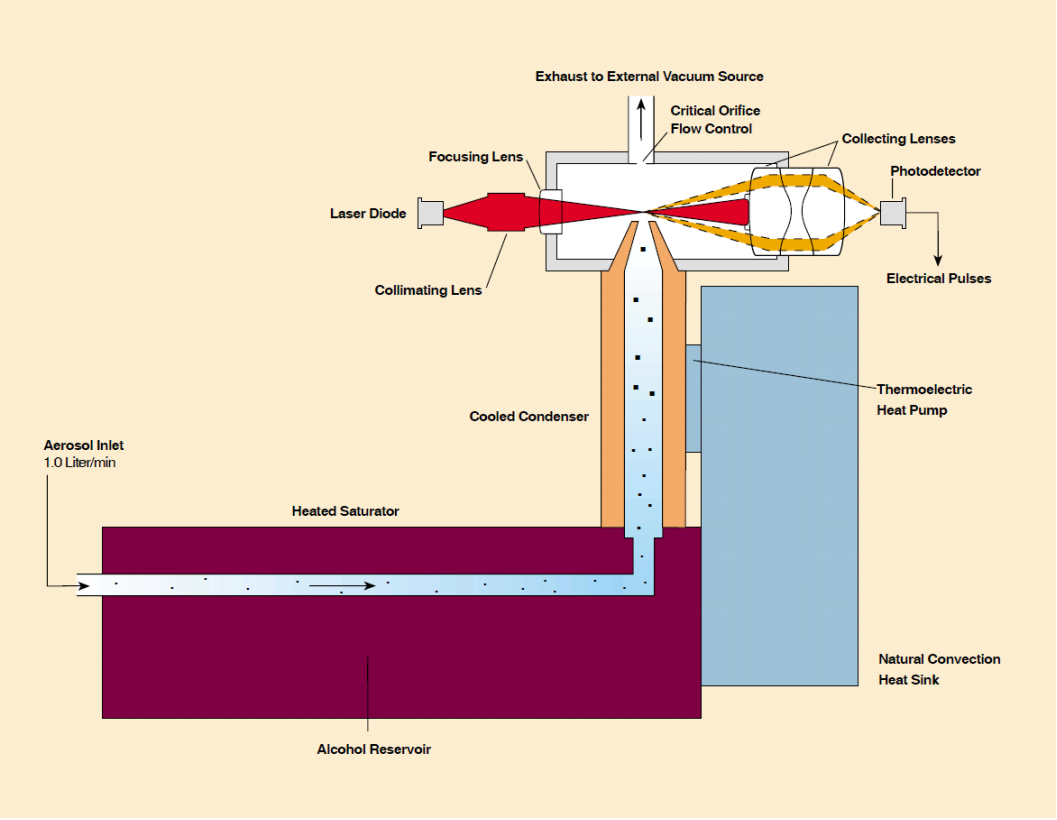

Figure 1.7. Schematic of the condensation particle counter (CPC, TSI Model 3010) that counts the concentration of particles between 0.01 and >3 μm. (Diagram courtesy of TSI, Inc.)

1.3.2.4 Scanning mobility particle sizer (SMPS)

When a DMA and CPC are combined in series, the system is referred to as a scanning mobility particle sizer (SMPS) that measures the size distributions of submicron aerosol particles. The DMA operates in scanning voltage mode and transmits the steadily changing sized particles through the DMA and to the CPC. By counting the particle concentration in each DMA size bin, the CPC determines the size distribution of the sampled aerosol. To accurately use SMPS measurements to obtain a size distribution, transfer functions are required to invert the raw data to account for charge equilibrium, the probability of an aerosol being electrically charged as a function of particle size, and to account for multiply charged particles [*Collins et al.*, 2004; *Stolzenburg and McMurry*, 2008]. As shown in Eq. 1.11, a particle with a particular mobility diameter and more than one charge will have a larger volume equivalent diameter than a singly-charged particle of the same mobility diameter; therefore it is important to account for the contribution of multiply-charged particles measured in each DMA size bin. The Model 3081 DMA and Model 3010 CPC used here generally measure the aerosol size distribution from ~11-600 nm using a sheath flow of 4.0 lpm and aerosol flow of 0.4 lpm with a scan time of 5 minutes.

1.3.3 Cloud condensation nuclei counter (CCNc)

A cloud condensation nuclei counter (CCNc) reproduces cloud formation by allowing the aerosol sample to be exposed to a controlled water supersaturation and then counting the number of particles that grow into cloud droplets [*Nenes et al.*, 2001]. The CCNcs used for this work were prototype miniature continuous-flow streamwise thermal gradient CCNcs that were constructed at Scripps Institution of Oceanography (SIO) based on the design of Roberts and Nenes [*Roberts and Nenes*, 2005]. The aerosol sample is sent to the center of the column and is surrounded by a sheath of humidified, filtered air. A water supersaturation is produced from a linear thermal gradient along the continuously wetted walls of the column. The

supersaturation is created because of the different rates of diffusion of heat (which controls P°_{H2O}) and water vapor (which controls P_{H2O}). This is shown in Figure 1.8. The aerosol sample is exposed to a well-defined and controlled water supersaturation that is a function of the column's thermal gradient (dT), and the total flow rate. Particles that take up water and grow considerably are detected by an OPC at the bottom of the column from the scattered laser light signal. The OPC is calibrated to record particles with optical diameters >1 μm, which corresponds to particles that have activated to form cloud drops, and are counted as CCN. The CCNc records the CCN concentration every second. The aerosol flow rate is ~15.0 cubic centimeters per minute (ccm) and the sheath flow is adjusted to produce a total flow of 100.0 ccm.

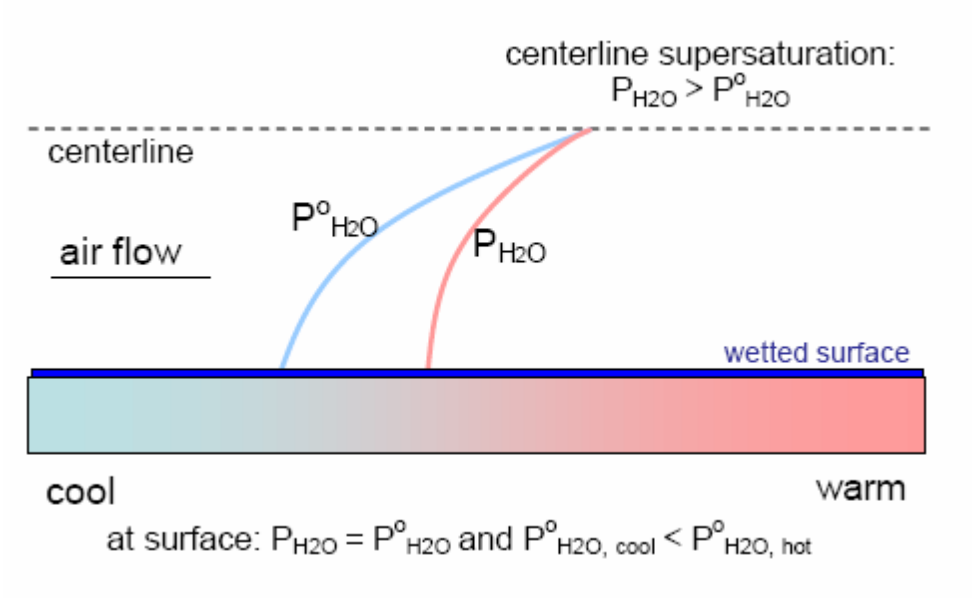

Figure 1.8. Schematic demonstrating the development of a constant water supersaturation in the CCNc. (Figure courtesy of Gregory Roberts.)

The supersaturation of the CCNc is a function of the thermal gradient (dT) and is calibrated using an atomized solution of 1.0 g/L ammonium sulfate (Sigma, 99.999%) to determine the activation diameter as a function of column dT. Thermodynamic data from the

Aerosol Inorganics Model (AIM) [*Wexler and Clegg*, 2002] and Köhler theory are used to determine the critical supersaturation (S_c) of the ammonium sulfate activation diameters. A linear fit of S_c versus column dT is then generated, usually with $R^2 > 0.995$. Typical ranges of column dT of 2.0-15.0 °C generates a supersaturations of ~ 0.08 -1.0%. Recently, there are two modes of CCNc operation. The first mode is performed using one supersaturation only, hereby referred to as static mode and is used in Chapters 2, 3, and 5. The second CCNc mode measures CCN by scanning supersaturation from ~0.1 – 1% continuously every 10 minutes, resulting in CCN spectra that give CCN concentration as a function of supersaturation, hereby referred to as scanning mode and is used in Chapter 4. While the static method yields insightful information, it is only for one supersaturation. The scanning method measures a range of supersaturations, allowing insights into CCN activity over a much larger range of particle sizes and chemical sensitivities.

1.3.3.1 CCN data analysis

To summarize the hygroscopicity measurements made with the CCNc, the CCN activation diameter (D_{act}) of atmospheric aerosols is estimated using measured size distributions, total CN, and CCN concentrations from

$$1-\frac{CCN}{CN}=\frac{\int_{D_o}^{D_{act}} n(D)dD}{N_{total}} \qquad (1.14)$$

where N_{total} is the cumulative concentration obtained by integrating the observed size distribution of $n(D)$ obtained from the SMPS measurements, D is the electric mobility diameter selected by the SMPS and D_o the smallest size measured by the SMPS (~11 nm). The CCN/CN ratio represents the fraction of the CCN-active aerosol (fCCN). Eqn. (1.12) assumes that all chemical compositions are internally mixed (i.e. homogeneous particle composition)

[*Furutani et al.*, 2008]. In the estimation of D_{act}, contributions from particles larger than the range of the SMPS (upper range = 600 nm) are not considered and are usually minimal.

Typical ambient data sets with static mode CCN data use hourly averages of CCN and CPC data to calculate fCCN, which is then used to calculate the hygroscopicity parameter, κ. For the scanning mode CCN data, the CCN and CPC data are filtered to eliminate any instrumental noise from the data and the instantaneous fCCN value is calculated every second and used to determine the instantaneous activation diameter from the cumulative SMPS size distribution as mentioned previously. Hygroscopicity parameter, κ is calculated from the instantaneous estimated activation diameter and the corresponding CCNc supersaturation values. Due to the high volume of data from the scanning mode, CCN concentrations and hygroscopicity parameter κ are binned by supersaturation. κ conveys the particle chemistry through hygroscopicity, allowing comparison with ATOFMS data to gain insights into the effect of particle composition on hygroscopicity.

1.4 Aerosol particle chemistry and cloud formation

1.4.1 Effect of particle composition on CCN activity

Aerosol particles can change the number concentration and size of droplets in a cloud, therefore affecting the radiative properties, precipitation and lifetime of the cloud [*Cess et al.*, 1997; *Finlayson-Pitts and Pitts*, 2000; *Lohmann and Feichter*, 2005; *Twomey*, 1974]. Soluble inorganic compounds, mainly a few inorganic salts, are relatively well understood in terms of their hygroscopic properties [*Ansari and Pandis*, 2000; *Clegg et al.*, 1998; *Heintzenberg*, 1989]. Insoluble inorganic compounds can also be important, especially for mineral dust particles [*McFiggans et al.*, 2006]. In general it has been shown that particles that are more hygroscopic are associated with sulfates and nitrates, where less hygroscopic particles are more associated with carbon [*Zhang et al.*, 1993]. On average, ~25-35% less water is

associated with inorganic particles mixed with organics [*Saxena et al.*, 1995]. WSOC is also very important, as an understanding of organic partitioning in cloud droplets is of the utmost importance to understanding their effect on CCN activation [*Facchini et al.*, 1999; *Jacobson et al.*, 2000; *Kiss et al.*, 2001; *Maria et al.*, 2003].

Long-chain organics ($>C_5$) with one or more polar functional groups can act as surfactants in aqueous aerosols, thereby forming a coating/film over the surface [*Finlayson-Pitts and Pitts*, 2000]. Organic films on particles are important because they can reduce the particle evaporation rate, inhibit transport of water and other trace gases into the droplet, reduce the efficiency by which the particle is scavenged by larger cloud and rain droplets and may therefore increase the lifetime of these particles in the atmosphere [*Gill et al.*, 1983; *Toossi and Novakov*, 1985]. However, depending on the nature of the organics, there can also be water associated with them as well, most likely the more oxidized and hydrophilic organics [*Saxena et al.*, 1995]. Surface-active organics present at the air-water interface, can reduce the Kelvin effect and induce CCN activation at lower supersaturations [*Finlayson-Pitts and Pitts*, 2000]. Surfactants have been shown to both enhance water uptake or did not alter activation of inorganic salts [*Cruz and Pandis*, 1998; *Kotzick et al.*, 1997; *Weingartner et al.*, 1997]. If the organics dissolve, they will contribute to the Raoult effect. Dissolution of organics in particles may lead to modified Köhler curves that have two maxima instead of one [*Shulman*, 1996]. In these modified cases, particles can become partially activated [*Shulman*, 1996], and therefore have metastable sizes that may behave in a very complex and poorly understood manner.

Further, as these films compress, the accommodation coefficient, or the fraction of collisions that result in uptake of gas by the condensed phase, for water and ammonia decreases [*Rubel and Gentry*, 1985]. The nature of the surface-active organics is also very important, as straight-chain compounds have been shown to decrease uptake, while branched molecules have not [*Daeumer et al.*, 1992; *McNeill et al.*, 2006; *Thornton and Abbatt*, 2005;

Xiong et al., 1998]. In general, urban organic particles are hydrophobic and inhibit water uptake while non-urban organic particles are hydrophilic and have increased water uptake [*Saxena et al.*, 1995]. Non-urban organic particles tend to be more hygroscopic due to the formation of smaller, more oxidized and water-soluble organics during long-range transport to the non-urban regions [*Saxena et al.*, 1995], but could also be due to the chemical nature of local biogenic emissions. Due to the complexity of mixed inorganic/organic aerosols and water uptake, more study is needed.

Field experiments have shown that particles < 100 nm in diameter, though highly dependent on location, are typically dominated by organic material and correlated with combustion sources [*Allan et al.*, 2003a]. The 40-200 nm threshold size for particle activation is highly complex. For particle sizes where the Aitken and accumulation modes overlap, external mixtures of low hygroscopicity hydrocarbon particles and oxygenated organic compounds mixed with inorganic compounds are likely [*McFiggans et al.*, 2006]. Most particles larger than ~200 nm have a fair amount of soluble material that activate under typical atmospheric supersaturations. Sizes more crucial to determining cloud droplet number are within the range of important contributions from both the Aitken and accumulation modes, ~100 nm [*McFiggans et al.*, 2006]; therefore it is necessary to know the aerosol size distribution in both of these modes to reasonably describe the activation behavior [*Martinsson et al.*, 1999]. Therefore, to predict CCN activation, the size-resolved chemistry and mixing state of particles ~40-200 nm is needed. Currently, no single technique is capable of providing this information.

1.4.2 Methods of comparing CCN and ambient aerosol composition

1.4.2.1 Offline bulk composition measurements

To use Köhler theory, such as Eqn. 1.6, chemical composition must be "converted" into concentration of molecules dissolved in cloud droplets, total insoluble mass and

concentration of limited/slightly soluble species [*McFiggans et al.*, 2006]. As previously mentioned, soluble inorganic components are relatively well understood in terms of their hygroscopic properties. However, the insoluble inorganic fraction (i.e. mineral dust) can also be important; and while many different measurements are available to determine the insoluble components, this is typically difficult to convert into total insoluble mass [*McFiggans et al.*, 2006].

Organic matter is typically measured with thermal techniques that report organic carbon (OC) and elemental carbon (EC)/black carbon (BC) in terms of carbon mass [*Jacobson et al.*, 2000; *Liousse et al.*, 1996; *Putaud et al.*, 2004] and gas chromatography/liquid chromatography with mass spectrometry (GC/MS, LC/MS) for molecular level indentification [*Engling et al.*, 2006a; *Gao et al.*, 2003; *Gorin et al.*, 2006; *Puxbaum et al.*, 2007; *Sullivan et al.*, 2008]. The conversion of carbon mass to aerosol mass is challenging without knowing the main chemical structure of the carbon [*Russell*, 2003; *Turpin and Lim*, 2001]. Additionally, BC, typically assumed insoluble, has been shown to be efficiently extracted with water [*Mayol Bracero et al.*, 2002; *Yu et al.*, 2004]. Molecular level identification and analysis is the conventional goal of aerosol organic analysis [*Carvalho et al.*, 2003; *Falkovich et al.*, 2005; *Graham et al.*, 2002; *Ion et al.*, 2005; *Pashynska et al.*, 2002; *Schkolnik et al.*, 2005], but only account for a small fraction of the total aerosol. Bulk sampling techniques used for such analyses have limited, if any size-segregation, making comparison with cloud activation properties unsuitable [*Carvalho et al.*, 2003; *Falkovich et al.*, 2005; *Matta et al.*, 2003; *Putaud et al.*, 2004]. Functional group analytical techniques analyze different types of chemical structures, while providing little or no information on the individual molecules [*Decesari et al.*, 2000; *Maria*, 2002]. Coupling functional group methods to solubility extraction-classification and other techniques provides a more comprehensive description of OC and is able to account for up to 90% of WSOC [*Decesari et al.*, 2001; *Varga et al.*, 2001].

Overall, offline bulk techniques can give information on both inorganic and organic chemical composition that can be clearly used by cloud models; however, there have only been a few studies that have presented a wide-ranging description of the chemical composition of different aerosol types as a function of size [*Cabada et al.*, 2004; *Chan et al.*, 1999; *Chio et al.*, 2004; *Maria et al.*, 2003; *Pakkanen et al.*, 2001; *Putaud*, 2000; *Sardar et al.*, 2005; *Sellegri et al.*, 2003; *Temesi et al.*, 2001; *Zappoli et al.*, 1999]. However, due to the nature of the method, there is limited information on highly resolved size chemistry and no determination of particle mixing state.

1.4.2.2 Online composition measurements

There are three main types of online methods that yield chemical composition of atmospheric aerosol particles: (1) single particle laser-based systems [*Noble and Prather*, 2000; *Sullivan and Prather*, 2005], (2) mass loadings by thermal volatilization [*Jayne et al.*, 2000; *Voisin et al.*, 2003; *Williams et al.*, 2006] and (3) liquid chromatography systems [*Orsini et al.*, 2003].

The first technique uses laser-based systems, such as the ATOFMS described previously, to desorb and ionize single particles and obtain a mass spectral fingerprint of the particle. These systems can probe the mixing state of aerosol particles close to the activation threshold dry diameter, but currently cannot quantify the mass of individual components. Field experiments show most tropospheric particles contained both organic and inorganic material [*Lee et al.*, 2002; *Middlebrook et al.*, 1998]. Single particle measurements have distinct repercussions for warm cloud activation. If almost all particles include some ionic species, this implies that completely hydrophobic particles will be rare. Even rather small amounts of ionic material can cause activation of organic particles [*Ervens et al.*, 2004a; *Lohmann*, 2004].

The second technique, thermal desorption, is used in many different instruments. The first main instrument that uses this technique is Aerodyne aerosol mass spectrometry (AMS),

uses thermal volatilization to vaporize the particles followed by electron bombardment to ionize the neutral gas provides mass loadings of non refractory submicron aerosol and obtain a mass size distribution of key species, but does not yield single particle mixing state information [*Allan et al.*, 2003b; *Jayne et al.*, 2000; *Jimenez et al.*, 2003]. AMS field experiments carried out in a broad range of environments show that sub 100 nm diameter particles are dominated by combustion-related organic material similar in signature to lubricating oil and fresh diesel exhaust, even in locations with large sulfate sources and nucleation of sulfuric acid [*Allan et al.*, 2003b; *Canagaratna et al.*, 2004; *Zhang et al.*, 2005b]. In a variety of locations in the Northern Hemisphere, the AMS has observed a single mass mode centered between 350-400 nm in diameter compromised of organic and acidified sulfate aerosol [*Allan et al.*, 2004; *Rupakheti et al.*, 2005; *Schneider et al.*, 2004; *Topping et al.*, 2004], and the mass spectral fingerprints of the organic fraction of the background continental accumulation mode aerosol are very similar to the combustion-related signature [*Zhang et al.*, 2005a]. Other instruments that use thermal desorption are the Thermal Desorption Aerosol GM/MS-FID (TAG) [*Lambe et al.*, 2010; *Williams et al.*, 2006] and thermal desorption chemical ionization mass spectrometry (TDCIMS) [*Voisin et al.*, 2003]. TAG collects aerosol into a thermal desorption cell by humidification and inertial impaction where they are then thermally desorbed and transferred into a gas chromatography (GC) column, with subsequent detection by both quadrupole mass spectrometer (MS) and a flame ionization detector (FID). TAG is capable of measuring speciated organic compounds in atmospheric aerosols with hourly time resolution [*Lambe et al.*, 2010; *Williams et al.*, 2006]. TDCIMS size classifies particles with a unipolar charger, a radial differential mobility analyzer and an electrostatic precipitator, and then analyzes then with thermal desorption and chemical ionization using an ion trap mass spectrometer. TDCIMS allows for a mass spectrum

to be collected every 0.5 s on particles below 20 nm [*Held et al.*, 2009; *Smith et al.*, 2004; *Smith and Rathbone*, 2008; *Voisin et al.*, 2003].

The third technique samples particles into a liquid and then analyses them with ion chromatography (PILS-IC). The PILS collects ambient particles into a small stream of high purity water, producing a solution containing the aerosol species. The aerosol sample is first mixed with a turbulent flow of hot supersaturated air that grow the particles into large droplets (D_p >1 mm) that are collected on an impactor. The droplets are then collected to produce a continuous flow of liquid for online analysis of the species in solution, usually analyzed by ion chromatography (IC) which can analyze aerosol composition with a time resolution of 4-30 minutes depending on the aerosol species to be analyzed [*Lee et al.*, 2003; *Orsini et al.*, 2003; *Song et al.*, 2005].

1.4.2.3 Direct comparison of ambient aerosol composition and CCN activity

CCN measurements can be used to assess agreement between measured and derived estimations of CCN concentrations or CCN spectra, known as CCN closure studies. Predicted CCN concentrations typically exceed measured CCN concentrations, and any deviation from the predicted-to-observed ratio of 1 can cause a sizeable error in model predictions of the aerosol indirect effect [*McFiggans et al.*, 2006]. Therefore continued efforts are needed in improving both the precision and accuracy of these measurements.

A large source of uncertainty in CCN closure studies is due to the unknown CCN activity of the organic fraction of the aerosol. The CCN activity of the organic aerosol fraction being included in CCN closure studies is on a case by case basis. In remote regions with a low organic fraction, organics are excluded from closure calculations [*Liu et al.*, 1996]. For locations with moderate organic contributions, consideration of the size-resolved chemical composition, such as surface tension reduction by organic aerosol is needed for closure [*Cantrell et al.*, 2001; *Dusek et al.*, 2003; *Ervens et al.*, 2010; *Gunthe et al.*, 2009; *Roberts et*

al., 2002]. In polluted or semi-urban locations, assuming insolubility of organics leads to good agreement [*Broekhuizen et al.*, 2006; *Lance et al.*, 2009; *Medina et al.*, 2007; *Quinn et al.*, 2008; *Stroud et al.*, 2007]. Inclusion of WSOC usually leads to an over prediction of CCN [*Broekhuizen et al.*, 2006; *Roberts et al.*, 2002]. Additionally, assuming an average composition of all aerosol can lead to good agreement [*Rose et al.*, 2010]. A CCN closure study employing AMS aerosol composition measurements in rural Ontario, Canada found good overall agreement when assuming organics were insoluble and assuming a surface tension of water, but during periods with high organic influence assuming surface tension reduction and inclusion of WSOC was necessary to improve agreement [*Chang et al.*, 2007]. AMS measurements have also been utilized for hygroscopicity closure studies by comparing the mole ratio of oxygen to carbon (O/C) in the organic mass fraction of the aerosol as a proxy for aerosol oxidation/processing to hygroscopicity parameter (κ) [*Chang et al.*, 2010]. By assuming the oxygenated component drives the hygroscopicity for the entire organic fraction of the aerosol, agreement was obtained with an empirically derived κ of the organic aerosol mass fraction [*Chang et al.*, 2010]. While this study did not include organosulfate or organonitrate compounds that could also contribute significantly to CCN activity, and assumed non-oxidized organics were not contributing to CCN; it is a significant step forward in CCN closure to associate distinctly derived κ values associated with the organic aerosol mass fraction types, rather than assuming only hydrophobic or hydrophilic species for the organic aerosol components [*Chang et al.*, 2010].

Single particle mixing state measurements utilize size distributions and estimated activation diameters for CCN closure, as they do not currently produce aerosol mass fractions. However, a comparison of ATOFMS single particle data with CCN measurements can allow for a relative assessment on the impact of atmospheric aerosol composition on CCN activity [*Furutani et al.*, 2008]. Field observations of simultaneous CCN and ATOFMS measurements

demonstrate changes in aerosol chemistry due to atmospheric aging play an important role in determining the CCN activity of atmospheric aerosols and that variations in aerosol chemistry must be taken into account to adequately predict the physicochemical properties of atmospheric aerosols and their CCN activity [*Furutani et al.*, 2008]. A CCN closure study combining both AMS aerosol mass fractions and ATOFMS single particle mixing state observed that size-resolved chemical composition is required to differentiate between the externally mixed non-CCN active EC and smaller organic particles from hygroscopic organic and inorganic aerosol components to obtain closure [*Cubison et al.*, 2008]. This CCN closure with inclusion of single particle mixing state as a requirement in addition to aerosol mass fraction highlights the importance of aerosol mixing state in understanding aerosol-cloud interactions. However, while CCN closure studies advance our understanding of the significance of physical and chemical properties for particle activation, they only refer to equilibrium conditions and neglect dynamic feedback processes in clouds that effect ambient supersaturations and droplet growth, which typically diminish the effects of deviations in CCN number. Continued measurements of ambient size-resolved chemical mixing state in parallel with CCN measurements are needed to continue to improve the scientific understanding of aerosol-cloud interactions and the aerosol indirect effect.

1.4.3 Major outstanding questions relating particle chemistry and cloud properties

A brief list of some major questions that remain regarding particle chemistry, cloud properties and their implications for climate:

1. How does the mixing of inorganic and organic compounds affect aerosol hygroscopicity? Are CCN active aerosols externally or internally mixed?

2. What are the physical and chemical parameters that determine the relationship between aerosol size distribution, chemical composition and CCN? What controls the number of CCN?
3. How does aerosol acidity affect hygroscopic properties?
4. What chemical compounds are present in the organic fraction? What physical properties do these compounds have?
5. How do the chemistry and size of the particles affect their ability to scatter and absorb radiation?

1.5 Objectives and synopsis

The majority of the research described here focuses on the chemistry of atmospheric aerosol particles and their related cloud properties, and attempts to address many of the questions mentioned above focusing on the effect of particle mixing state on CCN activity. Chapter 2 describes the effect of organics on the CCN activity of sea spray aerosols. During the fall of 2007 and 2008, over 300,000 acres burned in San Diego County wildfires. Chapter 3 explores the resulting particle chemistry, CCN activity and estimated hygroscopicity during these wildfire events. Chapter 4 investigates particle chemistry and estimated hygroscopicity of mineral dust at Owens (dry) Lake, east of the Sierra Nevada Mountain Range in California. The Cloud Indirect Forcing Experiment (CIFEX) took place to study the influence of aerosols on cloud properties at Trinidad Head, a coastal site in northern California representing clean marine air with periodic long-range transport. Chapters 5 & 6 explore particle chemistry, mixing state, optical properties and estimated hygroscopicity during CIFEX.

1.6 Acknowledgments

I would like to thank Melanie Zauscher and Lindsay Hatch for their help editing this chapter.

1.7 References

Albrecht, B.A., Aerosols, Cloud Microphysics, and Fractional Cloudiness, *Science, 245*, 1227-1230, 1989.

Allan, J.D., A.E. Delia, H. Coe, K.N. Bower, M.R. Alfarra, J.L. Jimenez, A.M. Middlebrook, F. Drewnick, T.B. Onasch, M. Canagaratna, J.T. Jayne, and D.R. Worsnop, A generalised method for extraction of chemically resolved mass spectra from aerodyne aerosol mass spectrometer data, *J. Atmos. Sci.*, *35*, 909-922, 2004.

Allan, J.D., J.L. Jimenenez, P.I. Willams, M.R. Alfarra, K.N. Bower, J.T. Jayne, H. Coe, and D.R. Worsnop, Quantitative sampling using an Aerodyne aerosol mass spectrometer, 1. Techniques of data interpretation and error analysis, *Journal of Geophysical Research*, *108* (4283), doi:10.1029/2002JD002358, 2003a.

Allan, J.D., J.L. Jimenez, P.I. Willams, M.R. Alfarra, K.N. Bower, J.T. Jayne, H. Coe, and D.R. Worsnop, Quantitative sampling using an Aerodyne aerosol mass spectrometer, 1. Techniques of data interpretation and error analysis, *Journal of Geophysical Research*, *108* (4283), doi:10.1029/2002JD002358, 2003b.

Andreae, M.O., Soot Carbon and Excess Fine Potassium: Long-Range Transport of Combustion-Derived Aerosols, *Science*, *220* (4602), 1148-1151, 1983.

Andreae, M.O., R.J. Charlson, F. Bruynseels, H. Storms, R. Van Grieken, and W. Maenhaut, Internal mixture of sea salt, silicates, and excess sulfate in marine aerosols, *Science*, *232* (4758), 1620-1623, 1986.

Ansari, A.S., and S.N. Pandis, Water absorption by secondar organic aerosol and its effect on inorganic aerosol behavior, *Environmental Science and Technology*, *34* (1), 71-77, 2000.

Ault, A.P., C. Gaston, Y. Wang, G. Dominguez, M.H. Thiemens, and K.A. Prather, Characterization of the Single Particle Mixing State of Individual Ship Plume Events Measured at the Port of Los Angeles, *Environmental Science and Technology*, *44* (6), 1954-1961, 2010.

Bassett, M.E., and J.H. Seinfeld, Atmospheric Equilibrium-Model of Sulfate and Nitrate Aerosols 2. Particle-Size Analysis, *Atmospheric Environment*, *18* (6), 1163-1170, 1984.

Bhave, P.V., J.O. Allen, B.D. Morrical, D.P. Fergenson, G.R. Cass, and K.A. Prather, A field-based approach for determining ATOFMS instrument sensitivities to ammonium and nitrate, *Environmental Science and Technology*, *36* (22), 4868-4879, 2002.

Broekhuizen, K., R.Y.-W. Chang, W.R. Leaitch, S.-M. Li, and J.P.D. Abbatt, Closure between measured and modeled cloud condensation nuclei (CCN) using size-resolved aerosol compositions in downtown Toronto, *Atmospheric Chemistry and Physics*, *6*, 2513-2524, 2006.

Cabada, J.C., S. Rees, S. Takahama, A. Khlystov, S.N. Pandis, C.I. Davidson, and A.L. Robinson, Mass size distributions and size resolved chemical composition of fine particulate matter at the Pittsburg supersite, *Atmospheric Environment*, *38*, 3127-3141, 2004.

Canagaratna, M., J.T. Jayne, D.A. Ghertner, S. Herndon, Q. Shi, J.L. Jimenez, P.J. Silva, P. Williams, T. Lanni, F. Drewnick, K.L. Demerjian, C.E. Kolb, and D.R. Worsnop, Chase studies of particulate emissions from in-use New York City vehicles, *Aerosol Science and Technology*, *38*, 555-573, 2004.

Cantrell, W., G.E. Shaw, G.R. Cass, Z. Chowdhury, L.S. Hughes, K.A. Prather, S.A. Guazzotti, and K.R. Coffee, Closure between aerosol particles and cloud condensation nuclei at Kaashidhoo Climate Observatory, *Journal of Geophysical Research*, *106*, 28711-28718, 2001.

Carvalho, A., C. Pio, and C. Santos, Water-soluble hydroxylated organic compounds in German and Finnish aerosols, *Atmospheric Environment*, *37*, 1775-1783, 2003.

Cess, R.D., M.H. Zhang, G.L. Potter, V. Alekseev, H.W. Barker, S. Bony, R.A. Colman, D.A. Dazlich, A.D. Del Genio, M. Deque, M.R. Dix, V. Dymnikov, M. Esch, L.D. Fowler, J.R. Fraser, V. Galin, W.L. Gates, J.J. Hack, W.J. Ingram, J.T. Kiehl, Y. Kim, H. Le Treut, X.-Z. Liang, B.J. McAvaney, V.P. Meleshko, J.J. Morcrette, D.A. Randall, E. Roeckner, M.E. Schlesigner, P.V. Sporyshev, K.E. Taylor, B. Timbal, E.M. Volodin, W. Wang, W.C. Wang, and R.T. Wetherald, Comparison of the Seasonal Change in Cloud-Radiative Forcing from Atmospheric General Circulation Models and Satellite Observations, *Journal of Geophysical Research*, *102*, 16593-16603, 1997.

Chan, Y.C., R.W. Simpson, G.H. McTanish, P.D. Vowles, D.D. Cohen, and G.M. Bailey, Source apportionment of PM2.5 and PM10 aerosols in Brisbane (Austrailia) by receptor modelling, *Atmospheric Environment*, *33*, 3251-3268, 1999.

Chang, R.Y.-W., P.S.K. Liu, W.R. Leaitch, and J.P.D. Abbatt, Comparison between measured and predicted CCN concentrations at Egbert, Ontario: Focus on the organic aerosol fraction at a semi-rural site, *Atmospheric Environment*, *41*, 8172-8182, 2007.

Chang, R.Y.-W., J.G. Slowik, N.C. Shantz, A. Vlasenko, J. Liggio, S.J. Sjostedt, W.R. Leaitch, and J.P.D. Abbatt, The hygroscopicity parameter (K) of ambient organic aerosol at a field site subject to biogenic and anthropogenic influences: relationship to degree of aerosol oxidation, *Atmospheric Chemistry and Physics*, *10*, 5047-5064, 2010.

Charlson, R.J., and J.H. Pilat, Climate: the influence of aerosols, *J. Appl. Meteorol.*, *8*, 3251-3268, 1969.

Chebbi, A., and P. Carlier, Carboxylic acids in the troposphere, occurence, sources and sinks: A review, *Atmospheric Environment*, *30*, 4233-4249, 1996.

Chio, C.-P., M.-T. Cheng, and C.-F. Wang, Source apportionment to PM10 in different air quality conditions for Taichung urban and coastal areas, Taiwan, *Atmospheric Environment*, *38*, 6893-6905, 2004.

Clegg, S.L., P. Brimblecombe, and A.S. Wexler, Thermodynamic model of the system H+-NH4+-SO42-NO3-H2O at tropospheric temperatures, *Journal of Physical Chemistry A*, *102*, 2137-2154, 1998.

Collins, D.R., D.R. Cocker, R.C. Flagan, and J.H. Seinfeld, The scanning DMA transfer function, *Aerosol Science and Technology*, *38* (8), 833-850, 2004.

Cruz, C.N., and S.N. Pandis, The effect of organic coatings on the cloud condensation nuclei activation of inorganic atmospheric aerosol, *Journal of Geophysical Research*, *103* (D11), 13,111-13,123, 1998.

Cubison, M.J., B. Ervens, G. Feingold, K.S. Docherty, I.M. Ulbrich, L. Shields, P. K., S. Hering, and J.L. Jimenenez, The influence of chemical composition and mixing state of Los Angeles urban aerosol on CCN number and cloud properties, *Atmospheric Chemistry and Physics*, *8*, 5649-5667, 2008.

Curry, J.A., and P.J. Webster, *Thermodynamics of Atmospheres and Oceans*, Academic Press, New York, 1999.

Daeumer, B., R. Niessner, and Klockow, Laboratory Studies of the Influence of Thin Organic Films on the Neutralization Reaction of H2SO4 Aerosol with Ammonia, *Journal of Aerosol Science*, *23*, 315-325, 1992.

DeCarlo, P.F., J.G. Slowik, D.R. Worsnop, P. Davidovits, and J.L. Jimenenez, Particle Morphology and Density Characterization by Combined Mobility and Aerodynamic Diameter Measurements. Part 1: Theory, *Aerosol Science and Technology*, *38*, 1185-1205, 2005.

Decesari, S., M.C. Facchini, S. Fuzzi, and E. Tagliavini, Characterization of water-soluble organic compounds in atmospheric aerosol: A new approach, *Journal of Geophysical Research*, *105*, 1481-1489, 2000.

Decesari, S., M.C. Facchini, E. Matta, F. Lettini, M. Mircea, S. Fuzzi, E. Tagliavini, and J.P. Putaud, Chemical features and seasonal variation of fine aerosol water-soluble organic compounds in the Po Valley, *Atmospheric Environment*, *35*, 3691-3699, 2001.

Dusek, U., D.S. Covert, A. Wiedensohler, C. Neususess, D. Weise, and W. Cantrell, Cloud condensation nuclei spectra derived from size distributions and hygroscopic properties of the aerosol in coastal south-west Portugal during ACE-2, *Tellus Series B - Chemical and Physical Meteorology*, *55*, 35-53, 2003.

Engling, G., C.M. Carrico, S.M. Kreidenweis, J.L. Collett, D.E. Day, W.C. Malm, E. Lincoln, W.M. Hao, Y. Iinuma, and H. Herrmann, Determination of levoglucosan in biomass combustion aerosol by high-performance anion-exchange chromatography with pluse amperometric detection, *Atmospheric Environment*, *40*, S299-311, 2006a.

Engling, G., C.M. Carrico, S.M. Kreidenweis, J.L. Collett, D.E. Day, W.C. Malm, E. Lincoln, W.M. Hao, Y. Iinuma, and H. Herrmann, Determination of levoglucosan in biomass combustion aerosol by high-performance anion-exchange chromatography with pulsed amperometric detection, *Atmospheric Environment*, *S2*, 299-311, 2006b.

Ervens, B., M.J. Cubison, E. Andrews, G. Feingold, J.A. Ogren, J.L. Jimenez, P.K. Quinn, T.S. Bates, J. Wang, Q. Zhang, H. Coe, M. Flynn, and J.D. Allan, CCN predictions using simplified assumptions of organic aerosol composition and mixing state: a synthesis from six different locations, *Atmospheric Chemistry and Physics*, *10*, 4795-4807, 2010.

Ervens, B., G. Feingold, S.L. Clegg, and S.M. Kreidenweis, A modeling study of aqueous production of dicarboxylic acids: 2. Implications for cloud microphysics, *Journal of Geophysical Research*, *109* (D15206), doi:10.1029/2004JD004575, 2004a.

Ervens, B., G. Feingold, G.J. Frost, and S.M. Kreidenweis, A modeling study of aqueous production of dicarboxylic acids: 1. Chemical pathways and speciated organic mass production, *Journal of Geophysical Research*, *109* (D15205), doi:10.1029/2003JD004387, 2004b.

Fabbri, D., L. Marynowski, M.I. Fabianska, M. Zaton, and B.R.T. Simoneit, Levoglucosan and Other Cellulose Markers in Pyrolysates of Miocene Lignites: Geochemical and Environmental Implications, *Environmental Science and Technology*, *42*, 2957-2963, 2008.

Facchini, M.C., M. Mircea, S. Fuzzi, and R.J. Charlson, Cloud albedo enhancement by surface-active organic solutes in growing droplets, *Nature*, *401*, 257-259, 1999.

Falkovich, A.H., E.R. Graber, G. Schkolnik, Y. Rudich, W. Maenhaut, and P. Artaxo, Low molecular weight organic acids in aerosol particles from Rondonia, Brazil, during the biomass-burning, transition and wet periods, *Atmospheric Chemistry and Physics*, *5*, 781-797, 2005.

Feingold, G., Modeling of the first indirect effectL Analysis of measurement requirements, *Geophysical Research Letters*, *30* (1997), doi:10.1029/2003GL017967, 2003.

Fine, P.M., G.R. Cass, and B.R.T. Simoneit, Chemical Characterization of Fine Particle Emissions from the Fireplace Combustion of Wood Types Grown in the Midwestern and Western United States, *Environmental Engineering Science*, *21* (3), 387-409, 2004.

Finlayson-Pitts, B.J., and J.N. Pitts, *Chemistry of the Upper and Lower Atmosphere*, Academic Press, New York, 2000.

Flagan, R.C., *Aerosol Measurement*, Wiley-InterScience, Inc., Hoboken, New Jersey, 2001.

Furutani, H.F., M. Dall'osto, G.C. Roberts, and K.A. Prather, Assessment of the relative importance of atmospheric aging on CCN activity derived from field observations, *Atmospheric Environment*, *42*, 3130-3142, 2008.

Gao, S., D.A. Hegg, P.V. Hobbs, T.W. Krirchstetter, B.I. Magi, and M. Sadilek, Water-soluble organic components in aerosols associated with savvana fires in southern Africa: Identification, evolution, and distribution, *Journal of Geophysical Research*, *108* (D13), 8491, doi:10.1029/2002JD002324, 2003.

Gard, E., J.E. Mayer, B.D. Morrical, T. Dienes, D.P. Fergenson, and K.A. Prather, Real-Time Analysis of Individual Atmospheric Aerosol Particles: Design and Performance of a Portable ATOFMS, *Analytical Chemistry*, *69*, 4083-4091, 1997.

Gill, P.S., T.E. Graedel, and C.J. Weschler, Organic Films on Atmospheric Aerosol Particles, Fog Droplets, Cloud Droplets, Raindrops, and Snowflakes, *Reviews of Geophysics and Space Physics*, *21* (4), 903-920, 1983.

Gorin, C.A., J.L. Collett, and P. Herckes, Wood smoke contribution to winter aerosol in Fresno, CA, *J. Air Waste Manage. Assoc.*, *56*, 1584-1590, 2006.

Graham, B., O.L. Mayol Bracero, P. Guyon, G. Roberts, S. Decesari, M.C. Facchini, P. Artaxo, W. Maenhaut, P. Koll, and M.O. Andreae, Water-soluble organic compounds in biomass burning aerosols over Amazonia- 1. Characterization by NMR and GC-MS, *Journal of Geophysical Research*, *107* (8047), doi:10.1029/2001JD000336, 2002.

Gray, H.A., G.R. Cass, J.J. Huntzicker, E.K. Heyerdahl, and J.A. Rau, Characteristics of Atmospheric Organic and Elemental Carbon Particle Concentrations in Los Angeles, *Environmental Science and Technology*, *20*, 580-589, 1986.

Grosjean, D., In Situ, Organic Aerosol Formation during a Smog Episode: Estimated Production and Chemical Functionality, *Atmospheric Environment*, *26A*, 953-963, 1992.

Grosjean, D., and J.H. Seinfeld, Parameterization of the Formation Potential of Secondary Organic Aerosols, *Atmospheric Environment*, *23*, 1733-1747, 1989.

Gross, D.S., M.E. Galli, P.J. Silva, and K.A. Prather, Relative sensitivity factors for alkali metal and ammonium cations in single particle aerosol time-of-flight mass spectra, *Analytical Chemistry*, *72* (2), 416-422, 2000.

Gunthe, S.S., S.M. King, D. Rose, Q. Chen, P. Roldin, D.K. Farmer, J.L. Jimenenez, P. Artaxo, M.O. Andreae, S.T. Martin, and U. Poeschl, Cloud condensation nuclei in pristine tropical rainforest air of Amazonia: size-resolved measurements and modeling of atmospheric aerosol composition and CCN activity, *Atmospheric Chemistry and Physics*, *9* (19), 7551-7575, 2009.

Hamilton, J.F., P.J. Webb, A.C. Lewis, J.R. Hopkins, S. Smith, and P. Davy, Partially oxidised organic components in urban aerosols using GCXGC-TOF/MS, *Atmospheric Chemistry and Physics*, *4*, 1279-1290, 2004.

Haywood, J.M., and O. Boucher, Estimates of the direct and indirect radiative forcing due to tropospheric aerosols: A review, *Reviews of Geophysics*, *38*, 513-543, 2000.

Heintzenberg, J., Fine particles in the global troposphere, A review, *Tellus Series B - Chemical and Physical Meteorology*, *41*, 149-160, 1989.

Held, A., G.J. Rathbone, and J.N. Smith, A Thermal Desorption Chemical Ionization Ion Trap Mass Spectrometer for the Chemical Characterization of Ultrafine Aerosol Particles, *Aerosol Science and Technology*, *43* (3), 264-272, 2009.

Hering, S.V., M.R. Stolzenburg, F.R. Quant, D.R. Oberreit, and P.B. Keady, A Laminar-Flow, Water-Based Condensation Particle Counter (WCPC), *Aerosol Science and Technology*, *39* (7), 659-672, 2005.

Hildemann, L.M., D.B. Klinedinst, G.A. Klouda, L.A. Currie, and G.R. Cass, Sources of Urban Contemporary Carbon Aerosol, *Environmental Science and Technology*, *28*, 1565-1576, 1994a.

Hildemann, L.M., M.A. Mazurek, G.R. Cass, and B.R.T. Simoneit, Seasonal Trends in Los Angles Ambient Organic Aerosol Observed by High-Resolution Gas Chromatography, *Aerosol Science and Technology*, *20*, 303-317, 1994b.

Hinds, W.C., *Aerosols Technology: Properties, Behavior, and Measurements of Airborne Particles*, John Wiley & Sons, New York, 1999.

Holecek, J.C., M.T. Spencer, and K.A. Prather, Analysis of rainwater samples: Comparison of single particle residues with ambient particle chemistry from the northeast Pacific and Indian oceans, *Journal of Geophysical Research*, *112* (D22S24), doi:10.1029/2006JD008269, 2007.

Hoppel, W.A., J.W. Fitzgerald, G.M. Frick, R.E. Larson, and E.J. Mack, Aerosol Size Distributions and Optical Properties Found in the Marine Boundary Layer Over the Atlantic Ocean, *Journal of Geophysical Research*, *95* (D4), 3659-3686, 1990.

Ion, A.C., R. Vermeylen, I. Kourtchev, J. Cafmeyer, X. Chi, A. Gelencser, W. Maenhaut, and M. Claeys, Polar organic compounds in rural PM2.5 aerosols from K-puszta, Hungary, during a 2003 summer field campaign: sources and diurnal variations, *Atmospheric Chemistry and Physics*, *5*, 1805-1814, 2005.

Jacobson, M.C., H.C. Hansson, K.J. Noone, and R.J. Charlson, Organic atmospheric aerosols: Review and state of the science, *Reviews of Geophysics*, *38*, 267-294, 2000.

Jayne, J.T., D.C. Leard, X.F. Zhang, P. Davidovits, K.A. Smith, C.E. Kolb, and D.R. Worsnop, Development of an aerosol mass spectrometer for size and composition analysis of submicron particles, *Aerosol Science and Technology*, *33*, 49-70, 2000.

Jimenez, J.L., J.T. Jayne, Q. Shi, C.E. Kolb, D.R. Worsnop, I. Yourshaw, J.H. Seinfeld, R.C. Flagan, X. Zhang, K.A. Smith, J. Morris, and P. Davidovits, Ambient Aerosol Sampling with an Aerosol Mass Spectrometer, *Journal of Geophysical Research*, *108* (8425), doi:10.1029/2001JD001213, 2003.

Kanakidou, M., J.H. Seinfeld, S.N. Pandis, I. Barnes, F.J. Dentener, M.C. Facchini, R. Van Dingenen, B. Ervens, A. Nenes, C.J. Nielsen, E. Swietlicki, J.P. Putaud, Y. Balkanski, S. Fuzzi, J. Horth, G.K. Moortgat, R. Winterhalter, C.E.L. Myhre, K. Tsigardis, E. Vignati, E.G. Stephanou, and W. J., Organic aerosol and global climate modelling: a review, *Atmospheric Chemistry and Physics*, *5*, 1053-1123, 2005.

Kiss, G., B. Varga, A. Gelencser, Z. Krivacsy, A. Molnar, T. Alsberg, L. Persson, H.C. Hansson, and M.C. Facchini, Characterisation of polar organic compounds in fog water, *Atmospheric Environment*, *25* (2193-2200), 2001.

Knutson, E.O., and K.T. Whitby, Aerosol classification by electric mobility: Apparatus, theory, and applications, *Journal of Aerosol Science*, *6*, 443-451, 1975.

Koehler, H., The Nucleus in and the Growth of Hygroscopic Droplets, *Trans. Farad. Soc.*, *32*, 1152-1161, 1936.

Kotzick, R., U. Panne, and R. Niessner, Changes in Condensation Properties of Ultrafine Carbon Particles Subjected to Oxidation by Ozone, *Journal of Aerosol Science*, *28*, 725-735, 1997.

Lambe, A.T., H.J. Chacon-Madrid, N.T. Nguyen, E.A. Weitkamp, N.M. Kreisberg, S.V. Hering, A.H. Goldstein, N.M. Donahue, and A.L. Robinson, Organic Aerosol Speciation: Intercomparison of Thermal Desorption Aerosol GC/MS (TAG) and Filter-Based Techniques, *Aerosol Science and Technology*, *44*, 141-151, 2010.

Lance, S., A. Nenes, C. Mazzoleni, M.K. Dubey, H. Gates, V. Varutbangkul, T.A. Rissman, S.M. Murphy, A. Sorooshian, R.C. Flagan, J.H. Seinfeld, and H. Jonsson, Cloud condensation nuclei activity, closure, and droplet growth kinetics of Houston aerosol during the Gulf of Mexico Atmospheric Composition and Climate Study (GoMACCS), *Journal of Geophysical Research*, *114* (D00F15), doi:10.1029/2008JD011699, 2009.

Lee, S.H., D.M. Murphy, D.S. Thomson, and A.M. Middlebrook, Chemical components of single particles measured with Particle Analysis by Laser Mass Spectrometry (PALMS) during the Atlanta SuperSite Project: Focus on organic/sulfate, lead, soot, and mineral particles Source, *Journal of Geophysical Research*, *107* (D1), 4003, doi:10.1029/2000JD000011, 2002.

Lee, Y.-N., R.J. Weber, Y. Ma, D. Orsini, K. Maxwell-Meier, D. Blake, S. Meinardi, G.W. Sachse, C. Harward, T.-Y. Chen, D. Thornton, F.-H. Tu, and A. Bandy, Airborne measurements of inorganic ionic components of fine aerosol particles using the particle-into-liquid sampler coupled to ion chromatography technique during ACE-Asia and TRACE-P, *Journal of Geophysical Research*, *108* (D23), 8646, doi:10.1029/2002JD003265, 2003.

Lewis, E.R., and S.E. Schwartz, *Sea salt aerosol production: mechanisms, methods, measurements and models: a critical review*, American Geophysical Union, Washington, D.C., 2004.

Li, J., M. Posfai, P.V. Hobbs, and P.R. Buseck, Individual aerosol particles from biomass burning in southern Africa: 2. Compositions and aging of inorganic particles, *Journal of Geophysical Research, 108(D13)* (8484), doi:10.1029/2002JD002310, 2003.

Liou, K.N., and S.C. Ou, The role of cloud microphysical processes in climate - an assesment from a one-dimensional perspective, *Journal of Geophysical Research, 94*, 8599-8607, 1989.

Liousse, C., E. Penner, C. Chuang, J. Walton, H. Eddleman, and H. Cachier, A global three-dimensional model study of carbonaceous aerosols, *Journal of Geophysical Research, 101*, 19,411-19,432, 1996.

Liu, P.S.K., W.R. Leaitch, C.M. Banic, S.-M. Li, D. Ngo, and W.J. Megaw, Aerosol observations at Chebogue Point during the 1993 North Atlantic Regional Experiment: relationships among cloud condensation nuclei, size distribution and chemistry, *Journal of Geophysical Research, 101*, 28971-28990, 1996.

Lohmann, U., and J. Feichter, Global indirect aerosol effects: a review, *Atmospheric Chemistry and Physics, 5*, 715-737, 2005.

Lohmann, U.B., K.; Leaitch, R.; Shantz, N.; Abbatt, J., How efficient is cloud droplet formation of organic aerosols? *Geophysical Research Letters, 31* (L05108), doi:10.1029/2003GL018999, 2004.

Maria, S.F., L.M. Russell, M.K. Gilles, and S.C.B. Myneni, Organic aerosol growth mechanisms and their climate-forcing implications, *Science, 306* (1921-1924), 2004.

Maria, S.F., L.M. Russell, B.J. Turpin, R.J. Porcja, T.L. Campos, R.J. Weber, and B.J. Huebert, Source signatures of carbon monoxide and organic functional groups in Asian Pacific Regional Aerosol Characterization Experiment (ACE-Asia) submicron aerosol types, *Journal of Geophysical Research, 108* (8637), doi:10.1029/2003JD003703, 2003.

Maria, S.F.R., L.M.; Turpin, B.J.; Porcja, R.J., FTIR measurements of functional groups and organic mass in aerosol samples over the Caribbean, *Atmospheric Environment, 36*, 5185-5196, 2002.

Martinsson, B.G., G. Frank, S.I. Cederfelt, E. Swietlicki, O.H. Berg, J.C. Zhou, K.N. Bower, C. Bradbury, W. Birmili, F. Stratmann, M. Wendisch, A. Wiedensohler, and B.A. Yuskiewicz, Source signatures of carbon monoxide and organic functional groups in Asian Pacific Regional Aerosol Characterization Experiment (ACE-Asia) submicron aerosol types, *Atmos. Res., 50*, 289-315, 1999.

Matta, E., M.C. Facchini, S. Decesari, M. Mircea, F. Cavalli, S. Fuzzi, J.P. Putaud, and A. Dell'Acqua, Mass closure on the chemical species in size-segregated atmospheric aerosol collected in an urban area of the Po Valley, Italy, *Atmospheric Chemistry and Physics, 3*, 623-637, 2003.

Mayol Bracero, O.L., P. Guyon, B. Graham, G. Roberts, M.O. Andreae, S. Decesari, M.C. Facchini, S. Fuzzi, and P. Artaxo, Water-soluble organic compounds in biomass

burning aerosols over Amazonia 2. Apportionment of the chemical composition and importance of the polyacidic fraction, *Journal of Geophysical Research*, *107* (D20), 8091, 2002.

McCormick, R., and J.H. Ludwig, Climate Modification by Atmospheric Aerosols, *Science*, *156*, 1358-1359, 1967.

McFiggans, G., P. Artaxo, U. Baltensperger, H. Coe, M.C. Facchini, G. Feingold, S. Fuzzi, M. Gysel, A. Laaksonen, U. Lohmann, T.F. Mentel, D.M. Murphy, C.D. O'Dowd, J.R. Snider, and E. Weingartner, The effect of physical and chemical aerosol properties on warm cloud droplet activation, *Atmospheric Chemistry and Physics*, *6*, 2593-2649, 2006.

McMurry, P.H., A review of atmospheric aerosol measurements, *Atmospheric Environment*, *34*, 1959-1999, 2000.

McNeill, V.F., J. Patterson, G.M. Wolfe, and J.A. Thornton, The effect of varying levels of surfactant on the reactive uptake of N2O5 to aqueous aerosol, *Atmospheric Chemistry and Physics*, *6*, 1635-1644, 2006.

Medina, J., A. Nenes, R.-E.P. Sotiropoulou, L.D. Cottrell, L.D. Ziemba, P.J. Beckman, and R.J. Griffin, Cloud condensation nuclei closure during the International Consortium for Atmospheric Research on Transport and Transformation 2004 campaign: effects of size-resolved composition, *Journal of Geophysical Research*, *112*, 2007.

Mertes, S., F. Schroder, and A. Wiedensohler, The Particle-Detection Efficiency Curve of the TSI-3010 CPC as a Function of the Temperature Difference between Saturator and Condenser, *Aerosol Science and Technology*, *23* (2), 257-261, 1995.

Middlebrook, A.M., D.M. Murphy, and D.S. Thomson, Observations of organic material in individual marine particles at Cape Grim during the First Aerosol Characterizaion Experiment (ACE1), *Journal of Geophysical Research*, *103* (D13), 16475-16483, 1998.

Mochida, M., A. Kawabata, K. Kawamura, H. Hatsushika, and K. Yamazaki, Seasonal variation and origins of dicarboxylic acids in the marine atmosphere over the western North Pacific, *Journal of Geophysical Research*, *108*, doi:10.1029/2002JD002355, 2003.

Moffet, R.C., B. De Foy, L.T. Molina, M.J. Molina, and K.A. Prather, Measurement of ambient aerosols in northern Mexico City by single particle mass spectrometry, *Atmospheric Chemistry and Physics*, *8*, 4499-4516, 2008.

Murphy, D.M., Something in the air, *Science*, *307*, 1888-1890, 2005.

Murphy, D.M., The design of single particle laser mass spectrometers, *Mass Spectrometry Reviews*, *26* (2), 150-165, 2007.

Murphy, D.M., D.J. Cziczo, K.D. Froyd, P.K. Hudson, B.M. Matthew, A.M. Middlebrook, R.E. Peltier, A.P. Sullivan, D.S. Thomson, and R.J. Weber, Single-particle mass

spectrometry of tropospheric aerosol particles, *Journal of Geophysical Research*, *111* (D23), doi:10.1029/2006JD007340, 2006.

Nenes, A., P.Y. Chuang, R.C. Flagan, and J.H. Seinfeld, A theoretical analysis of cloud condensation nucleus (CCN) instruments, *Journal of Geophysical Research*, *106* (D4), 3449-3474, 2001.

Niimura, N., K. Okada, X.B. Fan, K. Kai, K. Arao, G.Y. Shi, and S. Takahashi, Formation of Asian dust-storm particles mixed internally with sea salt in the atmosphere, *Journal of Meteorological Society of Japan*, *76* (2), 275-288, 1998.

Noble, C.A., and K.A. Prather, Real-time single particle mass spectrometry: A historical review of a quarter century of the chemical analysis of aerosols, *Mass Spectrometry Reviews*, *19* (4), 248-274, 2000.

O'Dowd, C.D., M.C. Facchini, F. Cavalli, D. Ceburnis, M. Mircea, S. Descesari, S. Fuzzi, Y. Jun Yoon, and J. Putaud, Biogenically driven organic contribution to marine aerosol, *Nature*, *431*, 676-680, 2004.

Orsini, D.A., Y. Ma, A.P. Sullivan, B. Sierau, K. Baumann, and R.J. Weber, Refinements to the particle-into-liquid sampler (PILS) for ground and airborne measurements of water soluble aerosol composition, *Atmospheric Environment*, *37*, 1243-1259, 2003.

Pakkanen, T.A., K. Loukkola, C.H. Korhonen, M. Aurela, T. Makela, R.E. Hillamo, T. Koskentalo, A. Kousa, and W. Maenhaut, Sources and chemical composition of atmospheric fine and coarse particles in the Helsinki area, *Atmospheric Environment*, *35*, 5381-5391, 2001.

Pandis, S.N., R.A. Harley, G.R. Cass, and J.H. Seinfeld, Secondary Organic Aerosol Formation and Transport, *Atmospheric Environment*, *26A*, 2269-2282, 1992.

Pashynska, V., R. Vermeylen, G. Vas, W. Maenhaut, and M. Claeys, Development of a gas chromatographic/ion trap mass spectrometic method for the determination of levoglucosan and saccharidic compounds in atmospheric aerosols: Application to urban aerosols, *J. Mass Spectr.*, *37*, 1249-1257, 2002.

Pekney, N.J., C.I. Davidson, A. Robinson, L. Zhou, P.K. Hopke, D. Eatough, and W.F. Rogge, Major Source Categories for PM2.5 in Pittsburg using PMF and UNMIX, *Aerosol Science and Technology*, *40*, 910-924, 2006.

Petters, M.D., C.M. Carrico, S.M. Kreidenweis, A.J. Prenni, P.J. DeMott, J.L. Collett, and H. Moosmueller, Cloud Condensation Nuclei Activity of Biomass Burning Aerosol, *Journal of Geophysical Research*, *114* (D22205), doi:10.1029/2009JD012353, 2009.

Petters, M.D., and S.M. Kreidenweis, A single parameter representation of hygroscopic growth and cloud condensation nucleus activity, *Atmospheric Chemistry and Physics*, *7* (8), 1961-1971, 2007.

Pratt, K.A., C.H. Twohy, S.M. Murphy, R.C. Moffet, A.J. Heymsfield, C.J. Gaston, P.J. DeMott, P.R. Field, T.R. Henn, D.C. Rogers, M.K. Gilles, J.H. Seinfeld, and K.A.

Prather, Observation of playa salts as nuclei in orographic wave clouds, *Journal of Geophysical Research*, *115* (D15301), doi:10.1029/2009JD013606, 2010.

Pruppacher, H.R., and J.D. Klett, *Microphysics of Clouds and Precipitation*, Kluwer Academic Publishers, Norwell, MA, 1997.

Putaud, J.-P.V.D., R.; Mangoni, M.; Virkkula, A.; Raes, F.; Maring, H.; Prospero, J.M.; Switetlicki, E.; Berg, O.H.; Hillamo, R.; Makela, T., Chemical mass closure and assesment of the origin of the submicron aerosol in the marine boundary layer and the free troposphere at Tenerife during ACE-2, *Tellus*, *52B*, 141-168, 2000.

Putaud, J.P., R. Van Dingenen, A. Dell'Acqua, F. Raes, E. Matta, S. Decesari, M.C. Facchini, and S. Fuzzi, Size-segregated aerosol mass closure and chemical composition in Monte Cimone(I) during MINATROC, *Atmospheric Chemistry and Physics*, *4*, 889-902, 2004.

Puxbaum, H., A. Caseiro, A. Sanchez-Ochoa, A. Kasper-Giebl, M. Claeys, A. Gelencser, M. Legrand, S. Preunkert, and C. Pio, Levoglucosan levels at background sites in Europe aerosol background, *Journal of Geophysical Research*, *112* (D23S05), doi:10.1029/2006JD008114, 2007.

Qin, X., and K.A. Prather, Impact of biomass emissions on particle chemistry during the California Regional Particulate Air Quality Study, *International Journal of Mass Spectrometry*, *258*, 142-150, 2006.

Quinn, P.K., T.S. Bates, D.J. Coffman, and D.S. Covert, Influence of particle size and chemistry on the cloud nucleating properties of aerosols, *Atmospheric Chemistry and Physics*, *8*, 1029-1042, 2008.

Ramaswamy, V., O. Boucher, J. Haigh, D. Hauglustaine, J. Haywood, G. Myhre, T. Nakajima, G.Y. Shi, and S. Solomon, Climate Change 2001: The Scientific Basis, Contribution of working group I to the Third Assessment Report of the Intergovernmental Panel on Climate Change, 2001.

Rebotier, T.P., and K.A. Prather, Aerosol time-of-flight mass spectrometry data analysis: A benchmark of clustering algorithms., *Analytica Chimica Acta*, *585* (1), 38-54, 2007.

Reid, J.S., R. Koppmann, T.F. Eck, and D.P. Eleuterio, A review of biomass burning emissions part II: intensive physical properties of biomass burning particles, *Atmospheric Chemistry and Physics*, *5*, 799-825, 2005.

Rissman, T.A., A. Nenes, and J.H. Seinfeld, Chemical amplification (or dampening) of the Twomey effect: Conditions derived from droplet activation theory, *J. Atmos. Sci.*, *61*, 919-930, 2004.

Roberts, G.C., P. Artaxo, J. Zhou, E. Swietlicki, and M.O. Andreae, Sensitivity of CCN spectra on chemical and physical properties of aerosol: A case study from the Amazon Basin, *Journal of Geophysical Research*, *107* (D20), 8070, doi:10.1029/2001JD000583, 2002.

Roberts, G.C., and A. Nenes, A Continuous-Flow Streamwise Thermal-Gradient CCN Chamber for Atmospheric Measurements, *Aerosol Science and Technology*, *39*, 206-221, 2005.

Rose, D., A. Nowak, P. Achtert, A. Wiedensohler, M. Hu, M. Shao, Y. Zhang, M.O. Andreae, and U. Poeschl, Cloud condensation nuclei in polluted air and biomass burning smoke near the mega-city Guangzhou, China - Part 1: Size-resolved measurements and implications for the modeling of aerosol particle hygroscopicity and CCN activity, *Atmospheric Chemistry and Physics*, *10*, 3365-3383, 2010.

Rubel, G.O., and J.W. Gentry, Measurement of Water and Ammonia Accommodation Coefficient at Surfaces with Adsorbed Monolayers of Hexadecanol, *Journal of Aerosol Science*, *16*, 571-574, 1985.

Rupakheti, M.W., R. Leaitch, U. Lohmann, K. Hayden, P. Brickell, G. Lu, S.-M. Li, D. Toom-Sauntry, J.W. Bottenheim, J.R. Brook, R. Vet, J.T. Jayne, and D.R. Worsnop, An intensive study of the size and composition of submicron atmospheric aerosols at a rural site in Ontario, Canada, *Aerosol Science and Technology*, *39*, 722-736, 2005.

Russell, L.M., Aerosol organic-mass-to-organic-carbon ratio measurements, *Abstracts of Papers of the American Chemical Society*, *225*, U817-U818, 2003.

Sardar, S.B., P.M. Fine, and C. Sioutas, Seasonal and spatial variability of the size-resolved chemical composition of particulate matter (PM10) in the Los Angeles Basin, *Journal of Geophysical Research*, *110* (D07S08), doi:10.1029/2004JD004627, 2005.

Saxena, P., L.M. Hildemann, P.H. McMurry, and J.H. Seinfeld, Organics Alter Hygroscopic Behavior of Atmospheric Particles, *Journal of Geophysical Research*, *100*, 18755-18770, 1995.

Saxena, P.H., L.M., Water-Soluble Organics in Atmospheric Particles: A Critical Review of the Literature and Application to Thermodynamics to Identify Candidate Compounds, *Journal of Atmospheric Chemistry*, *24*, 57-109, 1996.

Schkolnik, G., A.H. Falkovich, Y. Rudich, W. Maenhaut, and P. Artaxo, New analytical method for the determination of levoglucosan, polyhydroxy compounds, and 2-methylerythritol and its application to smoke and rainwater samples, *Environmental Science and Technology*, *39*, 2744-2752, 2005.

Schneider, J., S. Borrmann, A.G. Wollny, M. Blasner, N. Mihalopoulos, K. Oikonomou, J. Sciare, A. Teller, Z. Levin, and D.R. Worsnop, Online mass spectrometric aerosol measurements during the MINOS campaign (Crete, August 2001), *Atmospheric Chemistry and Physics*, *4*, 65-80, 2004.

Seinfeld, J.H., and S.N. Pandis, *Atmospheric Chemistry and Physics*, John Wiley & Sons, New York, 1998.

Sellegri, K., P. Laj, F. Peron, R. Dupuy, M. Legrand, S. Preunkert, J.P. Putaud, H. Cachier, and G. Ghermandi, Mass balance of free tropospheric aerosol at the Puy de

D(o)oververcapme (France) in winter, *Journal of Geophysical Research*, *108* (4333), doi:10.1029/2002JD002747, 2003.

Sempere, R., and K. Kawamura, Low Molecular Weight Dicarboxylic Acids and Related Polar Compounds in the Remote Marine Rain Samples Collected from Western Pacific, *Atmospheric Environment*, *30*, 1609-1619, 1996.

Shulman, M.L.J., M. C.; Carlson, R. J.; Synovec, R. E.; Young, T. E., Dissolution behavior and surface tension effects of organic compounds in nucleating cloud droplets, *Geophysical Research Letters*, *23* (3), 277-280, 1996.

Silva, P.J., Source Profiling and Apportionment of Airborne Particles: A New Approach Using Aerosol Time-of-Flight Mass Spectrometry, University of California Riverside, 2000.

Silva, P.J., D. Liu, C.A. Noble, and K.A. Prather, Size and Chemical Characterization of Individual Particles Resulting from Biomass Burning of Local Southern California Species, *Environmental Science and Technology*, *33* (18), 3068-3076, 1999.

Smith, J.N., K.F. Moore, P.H. McMurry, and F.L. Eisele, Atmospheric Measurements of Sub-20 nm Diameter Particle Chemical Composition by Thermal Desorption Chemical Ionization Mass Spectrometry, *Aerosol Science and Technology*, *38*, 100-110, 2004.

Smith, J.N., and G.J. Rathbone, Carboxylic acid characterization in nanoparticles by thermal desorption chemical ionization mass spectrometry, *International Journal of Mass Spectrometry*, *274*, 8-13, 2008.

Sodeman, D.A., S.M. Toner, and K.A. Prather, Determination of Single Particle Mass Spectral Signatures from Light-Duty Vehicle Emissions, *Environmental Science and Technology*, *39* ((12)), 4569-4580, 2005.

Solomon, S., D. Qin, M. Manning, Z. Chen, M. Marquis, K.B. Averyt, M. Tignor, and H.L. Miller, Climate Change 2007: The Physical Science Basis, Contribution of Working Group I to the Fourth Assessment Report of the Intergovernmental Panel on Climate Change, 2007.

Song, C.H., and G.R. Carmichael, The aging process of naturally emitted aerosol (sea-salt and mineral aerosol) during long range transport, *Atmospheric Environment*, *33*, 2203-2218, 1999.

Song, C.H., Y. Ma, D. Orsini, Y.P. Kim, and R.J. Weber, An Investigation into the Ionic Chemical Composition and Mixing State of Biomass Burning Particles Recorded During TRACE-P P3B Flight # 10, *Journal of Atmospheric Chemistry*, *51* (1), 43-64, 2005.

Song, X.H., P.K. Hopke, D.P. Fergenson, and K.A. Prather, Classification of single particles analyzed by ATOFMS using an artificial neural network, ART-2A, *Analytical Chemistry*, *71* (4), 860-865, 1999.

Sorooshian, A., V. Varutbangkul, F.J. Brechtel, B. Ervens, G. Feingold, R. Bahreini, S.M. Murphy, J.S. Holloway, E.L. Atlas, G. Buzorius, H. Jonsson, R.C. Flagan, and J.H. Seinfeld, Oxalic acid in clear and cloudy atmospheres: Analysis of data from International Consortium for Atmospheric Research on Transport and Transformation 2004, *Journal of Geophysical Research*, *111* (D23S45), doi:10.1029/2005JD006880, 2006.

Spencer, M.T., J.C. Holecek, C.E. Corrigan, V. Ramanathan, and K.A. Prather, Size-resolved chemical composition of aerosol particles during a monsoonal transition period over the Indian Ocean, *Journal of Geophysical Research*, *113* (D16305), doi:10.1029/2007JD008657, 2008.

Spencer, M.T., and K.A. Prather, Using ATOFMS to determine OC/EC mass fractions in particles, *Aerosol Science and Technology*, *40* (8), 585-594, 2006.

Stolzenburg, M.R., and P.H. McMurry, Equations governing single and tandem DMA configurations and a new lognormal approximation to the transfer function, *Aerosol Science and Technology*, *42* (6), 421-432, 2008.

Stroud, C.A., A. Nenes, J.L. Jimenez, P.F. DeCarlo, J.A. Huffman, R. Brunintjes, E. Nemitz, A.E. Delia, D.W. Toohey, A.B. Guenther, and S. Nandi, Cloud activating properties of aerosol observed during CELTIC, *Journal of the Atmospheric Sciences*, *64*, 441-459, 2007.

Su, Y.X., M.F. Sipin, H.F. Furutani, and K.A. Prather, Development and characterization of an aerosol time-of-flight mass spectrometer with increased detection efficiency, *Analytical Chemistry*, *76*, 712-719, 2004.

Sullivan, A.P., A.S. Holden, L.A. Patterson, G.R. McMeeking, S.M. Kreidenweis, W.C. Malm, W.M. Hao, C.E. Wold, and J.L. Collett, A method for smoke marker measurements and its potential application for determining the contribution of biomass burning from wildfires and prescribed fires to ambient PM2.5 organic carbon, *Journal of Geophysical Research*, *113* (D22302), doi:10.1029/2008JD010216, 2008.

Sullivan, R.C., and K.A. Prather, Recent advances in our understanding of atmospheric chemistry and climate made possible by on-line aerosol analysis instrumentation, *Analytical Chemistry*, *77* (12), 3861-3885, 2005.

Temesi, D., A. Molnar, E. Meszaros, T. Feczko, A. Gelencser, G. Kiss, and Z. Krivacsy, Size resolved chemical mass balance of aerosol particles over rural Hungary, *Atmospheric Environment*, *35*, 4347-4355, 2001.

Thornton, J.A., and J.P.D. Abbatt, N2O5 Reaction on Submicron Sea Salt Aerosol: Kinetics, Products, and the Effect of Surface Active Organics, *Journal of Physical Chemistry A*, *109* (44), 10004-10012, 2005.

Toner, S.M., D.A. Sodeman, and K.A. Prather, Single Particle Characterization of Ultrafine and Accumulation Mode Particles from Heavy Duty Diesel Vehicles Using Aerosol Time-of-Flight Mass Spectrometry, *Environmental Science and Technology*, *40* (12), 3912-3921, 2006.

Toossi, R., and T. Novakov, The Lifetime of Aerosols in Ambient Air: Consideration of the Effects of Surfactants and Chemical Reactions, *Atmospheric Environment*, *19*, 127-133, 1985.

Topping, D., H. Coe, G. McFiggans, R. Burgess, J.D. Allan, M.R. Alfarra, K. Bower, T.W. Choularton, S. Decesari, and M.C. Facchini, Aerosol chemical characteristics from sampling conducted on the Island of Jeju, Korea during ACE Asia, *Atmospheric Environment*, *38*, 2111-2123, 2004.

Turpin, B.J., and J.J. Huntzicker, Indentification of Secondary Organic Aerosol Episodes and Quantitation of Primary and Secondary Organic Aerosol Concentrations during SCAQS, *Atmospheric Environment*, *29*, 3527-3544, 1995.

Turpin, B.J., J.J. Huntzicker, S.M. Larson, and G.R. Cass, Los Angeles Summer Midday Particulate Carbon: Primary and Secondary Aerosol, *Environmental Science and Technology*, *25*, 1788-1793, 1991.

Turpin, B.J., and H.J. Lim, Species contributions to PM2.5 mass concentrations: Revisiting common assumptions for estimating organic mass, *Aerosol Science and Technology*, *35*, 602-610, 2001.

Twomey, S., Pollution and Planetary Albedo, *Atmospheric Environment*, *8*, 1251-1256, 1974.

Varga, B., G. Kiss, I. Ganszky, A. Gelencser, and Z. Krivacsy, Isolation of water-soluble organic matter from atmospheric aerosol, *Talanta*, *55*, 561-572, 2001.

Voisin, D., J.N. Smith, H. Sakurai, P.H. McMurry, and F.L. Eisele, Thermal Desorption Chemical Ionization Mass Spectrometer for Ultrafine Particle Chemical Composition, *Aerosol Science and Technology*, *37*, 471-475, 2003.

Volckens, J., and T.M. Peters, Counting and particle transmission efficiency of the aerodynamic particle sizer, *Journal of Aerosol Science*, *34* (3), 319-337, 2005.

Warner, J., A reduction in rain associated with smoke from sugarcane fires-An inadvertent weather modification, *J. Appl. Meteorol.*, *7*, 247-251, 1968.

Weingartner, E., H. Burtscher, and U. Baltensperger, Hygroscopic properties of carbon and diesel soot particles, *Atmospheric Environment*, *31* (15), 2311-2327, 1997.

Wenzel, R.J., and K.A. Prather, Improvements in ion signal reproducibility obtained using a homogeneous laser beam for on-line laser desorption/ionization of single particles, *Rapid Communications in Mass Spectrometry*, *18* (13), 1525-1533, 2004.

Wexler, A.S., and S.L. Clegg, Atmospheric aerosol models for systems including ions H+, NH4+, Na+, SO42-, NO3-, Cl-, Br- and H2O, *Journal of Geophysical Research*, *107* (D14), 4207, 2002.

Wiedensohler, A., An Approximation of the Bipolar Charge-Distribution for Particles in the Sub-Micron Size Range, *Journal of Aerosol Science*, *19* (3), 387-389, 1988.

Williams, B.J., A.H. Goldstein, N.M. Kreisberg, and S.V. Hering, An In-Situ Instrument for Speciated Organic Composition of Atmospheric Aerosols: Thermal Desorption Aerosol GC/MS-FID (TAG), *Aerosol Science and Technology*, *40*, 627-638, 2006.

Xiong, J.Q., M. Zhong, C. Fang, L.C. Chen, and M. Lippmann, Influence of Organic Films on the Hygroscopicity of Ultrafine Sulfuric Acid Aerosol, *Environmental Science and Technology*, *32*, 3536-3541, 1998.

Yu, J.Z., X.-F. Huang, J. Xu, and M. Hu, When Aerosol Sulfate Goes Up, So Does Oxalate: Implication for the Formation Mechanisms of Oxalate, *Environmental Science and Technology*, *39*, 128-133, 2005.

Yu, J.Z., H. Yang, H.Y. Zhang, and A.K.H. Lau, Size distributions of water-soluble organic carbon in ambient aerosols and its size-resolved thermal characteristics, *Atmospheric Environment*, *38*, 1061-1071, 2004.

Zappoli, S., A. Andracchio, S. Fuzzi, M.C. Facchini, A. Gelencser, G. Kiss, Z. Krivacsy, A. Molnar, E. Meszaros, H.C. Hanson, K. Rosman, and Y. Zebuhr, Inorganic, organic and macromolecular components of fine aerosol in different areas of Europe in relation to their water solubility, *Atmospheric Environment*, *33*, 2733-2743, 1999.

Zhang, Q., M.R. Alfarra, D.R. Worsnop, J.D. Allan, H. Coe, M. Canagaratna, and J.L. Jimenez, Deconvolution and quantification of hydrocarbon-like and oxygenated organic aerosols based on aerosol mass spectrometry, *Environmental Science and Technology*, *39*, 4938-4952, 2005a.

Zhang, Q., D.R. Worsnop, M.R. Canagaratna, J.T. Jayne, and J.L. Jimenenez, Hydrocarbon-like and Oxygenated Organic Aerosols in Pittsburgh: Insights into Sources and Processes of Organic Aerosols, *Atmospheric Chemistry and Physics*, *5*, 3289-3311, 2005b.

Zhang, X.Q., P.H. McMurry, and S.V. Hering, Mixing Characteristics and Water Content of Submicron Aerosols Measured in Los Angeles and at the Grand Canyon, *Atmospheric Environment*, *27A* (10), 1593-1607, 1993.

Ziemann, P.J., Particle mass and size measurement using mass spectrometry, *Trac-Trends in Analytical Chemistry*, *17* (6), 322-328, 1998.

Chapter 2

Effect of Organic Compounds on Cloud Condensation Nuclei (CCN) Activity of Sea Spray Aerosol Produced by Bubble Bursting

2.1 Synopsis

The ocean comprises over 70% of the surface of the earth and thus sea spray aerosols generated by wave processes represent a critical component of our climate system. Importantly, sea spray aerosols strongly impact the Earth's radiation balance through a number of mechanisms including by acting as nuclei upon which water condenses and clouds form. The manner in which different chemical species are distributed between individual particles in sea spray directly determines which particles will effectively form cloud nuclei. Complex oceanic mixtures of organic species and inorganic salts undergo complex interactions, causing them to segregate into poorly understood mixtures, thus creating significant challenges for predicting important climate-relevant particle properties such as water uptake and cloud forming potential. Controlled laboratory experiments were undertaken to better understand the full range of particle properties produced by bubbling solutions composed of simplistic model organic species, oleic acid and sodium dodecyl sulfate (SDS), mixed with NaCl to more complex artificial seawater mixed with complex organic mixtures produced by common oceanic microorganisms. Simple mixtures of NaCl and oleic acid or SDS had a significant effect on CCN activity, even in very small amounts. However, the artificial seawater (ASW) solution containing microorganisms, the common cyanobacteria (*Synechococcus*) and DMS-producing green algae (*Ostreococcus*), produced particles containing ~34 times more carbon than the particles produced from pure ASW, yet no

significant change was observed in the overall CCN activity. We hypothesize that these microorganisms produce diverse mixtures of organics with a wide range of properties that had an offsetting effect, leading to no change in the overall *average* measured hygroscopicity of the collection of sea spray particles. Changes in CCN activity account for < 3% of a change in CCN concentrations for these specific microorganisms, suggesting "bloom" conditions lead to small changes in CCN activity, and thus would have a negligible impact on cloud formation. However, the ocean contains a much broader range of organic species and biological processes and thus further studies are needed of sea spray particles and biological processes under a wide range of controllable conditions.

2.2 Introduction

Dust and sea spray aerosols are the two most abundant aerosols in the atmosphere [*Satheesh and Moorthy*, 2005]. The primary source of sea spray aerosol (SSA) is bubble bursting from breaking waves in the ocean [*Lewis and Schwartz*, 2004]. With oceans covering over 70% of the earth and marine stratus and stratocumulus clouds contributing 30-40% to the earth's albedo [*Niedermeier et al.*, 2008], sea spray aerosols represent an essential component of the climate system, both directly and indirectly. Bubbles burst and form drops that evaporate, leaving behind residual particles composed not only of sea salt but also other sea surface microlayer compounds [*Bigg and Leck*, 2008; *Garrett*, 1967; *Lion and Leckie*, 1981], as well as bacteria and other bioparticles [*Blanchard*, 1989; *Posfai et al.*, 2003]. Incorporation of the sea surface microlayer into marine aerosol particles can change their physical properties [*Bigg and Leck*, 2008; *Sellegri et al.*, 2006], affecting their ability to scatter light, take up water, and form clouds. Dissolved organic matter and decomposition products from microorganisms in the ocean accumulate in the sea surface microlayer [*Smoydzin and von Glasow*, 2007]. While the species in this layer are enriched in the top ~1 mm of the ocean, the

thickness varies depending on the extent of regional biological activity [*Smoydzin and von Glasow*, 2007]. This thin microlayer represents a chemically rich and diverse environment which directly impacts the composition of atmospheric aerosols [*MacIntyre*, 1974]. While it is known that sea spray is produced via bubble bursting and other wind-driven processes, it represents a tremendous challenge to deconvolute the effect of the microlayer on the initial marine aerosol composition, which is very important for understanding global atmospheric processes [*Bigg and Leck*, 2008].

Many aspects of sea spray production are affected by properties of the air-water interface, which in turn can affect marine aerosol production and behavior. Surface-active compounds (surfactants), such as those present in the ocean surface microlayer, are difficult to characterize in a systematic way [*Lewis and Schwartz*, 2004]. Over 25 years ago [*Gill et al.*, 1983], scientists looked into the importance of organic surfactants that can be present on SSA and how they could affect droplet activation and growth. More recent measurements show that up to 60% of the mass of marine particles can be organic, which is strongly size dependent and much higher for submicron particles [*Middlebrook et al.*, 1998; *O'Dowd et al.*, 2004; *Russell et al.*, 2010]. SSA that are 30% organic by mass show a 15% decrease in hygroscopic growth above 75% relative humidity (RH) [*Ming and Russell*, 2001]. These concentrations have been observed even in areas with decreased biological activity [*Novakov et al.*, 1997; *Russell et al.*, 2002]. The concentrations of organic material in marine particles can range over orders of magnitude due to changes in biological activity. While the organic mass fraction has been shown to be typically larger for smaller particles than larger particles[*O'Dowd et al.*, 2004], a recent study using volatility and hygroscopicity tandem differential mobility analysis (VH-TDMA) has shown that the naturally formed accumulation mode of SSA occurs around 100 nm, representing only ~8 % by volume organic material [*Modini et al.*, 2010]. Therefore,

a large uncertainty still surrounds the factors controlling the composition of accumulation mode SSA. Understanding the composition of this mode is critical for understanding the overall effect of the ocean on CCN and climate.

The extent to which the sea surface microlayer affects the initial formation and composition of marine aerosols is poorly understood and still under investigation [*Rinaldi et al.*, 2009; *Smoydzin and von Glasow*, 2007]. Facchini et al. [2008b] observed a size dependent transfer of marine organic matter being controlled by the solubility and surface tension properties of the organic material with water insoluble organic matter (WIOM) having the greatest contribution to smaller particles and water soluble organic matter (WSOM) having the greatest contribution to coarse particles due to the aggregation processes and surface active properties of the organic matter [*Facchini et al.*, 2008b]. Recent studies on ocean productivity and marine clouds, [*Meskhidze and Nenes*, 2006] focused on remote sensing secondary organic aerosol production from gases produced from phytoplankton. This previous study demonstrated that the role of primary organic carbon aerosol (POA) and reactive gases like isoprene and amines from ocean biota in modifying the chemical composition and size distribution of marine aerosols is an intriguing question [*Facchini et al.*, 2008a; *Langmann et al.*, 2008]. Single particle environmental transmission electron microscopy (ETEM) showed a large difference in subsatured water uptake and morphology between NaCl and laboratory generated sea spray aerosol (SSA) or natural seawater [*Wise et al.*, 2009]. Recent experiments relating the CCN activity of primary sea spray aerosol and phytoplankton-derived organic matter show a decrease in hygroscopic growth and CCN activity associated with the addition of organics [*Fuentes et al.*, 2010b]. Additionally, there were notable differences in CCN activity and hygroscopic growth between different types of organisms; diatomaceous associated organic matter was more hydrophobic than nanoplankton associated organic matter

[*Fuentes et al.*, 2010b]. This clearly illustrates the need for further experiments involving increasing numbers of different marine microorganisms, including detailed analysis of the organic material associated with these microorganisms, to better understand the effect of marine organic matter from primary production on the CCN activity and hygroscopic growth of sea spray aerosols.

In this chapter, we measure the CCN activity of SSA generated in the presence of surface-active organic material and marine microorganisms to show the potential impact of marine organic matter on cloud formation. The morphology and composition of the aerosol particles close to the CCN activation diameter of the particles are also explored using single particle techniques, Scanning Electron Microscopy and Near Edge X-ray Absorption Fine Structure Scanning Transmission X-ray Microscopy.

2.3 Materials and methods

2.3.1 Laboratory generation of sea salt aerosol

The bubble bursting apparatus that was used to generate particles in these experiments is an L-shaped sintered glass filter with porosity "C" rated at 25-50 μm (Ace Glass Vineland, NJ) that was immersed 2 cm below each of the 100 mL sample solutions in a 32oz Mason jar (approximately 3" D x 7"H). The glass filter was attached to a 1/8" stainless steel tube that protruded from a hole in a stainless steel cap on the jar. Another hole in the cap allowed for an additional 1/8" stainless steel tube to supply the sheath air. This sheath tube did not go below the surface of the water, it was approximately 1 cm from the surface and was bent in a spiral motion to have the flow almost perpendicular to the surface and towards a third hole, the exit port of the cap. All holes were sealed with o-rings and ferrules to prevent contamination with outside air. The glass was combusted for 4 hours at 450 °C to help prevent organic

contamination. The stainless steel components were cleaned by sonicating in water for 72 hours total prior to use; 24 hours with tap water, 24 hours with distilled water and 24 hours with ultra pure deionized water to remove contamination. A flow of 500 cm^3/min dry filtered nitrogen flowed through the glass filter to produce bubbles. While this apparatus is a very simplified and small scale proxy of breaking waves in the ocean, the bubbles produced were determined by image capture to be approximately 1-4 mm in diameter and are within actual bubble distributions measured on breaking ocean waves [*Deane and Stokes*, 1997]. Additionally, the size distributions of aerosols produced from this experimental setup are similar to other similar experimental generation methods [*Sellegri et al.*, 2006] (shown below), and of the various types of bubble generation methods that have been used, is considered a valid representation of marine aerosol [*Fuentes et al.*, 2010a]. Approximately 1 cm above the solution, a sheath flow ("surface wind") flowed perpendicular to the solution surface with a flow of 1500 cm^3/min dry filtered nitrogen to take ejected and suspended seawater droplets away from the bubbling chamber. A figure describing this apparatus is shown in Figure 2.1.

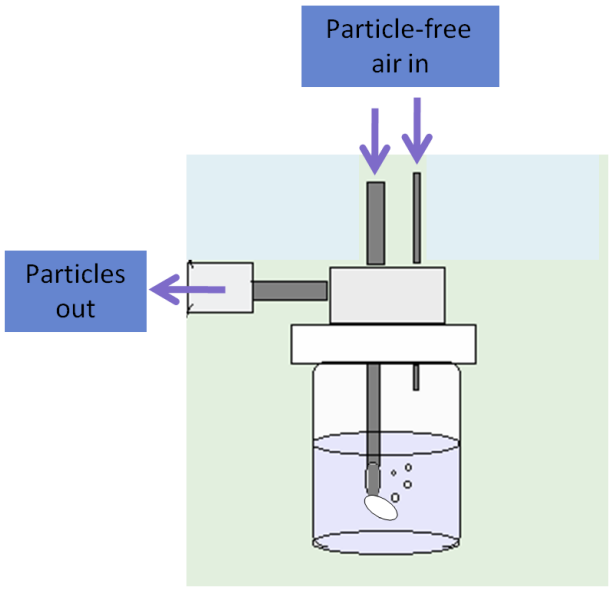

Figure 2.1. Schematic of bubbling apparatus.

The wet sea spray droplets from the bubbling chamber were then sent through two home-made diffusion dryers filled with silica gel, causing the relative humidity to become <10% at 25°C (room temperature), letting the droplets dry up and form solid SSA. The dry SSA were then split between a scanning mobility particle sizer (SMPS) and an aerosol particle sizer (APS) to observe particle size distributions; or the entire flow from the driers was sent to a differential mobility analyzer (DMA) where the output of the DMA was then split between a condensation particle counter (CPC) and cloud condensation nuclei counter (CCNc) for the CCN curves.

2.3.2 Size distributions

Size distributions of the bubbled particles less than 600 nm were measured using a Scanning Mobility Particle Sizer (SMPS), consisting of a differential mobility analyzer (DMA, TSI model 3080) and a condensation particle counter (CPC, TSI model 3010). Scans of particles from 11nm- 640 nm took 240 seconds with a sheath to aerosol ratio of 4.0/0.4. Particle sizes greater than 500 nm were measured with an Aerodynamic Particle Sizer (APS, TSI model 3020). Scans from 500-20 μm took 57 seconds to run. After bubbling started, the concentration of the aerosols reached a steady state within 5-10 min, after which 3 SMPS and 15 APS size distribution spectra were averaged for each experimental condition. The DMA used with the SMPS distributions produced sizes in mobility diameter (D_m). These were converted from D_m, to volume equivalent diameter, D_{ve}, as shown in Equation 2.1 [*DeCarlo et al.*, 2004].

$$\frac{D_m}{C_c(D_m)} = \frac{D_{ve}\chi}{C_c(D_{ve})} \qquad (2.1)$$

Where χ is the dynamic shape factor (1.08 for NaCl)[*Rose et al.*, 2008], $C_c(D_m)$ is the Cunningham slip correction factor for D_m, and $C_c(D_{ve})$ is the Cunningham slip correction factor for D_{ve}. C(D) can be approximated by the following relation, as shown in Equation 2.2 [*Rose et al.*, 2008]:

$$C(D) = 1 + \frac{2\lambda}{D}\left(1.142 + 0.558\exp\left(-0.999\frac{D}{2\lambda}\right)\right) \quad (2.2)$$

Where λ is the mean free path of the gas molecules (λ = 68 nm in air at 298 K and standard atmospheric pressure). D_{ve} was obtained by iteratively solving equation 2.1 with equation 2.2.

2.3.3 Cloud condensation nuclei (CCN) activity measurements

CCN curves were constructed using a differential mobility analyzer (DMA, TSI model 3080) at a sheath to aerosol ratio of 15.0 to 1.5. The monodisperse output of the DMA was split between a condensation particle counter (CPC, TSI model 3010) and a streamwise thermal gradient CCN column at a supersaturation (*SS*) of around 0.1% with an instrumental uncertainty of 10% [*Roberts and Nenes*, 2005]. The CCN supersaturation was calibrated before use with ammonium sulfate aerosol (99.999%, Sigma Aldrich). The mobility size was changed on the DMA and once particle concentrations stabilized, minute long averages of the CPC and CCN 1 Hz data were obtained and used to calculate the CCN/CPC ratio. Activation diameters are obtained from the x-half value of a sigmoidal fit to the activation curves after normalization of the activated plateau to 1. To take into account the change in morphology of the aerosols with uptake of organics, mobility diameters were corrected for a range of possible shapes from non-spherical to spherical using Equations 1 and 2, assuming an average dynamic

shape factor of 1.04 with uncertainty estimations on each of the curves ranging from shape factors 1.0 to 1.08 for NaCl [*Fuentes et al.*, 2010a; *Rose et al.*, 2008].

2.3.4 Model seawater solution, organic surfactants, and microorganisms

Salt solutions, either 3.5% NaCl (99.999% Sigma) in Mill-Q water or artificial seawater (ASW) made from analytical grade inorganic salts (without additional nutrients) in Mill-Q water[*Morel and Rueter*, 1979] were used as model seawater in the experiments. A concentrated solution of 0.025 mg/ml oleic acid (99+%, Aldrich) in hexanes (99.95%, EMD OmniSolv) was then cumulatively added to the surface of the NaCl or artificial seawater solution that was to be bubbled. Trials started with 10ul, then 100ul and finally 1000ul over the course of an experiment. After adding the necessary aliquot of oleic acid, only the sheath air flowed to allow the hexane to evaporate for 15 min, leaving only the surfactant on the surface. After the 15 min pre-preparation, both sheath and bubbling air were turned on and generation of sea spray aerosol was initiated. Once size distributions and CCN curve measurements were completed, the next aliquot was added and the process was repeated. The surfactant added to the solution surface was done with combusted glass Pasteur pipets attached to automated pipets which were calibrated previously to insure accuracy. A concentrated solution of 0.025 mg/ml sodium dodecyl sulfate (SDS) (99+%, Sigma Aldrich) was made in Milli-Q (18.2MΩ) water instead of hexane. Marine microorganisms *Ostreococcus lucimarinus* (sp. strain CCE9901) and *Synechococcus* (sp. strain CC9311) were grown in f/4 medium, which is half strength f/2 medium [*Guillard*, 1975]. *Ostreococcus* are the smallest known free-living eukaryotes and are DMS-producing unicellular coccoid green alga that is found in many ocean regions with an average size around 2 μm [*Courties et al.*, 1994; *Madigan et al.*, 2006]. *Synechococcus* are unicellular cyanobacteria that are very widespread in the marine environment and are preferentially found in well-lit surface temperate and tropical waters and

are between 0.6 µm and 1.6 µm in size. [*Madigan et al.*, 2006; *Waterbury et al.*, 1979]. These cells were then either bubbled by adding 'fresh' cells right from the incubating room; or 'frozen' cells which were placed in a plastic centrifuge tube and frozen for at least 24 hours at -30 °C to ensure that the cells had indeed ruptured to produce organic material. A cumulative amount of cells were then added to the artificial seawater solution starting with 0.5 ml then 5 ml then 50 ml to approximately 1x, 10x and 100x typical ocean concentrations of these particular cells in the ASW (10^6 cells/L)[*Worden et al.*, 2004]. 'Filtered' cells are fresh cells from the incubation room that were filtered with a 0.2 µm syringe filter before use to ensure no cell material was placed in solution, only the organic species from within the cells. 'Bulk' cells are the concentrated solution of cells before they are added to the salt solution for each bubbling experiment.

2.3.5 SEM collection

To collect sea spray aerosols generated in the laboratory bubble bursting experiments for off-line single particle analysis via SEM and STXM, 100 nm thick standard silicon nitride windows (Silson Ltd.) were used. Three windows were attached to each Micro-orifice uniform deposit impactor (MOUDI) foil with carbon tape (cut up old carbon SEM grids) and placed on stage 6 and 8 (0.5-1 µm and 0.1-0.3 µm, respectively). All other stages in the MOUDI used foil only. The aerosol output of the bubbler was sent through two diffusion dryers then diluted with dry nitrogen ~28 slpm into the MOUDI, with a HEPA vent on the MOUDI inlet having an excess flow of approximately 0.8 slpm. Stages were manually rotated every hour and particles were collected for 2 hours per experiment. A Phillips XL30 field emission scanning electron microscope (SEM) was used to take the images.

2.3.6 STXM/NEXAFS

Near Edge X-ray Absorption Fine Structure (NEXAFS) Scanning Transmission X-ray Microscopy (STXM) was carried out to help quantify the relative amounts of organics on the SSA at Lawrence Berkeley National Laboratory's Advanced Light Source. The STXMs at beamlines 5.3.2 and 11.0.2 were used to examine the laboratory generated particles. A brief description of the measurement follows: Energy selected X-rays from the synchrotron are focused onto the sample as it is raster scanned. After one complete sample scan completes, the X-ray energy is changed and the sample is re-scanned. This process is repeated until an entire spectral image "stack" is completed. For this study, the X-ray energy was scanned over the carbon K edge from 275-320 eV using approximately 120 variable step sizes [*Kilcoyne et al.*, 2003].

2.4 Results and Discussion

2.4.1 SMPS and APS size distributions

Figures 2.2-2.5 compare the SMPS and APS size distributions generated from all experiments. The size distribution curves clearly show that there were very minimal, if any, changes in the particle size distribution produced upon addition of surfactant or microorganisms to the seawater solution.

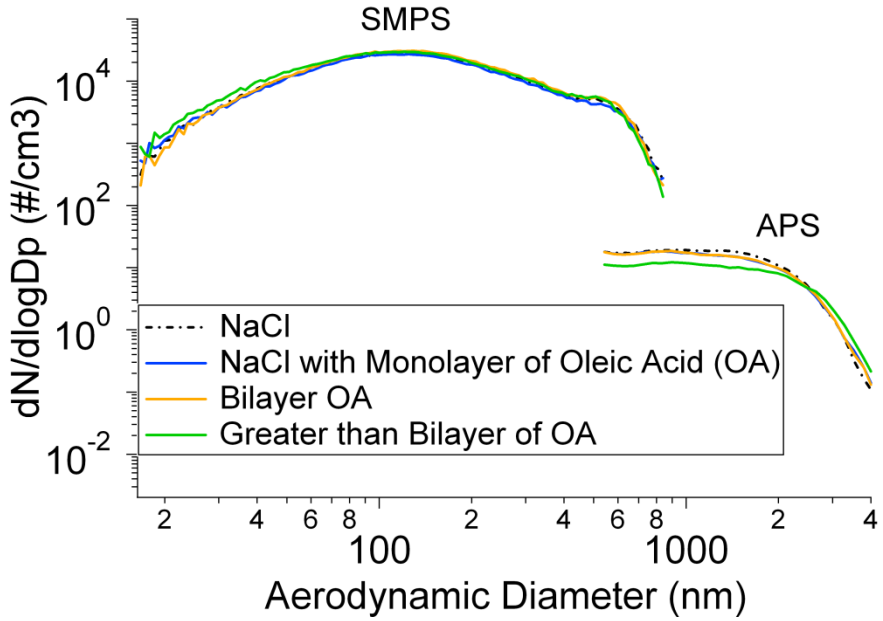

Figure 2.2. Scanning mobility particle sizer (SMPS) and Aerodynamic particle sizer (APS) size distributions of the bubbled particles for the NaCl and OA experiments. SMPS measurements were converted to aerodynamic diameter assuming a density of 2.165 g/cm3 (that of NaCl) and a dynamic shape factor of 1.08.

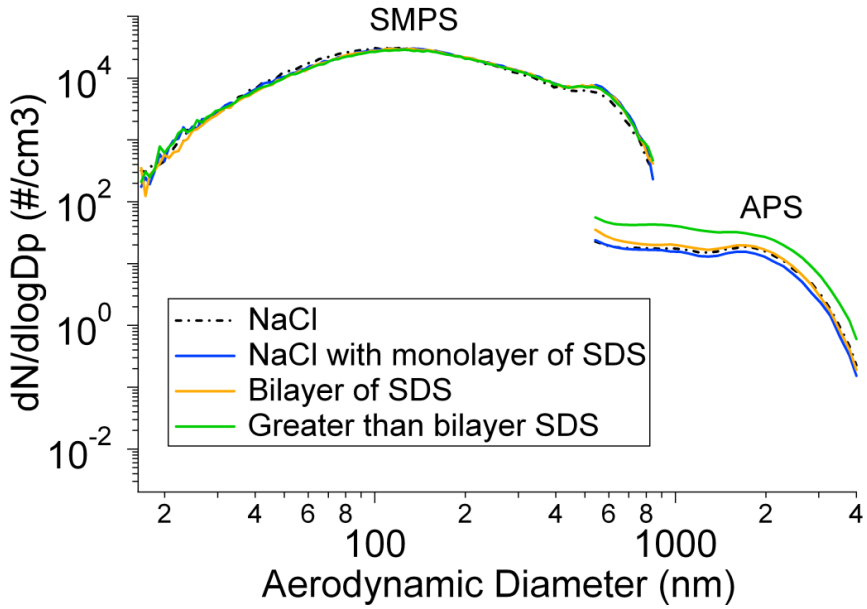

Figure 2.3. Scanning mobility particle sizer (SMPS) and Aerodynamic particle sizer (APS) size distributions of the bubbled particles for the NaCl and SDS experiments. SMPS measurements were converted to aerodynamic diameter assuming a density of 2.165 g/cm3 (that of NaCl) and a dynamic shape factor of 1.08.

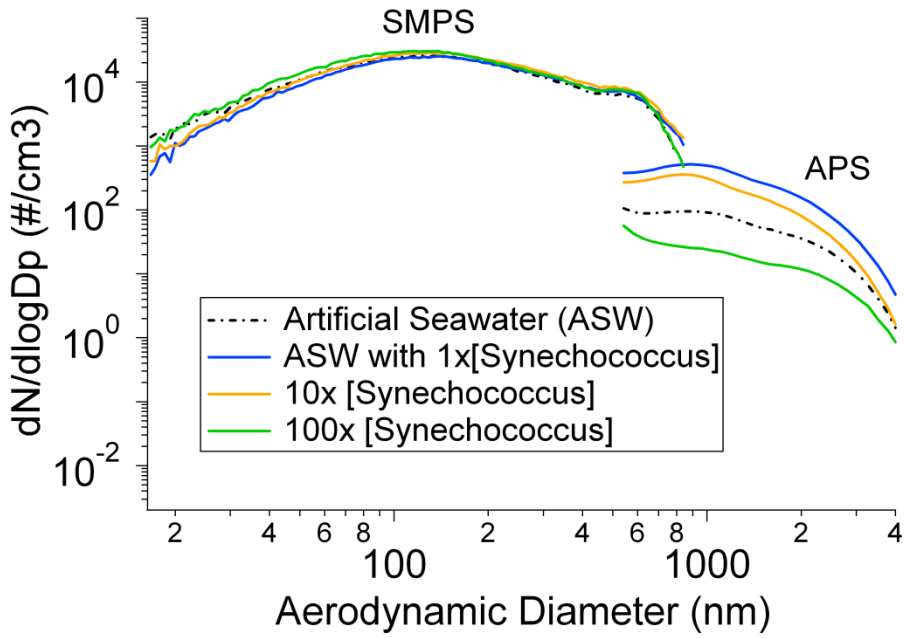

Figure 2.4. Scanning mobility particle sizer (SMPS) and Aerodynamic particle sizer (APS) size distributions of the bubbled particles for the ASW *Synechococcus* experiments.

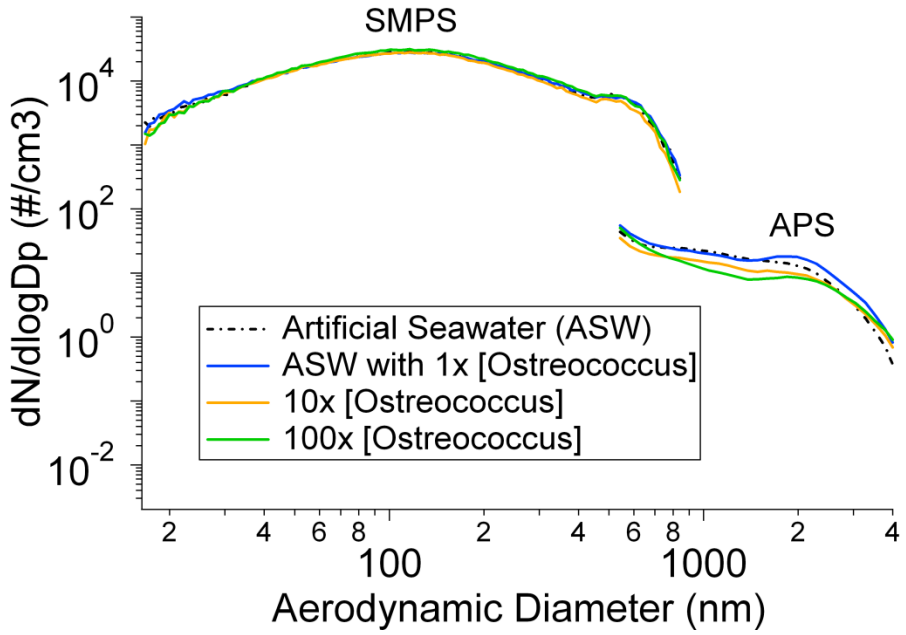

Figure 2.5. Scanning mobility particle sizer (SMPS) and Aerodynamic particle sizer (APS) size distributions of the bubbled particles for the ASW *Ostreococcus* experiments.

2.4.2 CCN activation curves for pure NaCl and surfactants

Figures 2.6 and 2.7 compare the CCN activation curves of NaCl aerosols generated from NaCl model seawater with 2 different types and concentration of organic surfactants, oleic acid, and SDS with an average shape factor 1.04 with uncertainty bars for a range of shape factors 1.0 to 1.08. The activation curves clearly show that even an addition of monolayer of organic surfactant *to the seawater solution* changes the CCN activity of the NaCl aerosols generated by the bubble bursting process. The activation diameter of pure NaCl in the oleic acid experiment with a shape factor of 1.04 was 106.1 ± 2.4 nm (±uncertainty from shape factor range 1.0-1.08), and 113.4 ± 2.6 nm for the SDS experiment.

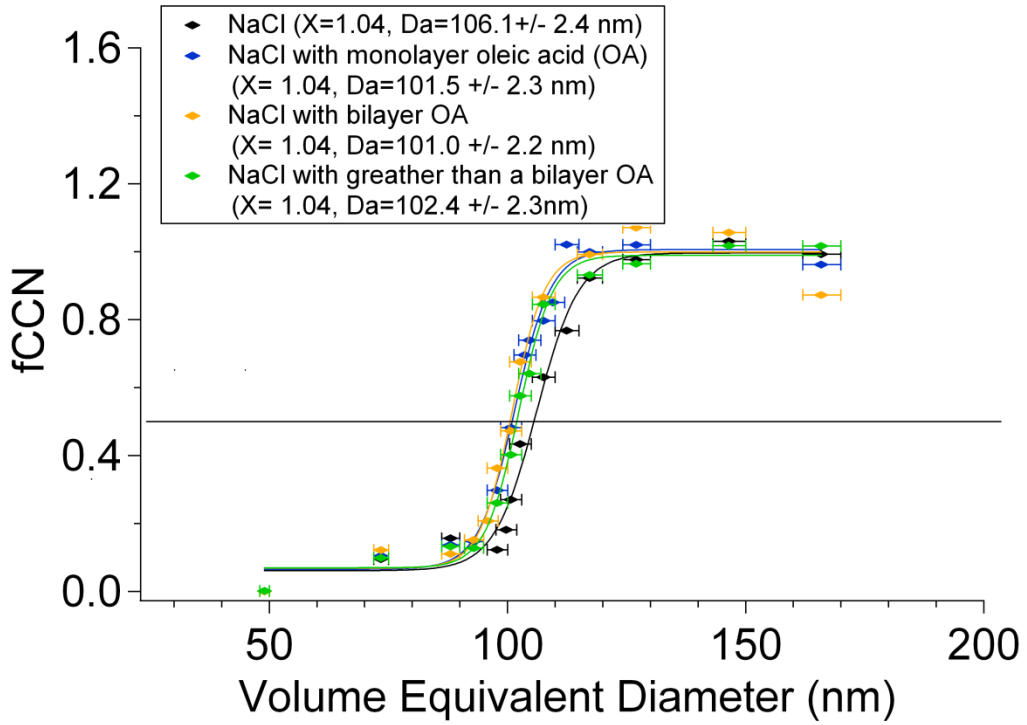

Figure 2.6. CCN curves of NaCl with Oleic Acid (OA). Markers are each of the data points collected during each curve. Curve is a sigmoidal fit of each of the markers for the experiment with a shape factor correction (X) of 1.04 for NaCl. Activation diameter (Da) was calculated from the x-half value of the sigmoidal fit. Error bars are +/- X of 1.0 and 1.08. The horizontal line indicates the approximate x-half value, set to 0.5 fCCN on the y-axis.

Upon addition of a monolayer of oleic acid *to the NaCl solution*, the activation diameter shifted to smaller sizes by 4.6 ± 3.3 nm. Additional oleic acid in solution of a bilayer and greater than a bilayer resulted in the shift of activation diameters to smaller sizes by 5.1 ± 3.3 and 3.7 ± 3.3 nm, respectively, when compared to the pure NaCl aerosol, indicating a clear increase in CCN activity with the addition of surfactant. Upon addition of a monolayer of SDS to the NaCl solution, the activation diameter shifted smaller by 1.9± 3.6 nm. Additional SDS *in solution* of a bilayer and greater than a bilayer resulted in the shift of activation diameters smaller by 5.6 ± 3.5 and 7.2 ± 3.5 nm, respectively when compared to the pure NaCl aerosol, indicating a clear increase in CCN activity.

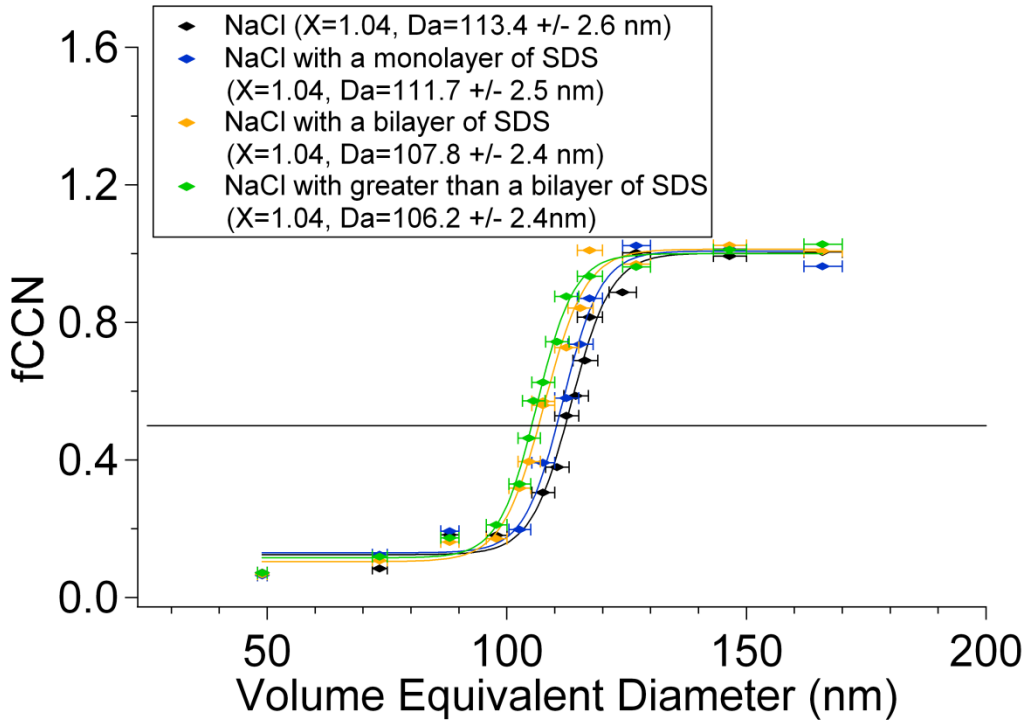

Figure 2.7. CCN curves of NaCl with Sodium dodecyl sulfate (SDS). Markers are each of the data points collected during each curve. Curve is a sigmoidal fit of each of the markers for the experiment with a shape factor correction (X) of 1.04 for NaCl. Activation diameter (Da) was calculated from the x-half value of the sigmoidal fit. Error bars are +/- X of 1.0 and 1.08. The horizontal line indicates the approximate x-half value, set to 0.5 fCCN on the y-axis.

For the NaCl with oleic acid experiment, a control experiment with just hexane and no oleic acid was run, to make sure that the effect observed was indeed due to the oleic acid and not the hexane itself. The effect of hexane was determined to be negligible (see Table 2.1) and all observations appear to be due to the presence of oleic acid and not an artifact of the use of hexane as a means to deliver the oleic acid to the NaCl solution surface. A summary of these two experiments and other trials under similar conditions can be found in Tables 2.1 and 2.2.

Table 2.1. Summary of NaCl with oleic acid CCN experiment activation diameters and experimental conditions with shape factor X=1.04. Uncertainty in Da is shown in parenthesis and is the difference between 1.04 and 1.0/1.08 shape factors. Averages of the shift are shown with standard deviations of all the experiments. Uncertainty in % S is 10%.
*Experiment 1 is shown in Figure 2.6
#Monolayer equivalent of hexane without oleic acid

Expt	NaCl Da (nm)	Monolayer oleic acid Da (nm)	Δ Monolayer	Bilayer oleic acid Da (nm)	Δ Bilayer	Greater than bilayer oleic acid Da (nm)	Δ Greater than bilayer	Hexane only Da (nm)#	Δ Hexane	%S
1*	106.1 (2.4)	101.5 (2.3)	-4.6 (3.3)	101.0 (2.2)	-5.1 (3.3)	102.4 (2.3)	-3.7 (3.3)	N/A	N/A	0.109 (0.011)
2	110.0 (2.5)	106.6 (2.4)	-3.4 (3.5)	107.2 (2.4)	-2.8 (3.5)	107.7 (2.4)	-2.3 (3.5)	109.7 (2.5)	-0.3 (3.5)	0.106 (0.011)
3	109.2 (2.4)	105.5 (2.4)	-3.7 (3.4)	107.6 (2.4)	-1.6 (3.4)	109 (2.4)	-0.2 (3.4)	N/A	N/A	0.106 (0.011)
Average	N/A	N/A	-3.9 (0.6)	N/A	-3.2 (1.8)	N/A	-2.1 (1.8)	N/A	N/A	N/A

Table 2.2. Summary of NaCl with SDS CCN experiment activation diameters and experimental conditions with shape factor X=1.04. Uncertainty in Da is shown in parenthesis and is the difference between 1.04 and 1.0/1.08 shape factors. Averages of the shift are shown with standard deviations of all the experiments. Uncertainty in % S is 10%. *Experiment 1 is shown in Figure 2.7

Expt	NaCl Da (nm)	Monolayer SDS Da (nm)	Δ Monolayer	Bilayer SDS Da (nm)	Δ Bilayer	Greater than bilayer SDS Da (nm)	Δ Greater than bilayer	%S
1*	113.4 (2.6)	111.5 (2.5)	-1.9 (3.6)	107.8 (2.4)	-5.6 (3.5)	106.2 (2.4)	-7.2 (3.5)	0.106 (0.011)
2	111.7 (2.5)	109.8 (2.5)	-1.9 (3.5)	110.0 (2.5)	-1.7 (3.5)	108.2 (2.4)	-3.5 (3.5)	0.106 (0.011)
Average	N/A	N/A	-1.9 (0.0)	N/A	-3.7 (2.8)	N/A	-5.4 (2.6)	N/A

2.4.3 CCN activation curves for ASW and microorganisms

Figures 2.8 and 2.9 compare the CCN activation curves of sea spray aerosols generated from ASW with two different types and concentration of marine microorganisms with an average shape factor of 1.04 with uncertainty bars for a range of shape factors 1.0 to 1.08 [*Fuentes et al.*, 2010a; *Rose et al.*, 2008]. The activation curves clearly show that even with one hundred times (100x) the oceanic concentration by volume of the microorganisms [*Worden et al.*, 2004], a minimal change occurs in the CCN activity of ASW aerosols generated by the bubble bursting process, and is well within the experimental uncertainty. The activation diameter of pure ASW in the *Synechococcus* experiment with a shape factor of 1.04 was 108.4 ± 2.4 nm, and 107.9 ± 2.4 nm for the *Ostreococcus* experiment.

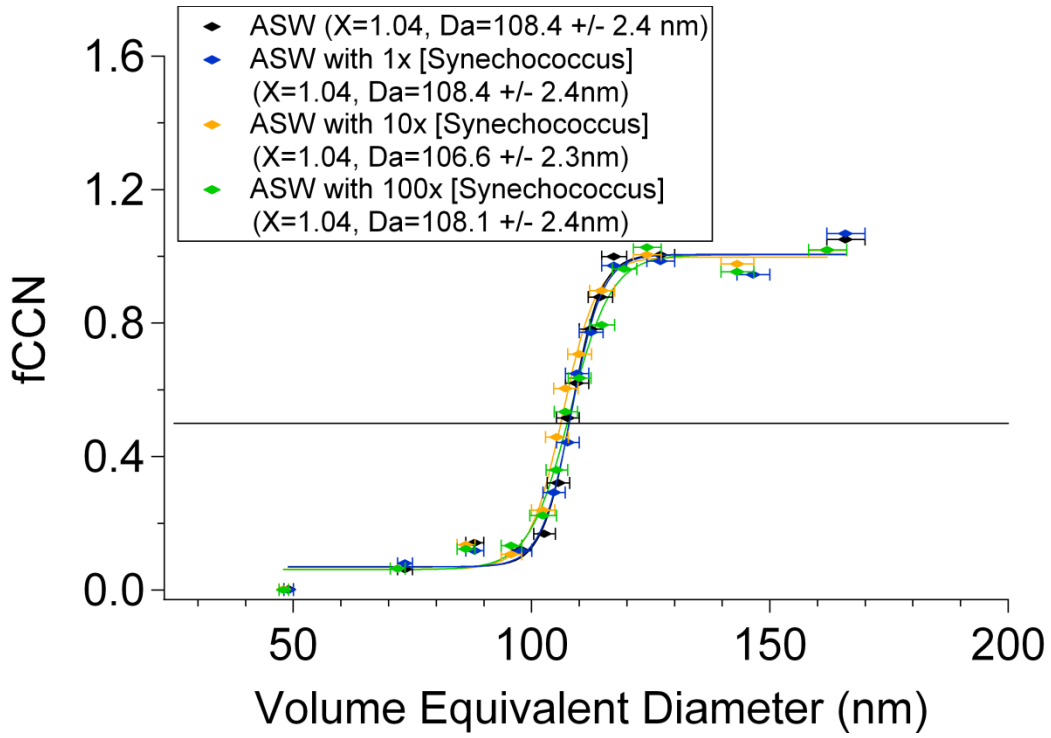

Figure 2.8. CCN curves of Artificial Seawater (ASW) with *Synechococcus*. Markers are each of the data points collected during each curve. Curve is a sigmoidal fit of each of the markers for the experiment with a shape factor correction (X) of 1.04 for ASW. Activation diameter (Da) was calculated from the x-half value of the sigmoidal fit. Error bars are +/- X of 1.0 and 1.08. The horizontal line indicates the approximate x-half value, set to 0.5 fCCN on the y-axis.

Upon addition of the typical oceanic concentration of *Synechococcus* (10^6 cells/L)[*Worden et al.*, 2004], (hereby referred to as 1x) to the ASW solution, the shift in activation diameter was negligible and within the errors of the experiment. Additional *Synechococcus* in solution of ten times (10x) and one hundred times (100x) typical oceanic concentrations (i.e. bloom conditions) also resulted in negligible shifts in the activation diameters when compared to the pure ASW aerosol, indicating a minimal change in CCN activity. Upon addition of the typical oceanic concentration of *Ostreococcus* (1x) to the ASW solution, the shift in activation diameter was negligible and within the errors of the experiment. Additional *Ostreococcus* in solution of 10x and 100x oceanic concentrations also resulted in negligible shifts in the

activation diameters when compared to the pure ASW aerosol. Experiments were also done with fresh cells as well as filtered cells, to try and separate the effect of the microorganism cells from the organics associated with the microorganisms. No significant difference was observed between fresh, frozen or filtered microorganism cells throughout the experiments. In addition, APS size distributions (Figures 2.4 and 2.5) show no significant changes around 1 μm, the approximate size of the intact microorganisms. This confirms that we are measuring the effect of the organics produced by the microorganisms and not the intact microorganisms themselves acting as CCN. A summary of these two experiments and other trials under similar conditions can be found in Tables 2.3 and 2.4. SMPS and APS size distributions of these experiments can be found in Figures 2.4 and 2.5.

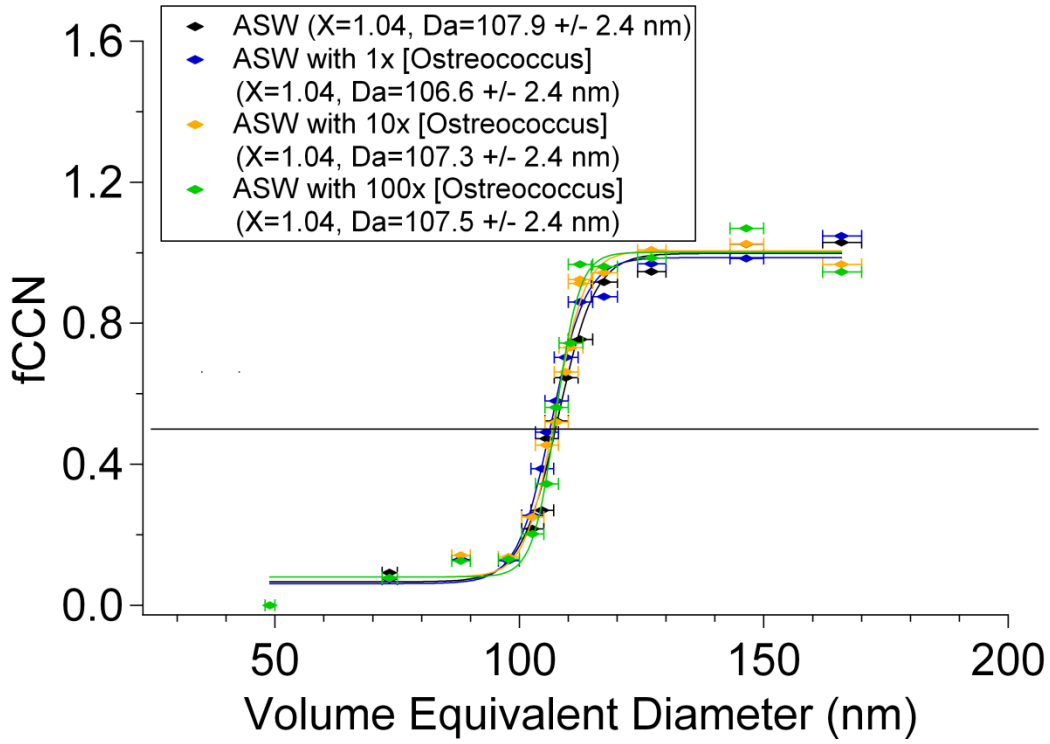

Figure 2.9. CCN curves of Artificial Seawater (ASW) with *Ostreococcus*. Markers are each of the data points collected during each curve. Curve is a sigmoidal fit of each of the markers for the experiment with a shape factor correction (X) of 1.04 for ASW. Activation diameter (Da) was calculated from the x-half value of the sigmoidal fit. Error bars are +/- X of 1.0 and 1.08. The horizontal line indicates the approximate x-half value, set to 0.5 fCCN on the y-axis

Table 2.3. Summary of ASW with Synechococcus CCN experiment activation diameters and experimental conditions with shape factor X=1.04. Uncertainty in Da is shown in parenthesis and is the difference between 1.04 and 1.0/1.08 shape factors. Averages of the shift are shown with standard deviations of all the experiments.
Uncertainty in % S is 10%.
*Experiment 4 is shown in Figure 2.8

Expt	ASW Da (nm)	1x [Synechococcus] Da (nm)	Δ 1x	10x [Synechococcus] Da (nm)	Δ 10x	100x [Synechococcus] Da (nm)	Δ 100x	Filtered Cells Da (nm)	Δ filtered cells	%S	Notes
1	104.5 (2.3)	102.2 (2.3)	-2.3 (3.3)	102.0 (2.3)	-2.5 (3.3)	102.9 (2.3)	-1.6 (3.3)	102.8 (2.3)	-1.7 (3.3)	0.105 (0.011)	fresh
2	112.1 (2.5)	112.1 (2.5)	0.0 (3.5)	111.5 (2.5)	-0.6 (3.5)	113.1 (2.6)	1.0 (3.6)	111.1 (2.5)	-1.0 (3.5)	0.09 (0.009)	fresh
3	110.1 (2.5)	110.3 (2.5)	+0.2 (3.5)	110.4 (2.5)	+0.3 (3.5)	110.1 (2.5)	0.0 (3.5)	109.5 (2.5)	-0.6 (3.5)	0.09 (0.009)	fresh
4*	108.4 (2.4)	108.4 (2.4)	0.0 (3.4)	106.6 (2.3)	-1.8 (3.3)	108.1 (2.4)	-0.3 (3.4)	N/A	N/A	0.106 (0.011)	frozen
Average	N/A	N/A	-0.5 (1.2)	N/A	-1.2 (1.2)	N/A	-0.2 (1.1)	N/A	-1.1 (0.6)	N/A	N/A

Table 2.4. Summary of ASW with Ostreococcus CCN experiment activation diameters and experimental conditions with shape factor X=1.04. Uncertainty in Da is shown in parenthesis and is the difference between 1.04 and 1.0/1.08 shape factors. Averages of the shift are shown with standard deviations of all the experiments. Uncertainty in % S is 10%.
#Experiment 3 repeated 100x experiment after bubbling for 3 hours and 5 hours respectively, pure ASW data invalid
*Experiment 4 is shown in Figure 2.9

Expt	ASW Da (nm)	1x [Ostreococcus] Da (nm)	Δ 1x	10x [Ostreococcus] Da (nm)	Δ 10x	100x [Ostreococcus] Da (nm)	Δ 100x	Filtered Cells Da (nm)	Δ filtered cells
1	111.6 (2.5)	111.2 (2.5)	-0.4 (3.5)	111.9 (2.5)	+0.3 (3.5)	113.0 (2.6)	+1.4 (3.6)	112.0 (2.5)	+0.4 (3.5)
2	107.8 (2.4)	108.5 (2.4)	+0.7 (3.4)	108.5 (2.4)	+0.7 (3.4)	109.2 (2.4)	+1.4 (3.4)	108.1 (2.4)	+0.3 (3.4)
3#	N/A	110.4 (2.5)	N/A	112.4 (2.5)	N/A	111.3 (2.5), 112.2 (2.5), 110.0 (2.5)	N/A	109.9 (2.5)	N/A
4*	107.9 (2.4)	106.6 (2.4)	-1.3 (3.4)	107.3 (2.4)	-0.6 (3.4)	107.5 (2.4)	-0.4 (3.4)	N/A	N/A
5	116.1 (2.6)	116.2 (2.6)	+0.1 (3.7)	115.5 (2.6)	-0.6 (3.7)	113.6 (2.6)	-2.5 (3.7)	N/A	N/A
Average	N/A	N/A	-0.2 (0.8)	N/A	-0.05 (0.7)	N/A	-0.03 (1.9)	N/A	+0.35 (0.07)

2.4.4. CCN activation curves for ASW with both surfactant and microorganisms

Figure 2.10 compares the CCN activation curves of ASW aerosols generated from ASW model seawater with both a surfactant (SDS) and a microorganism (*Ostreococcus*) with shape factors 1.04 with uncertainty bars for a range of shape factors 1.0 to 1.08. The activation curves clearly show that even with 100x the oceanic concentration of *Ostreococcus* and greater than a bilayer of surfactant SDS, there is very minimal change in the CCN activity of ASW aerosols generated by the bubble bursting process, well within the experimental uncertainty.

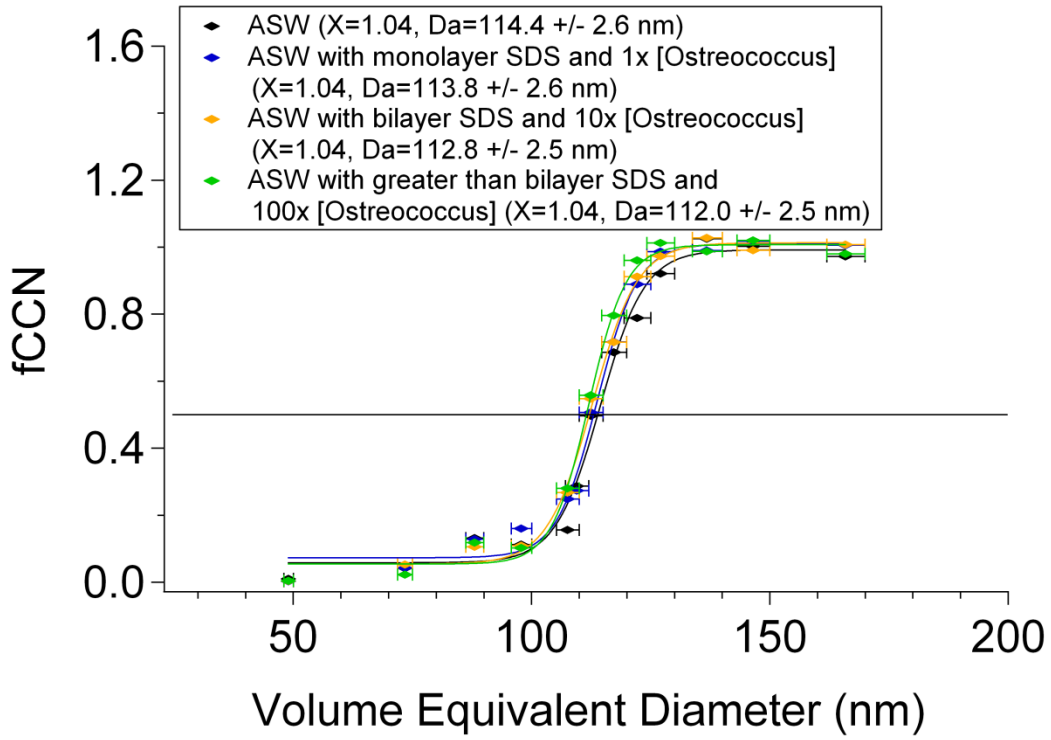

Figure 2.9.CCN curves of Artificial Seawater (ASW) with SDS and *Ostreococcus*. Markers are each of the data points collected during each curve. Curve is a sigmoidal fit of each of the markers for the experiment with a shape factor correction (X) of 1.04 for ASW. Activation diameter (Da) was calculated from the x-half value of the sigmoidal fit. Error bars are +/- X of 1.0 and 1.08. The horizontal line indicates the approximate x-half value, set to 0.5 fCCN on the y-axis.

The activation diameter of the pure ASW in this experiment with a shape factor of 1.04 was 114.4 ± 2.6 nm. Upon addition of 1x the typical oceanic concentration of *Ostreococcus* and a monolayer of SDS to the ASW solution, the activation diameter shifted to smaller sizes by 0.6 ± 3.7 nm. Additional *Ostreococcus* in solution of a 10x and 100x oceanic concentrations with a bilayer and greater than a bilayer of SDS, respectively, resulted in the shift of activation diameters smaller by 1.6 ± 3.6 and 2.4 ± 3.6 nm, respectively when compared to the pure ASW aerosol, indicating a minimal change in CCN activity. A summary of this experiment and another trial under similar conditions can be found in Table 2.5.

Table 2.5. Summary of ASW with SDS and Ostreococcus CCN experiment activation diameters and experimental conditions with shape factor X=1.04. Uncertainty in Da is shown in parenthesis and is the difference between 1.04 and 1.0/1.08 shape factors. Averages of the shift are shown with standard deviations of all the experiments. Uncertainty in % S is 10%.
*Experiment 2 is shown in Figure 2.10

Expt	ASW Da (nm)	Monolayer SDS/1x [Ostreococcus] Da (nm)	Δ 1x/monolayer	Bilayer SDS/10x [Ostreococcus] Da (nm)	Δ 10x/bilayer	Greater than Bilayer SDS/100x [Ostreococcus] Da (nm)	Δ 100x/greater than bilayer	%S	Notes
1	117.0 (2.7)	116.0 (2.6)	-1.0 (3.7)	112.6 (2.6)	-4.4 (3.7)	113.3 (2.6)	-3.7 (3.7)	0.106 (0.011)	frozen
2*	114.4 (2.6)	113.8 (2.6)	-0.6 (3.7)	112.8 (2.5)	-1.6 (3.6)	112.0 (2.5)	-2.4 (3.6)	0.106 (0.011)	frozen
Average	N/A	N/A	-0.8 (0.3)	N/A	-3.0 (2.0)	N/A	-3.1 (0.9)	N/A	N/A

2.4.5 SEM Images

Shown in Figure 2.11, ASW particles bubbled with 100x *Ostreoocccus* collected on stage 8 (0.1-0.3 µm) of the MOUDI show small morphological changes between the particles without *Ostreococcus* and those with *Ostreococcus*. Particles without *Ostreococcus* have a square particle shape characteristic of NaCl cubes. Particles bubbled with *Ostreococcus*, while some of them are square as expected for dried NaCl, some show slightly more rounded shapes. These small visible changes in particle morphology indicate the uptake of organics onto the salt particles, as has been shown previously [*Russell et al.*, 2010; *Wise et al.*, 2009].

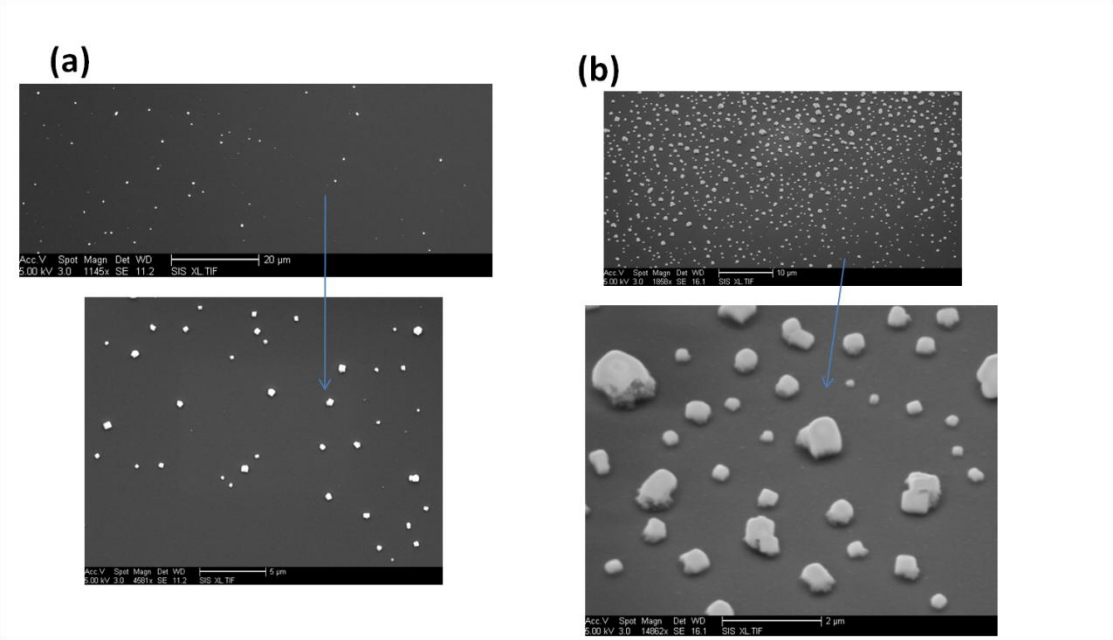

Figure 2.11. SEM images of ASW without (a) and with (b) *Ostreococcus*. Particles without *Ostreococcus* (a) show sharp, square-edged particles, characteristic of NaCl found in ASW. Particles with *Ostreococcus* (b) show more rounded, almost circular particles, indicative of a morphology change of the salt particles, due to the presence of organics from the microorganism cells.

2.4.6 NEXAFS /STXM results

Shown in Figure 2.12a, ASW particles produced without organics show a typical inorganic salt signal of COOH and carbonate, with 280eV and 380 eV edge values. Figure 2.12b shows an ASW particle generated when 100x microorganisms were present, with clear organic peaks for CH_x and C=C. Figure 2.12c shows bulk *Ostreococcus* cells, and matches very closely that of the organic particle shown in (b), suggesting that portions of the cells have been transferred to the SSA. However, the signal of the bulk filtered cells was not obtained, therefore it is unknown if the signal is directly from the cells or the filtered cell material.

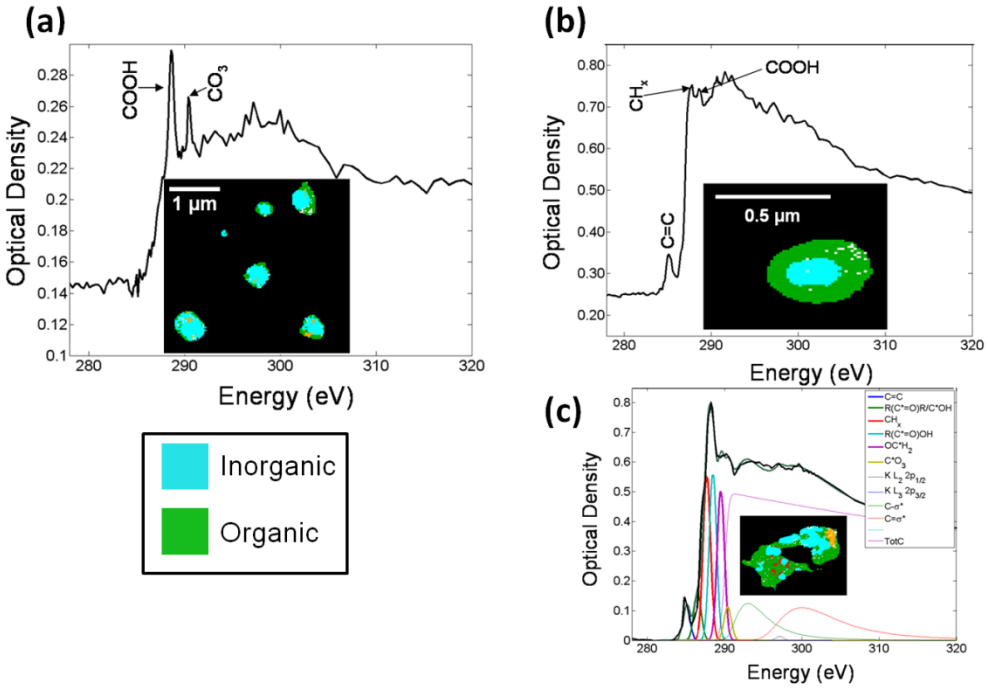

Figure 2.12. NEXAFS/STXM of Bubbled particles. Image (a) shows a STXM spectrum of an ASW particle without organics. Image (b) shows a STXM spectrum of an ASW particle with organics. Image (c) is that of a bulk *Ostreococcus* cell.

Based on the average total carbon derived from the NEXAFS/STXM spectrum for all particles, we determined that there is 34 times more carbon in the ASW particles bubbled with

100x ocean concentrations of organics from microorganisms than those without. Furthermore, there was more of a visible organic coating observed in the images at the carbon K-edge. The ratio of equivalent circular diameters for the organic material to the inorganic was 1.5 and 0.78 for the ASW bubbled with 100x organics from microorganisms and without organics, respectively. Assuming that the particles contain only NaCl and carbon, the mass fraction of carbon:NaCl is 0.27 for ASW particles bubbled with organics and 0.01 for the ASW without organics. This assumes no oxygen, and is considered an upper limit for the amount of carbon that is present. Mass fractions were calculated using Beer's law and absorption cross sections documented in [*Henke et al.*, 1993].

2.4.7 Effect of pure surfactants vs. complex microorganisms on Köhler theory: Possible film formation

Due to the fact that pure oleic acid and SDS caused a change in CCN activity while more the more chemically complex organics produced by *Synechococcus* and *Ostreococcus* did not, a closer look is needed as to what could be producing these results. It has been shown that surfactants such as SDS and hexanoic acid can decrease the uptake of N_2O_5 on sea salt aerosol [*McNeill et al.*, 2006; *Thornton and Abbatt*, 2005]. This is thought to occur due to the formation of a surface layer, or "inverted micelle" by the organic molecules that would affect the transport of molecules across the air-particle interface. In addition, a comparison of the uptake of N_2O_5 on a sulfuric acid solution coated with branched and straight chain organic surfactants showed a significant decrease in N_2O_5 uptake only with straight chain organic surfactants [*Cosman et al.*, 2008]. In those cases a decrease in the uptake coefficient of N_2O_5 was observed for straight chain organic films, while we have observed an increase in CCN activity for straight chain organic films. Another recent study on marine dissolved organic matter (DOM) showed that the primary chemical effect of marine DOM on CCN activity is

through its impact on surface tension [*Moore et al.*, 2008]. Previous theoretical studies of NaCl and SDS show that the SDS should decrease the CCN activity due to the surfactant having a greater effect on displacement of solute NaCl (Raoult effect) than decrease in surface tension (Kelvin effect) [*Li et al.*, 1998]. However, they assumed that the SDS was displacing the NaCl while holding size constant. Taking into account surface-to-bulk partitioning of the surfactants is additionally important for the solute effect (Raoult effect), especially for particles with high salt and low amounts of surface-active organics, which drives the surfactant to the surface [*Abdul-Razzak and Ghan*, 2004; *Prisle et al.*, 2010; *Sorjamaa and Laaksonen*, 2006; *Sorjamaa et al.*, 2004].

Here, we add a very small amount of surfactant to the same amount of soluble solute in the pure NaCl/ASW experiments, and because the CCN activity is increasing, the decrease in surface tension dominates over the solute effect. This could be the reason that there was a net change in CCN activity with the pure surfactants and not with the organics from the microorganisms; the neat film caused a decrease in surface tension which was not offset by a decrease in soluble solute, possibly due to a small amount of organics. Köhler theory calculations show that the increase in the CCN activity for the NaCl with OA and SDS cases would need a reduction in surface tension 1.5-5.7%, which is within previous study estimates for surface tension reduction (0.5-30%) [*Facchini et al.*, 1999; *Fuentes et al.*, 2010b]. Based on the surface tension of pure SDS, this indicates a 21-32% fraction of SDS to water in the droplet [*Mysels*, 1986]. While the organics from the microorganisms, which most likely have many different types of organics associated with them, did not form a film and therefore did not have a net effect on the transport of water across the air-aerosol interface. Figure 2.12 and stated previously in the STXM results, show that the particles produced from bubbling ASW with 100x *Ostreococcus* have 34x more carbon with 27% of the particle mass fraction being

organic. Therefore it appears that the absence of a net change in CCN activity for the microorganisms could be due to a decrease in surface tension being directly offset by a decrease in solute. Köhler theory calculations show that the lack of change in CCN activity for the ASW with *Synechococcus* and *Ostreococcus* cases would need a reduction in surface tension of 14-16% to offset a 27% decrease in solute, assuming the organics from the microorganisms are completely insoluble. A reduction in surface tension of 11-12.5% is needed assuming the organics from the microorganims have a solubility of 1.07 g/ml H_2O and a molecular weight of 132.13 g/mol (glutaric acid) as an upper limit. For the surface tension reduction needed in the cases with organics with microorganisms, the surface tension reduction is also within previous atmospheric calculations of surface tension reduction [*Facchini et al.*, 1999; *Fuentes et al.*, 2010b], similar to the NaCl and OA and SDS cases.

Others have shown via SEM that inorganic particles with submonolayer oleic acid coverage have island formation of the oleic acid molecules, and not films [*Garland et al.*, 2008]. Because it is not known how much oleic acid or SDS is making it to the particles from our bubbling technique, the overall structure is unknown for the oleic acid or SDS on the NaCl particles. However, it is important to note that the islands of oleic acid were found on alumina or polystyrene latex spheres of 1.6 μm in diameter when oleic acid was added via vapor-deposition [*Garland et al.*, 2008]. In our case, the smaller particles were formed from films drops on the surface of the NaCl solution, known to preferentially transfer organics from the surface of a solution [*Blanchard*, 1964]. Our particles could then have a very different structure of oleic acid, but we were not able to determine this via SEM. Size resolved chemical differences could explain the results, but we assume here a single composition for all sizes, which may not always be the case. In both cases, the aerosols were exposed to a much lower RH than would be encountered in the marine atmosphere. Interpretation of both our

results and Garland et al. 2008 results' impacts on understanding organic compounds' interaction with SSA may not be completely representative of what is occurring in the atmosphere.

To address the possibility that the numerous organics from the marine microorganisms may be forming a film, but there may not be surface-active compounds present, we look to the ASW with both *Ostreococcus* and SDS. The results from this experiment are very similar to ASW with *Synechococcus* and *Ostreococcus*; even with SDS, a known surface-active compound present, the mixture of diverse chemical compounds associated with the microorganisms cause a minimal change in the CCN activity, well within the experimental uncertainty. It appears that complex interactions of many organic compounds, including a known surface-active compound SDS, cause no net change in CCN activity when compared to the pure ASW aerosol. It is possible that some lead to a positive shift and some may lead to a negative shift, but the average shift is negligible.

2.4.8 Atmospheric Implications

To determine the potential impact of these findings on climate, we estimated the change in CCN concentrations due to measured CCN activity changes. Using the average shift in activation diameter and the cumulative size distributions from each experiment where a shift occurred, we have estimated the change in concentration of CCN. Our results show, that even for experiments with a larger shift in activation diameter, such as NaCl with SDS of -5.4 ± 2.6 nm, the percent change in the concentration of CCN increased by 2.5%, assuming our experimental particle concentrations 11-640 nm (~20,000 cm^{-3}) scale to remote marine boundary layer concentrations (< 700 cm^{-3})[*Sellegri et al.*, 2008]. Previous modeling studies have shown that for a ~20% increase in CCN concentration, there is a -1 W/m^2 feedback at the top of the atmosphere, as an upper bound [*Facchini et al.*, 1999]. A summary of these results

can be found in Table 2.6. These results show that even under extreme "bloom" conditions, the change in CCN concentrations induced by these two particular microorganisms, *Synechococcus* and *Ostreococcus*, would by themselves have a negligible effect on cloud formation from their resulting SSA, but cannot comprehensively address the role of organics from microorganisms for the entire SSA. This estimate assumes that the changes in organic species at the sea surface do not affect the overall number of particles formed, which the measured size distributions (Figures 2.2-2.5) seem to support.

Table 2.6. Change in CCN concentrations from calculated shifts in activation diameter and measured size distributions using a shape factor of 1.04.

Expt	Average shift (std dev)	Total # concentration 11-600 nm ($\#/cm^3$)	Change in number concentration due to shift ($\#/cm^3$)	Change in CCN concentration (%)
NaCl with greater than bilayer oleic Acid	-2.1 (1.8)	20,300	200	1.0
NaCl with greater than bilayer SDS	-5.4 (2.6)	22,200	550	2.5
ASW with 100x Synechococcus	-0.2 (1.1)	20,200	20	0.1
ASW with 100x Ostreococcus	-0.03 (1.9)	22,700	0	0.0
ASW with greater than bilayer SDS and 100x Ostereococcus	-3.1 (0.9)	22,800	300	1.3

2.5 Conclusions

The CCN activity is investigated for sea spray aerosols produced by bubbling artificial seawater and NaCl solutions containing a range of organic materials from simplistic model systems to more complex mixtures produced by representative marine microorganisms. While the simplistic mixtures showed a clear shift to smaller activation diameters, no significant shift in activation diameter was observed for ASW-complex organic solutions. These observations suggest the formation of a neat film could occur on the top layer of the solution when using the pure surfactants, causing a decrease in surface tension and therefore an increase in CCN activity. In contrast, the microorganisms most likely produce many different types of organic species and thus do not form such an organized film and therefore did not affect the transport of particles across the air-water interface or significantly change the particle surface tension. To show that organics from the microorganisms were indeed transferred to the particles during the bubble bursting process, SEM and NEXAFS/STXM images were acquired. SEM images showed a morphological change in submicron ASW particles upon bubbling with the marine microorganism *Ostreococcus*, supporting the uptake of organic species on these particles. NEXAFS/STXM showed that the organic signature from the ASW particles matched the bulk microorganism signature. Based on the average total carbon derived from the NEXAFS/STXM spectrum for all particles, we determined that there is 34 times more carbon in the ASW particles bubbled with microorganism *Ostreococcus* than those without. In addition, there was more of a visible organic coating observed in the images at the carbon K-edge. Therefore, even with a large increase in the fraction of carbon in the particle, the net change in CCN activity could be due to the decreased surface tension of the particle being offset by the decrease in solute from the displaced salt [*Asa-Awuku et al.*, 2009; *Asa-Awuku et al.*, 2010].

These findings indicate that organic matter from primary production in the ocean, when incorporated into sea spray aerosol particles, can cause a change in sea salt aerosol CCN activity. However, this is strongly dependent on the type and complex mixture of the organic compounds. Simple mixtures of NaCl and oleic acid or SDS were observed to have a small, but notable effect on CCN activity, even in small amounts. However, even in high amounts, diverse mixtures of organics from two marine microorganisms, did not form a film on the sea spray aerosol, even in the presence of a known surface-active compound; and therefore did not significantly change the sea salt aerosol hygroscopicity. These changes in CCN activity for both the NaCl and ASW experiments mixed with surfactants account for < 3% of a change in CCN number concentrations over the remote marine boundary layer and therefore show that under "bloom" conditions, changes in CCN concentration due to change in CCN activity from chemical changes due to inclusion of marine organic matter during bubble bursting sea spray aerosol formation appear to have a limited effect on the climate. However, additional consideration is needed with regard to the effect of the marine environment on the evolution of the organics; UV light can alter the nature of certain organic compounds, which may change the effect of these compound on the CCN activity of the aerosol before cloud droplet activation [*Orellana and Verdugo*, 2003]. While primary production from the ocean may add significant amounts of organic material to sea spray aerosols, this study shows how, as least for this set of microorganisms, the net effect of CCN activity is relatively small. This can most likely be accounted for by the existing large fraction of water-soluble salts having the largest effect on CCN activation.

2.6 Acknowledgements

The authors are grateful to Cassandra Gaston and Drs. Grant Deane and Dale Stokes, at Scripps Institution of Oceanography, for their assistance in validation of the bubbling technique via picture imaging used in these experiments. The authors are also grateful to Jessie Charrier and Ryan Sullivan, Department of Chemistry at UCSD, for helpful discussions on experimental techniques and data interpretation and the Lihini Aluware laboratory, Scripps Institution of Oceanography, for use of their oven for combustion of glassware. Funding for M.J.K.M. was provided by UCSD's Chancellor Interdisciplinary Collaboratories Fellowship. STXM/NEXAFS data was acquired at beamline 5.3.2.2 at the ALS, which is supported by the Director of the Office of Science, Department of Energy, under Contract No. DE-AC02-05CH11231.

Publication Acknowledgement

The text and figures of Chapter 2 of a submitted manuscript: Moore, M.J.K., Furutani, H.; Roberts, G.; Moffet, R.; Giles, M.; Palenik, B.; Prather, K.A., Effect of Organic Matter on Sea Spray Aerosol Production by Bubble Bursting and its Cloud Condensation Nuclei (CCN) Activity, submitted to Atmospheric Environment. The dissertation author was the primary investigator and author of this paper.

2.7 References

Abdul-Razzak, H., and S.J. Ghan, Parameterization of the influence of organic surfactants on aerosol activation, *Journal of Geophysical Research*, *109* (D03205), doi:10.1029/2003JD004043, 2004.

Asa-Awuku, A., G.J. Engelhart, B.H. Lee, S.N. Pandis, and A. Nenes, Relating CCN activity, volatility, and droplet growth kinetics of Beta-caryophyllene secondary organic aerosol, *Atmospheric Chemistry and Physics*, *9*, 795-812, 2009.

Asa-Awuku, A., A. Nenes, S. Gao, R.C. Flagan, and J.H. Seinfeld, Alkene ozonolysis SOA: inferences of composition and droplet growth kinetics from Köhler theory analysis, *Atmospheric Chemistry and Physics*, *10*, 1585-1597, 2010.

Bigg, E.K., and C. Leck, The composition of fragments of bubbles bursting at the ocean surface, *Journal of Geophysical Research*, *113* (D11209), doi:10.1029/2007JD009078, 2008.

Blanchard, D.C., Sea-to-Air Transport of Surface Active Material, *Science*, *146* (3642), 396-397, 1964.

Blanchard, D.C., The Ejection of Drops from the Sea and Their Enrichment with Bacteria and Other Materials: A Review, *Esturaries*, *12* (3), 127-137, 1989.

Cosman, L.M., D.A. Knopf, and A.K. Bertram, N2O5 Reactive Uptake on Aqueous Sulfuric Acid Solutions Coated with Branched and Straigh-Chain Insoluble Organic Surfactants, *Journal of Physical Chemistry A*, *112* (11), 2386-2396, 2008.

Courties, C., A. Vaquer, M. Troussellier, J. Lautier, M.J. Chretiennot-Dinet, J. Neveux, C. Machado, and H. Claustre, Smallest eukaryotic organism, *Nature*, *370*, 255, 1994.

Deane, G.B., and D. Stokes, Scale Dependence of bubble creation mechanisms in breaking waves, *Nature*, *418*, 839-844, 1997.

DeCarlo, P., J. Slowik, D.R. Worsnop, P. Davidovits, and J.L. Jimenez, Particle Morphology and Density Characterization by Combined Mobility and Aerodynamic Diameter Measurements. Part 1: Theory, *Aerosol Science and Technology*, *38* (12), 1185-1205, 2004.

Facchini, M.C., S. Decesari, M. Rinaldi, C. Carbone, E. Finessi, M. Mircea, S. Fuzzi, F. Moretti, E. Tagliavini, D. Ceburnis, and C.D. O'Dowd, Important Source of Marine Secondary Organic Aerosol from Biogenic Amines, *Environmental Science and Technology*, *42* (24), 9116-9121, 2008a.

Facchini, M.C., M. Mircea, S. Fuzzi, and R.J. Charlson, Cloud albedo enhancement by surface-active organic solutes in growing droplets, *Nature*, *401*, 257-259, 1999.

Facchini, M.C., M. Rinaldi, S. Decesari, C. Carbone, E. Finessi, M. Mircea, S. Fuzzi, D. Ceburnis, R. Flanagan, E.D. Nilsson, G. De Leeuw, M. Martino, and J. Woeltjen, Primary submicron marine aerosol dominated by insoluble organic colloids and aggregates, *Geophysical Research Letters*, *35* (L17814), doi:10.1029/2008GL034210, 2008b.

Fuentes, E., H. Coe, D. Green, G. deLeeuw, and G. McFiggans, Laboratory-generated primary marine aerosol via bubble-bursting and atomization, *Atmospheric Measurement Techniques*, *3*, 141-162, 2010a.

Fuentes, E., H. Coe, D. Green, and G. McFiggans, On the impacts of phytoplankton-derived organic matter on the properties of the primary marine aerosol - Part 2: Composition,

hygroscopicity and cloud condensation activity, *Atmospheric Chemistry and Physics Discussions*, *10*, 26157-26205, 2010b.

Garland, E.R., E.P. Rosen, L.I. Clarke, and T. Baer, Structures of submonolayer oleic acid coverages on inorganic aerosol particles: evidence of island formation, *Physical Chemistry Chemical Physics*, *10*, 3156-3161, 2008.

Garrett, W.D., Stabilization of air bubbles at the air-sea interface by surface-active material, *Deep-Sea Research*, *14*, 661-672, 1967.

Gill, P.S., T.E. Graedel, and C.J. Weschler, Organic Films on Atmospheric Aerosol Particles, Fog Droplets, Cloud Droplets, Raindrops, and Snowflakes, *Reviews of Geophysics and Space Physics*, *21* (4), 903-920, 1983.

Guillard, R.R.L., Culture of phytoplankton for feeding marine invertebrates, *In Smith, W.L. and Chanley, M.H. (Eds.) Culture of Marine Invertebrate Animals*, 26-60, 1975.

Henke, B.L., E.M. Gullikson, and J.C. Davis, X-ray interactions: photoabsorption, scattering, transmission, and reflection at E = 50-30,000 eV, Z = 1-92, *Atomic Data and Nuclear Data Tables*, *54* (2), 181-342, 1993.

Kilcoyne, A.L.D., T. Tyliszczak, W.F. Steele, S. Fakra, P. Hitchcock, K. Franck, E. Anderson, B. Harteneck, E.G. Rightor, G.E. Mitchell, A.P. Hitchcock, L. Yang, T. Warwick, and H. Ade, Interferometer-controlled scanning transmission X-ray microscopes at the Advanced Light Source, *Journal of synchrotron radiation*, *10* (2), 125-136, 2003.

Langmann, B., C. Scannell, and C.D. O'Dowd, New Directions: Organic matter contribution to marine aerosols and cloud condensation nuclei, *Atmospheric Environment*, *42*, 7821-7822, 2008.

Lewis, E.R., and S.E. Schwartz, *Sea salt aerosol production: mechanisms, methods, measurements and models: a critical review*, American Geophysical Union, Washington, D.C., 2004.

Li, Z., A.L. Williams, and R. M.J., Influence of Soluble Surfactant Properties on the Activation of Aerosol Particles Containing Inorganic Solute, *Journal of the Atmospheric Sciences*, *55*, 1859-1866, 1998.

Lion, L.W., and J.O. Leckie, The Biogeochemistry of the Air-Sea Interface, *Annual Reviews of Earth and Planetary Science*, *9*, 449-486, 1981.

MacIntyre, F., Top Millimeter of the Ocean, *Scientific American*, *230* (5), 62-69, 75-77, 1974.

Madigan, M.T., J.M. Martinko, P.V. Dunlap, and D.P. Clark, *Brock Biology of Microorganisms*, Pearson Benjamin Cummings, San Francisco, 2006.

McNeill, V.F., J. Patterson, G.M. Wolfe, and J.A. Thornton, The effect of varying levels of surfactant on the reactive uptake of N2O5 to aqueous aerosol, *Atmospheric Chemistry and Physics*, *6*, 1635-1644, 2006.

Meskhidze, N., and A. Nenes, Phytoplankton and Cloudiness in the Southern Ocean, *Science*, *314*, 1419-1424, 2006.

Middlebrook, A.M., D.M. Murphy, and D.S. Thomson, Observations of organic material in individual marine particles at Cape Grim during the First Aerosol Characterizaion Experiment (ACE1), *Journal of Geophysical Research*, *103* (D13), 16475-16483, 1998.

Ming, Y., and L.M. Russell, Predicted hygroscopic growth of sea salt aerosol, *Journal of Geophysical Research*, *106* (D22), 28,259-28,274, 2001.

Modini, R.L., B. Harris, and Z.D. Ristovski, The organic fraction of bubble-generated, accumulation mode Sea Spray Aerosol (SSA), *Atmospheric Chemistry and Physics*, *10*, 2867-2877, 2010.

Moore, R.H., E.D. Ingall, A. Sorooshian, and A. Nenes, Molar mass, surface tension, and droplet growth kinetics of marine organics from measurements of CCN activity, *Geophysical Research Letters*, *35* (L07801), doi:10.1029/2008GL33350, 2008.

Morel, F.M.M., and J.G. Rueter, AQUIL: A chemically defined phytoplankton culture medium for trace metal studies, *J. Phycol.*, *15* (2), 135-141, 1979.

Mysels, K.J., Surface Tension of Solutions of Pure Sodium Dodecyl Sulfate, *Langmuir*, *2*, 423-428, 1986.

Niedermeier, D., H. Wex, J. Voigtlaender, F. Stratmann, E. Brueggemann, A. Kiselev, H. Henk, and J. Heintzenberg, LACIS-measurements and parameterization of sea-salt particle hygroscopic growth and activation, *Atmospheric Chemistry and Physics*, *8*, 579-590, 2008.

Novakov, T., C.E. Corrigan, J.E. Penner, C.C. Chuang, O. Rosario, and O.L. Mayol Bracero, Organic aerosols in the Caribbean trade winds: A natural source? *Journal of Geophysical Research*, *102* (D17), 21,307-21,313, 1997.

O'Dowd, C.D., M.C. Facchini, F. Cavalli, D. Ceburnis, M. Mircea, S. Descesari, S. Fuzzi, Y. Jun Yoon, and J. Putaud, Biogenically driven organic contribution to marine aerosol, *Nature*, *431*, 676-680, 2004.

Orellana, M.V., and P. Verdugo, Ultraviolet radiation blocks the organic carbon exchange between the dissolved phase and the gel phase in the ocean, *Limnology and Oceanography*, *48* (4), 1618-1623, 2003.

Posfai, M., J. Li, J.R. Anderson, and P.R. Buseck, Aerosol bacteria over the Southern Ocean during ACE-1, *Atmospheric Research*, *66*, 231-240, 2003.

Prisle, N.L., T. Raatikainen, A. Laaksonen, and M. Bilde, Surfactants in cloud drop activation: mixed organic-inorganic particles, *Atmospheric Chemistry and Physics*, *10*, 5663-5683, 2010.

Rinaldi, M., M.C. Facchini, S. Decesari, C. Carbone, E. Finessi, M. Mircea, S. Fuzzi, D. Ceburnis, M. Ehn, M. Kulmala, G. De Leeuw, and C.D. O'Dowd, On the representativeness of coastal aerosol studies to open ocean studies: Mace Head – a case study, *Atmospheric Chemistry and Physics*, *9*, 9635-9646, 2009.

Roberts, G.C., and A. Nenes, A Continuous-Flow Streamwise Thermal-Gradient CCN Chamber for Atmospheric Measurements, *Aerosol Science and Technology*, *39*, 206-221, 2005.

Rose, D., G.P. Frank, U. Dusek, S.S. Gunthe, M.O. Andreae, and U. Poschl, Calibration and measurement uncertainties of a continuous-flow cloud condensation nuclei counter (DMT-CCNC): CCN activation of ammonium sulfate and sodium chloride aerosol particles in theory and experiment, *Atmospheric Chemistry and Physics*, *8*, 1153-1179, 2008.

Russell, L.M., L.N. Hawkins, A.A. Frossard, P.K. Quinn, and T.S. Bates, Carbohydrate-like composition of submicron atmospheric particles and their production from ocean bubble bursting, *Proceedings of the National Academy of Sciences of the United States of America*, *107* (15), 6652-6657, 2010.

Russell, L.M., S.F. Maria, and S.C.B. Myneni, Mapping organic coatings on atmospheric particles, *Geophysical Research Letters*, *29* (16), 10.1029/2002GL014874, 2002.

Satheesh, S.K., and K.K. Moorthy, Radiative effects of natural aerosols: A review, *Atmospheric Environment*, *39*, 2089-2110, 2005.

Sellegri, K., C.D. O'Dowd, Y.J. Yoon, S.G. Jennings, and G. de Leeuw, Surfactants and submicron sea spray generation, *Journal of Geophysical Research*, *111* (D22215), doi:10.1029/2005JD006658, 2006.

Sellegri, K., P. Villani, D. Picard, R. Dupuy, C.D. O'Dowd, and P. Laj, Role of the volatile fraction of submicron marine aerosol on its hygroscopic properties, *Atmospheric Research*, *90*, 272-277, 2008.

Smoydzin, L., and R. von Glasow, Do organic surface films on sea salt aerosols influence atmospheric chemistry?- A model study, *Atmospheric Chemistry and Physics*, *7*, 5555-5567, 2007.

Sorjamaa, R., and A. Laaksonen, The influence of surfactant properties on critical supersaturations of cloud condensation nuclei, *Journal of Aerosol Science*, *37*, 1730-1736, 2006.

Sorjamaa, R., B. Svenningson, T. Raatikainen, S. Henning, M. Bilde, and A. Laaksonen, The role of surfactants in Kohler theory reconsidered, *Atmospheric Chemistry and Physics*, *4*, 2107-2117, 2004.

Thornton, J.A., and J.P.D. Abbatt, N2O5 Reaction on Submicron Sea Salt Aerosol: Kinetics, Products, and the Effect of Surface Active Organics, *Journal of Physical Chemistry A*, *109* (44), 10004-10012, 2005.

Waterbury, J.B., S.W. Watson, R.R.L. Guillard, and L.E. Brand, Widespread occurence of a unicellular, marine, planktonic, cyanobacterium, *Nature*, *277*, 293-294, 1979.

Wise, M.E., E.J. Freney, C.A. Tyree, J.O. Allen, S.T. Martin, L.M. Russell, and P.R. Buseck, Hygroscopic behavior and liquid-layer composition of aerosol particles generated from natural and artificial seawater, *Journal of Geophysical Research*, *114* (D03201), doi:10.1029/2008JD010449, 2009.

Worden, A.Z., J.K. Nolan, and B. Palenik, Assessing the Dynamics and Ecology of Marine Picophytoplankton: The Importance of the Eukaryotic Component, *Limnology and Oceanography*, *49* (1), 168-179, 2004.

Chapter 3

A comparison of single particle mixing state and CCN activity during the 2007 and 2008 San Diego Wildfires

3.1 Synopsis

Individual particle size and chemical composition as well as condensation nuclei (CN) and cloud condensation nuclei (CCN) concentrations were measured in real-time during the San Diego wildfires in 2007 and 2008 at the University of California San Diego (UCSD) main campus and Scripps Institution of Oceanography (SIO) Pier. Aerosol hygroscopicity was estimated from the CCN measurements and compared to simultaneous aerosol chemistry and size distribution measurements. During 2007, the sampling sites were located in the much larger fresh fire plume, whereas in 2008 the plumes were smaller and more aged as they were transported from smaller fires 30 to 60 miles away. Near the beginning of the 2007 wildfires, CCN and CN concentrations were ten times higher than normal and biomass burning aerosol (BBA) made up more than 80% of the total number of particles with sizes smaller than 300 nm. In 2008, CCN concentrations were slightly above normal background conditions, while CN concentrations were up to ten times higher than background concentrations and BBA made up more than 60% of the total particles numbers smaller than 300 nm. The BBA chemical signatures were different between the years- in 2007, the two main BBA types were BB nitr-sulf and BB sulf-nitr; while in 2008 BB sulf-nitr and Aged BB were the main types, even though the biomass being burned was similar and included shrubs, duff and some building materials. The low values of the aerosol hygroscopicity parameter (κ) observed in 2007 (κ = 0.018-0.089) and 2008 (κ = 0.01-0.2) indicate that a significant fraction of the BBA particulate mass was composed of components with low hygroscopicities, similar to

ponderosa pine (0.04) [*Carrico et al.*, 2010], however, 2008 was closer to that of continental aerosol (0.27) [*Pringle et al.*, 2010]. The biomass burning emissions measured during these wildfires were on the lower end of the hygroscopicity range previously determined from both controlled burns and ambient measurements [*Carrico et al.*, 2010; *Petters et al.*, 2009a].

3.2 Introduction

Biomass burning represents a significant source of aerosols and gaseous pollutants in many regions of the world [*Kaufman et al.*, 2005]. Biomass burning aerosol particles (BBA) are a common component of tropospheric aerosol and have been observed in many locations [*Andreae*, 1983; *Guazzotti et al.*, 2003; *Hudson et al.*, 2004; *Kaufman et al.*, 2005; *Moffet et al.*, 2008a; *Posfai et al.*, 2003; *Yokelson et al.*, 2009]. Since most BBA are smaller than 400 nm [*Posfai et al.*, 2004; *Posfai et al.*, 2003; *Reid et al.*, 2005], their removal from the atmosphere is dominated by cloud droplet activation and wet deposition instead of dry deposition processes [*Lee et al.*, 2006]. BBA can also become transported to high altitudes and undergo long range transport, affecting global climate [*Guazzotti et al.*, 2003; *Ramanathan et al.*, 2001; *Tivanski et al.*, 2007]. Risk of wildfires represents a growing concern because of increased dryness in certain regions due to a warming climate [*Andreae and Rosenfeld*, 2008]. BBA can either increase or decrease cloud cover by modifying cloud microphysics, and can directly alter radiative transfer by absorbing and reflecting radiation. These aerosol-cloud-climate feedbacks represent some of the largest uncertainties in climate research [*Crutzen and Andreae*, 1990; *Kaufman and Fraser*, 1997; *Kaufman and Koren*, 2006; *Petters et al.*, 2009b; *Rosenfeld*, 1999; *Solomon et al.*, 2007]. Biomass burning can cause intense convection, transporting the aerosol to high altitudes in the atmosphere [*Andreae et al.*, 2004; *Mircea et*

al., 2005; *Val Martin et al.*, 2010]. The resulting high updraft velocities can produce large water supersaturations, causing the BBA to nucleate cloud droplets.

Due to the abundance, cloud interactions, and wet removal of BBA, it is especially important to understand its interaction with water. Uptake of water by aerosols is controlled by particle size and chemical composition. Heterogeneous interactions of BBA with water can in turn alter the physical and chemical properties of the particles [*Ansari and Pandis*, 2000; *Jacobson et al.*, 2000; *Khlystov et al.*, 2005]. Hygroscopicity strongly influences the size, refractive index, light scattering, and cloud condensation nuclei (CCN) activity of aerosols. Understanding how these properties evolve over time in the atmosphere is essential for understanding the aerosol direct and indirect effects on the global radiation budget [*Andreae and Rosenfeld*, 2008; *Solomon et al.*, 2007].

The fire type, fuel type, and age of the smoke all represent important factors that determine the size, chemical composition and resulting hygroscopic and optical properties of BBA [*Carrico et al.*, 2008; *Carrico et al.*, 2010; *Hungershoefer et al.*, 2008; *McMeeking et al.*, 2009; *Petters et al.*, 2009a; *Reid et al.*, 2005]. Flaming fires (pyrolysis) tend to produce particles with higher inorganic content and more elemental carbon, while smoldering fires (charring) tend to produce more organic carbon rich aerosol [*Carrico et al.*, 2010; *Hopkins et al.*, 2007; *Li et al.*, 2003; *Petters et al.*, 2009a; *Posfai et al.*, 2003; *Reid et al.*, 2005; *Semeniuk et al.*, 2006; *Yamasoe et al.*, 2000]. If the particles contain relatively low levels of inorganic salts that can absorb water, they may exist as tarballs [*Posfai et al.*, 2004]. In fact, fire type can be more important than fuel type in determining the chemical signatures of the resulting particles [*Weimer et al.*, 2008]. A wide range of aerosol hygroscopicity (κ = 0.04-0.7) has been measured during laboratory fuel burns that strongly depended on the fuel type [*Carrico et al.*, 2010; *Petters et al.*, 2009a]. Large particle volume fractions of soluble inorganic and

organic compounds can make BBA hygroscopic and thus efficient CCN [*Jacobson et al.*, 2000; *Novakov and Corrigan*, 1996]. The hygroscopicity of some of these organic compounds enable cloud droplet activation without the addition of inorganic compounds [*Novakov and Corrigan*, 1996]. Previous field studies have shown that knowledge of the contribution of water soluble organic carbon (WSOC) is essential for predicting the hygroscopicity of ambient aerosol [*Chang et al.*, 2007; *Mircea et al.*, 2005; *Rissler et al.*, 2004; *Roberts et al.*, 2002].

Fresh biomass burning particles, consisting primarily of potassium chloride salts and organic carbon [*Allen and Miguel*, 1995; *Formenti et al.*, 2003; *Li and Shao*, 2010], can be readily converted to potassium nitrate (KNO_3) and potassium sulfate (K_2SO_4) via heterogeneous reactions with secondary acids such as HNO_3 and H_2SO_4 during atmospheric transport [*Gaudichet et al.*, 1995; *Li et al.*, 2003; *Li and Shao*, 2010; *Liu et al.*, 2000; *Trebs et al.*, 2005]. These heterogeneous reactions have important implications for BBA hygroscopic properties; the deliquescence relative humidity (DRH) of K_2SO_4 and KNO_3 are 97.4 and 92.5%, respectively, while that of KCl is 84.3% [*Li et al.*, 2003]. These reactions are also an important source of chlorine gases to the atmosphere [*Thornton et al.*, 2010].

A total of 300,000 and 4,000 acres burned in San Diego County (SDC) during the fall 2007 and 2008 fires, respectively [*CalFire*, 2008; *Grijalva et al.*, 2008]. While the locations of the fires varied from 2007 to 2008, the main biomass that was burned during these fire events was Chaparral, typically found in Southern California, consisting of shrubs and duff including chamise, hoaryleaf ceanothus, and manzanita [*McMeeking et al.*, 2009]; in addition to the burning of many more buildings in 2007. In 2007 and 2008, particle number concentrations were 10 times higher than normal background, especially for particles with diameters < 300 nm. In this study, we compare CCN concentrations and aerosol hygroscopicity with submicron single-particle size and chemical composition in various air masses during these

two different fire-influenced periods in San Diego County. We investigate the different factors that influenced aerosol chemical composition and the resulting hygroscopicity during periods influenced by the wildfires.

3.3 Materials and Methods

3.3.1 Sampling locations and instrumentation 2007

Ambient particles were sampled from outside the laboratory on the second floor of Urey Hall (32°52'31.66"N, 117°14'28.64"W) on the campus of the University of California, San Diego (UCSD) from Sunday, October 21 to Thursday, November 1, 2007. The aerosol was sampled through a 3/8" stainless steel tube that extended outside through the exterior wall, and was delivered to the various instruments. The lab is located approximately 1 km from the Pacific Ocean coastline at an elevation of ~130 m above sea level. Single particle aerodynamic size and chemical composition were measured in real-time with an ultrafine aerosol time-of-flight mass spectrometer (UF-ATOFMS) equipped with an aerodynamic lens that transmitted an aerodynamic diameter (D_a) size range from 100 to 1000 nm. Single particles are sized based on their time-of-flight between two 532 nm CW lasers and then ablated and ionized by a Q-switched 266 nm Nd:YAG laser. The resulting positive and negative ions are analyzed by a dual-polarity reflectron time-of-flight mass spectrometer. Further details on the UF-ATOFMS instrument design and operation are described elsewhere [*Su et al.*, 2004], however, a Micro-Orifice Uniform Deposit Impactor (MOUDI) was not used upstream of the UF-ATOFMS to cut out larger particles. The particle size distributions were measured concurrently by a scanning mobility particle sizer (SMPS, TSI Model 3936) with sheath and aerosol flows of 4.0 and 0.4 slpm, respectively. CCN concentrations were measured with a streamwise thermal-gradient CCN counter at a supersaturation of 0.29%

[*Roberts and Nenes*, 2005]. The instrument was calibrated before use with ammonium sulfate aerosol (99.999%, Sigma Aldrich) using thermodynamics from the Aerosol Inorganic Model (AIM) [*Wexler and Clegg*, 2002], and a surface tension of pure water at 298.15 K. Total particle condensation nuclei (CN) concentrations were measured with a condensation particle counter (CPC, TSI model 3007). The fraction of CCN active particles, or fCCN, was obtained from the CCN/CN ratio. Due to the 10 nm lower size limit of the CPC, CN is more precisely CN_{10}, and therefore fCCN is more precisely $fCCN_{10}$. For simplicity, we will refer to $fCCN_{10}$ as fCCN for the remainder of the paper. A second CCN counter and CPC (TSI model 3010) was located at the Scripps Institution of Oceanography (SIO) Pier (32° 51'47.232"N, 117° 15'21.6"W) and the CCN operated at a supersaturation of 0.13%. The sampling inlet on the SIO Pier was approximately 12 meters above sea level and 400 meters out over the water from the beach. We will refer to the Urey Hall CCN as CCN_0.3 and the SIO Pier CCN as CCN_0.1. Meteorological data (relative humidity, wind speed, and wind direction) was also obtained from the SIO pier.

3.3.2 Sampling locations and instrumentation 2008

During 2008, the same experimental setup was used as in 2007, in Urey Hall at UCSD, from Tuesday October 14th through Tuesday October 21st, with the following differences. The CCN counter previously used in 2007 was calibrated to have a supersaturation (SS) of 0.33%. Total particle condensation nuclei (CN) concentrations were measured with a condensation particle counter (CPC, TSI model 3010) and meteorological data was obtained from Tioga Hall, approximately 400 meters to the north of Urey Hall on the UCSD upper campus. There were no measurements at the SIO Pier in 2008.

3.3.3 ATOFMS data analysis

The UF-ATOFMS single particle data were automatically sorted and grouped into clusters of particles with similar mass spectral characteristics using the adaptive resonance theory neural network algorithm, ART-2a. The main user-defined parameters for ART-2a are the learning rate, number of iterations, and vigilance factor, which were set to 0.05, 20, and 0.80, respectively [*Rebotier and Prather*, 2007]. The resulting clusters were then analyzed manually and classified into distinct particle types based on their mass spectral features [*Furutani et al.*, 2008; *Guazzotti et al.*, 2003; *Moffet et al.*, 2008a; *Silva et al.*, 1999; *Sullivan et al.*, 2007]. The specific focus of this manuscript is on particles with vacuum aerodynamic diameters of 100-300 nm. Temporal-mass searches were run on specific biomass burning and aging markers as shown in Table 3.1.

Table 3.1. Overview of various chemical markers used in this study [*Silva et al.*, 1999].

Mass to charge (m/z)	Ion marker/chemical formula	Name/identification	Mass to charge (m/z)	Ion marker/chemical formula	Name/identification
+18	NH_4^+	Ammonium	-46	NO_2^-	Nitrite
+39/41	K^+	Potassium	-62	NO_3^-	Nitrate
+86	$(C_2H_5)_2NCH_2^+$	Amine	-80	SO_3^-	Sulfite
+101	$(C_2H_5)_3N^+$	Amine	-89	$COOHCO_2^-$	Oxalate
+113	K_2Cl^+	Potassium chloride	-97	HSO_4^-	Bisulfate
+159	$NaKHSO_4^+$	Sodium potassium bisulfate	-125	$H(NO_3)_2^-$	Nitrate
+213	$K_3SO_4^+$	Potassium sulfate			

3.3.4 Single hygroscopicity parameter

To directly compare the hygroscopicity measurements made with the CCNcs to the composition measurements, a single parameter for particle hygroscopicity (κ) is used [*Petters and Kreidenweis*, 2007]. The following equation defines the relationship between a growing particle's equilibrium water saturation ratio, S, droplet diameter, D, dry diameter, D_{dry}, and hygroscopicity, κ:

$$S(D) = \frac{D^3 - D_{dry}^3}{D^3 - D_{dry}^3(1-\kappa)} \exp\left(\frac{A}{D}\right) \qquad (3.1)$$

where $A = 2.1\text{x}10^{-9}$ m is a constant evaluated for a surface tension of 0.072 J m^{-2} (pure water) and temperature of 298.15 K [*Petters and Kreidenweis*, 2007]. κ describes a particle's water activity and typical values range from 1.4 (hygroscopic soluble salt; NaCl) to about 0 (insoluble but wettable) for atmospherically relevant systems. The CCN activation diameter (D_{act}) of atmospheric aerosols was estimated using the measured size distributions, CN, and CCN concentrations:

$$1 - \frac{CCN}{CN} = \frac{\int_{D_0}^{D_{act}} n(D)dD}{N_{total}} \qquad (3.2)$$

where N_{total} is the cumulative concentration obtained by integrating the observed size distribution of $n(D)$, D is the electric mobility diameter selected by the SMPS and D_o the smallest size measured by the SMPS (~11 nm). The CCN/CN ratio represents the fraction of the CN that activate to form CCN (fCCN). Eqn. (3.2) assumes that all particles are internally mixed and have the same average composition. This approach was taken to simplify the data analysis yet still reflects how much the relative degree of variation in the chemical composition affects CCN activity, as the size resolved chemistry was simultaneously

measured [*Furutani et al.*, 2008]. Therefore, the changes in κ represent the overall changes in both the fractions of particle types and the changes in temporal chemistry on each of those particle types, including particles below the limit of detection of chemical measurements (< 100 nm). We use the previously estimated approximate relationship $D_{act} \sim \kappa^{-1/3}$ [*Shinozuka et al.*, 2009]. In estimating D_{act}, contributions from particles larger than the 600 nm upper limit of the SMPS were not considered. However, contributions of particles > 600 nm were most likely low and made minor contributions to the total aerosol concentration, as biomass burning particles are primarily less than 400 nm [*Reid et al.*, 2005].

In order to determine D_{act}, and therefore κ, particle size distributions are needed. Since particle size distributions were only measured on the UCSD upper campus, we used the UCSD CN and SMPS data with SIO CCN data to estimate κ_0.1. Due to the good correlation between UCSD CCN_0.3 and SIO CCN_0.1 (R^2=0.88) (the two instruments were about 1 km apart); the use of UCSD SMPS data for determining κ_0.1 should provide a reasonable approximation (see Figure 3.1). SIO CN concentrations were systemically lower than UCSD CN, while CCN_0.1 (SIO) was systemically higher than CCN_0.3 (UCSD), though most of the time within 10%. The systematic difference between the two sites was probably due to differences in the particle size distributions; the SIO pier most likely had a higher number of larger particles with a lower cumulative concentration. Assuming the size distributions at the pier were slightly larger than upper campus, the κ_0.1 values reported represent an upper limit.

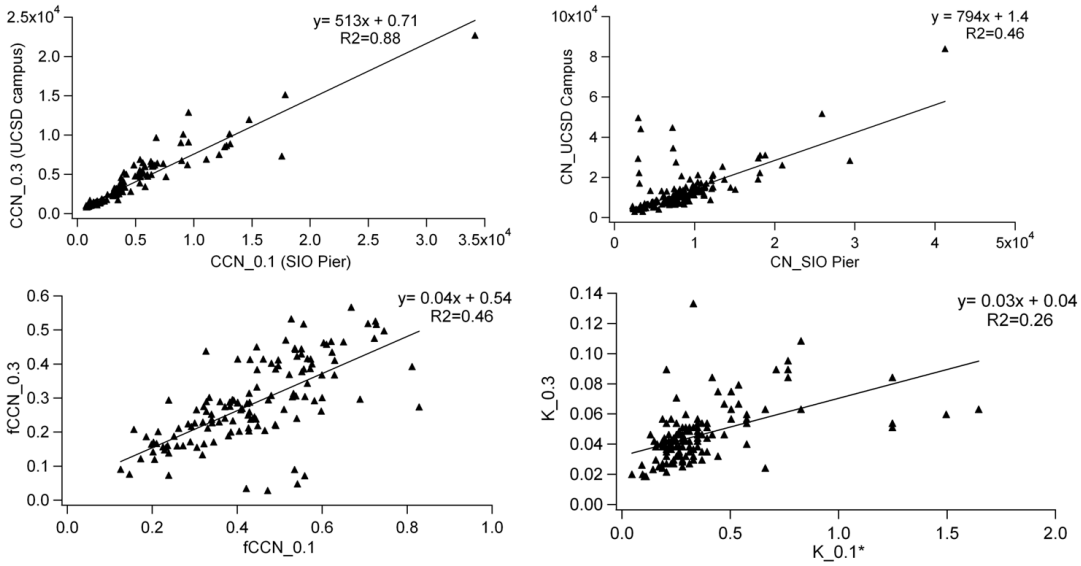

Figure 3.1. Scatter plots of CCN_0.3 vs. CCN_0.1, total particle concentration at both sites (CN), hygroscopicity parameter (κ) and CCN/CN activation ratio (fCCN).
* κ _0.1 was calculated with the SIO Pier CCN and UCSD main campus CN and SMPS.

3.4 Results and Discussion

3.4.1 Meteorology and wildfire observations

From October 21st to November 1st 2007, biomass burning aerosols dominated the atmosphere in San Diego County due to the proximity of large fires less than 25 km away from UCSD. Again in 2008, from October 14th through October 21st, another wildfire event occurred in San Diego County, but this time the fires were much smaller, centered farther away, and produced a smaller footprint in the region. Both years, the study can be divided into five different time periods based on the Urey Hall laboratory-based CCN and fCCN (CCN_0.3, fCCN_0.3), size distributions, particle chemistry, and air mass back trajectories. HYSPLIT air mass back trajectories during different time periods (1 though 5) are displayed in Figure.3.2. Figure 3.3 shows an overview of CCN, κ, size distributions, and meteorological data; a summary of time periods and their CCN, fCCN, κ, CN, size distributions, particle chemistry and HYSPLIT is provided in Table 3.2a and 3.2b for 2007 and 2008, respectively.

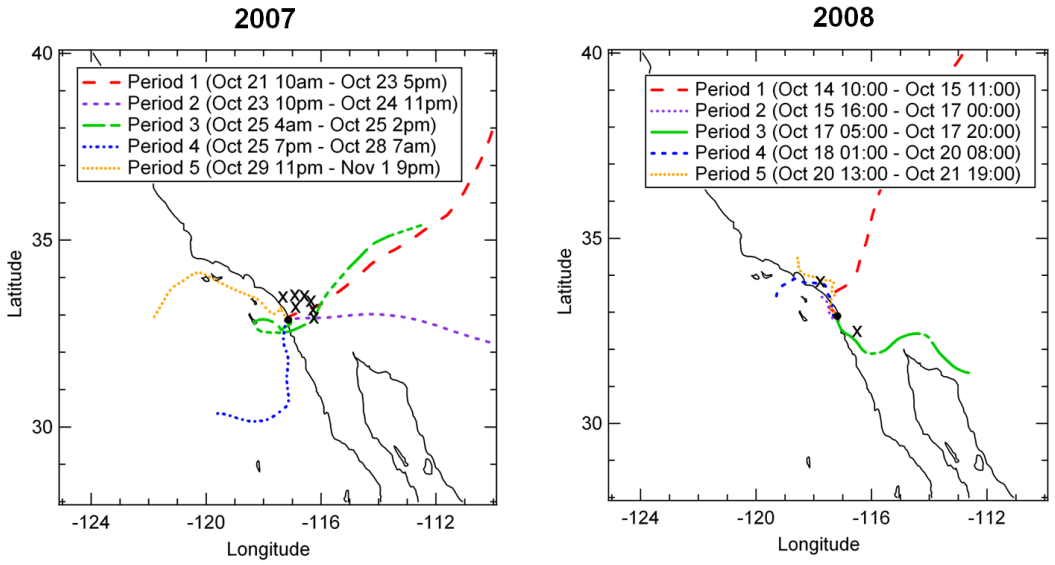

Figure 3.2. HYSPLIT back trajectories during wildfire sampling period during 2007 (left) and 2008 (right) fires. Each line is a representative 48 hour back-trajectory during that period at 500 m. Corresponding periods for comparison to sampling data are in parenthesis. Black circle marks approximate sampling location, 'X' marks note the approximate locations of the fires.

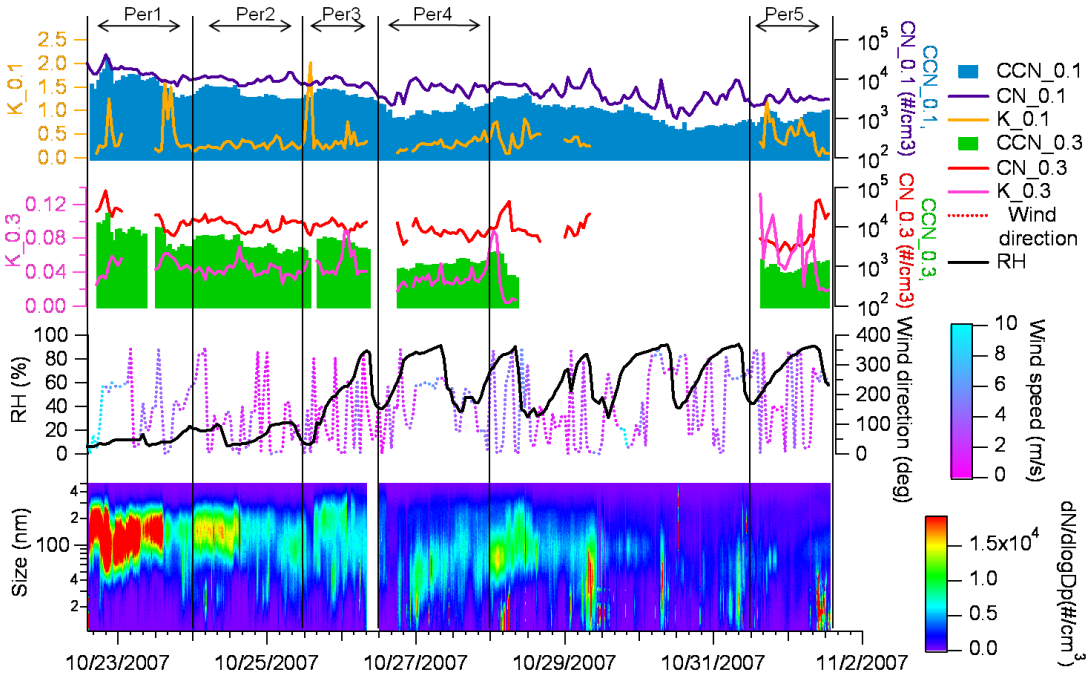

Figure 3.3a. 2007 overview of SIO CCN (CCN_0.1) and Urey Hall CCN (CCN_0.3) concentrations (S = 0.13%, 0.29% respectively), κ_0.1, κ_0.3, meteorological data and Urey Hall SMPS.

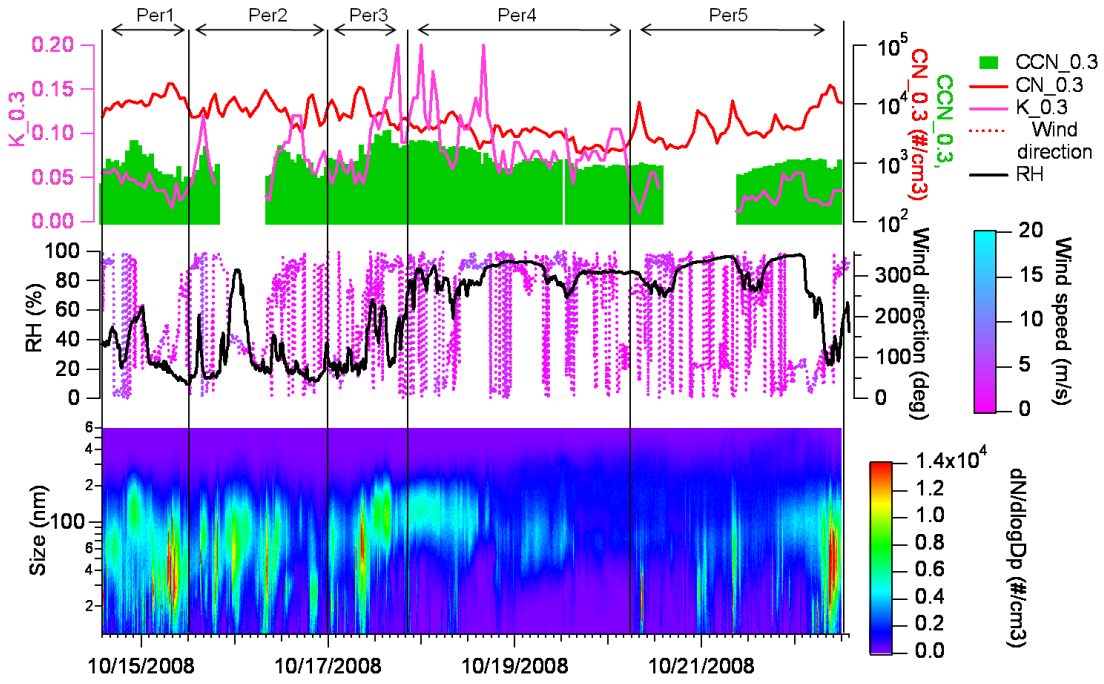

Figure 3.3b. 2008 overview of CCN, κ, meteorological data and SMPS.

Table 3.2a. 2007 overview of different Urey Hall and SIO CCN periods based on CCN activity, size distributions, particle chemistry and HYSPLIT back trajectories (see dividing lines in Fig. 3.3a). All numbers are averages for those time periods with one standard deviation.

Period Name time	fCCN_0.1	CCN_0.1 (#/cm^3)	CN_0.1 (#/cm^3)	K_0.1	fCCN_0.3	CCN_0.3 (#/cm^3)	CN_0.3 (#/cm^3)	K_0.3	SMPS dN/dlog D_p mode (min/max)	Biomass Particle Chemistry	HYSPLIT
1. Santa Ana Fire 10/22-10/23	0.60 +/- 0.15	9600 +/- 5974	15477 +/- 6896	0.5 +/- 0.4	0.36 +/- 0.09	7448 +/- 4453	21984 +/- 17906	0.05 +/- 0.05	125 nm (11.8/209.1)	Larger inorganic signatures	Strong Santa Ana
2. Local stagnation 10/24-10/25 12:00	0.47 +/- 0.13	4567 +/- 1437	9941 +/- 1948	0.3 +/- 0.08	0.34 +/- 0.11	4114 +/- 1531	12495 +/- 3485	0.04 +/- 0.008	150 nm (25.9/209.1)	Small increase in ammonium	Stagnated; from ocean and inland
3. 1st Ammonium Period 10/25 12:00- 10/26 12:00	0.53 +/- 0.08	4267 +/- 990	8160 +/- 1843	0.4 +/- 0.4	0.36 +/- 0.10	4013 +/- 1208	11047 +/- 2578	0.05 +/- 0.02	190 nm (27.9/299.6)	Large increase in ammonium	From ocean
4. 2nd Ammonium period 10/26 12:00- 10/28 00:00	0.33 +/- 0.15	1610 +/- 446	5641 +/- 2136	0.3 +/- 0.1	0.17 +/- 0.06	1195 +/- 243	7570 +/- 2627	0.03 +/- 0.008	60 nm (15.1/278.8)	Ammonium signal still high	From coast, ocean, inland
5. Local background 10/31 12:00- 11/1 12:00	0.39 +/- 0.11	1177 +/- 352	3106 +/- 722	0.5 +/- 0.3	0.20 +/- 0.09	1035 +/- 275	10038 +/- 13227	0.06 +/- 0.03	20nm (14.6/117.6)	Many particle types; none specifically tracking CCN	From North along coast

Table 3.2b. 2008 overview of different CCN periods based on CCN activity, size distributions, particle chemistry and hysplit back trajectories see dividing lines in Fig 3.3b). All numbers are averages for those time periods with one standard deviation.

Period	CCN (#/cm^3)	CN (#/cm^3)	fCCN	K	SMPS mode (min/max)	Biomass Particle Chemistry	HYSPLIT
1. Santa Ana 10/14 13:00-10/15 11:00	1076.86 +/- 564.39	11982.90 +/- 4097.30	0.1 +/- 0.06	0.04 +/- 0.01	35 nm (12.6/135.8)	Larger inorganic signatures, lower ammonium	Strong Santa Ana
2. Stagnated local 10/15 12:00-10/16	1020.46 +/- 418.93	8486.20 +/- 3385.16	0.15 +/- 0.09	0.07 +/- 0.03	62 nm (11.8/113.4)	Similar to Period 1	Stagnated; from ocean and inland
3. S/SE 10/17-10/17 20:00	1812.45 +/- 827.10	8254.39 +/- 4251.14	0.27 +/- 0.17	0.09 +/- 0.04	85 nm (16.8/135.8)	Gradual increase in ammonium and amines	From south, SE over land
4. Fog 10/17 21:00-10/20 08:00	1291.29 +/- 527.96	3347.34 +/- 1605.09	0.42 +/- 0.13	0.09 +/- 0.04	95 nm (24.1/259.5)	Large decrease in nitrate, sulfate, organic acids	From North over ocean
5. North over land 10/20 09:00-10/22 12:00	933.70 +/- 169.89	5425.01 +/- 4252.26	0.21 +/- 0.10	0.03 +/- 0.01	69 nm (11.8/216.7)	Ammonium still higher, nitrate, sulfate and organic acids increase again	From North over land

In 2007, the surface winds were much stronger and transported over longer distances, allowing the fires to arrive much more quickly at the sampling site, whereas in 2008 the winds were weaker and more stagnant for all periods, resulting in larger impacts from local sources. During period 1 for both wildfire studies, the air mass back trajectories were coming from northeast of the sampling location (Santa Ana Winds), bringing hot and dry air to San Diego (Figures 3.2 a,b). In 2007, these back trajectories then shifted to the east (during period 2), while in 2008, the back trajectories stagnated over San Diego. During period 3 in both 2007 and 2008, the airmass back trajectories passed over the ocean, which contributed to a large increase in RH, going from dry air (RH~20%) to humid air (~80%) (Figures 3.3 a,b). However, in 2007 these back trajectories, while locally stagnated, did still have some inland influence from the NE direction; while in 2008, the back trajectories were from the south along the coast and then inland. This difference contributed to sustained high RH (around

80%) in 2008, while in 2007, the time series exhibit a diurnal pattern of RH, peaking at 80% at night and decreasing to ~40% during the day. For period 4 in 2007, the airmass back trajectories came from the south over the ocean (like period 3 in 2008), while period 4 in 2008 was from the north over the land and the ocean along the coast. The RH trends continued during this period with 2007 having a diurnal pattern and 2008 staying constantly high, which was due to a prolonged fog event. During period 5, both 2007 and 2008 experienced normal San Diego conditions, with air masses coming from the NW along the coast, however, during 2008 the fog event still persisted during Period 5. The similar airmass back trajectories during the biomass burning dominated periods make it possible to perform an inter-year comparison of aerosol size, composition, and hygroscopicity. Figure 3.3a shows that during 2007, both CCN_0.3 and CCN_0.1 concentrations were highest during the beginning of the fires (~14,000 and 17,000/cm^3, respectively) when the SMPS also showed the highest particle concentrations while the RH and wind speed were low. After this initial period, CCN and SMPS concentrations decreased and RH and wind speed increased. However, in 2008, CCN_0.3 was the highest during the middle of the fires (2600/cm^3) around October 17th and 18th while RH shifted to higher values and the SMPS shifted to larger sizes as shown in Figure 3.3 b. For both years, the highest impact from fresh fires was at the very beginning of both studies, before and including October 23rd in 2007, and before October 15th in 2008.

3.4.2 Overall Particle Composition

The ATOFMS has previously been used to determine biomass burning markers from burning Southern California biota [*Silva et al.,* 1999]. Fine particle potassium with carbonaceous signatures are known to be markers for biomass combustion [*Andreae,* 1983; *Fine et al.,* 2004; *Li et al.,* 2003; *Reid et al.,* 2005; *Silva et al.,* 1999]. Single-particle mass spectrometry in real time with the ATOFMS allows us to track mixing state and chemical

composition changes with high time resolution. During both wildfire events, the dominant particle types in the 100-300 nm size range were from biomass burning. The top biomass burning particle type for period 1 for each year is shown in Figure 3.4. Characteristics of biomass particles include an intense potassium peak (m/z +39), with smaller sodium (m/z +23), organic markers ($C_2H_3^+$, m/z +27), potassium chloride (K_2Cl^+, m/z +113), sodium potassium sulfate ($NaKHSO_4^+$, m/z +159) and potassium sulfate ($K_3SO_4^+$, m/z +213) ions in the positive mass spectrum. The negative ion mass spectrum shows nitrate (NO_2^-, NO_3^-, m/z -46,-62), sulfate (HSO_4^-, m/z -97) and some sugar markers (CN^-, CNO^-, m/z -26, -42). It has been shown that both sulfate (KSO_4^-, m/z -135; $K(HSO_4)_2^-$, m/z -233; $K_2HSO_4^+$, m/z +175; $Na_2KSO_4^+$, m/z +181; $Na_2K_2SO_4^+$, m/z +197; $K_3SO_4^+$, m/z +213) and nitrate (K_2NO_2, m/z +124; K_2NO_3, m/z +140; $K(NO_3)_2$, m/z -163) can be internally mixed with potassium in biomass burning single particles produced from flaming fires [*Silva et al.*, 1999]. In 2007 the top biomass particle type 100-300 nm was characterized by an intense potassium peak with nitrate peaks more intense than the sulfate peak (BB nitr-sulf), representing up to 60% of all biomass burning particles over the course of the study. In 2008, the top biomass particle type in the 100- 300 nm size range was characterized by an intense potassium peak with the sulfate peak more intense than nitrate peaks (BB sulf-nitr), and made up > 50% of all biomass particles over the course of the study. The higher intensity of sulfate over nitrate in 2008 compared to 2007 in the main BBA particle types was most likely due to the higher RH during period 1 in 2008, (~20-60%) which most likely contributed to increased aqueous phase production of particulate sulfate [*Hegg et al.*, 1996; *Sorooshian et al.*, 2006]. Other BBA types also had an intense potassium peak mixed with soot and/or organic carbon; and sometimes with no negative ions (pos only). Positive ion only spectra (pos only) were most likely highly aged and as a result classified as aged throughout this study; it is well documented that as

particles become atmospherically processed they increase their hygroscopicity, causing an increase in water uptake. This uptake of water on the particles suppresses negative ion formation, resulting in spectra with no negative ions [*Moffet et al.*, 2008b; *Neubauer et al.*, 1998]. A higher prevalence of pos only BBA in 2008 indicates the particles contained more water and most likely underwent a higher degree of atmospheric processing, due to the higher RH/fog in 2008.

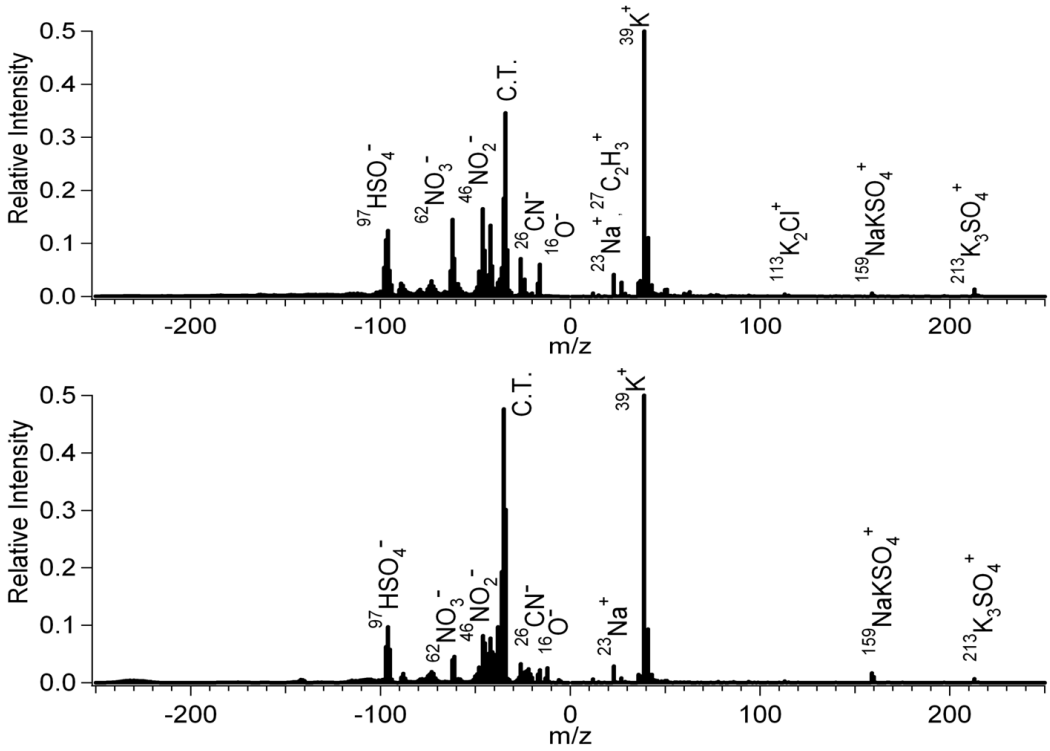

Figure 3.4a,b. Top biomass particle type mass spectrum/weight matrix for period 1 of each year, 2007 (BB nitr-sulf, top) and 2008 (BB sulf-nitr, bottom). Positive ions are shown to the right of center and negative ions to the left of center. Peak labeled CT in the negative ion spectrum indicates signal cross-talk, or noise, from the positive ion detector.

Other particle types observed were soot, soot mixed with organic carbon (soot-OC), organic carbon (OC), metals, and amines. Soot particles are defined by their distinctive carbon atom clusters every 12 m/z in both the positive and negative mass spectrum. Soot-OC particles

are defined by the presence of some distinctive carbon atom clusters with the presence of other smaller organic peaks (C_3H^+, m/z +37; $C_2H_3O^+$, m/z +43). OC particles are similar to the biomass burning mass spectrum described previously without the characteristic potassium marker [*Toner et al.*, 2008]. The relatively constant matrix of the BBA particles allows us to examine relative abundances of various chemical species by tracking their ion peak areas in a specific particle type [*Sullivan et al.*, 2007; *Sullivan and Prather*, 2007]. The main ion peaks used in this manuscript are listed in Table 3.1.

3.4.2.1 2007 Overall Particle Composition

Near the beginning of the wildfires, the biomass burning particles were relatively fresh and consisted generally of KCl and organic compounds, as has been reported in other studies [*Allen and Miguel*, 1995; *Formenti et al.*, 2003; *Li and Shao*, 2010]. As the biomass particles aged and the fires transitioned from flaming to smoldering fires, they showed increasing amounts of $KHSO_4$ compounds, and aged organic compounds as shown in similar studies [*Gaudichet et al.*, 1995; *Li et al.*, 2003; *Li and Shao*, 2010; *Liu et al.*, 2000; *Trebs et al.*, 2005]. The temporal counts and fraction of >90% of classified 100-300 nm particles are shown in Figure 3.5a. After October 25th 2007, the contribution of BBA to particles 100-300nm decreased from greater than 90% to around 60% (Figure 3.5a). The top two BBA types, BB nitr-sulf and BB sulf-nitr, make up > 90% of the BBA with the contributions of the top 5 types making up > 98% of the BBA. Soot and soot with OC (soot-OC) particle types composed the remaining ~ 40% of total particles 100-300 nm with minor contributions from particles classified as metals, amines, and organic carbon (OC). The main soot-OC type was mixed with sulfate and nitrate while the main soot particle type was aged (pos only), indicating the presence of water and secondary species produced by atmospheric processing. During the beginning of the fires, there was a dramatic decrease in vehicular travel and after a

few days, vehicle traffic once again increased leading to a decrease in the relative contributions of the fires. The sampling site at Urey Hall is approximately 1 km from the I-5 freeway. These soot and soot-OC particles signatures matched previous source apportionment studies of vehicles and fossil fuel combustion [*Shields et al.*, 2007; *Sodeman et al.*, 2005; *Toner et al.*, 2008; *Toner et al.*, 2006]. When the fraction of soot and soot-OC particles increased, the SMPS size mode also decreased to sizes indicative of fresh vehicle emissions, going from ~190 nm during period 3 to ~60 nm during period 4 (Figure 3.3a).

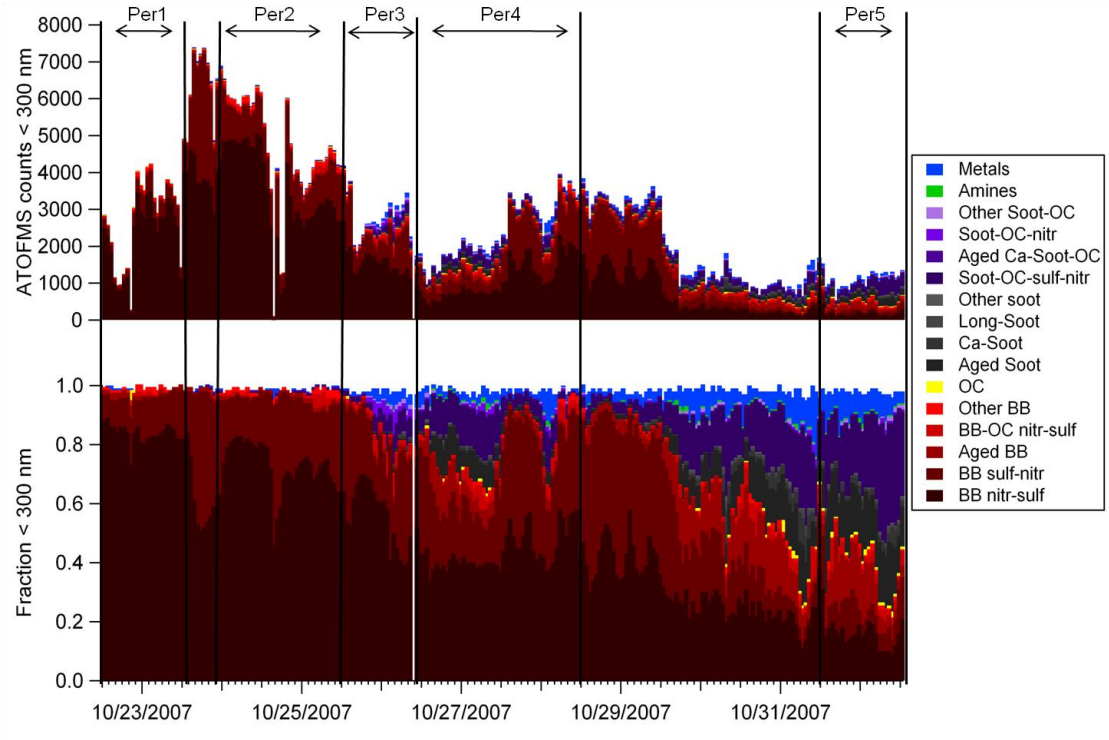

Figure 3.5a. Particle classification time series for 2007. Shown are the top 90 clusters classification (90%) of particles < 300 nm counts (top) and fraction of the total (bottom). Biomass types are shown in red and were the dominant type during most of the periods. Gray types are soot and purple types are soot with organic carbon (Soot-OC) and grow in as biomass decreases.

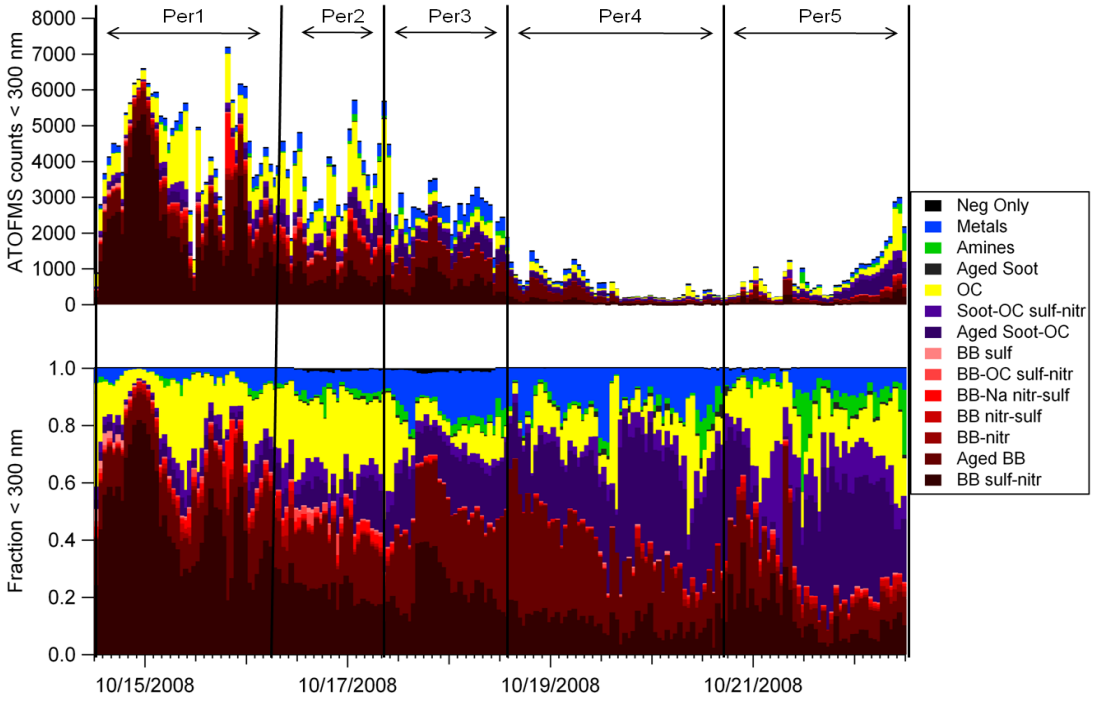

Figure 3.5b. Particle classification time series for 2008. Shown are the top 50 clusters classification (90%) of particles < 300 nm counts (top) and fraction of the total (bottom). Biomass types are shown in red and were the dominant types during most of the periods. Yellow are organic carbon (OC) types and purple are soot with organic carbon (Soot-OC) types and grow in as biomass decreases.

3.4.2.2 2008 Overall Particle Composition

The temporal counts and fraction of classified particles for 100-300 nm are shown in Figure 3.5b. After October 15th 2008, the contribution of BBA to the total aerosol number fraction < 300 nm decreased from approximately 80% to < 50% going from Period 1 to Period 2 (Figure 3.5b). The top two BBA types, BB sulf-nitr and Aged BB, make up > 85% of the BBA with the contributions of the top 5 types making up > 90% of the BBA (see Figure 3.5b). Soot-OC and OC particles composed ~ 50% of all particles with minor contributions from particles classified as metals, amines, and soot. The main soot-OC and OC types were highly aged due to their positive only spectra, indicating the presence of water due

to significant atmospheric processing. The soot-OC and OC particles are most likely are from the regional background, as they were observed in somewhat high abundance during the beginning of the fires and persisted well after the main BBA dominated period, however, they could also be from biomass burning a previous study has shown a high fraction of organic matter in San Diego was from biomass burning [*Hawkins and Russell*, 2010].

3.4.2.3 Particle Composition Comparison between 2007 and 2008

BBA emissions dominated the contribution of particles 100-300 nm during both years. However, there are notable differences between the years. In 2007, BBA represented a higher fraction of the particles for a more extended period of time; ~ 95% of particles 100-300 nm were BBA over the course of about 4 days. In 2008, BBA made up the majority of the particles, but contributed to ~80% of sub-300 nm particles during the highest wildfire influence during one day and quickly decreased in contribution to less than ~50% within three days. This difference can be attributed to the smaller size and more distant location of the fires in 2008.

Figure 3.6a highlights the fraction of different BBA types for both years. In 2007, the two main BBA types are BB nitr-sulf and BB sulf-nitr through period 4, where in period 5 there are increased contributions Aged BB and BB-OC nitr-sulf. In 2008, the two main BBA types are BB sulf-nitr and Aged BB for all 5 periods. The influence of soot and soot-OC particles increased as the contribution of BBA began to decrease in 2007 (Figure 3.5a,b). The overall signatures of the BBA types are very similar between the years, however, there was a more intense signal of sulfate than nitrate in 2008, while in 2007, nitrate signals were more intense than sulfate. The main overall difference in the particle chemistry 100-300 nm is the larger presence of fossil fuel soot after the fires in 2007 (and lack thereof in 2008); while in

2008 there were more OC particles during and after the fires than in 2007, most likely due to higher RH conditions leading to gas to particle conditioning and subsequent processing.

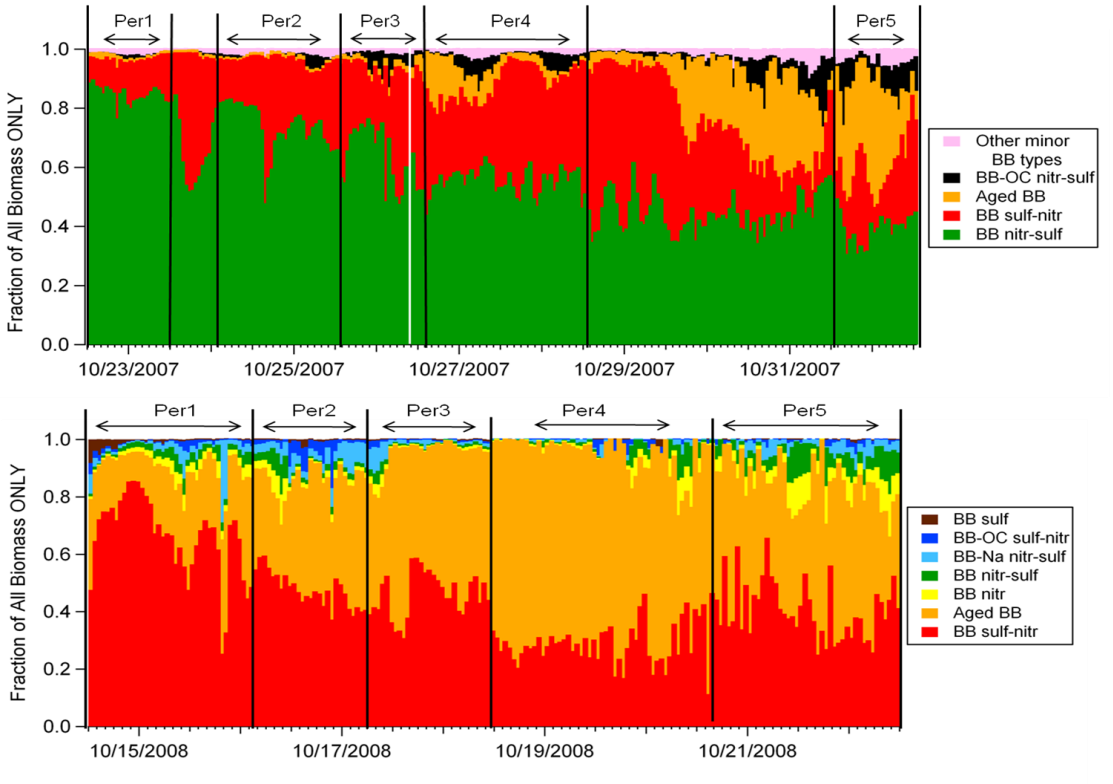

Figure 3.6a,b. Fraction of biomass types (only) for 2007 (top) and 2008 (bottom) by period.

3.4.2.4 2007 and 2008 size-resolved chemistry

In 2007, the chemistry of aerosol particles < 300 nm was largely dominated by BBA, soot-OC and soot (Figure 3.7a); with soot-OC and soot dominating the fraction of particles < 200 nm and biomass burning dominating the fraction of particles > 200 nm. In 2008, the fraction of classified particles as a function of size shows that soot-OC and OC dominated the fraction of particles < 200 nm, while particles > 200 nm were dominated by BBA and OC (Figure 3.7b). This contrasts 2007, which showed soot, rather than OC, as being more

abundant for particles smaller than 200 nm. While the soot-OC particles dominated the smallest sizes and the BBA dominated the larger sizes both years, in 2007, the main mode of the BBA was smaller, ~ 200 nm, whereas in 2008, the BBA mode was closer to ~ 300 nm (Figure 3.7a,b). Assuming that the primary BBA are same size initially for both years, this supports the fact that the BBA in 2008 was more aged than in 2007.

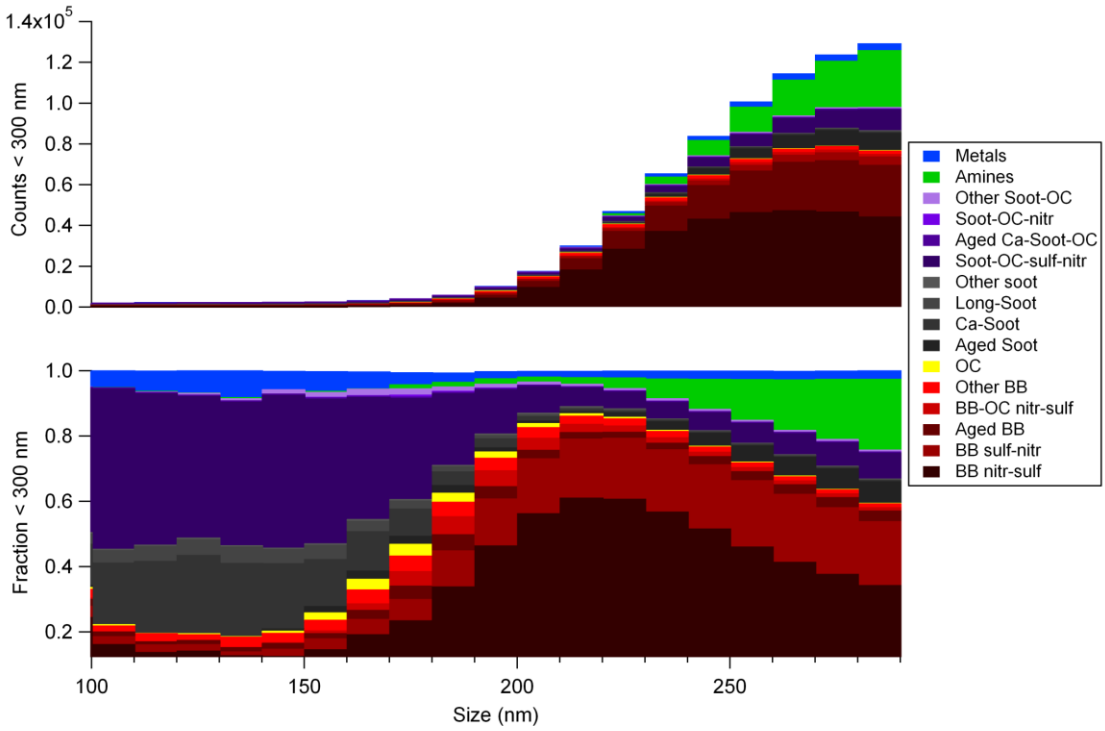

Figure 3.7a. Size resolved particle classification for 2007. Shown are the classification of the top 90 cluster counts (90% of total particles) between 100 and 300 nm detected by the ATOFMS during the study(top) and fraction of the total (bottom). Biomass is shown in red and is the dominant type for larger sizes, while EC, shown in gray, and ECOC in purple are more dominant for the smaller sizes.

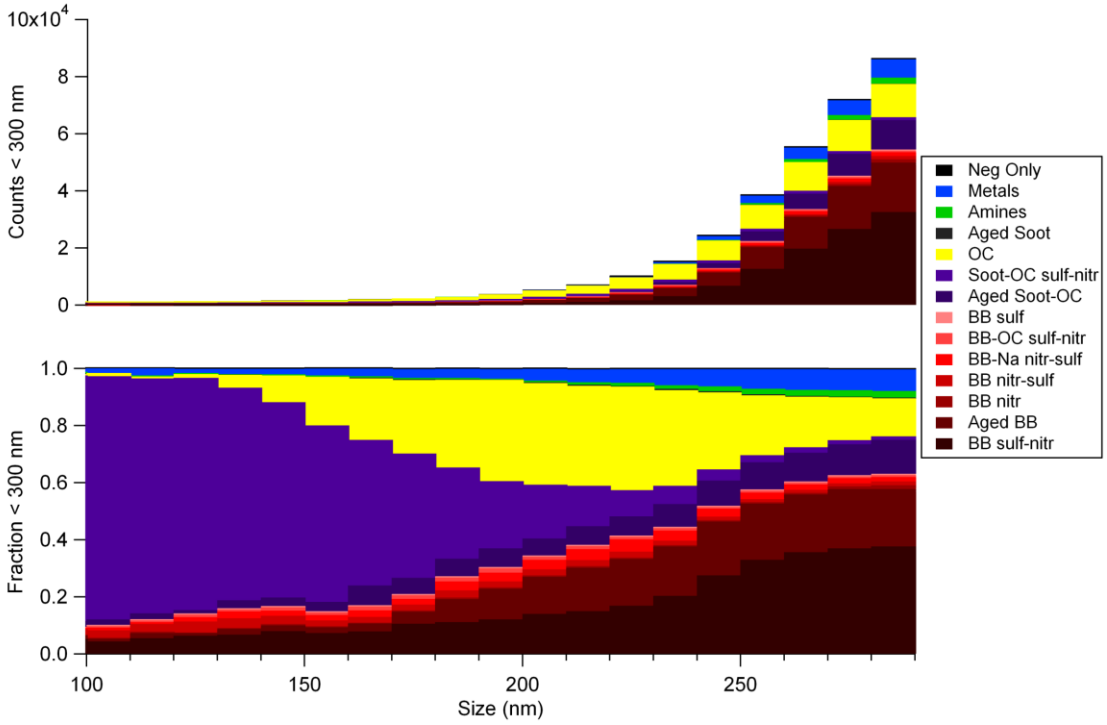

Figure 3.7b. Size resolved particle classification for 2008. Shown are the classification of the top 50 cluster counts (90% of total particles) between 100 and 300 nm detected by the ATOFMS during the study(top) and fraction of the total (bottom). Biomass is shown in red and is the dominant type for larger sizes, while ECOC, shown in purple and OC, shown in yellow, are more dominant for the smaller sizes.

3.4.3 Biomass burning aerosol markers and particle aging

Oxalate is often used as a marker of particle aging and atmospheric oxidation [*Chebbi and Carlier*, 1996; *Mochida et al.*, 2003; *Sullivan and Prather*, 2007], and $KHSO_4$ compounds have been shown in aged biomass particles [*Gaudichet et al.*, 1995; *Li et al.*, 2003; *Li and Shao*, 2010; *Liu et al.*, 2000; *Trebs et al.*, 2005]. Potassium chloride is a good marker indicating fresh biomass burning [*Allen and Miguel*, 1995; *Formenti et al.*, 2003; *Li and Shao*, 2010]. Figure 3.8a,b shows the hourly-averaged ion marker values from individual BBA particles during different air mass periods for oxalate (m/z -89), potassium chloride (m/z +113), and potassium sulfate (m/z +213) for both 2007 and 2008. In 2007, the initial

increase in the oxalate and potassium sulfate aging markers and the rapid decrease of fresh BBA marker potassium chloride from period 1 in the BBA (Figure 3.8a) indicates that the BBA was initially fresher during period 1 and likely aged very rapidly in the fire plume or during transport to the site during period 2. In 2008, due to the low intensity and steady decrease of oxalate and potassium sulfate in the BBA (Figure 3.8b) and the general lack of temporal variation of potassium chloride (Figure 3.8b), the BBA appears to most likely have already been aged before reaching the sampling site; only at the very beginning of 2008 is there fresher BBA. Therefore, due to lack of temporal variation, most likely due to decreased proximity to the fires, it appears that the BBA in 2008 was already completely aged before sampling, whereas in 2007, the BBA aged rapidly over the course of the study.

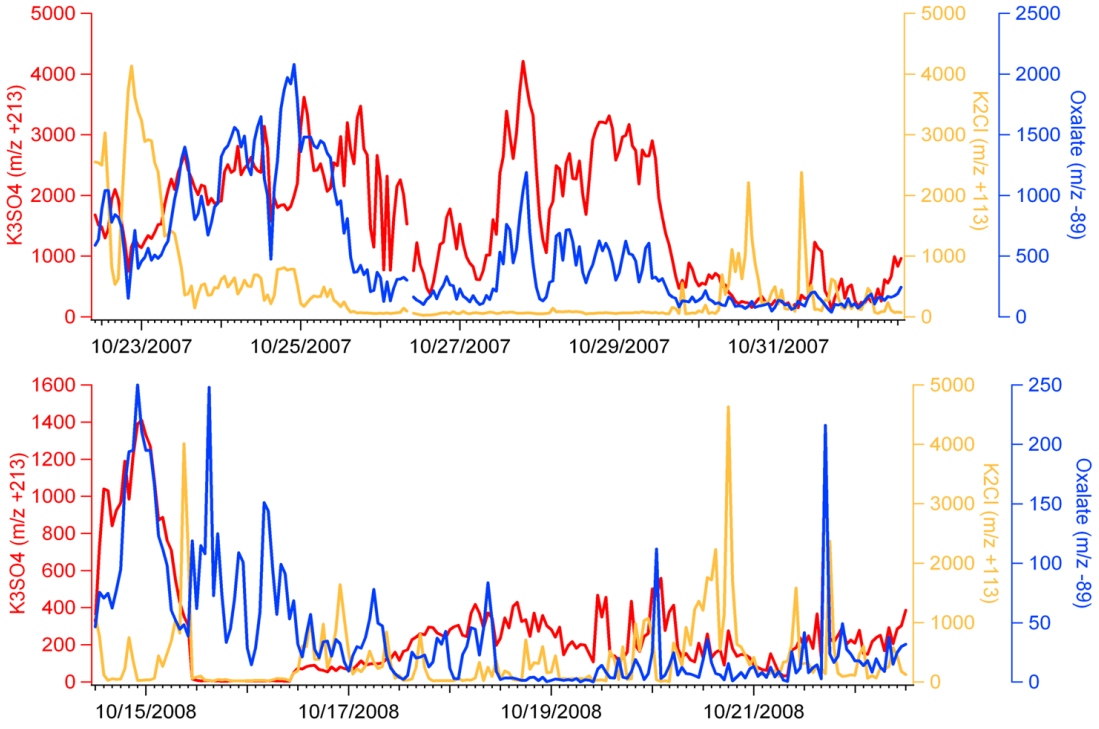

Figure 3.8a,b. 2007 (top) and 2008 (bottom) hourly-averaged ion marker values of the BBA particles during different air mass periods, shown here are potassium sulfate (m/z +213), m/z +113(potassium chloride), and oxalate (m/z -89) peak areas.

3.4.4 CCN overview

3.4.4.1 2007 CCN overview

During the peak influence of the biomass burning, CCN_0.3 concentrations were as high as 14,000/cm^3 and UCSD CN concentrations up to 58,000/cm^3; while CCN_0.1 concentrations were up to 17,000/cm^3 and SIO CN concentrations up to 24,000/cm^3. With the decreased contribution of fires, CCN_0.3 concentrations, fCCN_0.3, total particle concentrations, and the average particle size all decreased overtime, indicating the dominant contribution of BBA to the CCN and total aerosol populations (Figure 3.3a). The decrease in particle concentrations correlated with a reduction in the contribution of biomass burning particle counts. In addition, the decreased peak areas from inorganic compounds such as potassium chloride in the BBA could indicate a decrease in water soluble and hygroscopic particle composition, and therefore explain the decrease in CCN concentrations as the wildfires died out and the BBA became less dominant and more aged. During a shift in RH from ~20 to 80% when the winds shifted direction from offshore to onshore, the overall fCCN increased from ~0.2 to ~0.5 which coincided with a shift to larger particle size mode from ~125 nm to ~190 nm (Figure 3.3a). These particles were stagnated over the ocean had further time to become atmospherically processed, and therefore were more aged. Soot and soot-OC particles then became more dominant and the relative contribution of BBA decreased as the air mass back trajectories shifted to non-fire regions (Figure 3.5a).

Periods 1 -3 were dominated by BBA (Figure 3.5a) with a median κ_0.3 value during these periods of 0.043 and median κ_0.1 value of 0.26 (Figure 3.9a). Periods 4 and 5 with the lowest contributions from BBA had median κ_0.3 values of 0.029 and 0.062 and median κ_0.1 values of 0.28 and 0.47, respectively. The activation diameters for κ_0.1 were larger in size, due to the lower supersaturation of CCN_0.1, therefore, those larger particles were most likely

more aged and generally more hygroscopic overall [*Gunthe et al.*, 2009; *Roberts et al.*, 2010]. Additionally, the stagnation over the ocean gave further time for these particles to become atmospherically processed, and therefore could explain the higher κ_0.1 values seen with CCN_0.1 compared to CCN_0.3. By varying the hygroscopicity parameter κ by ± 50% resulted in changes in CCN number concentrations within 15% for 2007. The activation diameters in 2007 (117 – 195 nm, 0.3% SS) were around the main particle size mode (~100-200 nm), which was attributed to the large impact of biomass emissions that year. The overall hygroscopicity of the BBA was κ ~0.04 (SS=0.29), similar to soot-rich biomass (0.01) [*Andreae and Rosenfeld*, 2008] and fresh anthropogenic emissions (0.05) [*Furutani et al.*, 2008], and considerably lower than laboratory produced secondary organic aerosol (SOA), ambient organic aerosol (~0.1-0.2) [*Andreae and Rosenfeld*, 2008; *Prenni et al.*, 2007; *VanReken et al.*, 2005], and polluted continental (~0.15-0.3) [*Dusek et al.*, 2006; *Hudson*, 2007; *Pringle et al.*, 2010; *Rose et al.*, 2010]. Therefore, the κ_0.3 range observed in this study (0.018-0.13) indicates that a significant fraction of biomass burning aerosol is comprised of low hygroscopicity and relatively insoluble compounds.

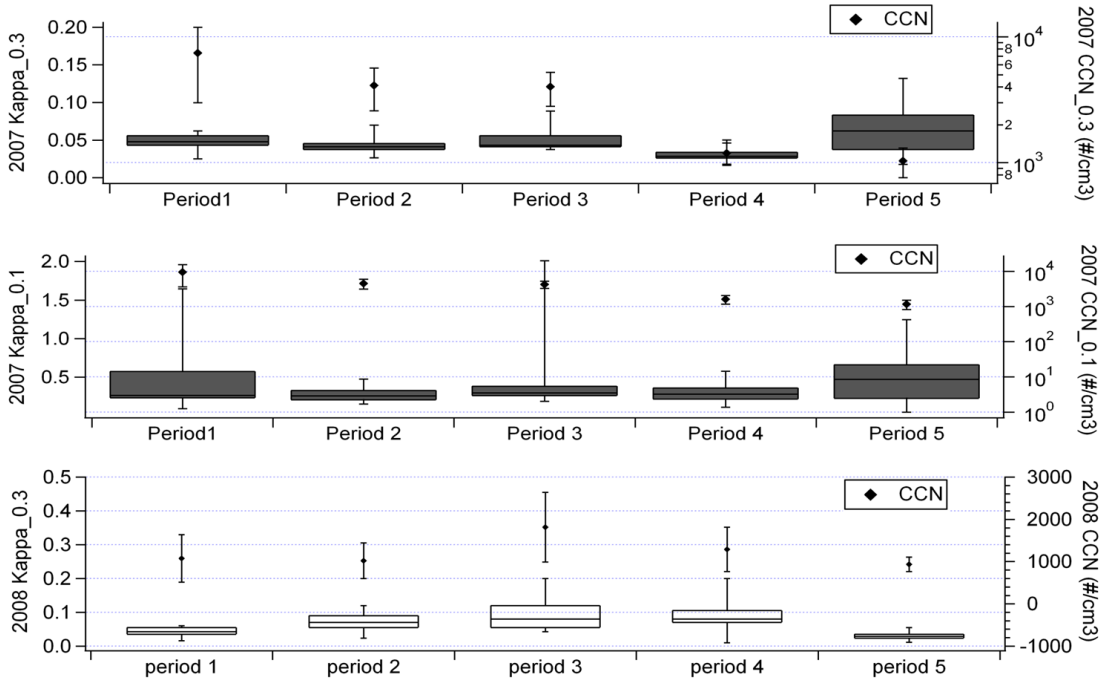

Figure 3.9. 2007 (top, middle) and 2008 (bottom) single parameter hygroscopicity (κ) values of the particles during different air mass periods. The top of the boxes are the 3rd quartile of κ values for that period, the bottoms are the 1st quartile values for that period. Whiskers show the minimum and maximum values for each period. Median values are the middle lines dividing the top and bottom of the boxes. Black diamonds are average CCN concentrations for those periods with standard deviation as error bars.

3.4.4.2 2008 CCN overview

During the peak influence of the biomass burning, CCN_0.3 concentrations were 1500/cm^3 and CN concentrations were up to 16,000/cm^3, much lower than 2007. The lower CCN_0.3 concentrations were due to a decreased influence of the fires in 2008 relative to 2007 and also a smaller particle size mode ~35-62 nm) that were probably too small to be CCN. As CCN_0.3 concentrations and fCCN increased over time, total particle concentrations decreased and the average particle size increased (Figure 3.3b). As the contribution of BBA (by number) was decreasing, the CCN concentrations and fCCN increased. During periods 1-2 when the influence of BBA was highest, κ was lower than in period 3. This was most likely

caused by the smaller particle size mode in periods 1-2 (~35-62 nm), while in period 3 the size mode increased to ~ 85 nm.

Figure 3.9 shows the κ_0.3 values for the various air masses sampled during the fires, derived from CCN_0.3 with corresponding average CCN concentrations for each time period. Period 1 was the most dominated by BBA (Figure 3.5b) and the range of κ_0.3 values during that period was 0.02 - 0.06, with a median value of 0.04. The most hygroscopic period was period 3, corresponding with a shift in higher RH and air mass back trajectory shifting from the north along the coast to from the south over land, with a range of κ_0.3 values from 0.04-0.2 and a median value of 0.09. The large variability of κ during period 3 is most likely due to local meteorological events that were not captured using the HYSPLIT back trajectories, such as variability in local pollution and marine sources, demonstrated by an increase in metal-containing and amine particle types in addition to changes in fractions of soot-OC, OC, and BBA particles. Period 5 was more representative of the regional background, with air masses coming from the northwest along the coast, and was the least hygroscopic, with a range of κ_0.3 values from 0.01- 0.06 and a median κ of 0.03. Activation diameters at 0.3% SS were 90-235 nm. By varying the hygroscopicity parameter κ by ± 50% resulted in changes in CCN number concentrations <3% for period 1. The activation diameters were much larger (90-235 nm) than the particle size mode (~40-60 nm) and varying the hygroscopicity did not have a large effect, as most of the particles were too small to activate regardless and reflects the much lower influence of larger-sized biomass burning and the much larger impact of the smaller-sized local emissions that year.

During the most BBA impacted periods 1-2 in 2008, the aerosol size mode peaked at sizes of ~30-60 nm and increased over time to ~85-95 nm in periods 3 and 4 when CCN and fCCN increased (Figure 3.3b, Table 3.2b). During this study there were strong contributions

from local sources based on the smaller size mode at 30-60 nm during all periods. This differs strongly from 2007 when these ultrafine particles could not exist due to coagulation with the larger particle surface area produced from the fires. The 85-95 nm mode in 2008 is still smaller than observed for wildfires, therefore is most likely from vehicles, and reflects the much smaller contribution of biomass burning relative to stronger contributions of other local sources in 2008. A summary of the statistics on CCN_0.3 by period can be found in Table 3.2b.

3.4.5 Hygroscopicity in 2007 and 2008

The contribution of wildfire emissions were much larger and played a more significant role in affecting CCN and CN concentrations in 2007 than in 2008 (Figure 3.3a,b). In 2007, 300,000 acres were burned whereas in 2008 just over 4,000 acres were burned in San Diego County. In 2007, the CCN_0.3 and CN concentrations peaked at the beginning of the fires, during period 1, at around 14,000/cm^3 and 58,000/cm^3. In 2008, the CCN_0.3 concentrations peaked at 2,600/cm^3 during period 3, a period not dominated by biomass burning; while the CN concentrations peaked during the only period dominated by fires at 16,000/cm^3 with a larger urban influence compared to the BBA. The decrease in CN over time during 2007 and 2008 was due to decreasing fire activity, supported by lower BBA contributions (Figure 3.5a,b). However, the simultaneous decreases in CCN (and fCCN, κ _0.3) and BBA in 2007 indicate that the BBA had a major influence on CCN activity in periods 1-3 (Figure 3.3a). Conversely, the CCN concentration (and fCCN, κ _0.3) increased as BBA contribution decreased in 2008, which can be attributed to increased atmospheric processing due to the high RH and fog.

The differences in inferred hygroscopicity could also be due to the size distributions and size-resolved chemistry of the particles. In 2007, there was a large particle mode around

~125 nm diameter during periods 1-3 that slowly decreased in size over time as the contributions from fires decreased and local vehicle emissions increased, while the composition of the aerosol population 100-300 nm was largely dominated by biomass burning, soot and soot-OC. In 2008, during periods 1-2 the size mode was much smaller ~30-60 nm diameter due to domination of local sources. The size mode and increased over time to ~85-95 nm in periods 3 and 4 when the CCN (and fCCN, κ _0.3) increased, suggesting atmospheric processing increased both the particle size and hygroscopicity. The composition of the particles 100-300 nm was fairly similar to 2007, with the exception that the soot in 2007 was replaced by OC in 2008 (Figure 3.7 a,b).

In 2007, over periods 1 to 3, the fraction of BBA total particles is quite high and fairly constant (Figure 3.5a). Also during these time periods, there is a decrease in BB nitr-sulf relative to BB sulf-nitr as the fraction of all BBA, as shown in Figure 3.6a. During these three periods, the κ_0.3 values were ~0.04, indicating that these two BBA types have similar hygroscopicities. However, due to the larger size and presence of soluble compounds on the BBA observed with the ATOFMS, these particles would most likely all be activated as CCN. Therefore, the differences observed in BBA particle types could be a proxy for chemical changes in the smaller particles below the detection limit of the ATOFMS, and are carefully compared to the estimated hygroscopicity of all particle sizes (κ_0.3). In period 4, the fraction of BBA to total particles 100-300 nm begins to decrease as the contributions from fossil fuel combustion types (soot-OC and soot) begin to increase (Figure 3.5a). The fraction of BBA had increased contributions from Aged BB and BB-OC nitr-sulf (Figure 3.6a). During period 4, the median κ_0.3 value decreased to 0.029. While this decrease in average particle hygroscopicity could indicate that the new BBA types and the soot-OC and soot were less hygroscopic than the BB nitr-sulf and BB sulf-nitr, the decrease in hygroscopicity is most

likely due to the significant shift in particle size mode from ~125-190 to ~60 nm (Figure 3.3a). In period 5, continued contributions from soot and soot-OC types were made to the fraction of total particles (Figure 3.5a), while the fraction of BBA particles had significant contributions of the aged BB and BB-OC nitr-sulf types (Figure 3.6a). The median κ_0.3 value for period 5 is 0.062, the highest for the study and the period with the most variability in hygroscopicity, as shown in Figure 3.9. Concurrent with the increase in hygroscopicity is a decrease in particle size mode to ~20 nm, indicative of local emission sources. The increase in hygroscopicity could indicate that the aged BBA types are more hygroscopic than the fresher BBA types, assuming that the increased contributions of the smaller and fresh soot and soot-OC were not more hygroscopic than fresher BBA. As previously stated, BBA can range in hygroscopicity from 0.01 to 0.7, while continental and fresh anthropogenic emissions can range from 0.05-0.3. Therefore, the nature of the specific BBA and continental emissions is case-dependent to determine which source is more hygroscopic and CCN active; in addition to the different size particles produced by these different sources. The lower median κ_0.3 value for period 4 with the increased contributions of soot and soot-OC, and smaller size mode indicates that the soot and soot-OC were less hygroscopic than the BBA, because they were smaller and fresher (Figures 3.3a, 3.7a). Overall, it appears that the aged biomass types (Aged BB and BB-OC nitr-sulf) were slightly more hygroscopic than the fresher biomass types (BB nitr-sulf and BB sulf-nitr); in general all BBA types were more hygroscopic than the fossil fuel emissions (soot and soot-OC) due to their larger and more aged signatures.

In 2008, over periods 1 to 2, the fraction of total BBA decreased strongly as the contributions of OC and soot-OC increased considerably (Figure 3.5b). Also during these time periods, there is a decrease in BB sulf-nitr relative to Aged BB as a fraction of all BBA, as shown in Figure 3.6b, indicating an evolution from a fresher to an aged BBA. During these

two periods, the median κ_0.3 values changed from 0.04 to 0.07, concurrent with an increase in particle size mode from ~35 nm to ~ 62 nm. This increase in hygroscopicity is most likely due to the shift to larger particle sizes, as the BB sulf-nitr, Aged BB, OC, and soot-OC particle types are much larger than the main particle size mode, and most likely completely activated as CCN due to their soluble inclusions and/or being aged. In period 3 the relative contribution of soot-OC increased relative to OC for total particles, while the contributions of the fresher and aged to total BBA are similar to those in period 2. The median κ_0.3 value for period 3 increased slightly to 0.09, concurrent with an increase in size mode to ~85 nm. The increase in hygroscopicity is most likely due to the increase in larger particles concurrent with the shift to higher RH, indicative of atmospheric processing. In period 4, the fraction of BBA to total particles continues to decrease further as the contribution of soot-OC continues to increase and the relative contributions to the fraction of BBA remain similar to period 3. During period 4, the median κ_0.3 value remains at 0.09 concurrent with a small increase in size mode to ~95 nm, indicating similar hygroscopicities of particles ~85-95 nm. In period 5, there is continued decrease of the relative fraction of BBA with slight increases in the contribution of OC to the fraction of total particles (Figure 3.5b), while the relative fraction of Aged BB decrease relative to BB sulf-nitr and new BBA types, BB nitr and BB nitr-sulf (Figure 3.6b). The median κ_0.3 value for period 5 is 0.03, the lowest of the study, as shown in Figure 3.9, concurrent with a shift to smaller particle size mode of ~69 nm. This indicates that the smaller, fresher soot-OC particles are most likely less hygroscopic than the BBA, which are more aged, larger, and most likely fully activated. Overall in 2008, it appears that small, fresh local sources below the chemical detection limit of the ATOFMS dominated the hygroscopicity, while the larger, mostly aged BBA were completely activated.

During the BBA dominant periods in both 2007 (periods 1-3) and 2008 (period 1), the median κ_0.3 values were ~0.04. Despite the large differences in submicron size distributions (Figure 3.3a,b), there were similar BBA signatures between the two years for particles 100-300 nm (Figures 3.4a,b; 3.5a,b; 3.6a,b), yielding similar κ values (Figure 3.9). The large particle size modes in 2007 (~125-190 nm) indicate that the BBA emissions were dominating the particle hygroscopicity. The much smaller size modes in 2008 (~35-95 nm) indicate that local sources dominated particle hygroscopicity that year, yielding hygroscopicity values that were more representative of urban pollution and background continental aerosol than BBA. Therefore, while similar biofuel burned each year and produced similar BBA signatures, which most likely had similar hygroscopicities; these particles were large and had many soluble markers, indicating that they would most likely have been completely CCN active.

Previous measurements of BBA hygroscopicity show a large range of κ from 0.01 for fresh soot-rich biomass [*Andreae and Rosenfeld*, 2008], 0.06 for ponderosa pine [*Petters et al.*, 2009a], 0.2 for levoglucosan [*Rose et al.*, 2008], 0.55 for grass burning [*Andreae and Rosenfeld*, 2008] and 0.7 for swamp sawgrass [*Petters et al.*, 2009a]. Andreae and Rosenfeld (2008) have noted aged biomass κ ranging from 0.1 to 0.3 [*Andreae and Rosenfeld*, 2008]. Carrico et al. (2008) observed the smallest κ of 0.064 for filter samples of burned duff core extracted in methanol and the largest κ of 0.252 from burned sagebrush extracted in water [*Carrico et al.*, 2008]. As mentioned previously, the main biomass fuel in San Diego was Chaparral, consisting of shrubs and duff including chamise, hoaryleaf ceanothus and manzanita [*McMeeking et al.*, 2009]. Petters et al. (2009) measured a κ of 0.33 for chamise, 0.4 for ceanothus and 0.1 for manzanita branches. Therefore, it appears that the BBA in San Diego during 2007 were on the lower end of previously determined biomass hygroscopicities and similar to soot rich biomass (0.01) and fresh anthropogenic emissions (0.05). The BBA

particles likely had a large volume fraction of unidentified weakly hygroscopic and/or insoluble compounds present. It is notable that κ is quite low even though many soluble inorganic compounds, such as $KCl/KNO_3/KSO_4$, were observed on the BBA. In 2008, local sources dominated the particle size modes. Fresh anthropogenic emissions measured near Los Angeles have an estimated κ of 0.05 [*Furutani et al.*, 2008], while laboratory produced secondary organic aerosol (SOA) and ambient organic aerosol have estimated κ values of ~0.1-0.2 [*Andreae and Rosenfeld*, 2008; *Prenni et al.*, 2007; *VanReken et al.*, 2005]. Continental aerosol has been shown for many different studies to have κ values of ~0.15-0.3 [*Dusek et al.*, 2006; *Hudson*, 2007; *Pringle et al.*, 2010; *Rose et al.*, 2010]. Therefore, the local pollution aerosol sampled in San Diego during 2008 was below and on the lower end of previously determined continental aerosol hygroscopicities, similar to fresh anthropogenic emissions. However, for both years the size range of the particle composition measurements (100-300 nm) is on the higher end of the particle activation range and there were significant amounts of particles < 100 nm (Figure 3.3a,b). Therefore, some of the changes taking place that are dictating CCN activity are below what was possible to detect chemically, and the chemical measurements 100-300 nm may be a proxy for what is occurring to particles below 100 nm.

3.4.5.1 Ammonium and aerosol base to acid ratio

Biomass burning can be a significant source of ammonia and amines [*Andreae et al.*, 1988; *Sorooshian et al.*, 2008]. While acidic aerosols tend to be more hygroscopic than their neutral counterparts [*Khlystov et al.*, 2005; *Pathak et al.*, 2004; *Zhang et al.*, 2007], the formation of ammonium salts due to reaction of ammonia with slightly soluble organic acids can affect the CCN activity and hygroscopic growth of aerosols with a significant organic component [*Pathak et al.*, 2004]. For example, [*Dinar et al.*, 2008] found that the activation

diameter of adipic acid decreased after exposure to ammonia due to the formation of more water-soluble products. Given the high abundance of ammonium and amines during this study, further investigation into their role in particle acidity and hygroscopicity is warranted.

To determine relative particle-phase acidity, the ratio of ammonium to inorganic acids is most commonly examined [*Pathak et al.*, 2004; *Pratt et al.*, 2009; *Sullivan et al.*, 2007; *Zhang et al.*, 2007]. Total base is the sum of the peak areas of ammonium and three amine markers at m/z +18, +86, and +101 [*Angelino et al.*, 2001; *Pratt et al.*, 2009]. Total inorganic acids are the sum of the peaks areas from nitrate markers (NO_2^-, NO_3^-, $H(NO_3)_2^-$, m/z -46, m/z-62, m/z -125) and sulfate markers (SO_3^-, HSO_4^-, m/z-80, m/z -97). Chloride (m/z -35) was not included in the total inorganic acid ratio due to its overlap with instrumental interference at m/z -33 from the strong m/z +39 signal, known as "cross talk" (see Figure 3.4a,b). Our measurements of total-base-to-inorganic-acids are relative measurements and do not indicate actual quantities of total base or acid in the BBA particles. However, as the base-to-acid ratio does increase, it is likely that the ammonium and amines shift the acid-base neutrality of the aerosols towards more alkaline. This would neutralize H_2SO_4 allowing additional weaker acids including organic acids, to now partition to the particle phase [*Gaudichet et al.*, 1995; *Li et al.*, 2003; *Liu et al.*, 2000; *Sullivan and Prather*, 2007; *Trebs et al.*, 2005]. As particle acidity has been shown to have implications for hygroscopicity [*Khlystov et al.*, 2005], understanding the relationship between the base to acid ratio and κ can further our understanding of the effects of particle chemistry on CCN activity.

In 2007 period 3 (1st ammonium period), a large increase occurred in the peak area of NH_4 (m/z +18) and total base-to -inorganic acids ratio (Figure 3.10a). In 2008, analogous to 2007, ammonium and particle acidity on BBA also showed very similar trends (Figure 3.10b). While the BBA were most likely completely CCN active due to the large sizes and

soluble material present, the chemical measurements 100-300 nm may be a proxy for what is occurring to particles below 100 nm. In 2007, κ did not increase during the high ammonium and base-to-acid ratio periods, most likely indicating that the BBA were already activated due to the soluble material already present in the particle, and the particle acidity may not have greatly impacted the hygroscopicity. In 2008, the periods of high ammonium and base-to-acid ratio in 2008 were concurrent with a shift to higher RH, larger particle size modes, and the periods with the highest κ values, indicating that atmospheric processing, most likely aqueous processing in this case, can significantly increase particle size and CCN activity, and could therefore have a significant impact on climate.

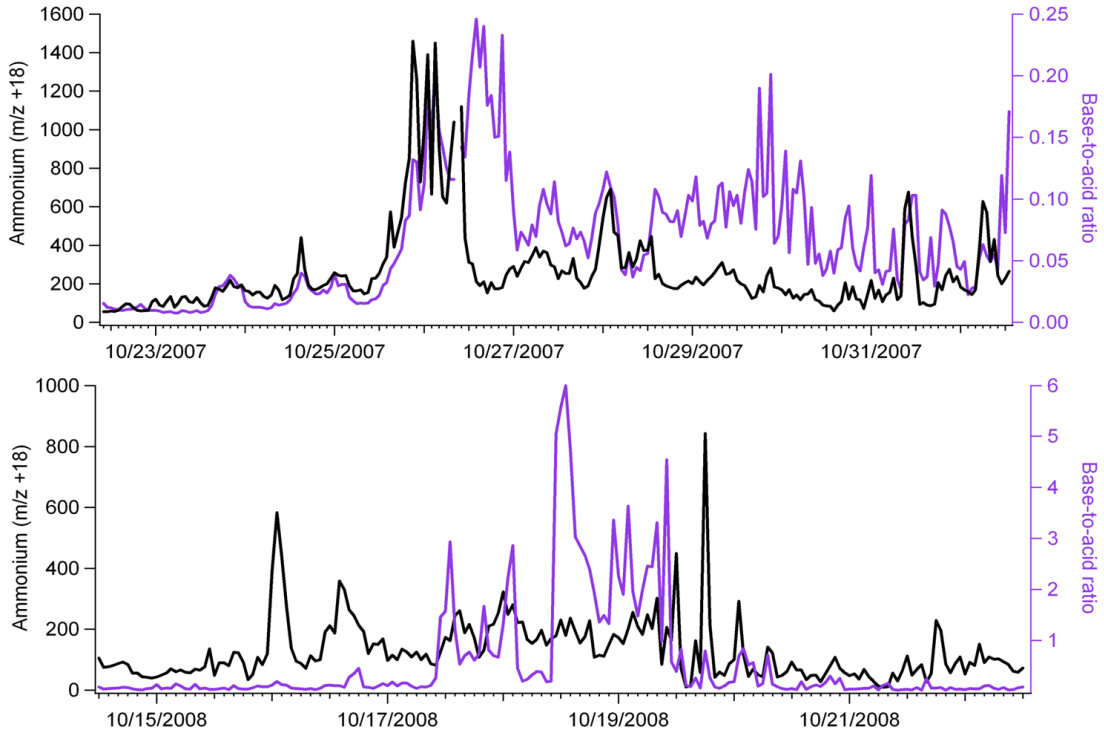

Figure 3.10a,b. 2007 (top) and 2008 (bottom) hourly-averaged ion marker values of the BBA particles during different air mass periods, shown here is ammonium (m/z +18) and total base-to-total-inorganic-acid ratio.

3.5 Conclusions

Aerosol size and composition were measured in real-time and particle hygroscopicity estimated from CCN measurements during the 2007 and 2008 wildfire events in San Diego. The contribution of wildfire emissions were much larger and played a more significant role in affecting CCN and CN concentrations in 2007 than in 2008. Particle size distributions indicate that 2007 was dominated by biomass burning emission with size modes (~125-190 nm), while in 2008 emissions were dominated by local pollution sources with much smaller particle size modes (~35-95 nm). During both of these studies, chemical measurements showed that biomass burning was the dominant particle type for sizes 100-300 nm. In addition to BBA, in 2007 there was more fossil fuel soot, while in 2008 there was more organic carbon. The increased fraction of organic carbon particles less than 300 nm in 2008 relative to 2007 may be because of aqueous processing due to higher RH/fog during the later portion of this study. The BBA in 2008 was already processed by the time it was sampled as indicated by the consistent contributions from several aging markers, whereas in 2007, aging markers in BBA increased over the course of several days.

The overall particle hygroscopicity (κ) during the BBA dominant periods (periods 1-3 in 2007; period 1 in 2008) was very similar (~0.04), however in 2008, the particle hygroscopicity was dominated by local sources rather than biomass burning, due to the much smaller particle size mode. In 2007, the two main BBA types were BB nitr-sulf and BB sulf-nitr; while in 2008 BB sulf-nitr and Aged BB were the main types. Even though the BBA chemical signatures were different between the years, they had similar hygroscopicities. However, due to the large sizes and soluble material of the BBA, they were likely completely CCN activated. Hygroscopicity parameter values are within previously measured values from

various BBA sources (0.01-0.7), and close to that of soot-rich biomass (0.01), ponderosa pine (0.04) and fresh anthropogenic emissions (0.05).

BBA makes an important contribution to global CCN concentrations because they are large in initial size for combustion particles, and hygroscopic enough to activate into cloud droplets under typical cloud supersaturations. Changes in the BBA chemical composition and a high fraction of total particles consisting of BBA, as observed here, can produce up to a fifteen-fold increase in CCN concentrations at 0.3% supersaturation. However, while biomass burning aerosol can contribute a large amount of CCN which can increase cloud reflectivity and therefore have a cooling effect, the absorbing carbonaceous species produced during the biomass combustion process have high absorption, therefore a warming effect; consequently, the net effect of the San Diego wildfires on the region is highly uncertain.

3.6 Acknowledgments

The authors are grateful to Dr. Andrew Ault and Cassandra Gaston for their help with data collection, and to Dr. Satoshi Takahama (SIO, UCSD) for his helpful discussions and assistance with data analysis. We acknowledge Prof. Markus Petters (North Carolina State University) and Prof. Sonia Kreidenweis (Colorado State University) for use of their code in estimating hygroscopicity parameter kappa. We are also grateful to NOAA for the NOAA HYSPLIT back trajectory model used, the UCSD personnel responsible for SIO Pier meteorological data in 2007, and Dr. Jan Kleissl/DEMROES (UCSD) for meteorological data in 2008. Funding was provided by the California Air Resources Board Grant # 04-336.

Publication Acknowledgement

The contents of Chapter 3 are part of a manuscript in preparation, Moore, M.J.K., Sullivan, R.C., Roberts, G.C., Wang, Y., Zauscher, M.D., Prather, K.A., A comparison of single particle mixing state and CCN activity during the 2007 and 2008 San Diego Wildfires, to be submitted to Atmospheric Environment. The dissertation author was the primary investigator and author of this paper.

3.7 References

Allen, A.G., and A.H. Miguel, Biomass Burning in the Amazon: Characterization of the Ionic Component of Aerosols Generated from Flaming and Smoldering Rainforest and Savannah, *Environmental Science and Technology*, *29* (2), 486-493, 1995.

Andreae, M.O., Soot Carbon and Excess Fine Potassium: Long-Range Transport of Combustion-Derived Aerosols, *Science*, *220* (4602), 1148-1151, 1983.

Andreae, M.O., E.V. Browell, G.L. Garstang, G.L. Gregory, R.C. Harriss, G.F. Hill, D.J. Jacob, M.C. Pereira, G.W. Sachse, A.W. Setzer, P.L. Silva Dias, R.W. Talbot, A.L. Torres, and S.C. Wofsy, Biomass-Burning Emissions and Associated Haze Layers Over Amazonia, *Journal of Geophysical Research*, *93* (D2), 1509-1527, 1988.

Andreae, M.O., and D. Rosenfeld, Aerosol-cloud-precipitation interactions. Part 1. The nature and sources of cloud-active aerosols, *Earth Science Reviews*, *89*, 13-41, 2008.

Andreae, M.O., D. Rosenfeld, P. Artaxo, A.A. Costa, G.P. Frank, K.M. Longo, and M.A.F. Silva Dias, Smoking Rain Clouds over the Amazon, *Science*, *303* (5662), 1337-1342, 2004.

Angelino, S., D.T. Suess, and K.A. Prather, Formation of aerosol particles from reactions of secondary and tertiary alkylamines: Characterization by aerosol time-of-flight mass spectrometry, *Environmental Science and Technology*, *35* (15), 3130-3138, 2001.

Ansari, A.S., and S.N. Pandis, Water absorption by secondar organic aerosol and its effect on inorganic aerosol behavior, *Environmental Science and Technology*, *34* (1), 71-77, 2000.

CalFire, California Department of Forestry and Fire Protection: Archieved Fires 2008, 2008.

Carrico, C.M., M.D. Petters, S.M. Kreidenweis, J.L. Collett, G. Engling, and W.C. Malm, Aerosol hygroscopicity and cloud droplet activation of extracts of filters from biomass

burning experiments, *Journal of Geophysical Research*, *113* (D08206), doi:10.1029/2007JD009274, 2008.

Carrico, C.M., M.D. Petters, S.M. Kreidenweis, A.P. Sullivan, G.R. McMeeking, E.J.T. Levin, G. Engling, W.C. Malm, and J.L. Collett, Water uptake and chemical composition of fresh aerosols generated in open burning of biomass, *Atmospheric Chemistry and Physics*, *10*, 5165-5178, 2010.

Chang, R.Y.-W., P.S.K. Liu, W.R. Leaitch, and J.P.D. Abbatt, Comparison between measured and predicted CCN concentrations at Egbert, Ontario: Focus on the organic aerosol fraction at a semi-rural site, *Atmospheric Environment*, *41*, 8172-8182, 2007.

Chebbi, A., and P. Carlier, Carboxylic acids in the troposphere, occurence, sources and sinks: A review, *Atmospheric Environment*, *30*, 4233-4249, 1996.

Crutzen, P.J., and M.O. Andreae, Biomass Burning in the Tropics: Impact on Atmospheric Chemistry and Biogeochemical Cycles, *Science*, *250* (4988), 1669-1678, 1990.

Dinar, E., T. Anttila, and Y. Rudich, CCN Activity and Hygroscopic Growth of Organic Aerosols Following Reactive Uptake of Ammonia, *Environmental Science and Technology*, *42*, 793-799, 2008.

Dusek, U., G.P. Frank, L. Hildebrant, J. Curtius, J. Schneider, S. Walter, D. Chand, F. Drewnick, S.S. Hings, D. Jung, S. Borrmann, and M.O. Andreae, Size Matters More Than Chemistry for Cloud-Nucleating Ability of Aerosol Particles, *Science*, *312* (5778), 1375-1378, 2006.

Fine, P.M., G.R. Cass, and B.R.T. Simoneit, Chemical Characterization of Fine Particle Emissions from the Fireplace Combustion of Wood Types Grown in the Midwestern and Western United States, *Environmental Engineering Science*, *21* (3), 387-409, 2004.

Formenti, P., W. Elbert, W. Maenhaut, J.M. Haywood, S. Osborne, and M.O. Andreae, Inorganic and carbonaceous aerosols during Southern African Regional Science Initiative (SAFARI 2000) experiment: Chemical characteristics, physical properties, and emission data for smoke from African biomass burning, *Journal of Geophysical Research*, *108(D13)* (8488), doi:10.1029/2002JD002408, 2003.

Furutani, H.F., M. Dall'osto, G.C. Roberts, and K.A. Prather, Assessment of the relative importance of atmospheric aging on CCN activity derived from field observations, *Atmospheric Environment*, *42*, 3130-3142, 2008.

Gaudichet, A., F. Echalar, B. Chatenet, J.P. Quisefit, G. Malingre, H. Cachier, P. Buatmenard, P. Artaxo, and W. Maenhaut, Trace-Elements in Tropical African Savanna Biomass Burning Aerosols, *Journal of Atmospheric Chemistry*, *22* (1-2), 19-39, 1995.

Grijalva, R., R. Moore, and H. Renteria, California Fire Siege 2007, An Overview, *California Department of Forestry and Fire Protection*, 2008.

Guazzotti, S.A., D.T. Suess, K.R. Coffee, P.K. Quinn, T.S. Bates, A. Wisthaler, A. Hansel, W.P. Ball, R.R. Dickerson, C. Neusuess, P.J. Crutzen, and K.A. Prather, Characterization of carbonaceous aerosols outflow from India and Arabia: Biomass/biofuel burning and fossil fuel combustion, *Journal of Geophysical Research*, *108* (D15), 4485, doi:10.1029/2002JD003277, 2003.

Gunthe, S.S., S.M. King, D. Rose, Q. Chen, P. Roldin, D.K. Farmer, J.L. Jimenez, P. Artaxo, M.O. Andreae, S.T. Martin, and U. Poeschl, Cloud condensation nuclei in pristine tropical rainforest air of Amazonia: size-resolved measurements and modeling of atmospheric aerosol composition and CCN activity, *Atmospheric Chemistry and Physics*, *9* (19), 7551-7575, 2009.

Hawkins, L.N., and L. Russell, Oxidation of ketone groups in transported biomass burning aerosol from the 2008 Northern California Lighting Series fires, *Atmospheric Environment*, *44*, 4142-4154, 2010.

Hegg, D.A., R. Majeed, P.F. Yuen, M.B. Baker, and T.V. Larson, The impact of SO2 oxidation in cloud droplets and in haze particles on aerosol light scattering and CCN activity, *Geophysical Research Letters*, *23*, 2613-2626, 1996.

Hopkins, R.J., K. Lewis, Y. Desyaterik, Z. Wang, A.V. Tivanski, W.P. Arnott, A. Laskin, and M.K. Giles, Correlations between optical, chemical and physical properties of biomass burn aerosols, *Geophysical Research Letters*, *34* (L18806), doi:10.1029/2007GL030502, 2007.

Hudson, J.G., Variability of the relationship between particles size and cloud-nucleating ability, *Geophysical Research Letters*, *34* (8), L08801, doi:10.1029/2006GL028850, 2007.

Hudson, P.K., D.M. Murphy, D.J. Cziczo, D.S. Thomson, J.A. de Gouw, C. Warneke, J. Holloway, H. Jost, and G. Huebler, Biomass-burning particle measurements: Characteristic composition and chemical processing, *Journal of Geophysical Research*, *109* (D23S27), doi:10.1029/2003JD004398, 2004.

Hungershoefer, K., K. Zeromskiene, Y. Iinuma, G. Helas, J. Trentmann, T. Trautmann, R.S. Parmar, A. Wiedensohler, M.O. Andreae, and O. Schmid, Modelling the optical properties of fresh biomass burning aerosol produced in a smoke chamber: results from EFEU campaign, *Atmospheric Chemistry and Physics*, *8*, 3427-3439, 2008.

Jacobson, M.C., H.C. Hansson, K.J. Noone, and R.J. Charlson, Organic atmospheric aerosols: Review and state of the science, *Reviews of Geophysics*, *38*, 267-294, 2000.

Kaufman, Y.J., and R.S. Fraser, The Effect of Smoke Particles on Clouds and Climate Forcing, *Science*, *277* (5332), 1636-1639, 1997.

Kaufman, Y.J., and I. Koren, Smoke and Pollution Aerosol Effect on Cloud Cover, *Science*, *313*, 655-658, 2006.

Kaufman, Y.J., I. Koren, L.A. Remer, D. Rosenfeld, and Y. Rudich, The effect of smoke, dust, and pollution aerosol on shallow cloud development over the Atlantic Ocean, *Proceedings of the National Academy of Sciences of the United States of America*, *102* (32), 11207-11212, 2005.

Khlystov, A., C.O. Stanier, S. Takahama, and S.N. Pandis, Water content of ambient aerosol during the Pittsburg Air Quality Study, *Journal of Geophysical Research*, *110* (D07S10), doi:10.1029/2004JD004651, 2005.

Lee, Y.S., D.R. Collins, R. Li, K.P. Bowman, and G. Feingold, Expected impact of an aged biomass burning aerosol on cloud condensation nuclei and cloud droplet concentrations, *Journal of Geophysical Research*, *111* (D22204), doi:10.1029/2005JD006464, 2006.

Li, J., M. Posfai, P.V. Hobbs, and P.R. Buseck, Individual aerosol particles from biomass burning in southern Africa: 2. Compositions and aging of inorganic particles, *Journal of Geophysical Research*, *108(D13)* (8484), doi:10.1029/2002JD002310, 2003.

Li, W.Y., and L.Y. Shao, Direct observation of aerosol particles in aged agricultural biomass burning plumes impacting urban atmospheres, *Atmospheric Chemistry and Physics Discussions*, *10* (4), 10589-10623, 2010.

Liu, X.D., P. Van Espen, F. Adams, J. Cafmeyer, and W. Maenhaut, Biomass burning in southern Africa: Individual particle characterization of atmospheric aerosols and savanna fire samples, *Journal of Atmospheric Chemistry*, *36* (2), 135-155, 2000.

McMeeking, G.R., S.M. Kreidenweis, S. Baker, C.M. Carrico, J.C. Chow, J.L. Collett, W.M. Hao, A.S. Holden, T.W. Kirchstetter, W.C. Malm, H. Moosmueller, A.P. Sullivan, and C.E. Wold, Emissions of trace gases and aerosols during the open combustion of biomass in the laboratory, *Journal of Geophysical Research*, *114* (D19210), doi:10.1029/2009JD011836, 2009.

Mircea, M., M.C. Facchini, S. Decesari, F. Cavalli, L. Emblico, S. Fuzzi, A. Vestin, J. Rissler, E. Swietlicki, G. Frank, M.O. Andreae, W. Maenhaut, Y. Rudich, and P. Artaxo, Importance of the organic aerosol fraction for modeling aerosol hygroscopic growth and activation: a case study in the Amazon Basin, *Atmospheric Chemistry and Physics*, *5*, 3111-3126, 2005.

Mochida, M., A. Kawabata, K. Kawamura, H. Hatsushika, and K. Yamazaki, Seasonal variation and origins of dicarboxylic acids in the marine atmosphere over the western North Pacific, *Journal of Geophysical Research, 108*, doi:10.1029/2002JD002355, 2003.

Moffet, R.C., B. de Foy, L.T. Molina, M.J. Molina, and K.A. Prather, Measurement of ambient aerosols in northern Mexico City by single particle mass spectrometry, *Atmospheric Chemistry and Physics*, *8*, 4499-4516, 2008a.

Moffet, R.C., X. Qin, T.P. Rebotier, H.F. Furutani, and K.A. Prather, Chemically segregated optical and microphysical properties of ambient aerosols measured in a single-particle

mass spectrometer, *Journal of Geophysical Research*, *113* (D12213), doi:10.1029/2007JD009393, 2008b.

Neubauer, K.R., M.V. Johnston, and A.S. Wexler, Humidity effects on the mass spectra of single aerosol particles, *Atmospheric Environment*, *32* (14-15), 2521-2529, 1998.

Novakov, T., and C.E. Corrigan, Cloud condensation nucleus activity of the organic component of biomass smoke particles, *Geophysical Research Letters*, *23* (16), 2141-2144, 1996.

Pathak, R.V., P.K.K. Louie, and C.K. Chan, Characteristics of aerosol acidity in Hong Kong, *Atmospheric Environment*, *38*, 2965-2974, 2004.

Petters, M.D., C.M. Carrico, S.M. Kreidenweis, A.J. Prenni, P.J. DeMott, J.L. Collett, and H. Moosmueller, Cloud Condensation Nuclei Activity of Biomass Burning Aerosol, *Journal of Geophysical Research*, *114* (D22205), doi:10.1029/2009JD012353, 2009a.

Petters, M.D., and S.M. Kreidenweis, A single parameter representation of hygroscopic growth and cloud condensation nucleus activity, *Atmospheric Chemistry and Physics*, *7* (8), 1961-1971, 2007.

Petters, M.D., M.T. Parsons, A.J. Prenni, P.J. DeMott, S.M. Kreidenweis, C.M. Carrico, A.P. Sullivan, G.R. McMeeking, E. Levin, C.E. Wold, J.L. Collett, and H. Moosmueller, Ice nuclei emissions from biomass burning, *Journal of Geophysical Research*, *114* (D07209), doi:10.1029/2008JD011532, 2009b.

Posfai, M., A. Gelencser, R. Simonics, K. K. Arato, J. Li, P.V. Hobbs, and P.V. Buseck, Atmospheric tar balls: Particles from biomass and biofuel burning, *Journal of Geophysical Research*, *109* (D06213), doi:10.1029/2003JD004169, 2004.

Posfai, M., R. Simonics, J. Li, P.V. Hobbs, and P.R. Buseck, Individual aerosol particles from biomass burning in southern Africa: 1. Compositions and size distributions of carbonaceous particles, *Journal of Geophysical Research*, *108* (D13), 8483, doi:10.1029/2002JD002291, 2003.

Pratt, K.A., L.E. Hatch, and K.A. Prather, Seasonal volatility dependence of ambient particle phase amines, *Environmental Science and Technology*, *43* (14), 5276-5281, 2009.

Prenni, A.J., M.D. Petters, S.M. Kreidenweis, P.J. DeMott, and P.J. Ziemann, Cloud droplet activation of secondary organic aerosol, *Journal of Geophysical Research*, *112* (D10), D10223, doi:10.1029/2006JD007963, 2007.

Pringle, K.J., H. Tost, A. Pozzer, U. Poeschl, and J. Lelieveld, Global distribution of the effective aerosol hygroscopicity parameter for CCN activation, *Atmospheric Chemistry and Physics*, *10*, 5241-5255, 2010.

Ramanathan, V., P.J. Crutzen, J. Lelieveld, A.P. Mitra, D. Althausen, J. Anderson, M.O. Andreae, W. Cantrell, G.R. Cass, C.E. Chung, A.D. Clarke, J.A. Coakley, W.D. Collins, W.C. Conant, F. Dulac, J. Heintzenberg, A.J. Heymsfield, B. Holben, S.

Howell, J. Hudson, A. Jayaraman, J.T. Kiehl, T.N. Krishnamurti, D. Lubin, G. McFarquhar, T. Novakov, J.A. Ogren, I.A. Podgorny, K.A. Prather, K. Priestley, J.M. Prospero, P.K. Quinn, E. Rajeev, P. Rasch, S. Rupert, R. Sadourny, S.K. Satheesh, G.E. Shaw, P. Sheridan, and F.P.J. Valero, Indian Ocean Experiment: An integrated analysis of the climate forcing and effects of the great Indo-Asian haze, *Journal of Geophysical Research*, *106* (D22), 28,371-28,398, 2001.

Rebotier, T.P., and K.A. Prather, Aerosol time-of-flight mass spectrometry data analysis: A benchmark of clustering algorithms., *Analytica Chimica Acta*, *585* (1), 38-54, 2007.

Reid, J.S., R. Koppmann, T.F. Eck, and D.P. Eleuterio, A review of biomass burning emissions part II: intensive physical properties of biomass burning particles, *Atmospheric Chemistry and Physics*, *5*, 799-825, 2005.

Rissler, J., E. Swietlicki, J. Zhou, G. Roberts, M.O. Andreae, L.V. Gatti, and P. Artaxo, Physical properties of the sub-micrometer aerosol over the Amazon rain forest during the wet-to-dry season transition- comparison of modeled and measured CCN concentrations, *Atmospheric Chemistry and Physics*, *4*, 2119-2143, 2004.

Roberts, G.C., P. Artaxo, J. Zhou, E. Swietlicki, and M.O. Andreae, Sensitivity of CCN spectra on chemical and physical properties of aerosol: A case study from the Amazon Basin, *Journal of Geophysical Research*, *107* (D20), 8070, doi:10.1029/2001JD000583, 2002.

Roberts, G.C., D.A. Day, L.M. Russell, E.J. Dunlea, J.L. Jimenenez, J.M. Tomlinson, D.R. Collins, Y. Shinozuka, and A.D. Clarke, Characterization of particle cloud droplet activity and composition in the free troposphere and the boundary layer during INTEX-B, *Atmospheric Chemistry and Physics*, *10*, 6627-6644, 2010.

Roberts, G.C., and A. Nenes, A Continuous-Flow Streamwise Thermal-Gradient CCN Chamber for Atmospheric Measurements, *Aerosol Science and Technology*, *39*, 206-221, 2005.

Rose, D., A. Nowak, P. Achtert, A. Wiedensohler, M. Hu, M. Shao, Y. Zhang, M.O. Andreae, and U. Poeschl, Cloud condensation nuclei in polluted air and biomass burning smoke near the mega-city Guangzhou, China - Part 1: Size-resolved measurements and implications for the modeling of aerosol particle hygroscopicity and CCN activity, *Atmospheric Chemistry and Physics Discussions*, *8*, 17343-17392, 2008.

Rose, D., A. Nowak, P. Achtert, A. Wiedensohler, M. Hu, M. Shao, Y. Zhang, M.O. Andreae, and U. Poeschl, Cloud condensation nuclei in polluted air and biomass burning smoke near the mega-city Guangzhou, China - Part 1: Size-resolved measurements and implications for the modeling of aerosol particle hygroscopicity and CCN activity, *Atmospheric Chemistry and Physics*, *10*, 3365-3383, 2010.

Rosenfeld, D., TRMM Observed First Direct Evidence of Smoke from Forest Fires Inhibiting Rainfall, *Geophysical Research Letters*, *26* (20), 3105-3108, 1999.

Semeniuk, T.A., M.E. Wise, S.T. Martin, L.M. Russell, and P.R. Buseck, Hygroscopic behavior of aerosol particles from biomass fires using environmental transmission electron microscopy, *Journal of Atmospheric Chemistry*, *56*, 259-273, 2006.

Shields, L., D.T. Suess, and K.A. Prather, Determination of single particle mass spectral signatures from heavy-duty diesel vehicle emissions for PM2.5 source apportionment, *Atmospheric Environment*, *41* (18), 3841-3852, 2007.

Shinozuka, Y., A.D. Clarke, P.F. DeCarlo, J.L. Jimenez, E.J. Dunlea, G.C. Roberts, J.M. Tomlinson, D.R. Collins, S.G. Howell, V.N. Kapustin, C.S. McNaughton, and J. Zhou, Aerosol optical properties relevant to regional remote sensing of CCN activity and links to their organic mass fraction: airborne observations over Central Mexico and the US West Coast during MILAGRO/INTEX-B, *Atmospheric Chemistry and Physics Discussions*, *9*, 12519-12558, 2009.

Silva, P.J., D. Liu, C.A. Noble, and K.A. Prather, Size and Chemical Characterization of Individual Particles Resulting from Biomass Burning of Local Southern California Species, *Environmental Science and Technology*, *33* (18), 3068-3076, 1999.

Sodeman, D.A., S.M. Toner, and K.A. Prather, Determination of Single Particle Mass Spectral Signatures from Light-Duty Vehicle Emissions, *Environmental Science and Technology*, *39* ((12)), 4569-4580, 2005.

Solomon, S., D. Qin, M. Manning, Z. Chen, M. Marquis, K.B. Averyt, M. Tignor, and H.L. Miller, Climate Change 2007: The Physical Science Basis, Contribution of Working Group I to the Fourth Assessment Report of the Intergovernmental Panel on Climate Change, 2007.

Sorooshian, A., S.M. Murphy, S. Hersey, H. Gates, L.T. Padro, A. Nenes, F.J. Brechtel, H. Jonsson, R.C. Flagan, and J.H. Seinfeld, Comprehensive airborne characterization of aerosol from a major bovine source, *Atmospheric Chemistry and Physics Discussions*, *8*, 10415-10479, 2008.

Sorooshian, A., V. Varutbangkul, F.J. Brechtel, B. Ervens, G. Feingold, R. Bahreini, S.M. Murphy, J.S. Holloway, E.L. Atlas, G. Buzorius, H. Jonsson, R.C. Flagan, and J.H. Seinfeld, Oxalic acid in clear and cloudy atmospheres: Analysis of data from International Consortium for Atmospheric Research on Transport and Transformation 2004, *Journal of Geophysical Research*, *111* (D23S45), doi:10.1029/2005JD006880, 2006.

Su, Y.X., M.F. Sipin, H.F. Furutani, and K.A. Prather, Development and characterization of an aerosol time-of-flight mass spectrometer with increased detection efficiency, *Analytical Chemistry*, *76*, 712-719, 2004.

Sullivan, R.C., S.A. Guazzotti, D.A. Sodeman, and K.A. Prather, Direct observations of the atmospheric processing of Asian mineral dust, *Atmospheric Chemistry and Physics*, *7* (5), 1213-1236, 2007.

Sullivan, R.C., and K.A. Prather, Investigations of the Diurnal Cycle and Mixing State of Oxalic Acid in Individual Particles in Asian Aerosol Outflow, *Environmental Science and Technology*, *41*, 8062-8069, 2007.

Thornton, J.A., J.P. Kercher, T.P. Riedel, N.L. Wagner, J. Cozic, J.S. Holloway, W.P. Dube, G.M. Wolfe, P.K. Quinn, A.M. Middlebrook, B. Alexander, and S.S. Brown, A large atomic chlorine source inferred from mid-continental reactive nitrogen chemistry, *Nature*, *464*, 271-274, 2010.

Tivanski, A.V., R.J. Hopkins, T. Tyliszczak, and M.K. Gilles, Oxygenated Interface on Biomass Burn Tar Balls Determined by Single Particle Scanning Transmission X-ray Microscopy, *Journal of Physical Chemistry A*, *111*, 5448-5458, 2007.

Toner, S.M., L.G. Shields, D.A. Sodeman, and K.A. Prather, Using mass spectral source signatures to apportion exhaust particles from gasoline and diesel powered vehicles in a freeway study using UF-ATOFMS, *Atmospheric Environment*, *42* (3), 568-581, 2008.

Toner, S.M., D.A. Sodeman, and K.A. Prather, Single Particle Characterization of Ultrafine and Accumulation Mode Particles from Heavy Duty Diesel Vehicles Using Aerosol Time-of-Flight Mass Spectrometry, *Environmental Science and Technology*, *40* (12), 3912-3921, 2006.

Trebs, I., S. Metzger, F.X. Meixner, G. Helas, A. Hoffer, Y. Rudich, A.H. Falkovich, M.A.L. Moura, R.S. da Silva, P. Artaxo, J. Slanina, and M.O. Andreae, The NH4+ -NO3- -Cl- -SO42- -H2O aerosol system and its gas phase precursors at a pasture site in the Amazon Basin: How relevant are mineral cations and soluble organic acids? *Journal of Geophysical Research*, *110*, D07303, 2005.

Val Martin, M., J.A. Logan, R.A. Kahn, F.-Y. Leung, D.L. Nelson, and D.J. Diner, Smoke injection heights from fires in North America: analysis of 5 years of satellite observations, *Atmospheric Chemistry and Physics*, *10* (4), 1491-1510, 2010.

VanReken, T.M., N.L. Ng, R.C. Flagan, and J.H. Seinfeld, Cloud condensation nucleus activation properties of biogenic secondary organic aerosol, *Journal of Geophysical Research*, *110* (D7), D07206, doi:10.1029/2004JD005465, 2005.

Weimer, S., M.R. Alfarra, D. D. Schreiber, M. M. Mohr, A.S.H. Prevot, and U. Baltensperger, Organic aerosol mass spectral signatures from wood-burning emissions: Influence of burning conditions and wood type, *Journal of Geophysical Research*, *113* (D10304), doi:10.1029/2007JD009309, 2008.

Wexler, A.S., and S.L. Clegg, Atmospheric aerosol models for systems including ions H+, NH4+, Na+, SO42-, NO3-, Cl-, Br- and H2O, *Journal of Geophysical Research*, *107* (D14), 4207, 2002.

Yamasoe, M.A., P. Artaxo, A.H. Miguel, and A.G. Allen, Chemical composition of aerosol particles from direct emissions of vegetation fires in the Amazon Basin: water-soluble species and trace elements, *Atmospheric Environment*, *34*, 1641-1653, 2000.

Yokelson, R., J.D. Crounse, P. DeCarlo, T. Karl, S. Urbanski, E. Atlas, T. Campos, Y. Shinozuka, V.N. Kapustin, A.D. Clarke, A. Weinheimer, D.J. Knapp, D.D. Montzka, J. Holloway, P. Weibring, F. Flocke, W. Zheng, D. Toohey, P.O. Wennberg, C. Wiedinmyer, L. Mauldin, A. Freid, D. Richter, J. Walega, J.L. Jimenez, K. Adachi, P.R. Buseck, S.R. Hall, and R. Shetter, Emissions from biomass burning in the Yucatan, *Atmospheric Chemistry and Physics Discussions*, *9*, 767-835, 2009.

Zhang, Q., J.L. Jimenez, D.R. Worsnop, and M. Canagaratna, A Case Study of Urban Particle Acidity and Its Influence on Secondary Organic Aerosol, *Environmental Science and Technology*, *41*, 3213-3219, 2007.

Chapter 4

Real-time Single Particle Composition and Cloud Condensation Nuclei (CCN) Activity at Owens (dry) Lake Bed

4.1 Synopsis

Owens Lake is one of the largest sources of $PM_{2.5}$ in the Western Hemisphere [*Gill and Gillette*, 1991]. Alkaline and saline dust particles can be lofted high in the atmosphere and transported over long distances, thus having the potential to impact climate over a large region. Because the formation of salty crusts on dry lakebeds is caused by fast evaporation of water, soluble salts can be concentrated at the top of the lakebed, forming a thin surface that is very heterogeneous in nature, and is easily eroded by wind perturbations. Thus, there is great potential for a large percentage of the windblown Owens Lake dust to be highly soluble, impact cloud formation, and possibly precipitation in the Sierra region. Individual particle size and composition, along with condensation nuclei (CN) concentrations and cloud condensation nuclei (CCN) spectra were measured in real time at a Great Unified Basin Air Pollution Control District air quality monitoring station on the south east end of Owens Lake during November 2009 to understand the effect of particle mixing state on CCN activity. Aerosol hygroscopicity was estimated from the CCN measurements and compared to simultaneous aerosol chemistry and size distribution measurements. Over the course of the study, two dust events occurred when wind speeds increased and came predominantly from the south, leading to increases in both PM_{10} and $PM_{2.5}$. An increase in detected dust particles was measured during the dust events with changes in particle chemistry, a shift from more salt-like dust to more alumina-silicate type dust, compared to the non-events, and an increase in particles 100-4000 nm, including those within the range of activation diameters, 129-300

nm. Size-resolved particle composition measurements close to the activation threshold indicate that particles 250-500 nm were significantly impacted by dust, as 25-40% of the particles of those sizes were K-rich dust. However, there was no significant change in particle hygroscopicity observed during the dust events with a median $\kappa_{0.1}$ value of 0.06, compared to the median value of $\kappa_{0.1}$= 0.05 for the entire study; and the median $\kappa_{0.7}$ was 0.01, similar to the entire study, $\kappa_{0.7}$ =0.01, indicating the dust is moderately hygroscopic. Most of the dust particles observed during the event were ~ 100-4000 nm and chemical measurements show the dust > 200 nm has soluble inclusions of nitrate, chloride and sulfate. Therefore, a majority of the dust particles are large enough and would activate to become CCN (or GCCN). As most of the particles > 500 nm were dust and most CCN were > 500 nm at 0.1% S_c, the dust needs to be CCN active to explain the NCCN observed.

4.2 Introduction

Alkaline and saline mineral dust particles can be lofted high in the atmosphere and transported over long distances, thus having the potential to impact regional climate over a large area. Mineral dust can both absorb and scatter radiation, and act as cloud condensation nuclei (CCN) [*(IPCC)*, 2007; *Satheesh and Moorthy*, 2005]. Dust has been shown to both enhance and suppress precipitation, depending on its physical and chemical properties and local meteorological conditions [*Levin et al.*, 1996; *Rosenfeld et al.*, 2001; *Rudich et al.*, 2002; *Yin et al.*, 2002]. Over the Aral sea, where dust particles are large and soluble, precipitation was enhanced due to an increase in the effective radius of the cloud droplets [*Rudich et al.*, 2002]. However, submicron and insoluble Saharan dust has been shown to suppress precipitation by causing a decrease in the cloud droplet effective radius [*Rudich et al.*, 2002]. As the sizes of arid regions increase due to warming and changes in precipitation from anthropogenic activities, further studies of the effect of dust on climate are needed.

Often, fresh submicron mineral dust particles are considered to be insoluble and assumed not to act as CCN until they undergo processing in the atmosphere [*Andreae and Rosenfeld*, 2008; *Liu et al.*, 2005]. However, mineral dust particles have different mineralogies which control how they react in the atmosphere. Calcium-rich mineral dust particles have been shown to be more nitrate-rich, while alumina-silicate particles have been shown to be more associated with sulfate after undergoing atmospheric processing [*Sullivan et al.*, 2007]. These differences in reactivity have significant implications on the hygroscopicity of the particles with different mineralogies. Previous laboratory studies have shown that the reaction of calcite (calcium carbonate) dust with trace nitric acid to form calcium nitrate can increase the hygroscopicity of the original source dust by over 100-fold [*Sullivan et al.*, 2009a]. However, not all proxies for aged mineral dust are more soluble and hygroscopic than the original dust. While calcium nitrate and calcium chloride are very soluble and hygroscopic, calcium sulfate, a proxy for reacted dust, is as non-hygroscopic as calcium oxalate and calcium carbonate [*Sullivan et al.*, 2009b].

Previous field measurements have highlighted the importance of dry lakebed/playa dust in the formation of North American continental clouds [*Pratt et al.*, 2009; *Pratt et al.*, 2010]. Dry lakebed salts containing sodium, potassium, magnesium, calcium and chloride from the Great Basin region of the U.S. were detected in clouds over Wyoming [*Pratt et al.*, 2010]. Dry lakebed salts are moderately soluble, with ~3-44% of the mass consisting of soluble salts [*Abuduwaili et al.*, 2008; *Blank et al.*, 1999; *Koehler et al.*, 2007; *Reheis*, 1997; *Singer et al.*, 2003]. The formation of salty crusts on dry lakebeds is caused by fast evaporation of water [*Reynolds et al.*, 2007]. This process concentrates soluble salts at the top of the lakebed, which form a thin surface that is very heterogeneous in nature, and is easily eroded by wind perturbations [*Blackwelder*, 1931; *Cahill et al.*, 1996; *Lowenstein and Hardie*, 1985; *Reheis*, 1997].

Owens (dry) Lake is one of the largest sources of $PM_{2.5}$ in the Western Hemisphere [*Gill and Gillette*, 1991]. Owens lakebed contained water for the last 800,000 years, but in 1913 the source of the water was diverted to Los Angeles County and within 15 years, the lake became completely dry [*Koehler et al.*, 2007]. Currently, Owens Lake playa obtains moisture from a natural underground brine pool which floods often in the winter and spring [*Cahill et al.*, 1996] in addition to having parts of the lake flooded intentionally to reduce the impact of the airborne dust on local air quality. As previously mentioned, because of the formation mechanism of the salt crust at Owens Lake, a large percentage of the dust is highly soluble. Dust plumes from Owens Lake have been lofted to 2 km above the ground, transported 250 km, and have extended to cover 90,000 square miles due to the complex topography of the area [*Reid et al.*, 1994]. Thus, there is potential for these particles to impact cloud formation and precipitation in the region. Previous analysis of Owens Lake dust has shown that 60-90% of dust is D < 10 μm and 10-50% of dust D < 2 μm. Additionally, 3-37% of the dust is soluble salt by mass, 40-75% calcite, smectites, illites, kaolinites, quartz and plagioclase feldspar by mass, and 0.9-30% organic species by mass [*Koehler et al.*, 2007; *Niemeyer et al.*, 1999; *Reheis*, 1997; *Reid et al.*, 1994]. The dominant salts of Owens Lake crust are sodium sulfate, sodium carbonate and their hydrates, and sodium chloride.

Previous humidified tandem differential mobility analyzer (HTDMA) experiments of both wet- and dry-generated Owens Lake dust samples showed a high degree of heterogeneity in the samples with hygroscopicity parameter (κ) values ranging from 0.05-0.82 [*Koehler et al.*, 2007]. Previous wet-generated CCN experiments of Owens Lake dust samples gave κ values between 0.39 and 1.07, close to those of sodium carbonate (κ=1.29) and sodium sulfate (κ=1.02) [*Koehler et al.*, 2007]. The predicted κ value of dry-generated dust from CCN experiments is 0.04 based on extrapolation of subsaturated hygroscopicity measurements, which indicates that a 300 nm particle would activate to form a cloud drop at 0.1%

supersaturation, showing that even a low concentrations of moderately hygroscopic dust could significantly contribute to the CCN or giant (GCCN) populations [*Koehler et al.*, 2007; *Rudich et al.*, 2002]. Due to the mixture of the thin surface of soluble salts and other less soluble minerals below the top layer, the aerosol produced from these samples is very heterogeneous in nature of as reflected in the range of measured hygroscopicities.

Because of the combination of heterogeneous aerosol composition and mineralogy produced at Owens Lake, further investigation into the mixing state and resulting hygroscopicity of is needed. For the first time, individual particle size and composition, alongside CN concentrations and CCN spectra were measured in real time at the Great Unified Basin Air Pollution Control District air quality monitoring station on the southeast end of Owens Lake during November 2009. The chemical, size and concentration variations of aerosol before, during, and after local dust events were characterized and evaluated. Aerosol hygroscopicity was estimated from CCN measurements and compared to simultaneous aerosol chemistry and size distribution measurements. Additionally, soil and suspended dust samples were collected from the lake bed and run after the completion of the study.

4.3 Materials and Methods

4.3.1 Sampling location

Measurements took place at the Great Unified Basin Air Pollution Control District air quality monitoring station “Dirty Socks” (36.33N, 117.96W, 1,084 m above sea level) on the south east end of Owens (dry) Lakebed from November 5 - 27th 2009. This site is a remote monitoring site that is periodically influenced by local dust storms. The aerosol was sampled through an insulated 2 m stainless steel sampling line (3/2” I. D.) from the Prather Lab Mobile Trailer and insulated conductive silicone tubing (1/4” or 3/8” I.D.) was used to transport the aerosol from the bottom of the sampling line to each of the various instruments in

the trailer. During the study, there were two significant dust events, one from November 11-12 and a second November 20-21.

4.3.2 Instrumentation

4.3.2.1 Single particle mass spectrometry

Single particle aerodynamic size and chemical composition were measured in real-time using an aerosol time-of-flight mass spectrometer (ATOFMS) equipped with a nozzle based inlet that transmits particles with an aerodynamic diameter (D_a) between 200 to 3000 nm. Single particle size is determined from the particle's velocity using the time-of-flight between two 532 nm CW lasers. The particle velocity is then used to time a Q-switched 266 nm Nd:YAG laser at the moment the particle enters the source region of the dual ion time-of-flight mass spectrometer that desorbs the particle and ionizes the desorbed species. The resulting positive and negative ions are then analyzed. An introduction of the ATOFMS instrument design and operation are described elsewhere [*Gard et al.*, 1997].

4.3.2.2 Size distributions and number concentrations

The submicron particle size distributions and number concentrations were measured concurrently by a scanning mobility particle sizer (SMPS, TSI Model 3936) with sheath and aerosol flows of 4.0 and 0.4 lpm, respectively. SMPS size distributions of particles 11-600 nm were collected every 5 minutes. An aerosol particle sizer (APS, TSI Model 3321) was also used to measure the particle size distribution of particles ~0.6 – 10 μm every minute. Total particle condensation nuclei (CN) concentrations were measured with a condensation particle counter every second (CPC, TSI model 3010).

4.3.2.3 Cloud condensation nuclei

CCN spectra were measured by scanning supersaturation from 0.11 – 1% continuously every 10 minutes while recording CCN concentrations every second with a miniaturized streamwise thermal-gradient CCN counter (mCCNc) based on Roberts and

Nenes (2005) [*Roberts and Nenes*, 2005]. The fraction of CCN active particles, or fCCN, was obtained from the CCN/CN ratio. Due to the lower size limit of the CPC, CN is more accurately described as CN_{10}, and therefore fCCN is more precisely $fCCN_{10}$. For simplicity, $fCCN_{10}$ will be referred to as fCCN for the remainder of the paper. During short periods throughout the study, the CCN was not scanning supersaturation, but was measuring CCN at one supersaturation only (S_c=0.08%), hereafter referred to as static mode. The instrument was calibrated in both static and scanning modes at the beginning and the end of the study with ammonium sulfate aerosol (99.999%, Sigma Aldrich) using thermodynamics from the Aerosol Inorganic Model (AIM) [*Wexler and Clegg*, 2002] and a surface tension of pure water at 298.15 K.

4.3.2.4 $PM_{2.5}$ and PM_{10} measurements

Hourly-averaged total particulate mass ≤ 2.5 μm was measured using a Met One Beta Attenuation Monitor (BAM) model 1020 with a particle inlet approximately 4 m above the ground. Hourly-averaged total particulate mass ≤ 10 μm was measured using a Rupprecht & Patashnick Tapered Element Oscillating Microbalance (TEOM) model 1400ab provided by the Great Basin Unified Air Pollution Control District in a separate enclosure 5 m northeast of the Prather Mobile Lab trailer.

4.3.2.5 Meteorological measurements

Wind speed and wind direction were measured using a RM Young Wind Monitor model 41010. Relative humidity (RH) and temperature were measured using a Vaisala temperature and RH sensor model HMP45AC. Meteorological measurements were made approximately 3.5 m above the ground and recorded every minute. There were no precipitation events over the course of the study. The NOAA HYSPLIT software version 4.9 (updated February of 2009) was used to calculate air mass back trajectories.

4.3.2.6 Soil and dust sample collection and analysis

Approximately 500 g of top soil (~ 1 inch) from various sites around the lakebed were collected with a clean shovel and placed in clean, quart-sized resealable plastic bags. The shovel used to collect the samples was thoroughly cleaned with ultrapure water and dried in between samples. Two to three grams of suspended dust were collected during the second dust event by attaching a plastic centrifuge tube downstream of a plastic funnel on a 2nd, unused Wind Monitor ~3.5 m above the ground. Samples were stored in a cool, dry place until they were analyzed. Details regarding each of the samples can be found in Table 4.1. It has been shown that dry generation of samples is more representative of the original soil and dust samples [*Koehler et al.*, 2007; *Sullivan et al.*, 2010], but due to the wet and bulky nature of the samples collected, a steady and constant flow of relatively high concentrations of submicron particles would not be possible to produce via this method. The formation process of the Owens Lake salt crust involves hydration and recrystallization of the crustal layers, therefore to some extent the wet-generation method may also be producing particles via a similar process to those that occur naturally [*Koehler et al.*, 2007], but some of the original mixing state and mineralogy of the dust will be lost. To analyze the various soil and dust samples, a wet-generation method was used to send the aerosol to either the ATOFMS to analyze the single particle chemistry or to the CCNc to analyze the hygroscopicity within 1 month after the field study. Due to the heterogeneous nature of the dust samples, the original size-dependent particle composition will become altered when the bulk samples are suspended in water and then atomized, mainly the soluble compounds become redistributed across all particles; some particles which were not originally associated with soluble material can have become transformed into an internally mixed particle [*Sullivan et al.*, 2010]. The wet-generation method involved atomization of aqueous solutions using high purity compressed air at 2–3 lpm, and then venting excess flow through a HEPA filter before passing the aerosol

through two silica gel diffusion driers to reduce the RH below 20%. Depending on the solubility and nature of the various samples, 0.1 to several grams of each sample were added into ~150mL milli-Q water (>18.2MΩ). At least 500 non-size-selected particles were collected per sample for ATOFMS analysis of the samples. A total of 13,106 single particle mass spectra were collected for the lab samples. For CCN analysis of the samples, the dry aerosol was sent to a differential mobility analyzer (DMA, Model 3081, TSI Inc.) for size selection with sheath and aerosol flows of 10.0 and 1.0, respectively. The monodisperse aerosol output from the DMA was then sent through a flow splitter where the aerosol was divided into a condensation particle counter (CPC, Model 3010, TSI Inc.) and the CCNc (described previously). A small excess aerosol flow of ~0.3 lpm was vented through a HEPA filter to eliminate pressure build up that could cause flow imbalances. Conductive silicone tubing was used to transport the aerosol. CCN activation curves were generated by scanning the dry particle diameter (D_{dry}) at a fixed supersaturation (SS). Both the CCNc and CPC record 1Hz averaged data, which were averaged to one minute to calculate fCCN. The critical activation diameter (D_{act}=D_{dry}) was determined by scaling all ratios to the maximum observed CCN/CN ratio (~1). The contribution from larger multiply charged particles to the size selected monodisperse aerosol was then accounted for following the procedure used by [*Rose et al.*, 2008]. Each activation curve was then fitted with a sigmoidal curve to determine the particle diameter at which ~50% of the particles activated. Each sample was analyzed with a size scan at three different supersaturations: 0.22, 0.36 and 0.57%.

Table 4.1. Soil and dust samples details.

Sample ID	Description/appearance	Approximate location
1a	Harder crust	Sandy dunes 100 m east of sampling site
1b	Softer, finer sand	Sandy dunes 100 m east of sampling site
2a	Finer, white soil	Dirty Sock pond untouched lake bed, 200 m east of sampling site
2c	Harder, brown crust	Dirty Sock pond untouched lake bed, 200 m east of sampling site
3a	White soil at edge of grass	Grass farm area, about 1000 m northeast of sampling site
3b	Soil in middle of grass	Grass farm area, about 1000 m northeast of sampling site
3c	Harder, brown crust at edge of grass	Grass farm area, about 1000 m northeast of sampling site
4a	Brown/orange crust at edge of lake	Large "C" shaped lake, about 1000 m north of sampling site
4b	Square/hard brown crust at edge of lake	Large "C" shaped lake, about 1000 m north of sampling site
4c	Wetter soil near edge of lake	Large "C" shaped lake, about 1000 m north of sampling site
5	Dried brown crust by water bubbler	"Large" lake, about 2000 m north of sampling site
6b	Sandy/gravel soil	10 m east of sampling site
6c	Dry, sandy soil	10 m west of sampling site
Suspended dust	Fine sand	Airborne at sampling site, 2nd dust event

4.3.3 Data analysis

4.3.3.1 ATOFMS data analysis

A total of 121,225 single ambient particle mass spectra were collected over the course of the study. Analysis based on particular mass spectral features within the data set was performed with a Matlab-based (ver. 6.5.1) toolset, YAADA (ver. 1.2) (http://www.yaada.org). The single particle data was first divided into sub- and supermicron particles before being automatically sorted and grouped into clusters of particles with similar mass spectral characteristics using the adaptive resonance theory neural network algorithm, ART-2a [*Song and Hopke*, 1999]. The main user-defined parameters for ART-2a are the learning rate, number of iterations, and vigilance factor, which were set to 0.05, 20, and 0.80,

respectively [*Rebotier and Prather*, 2007]. The resulting clusters were then analyzed manually and classified into distinct particle types based on their mass spectral features [*Furutani et al.*, 2008; *Guazzotti et al.*, 2003; *Moffet et al.*, 2008; *Silva et al.*, 1999; *Sullivan et al.*, 2007]. The 50 largest particle clusters, representing over 89% of submicron and 92% of supermicron classified particles were labeled as mineral dust, biomass burning, elemental carbon (EC), elemental carbon with organic carbon (ECOC), organic carbon (OC), biogenic, and particles with negative spectra only (Neg only). Further details on specific dust types are discussed in the results section. The appearance or nonexistence of secondary aerosol species like nitrate, sulfate and ammonium was not used as part of the previous classifications.

4.3.3.2 Single hygroscopicity parameter

To directly compare the hygroscopicity measurements made with the mCCNc to the composition measurements, a single parameter for particle hygroscopicity (κ) is used [*Petters and Kreidenweis*, 2007]. The following equation defines the relationship between a growing particle's equilibrium water saturation ratio, S, droplet diameter, D, dry diameter, D_{dry}, and hygroscopicity, κ:

$$S(D) = \frac{D^3 - D_{dry}^3}{D^3 - D_{dry}^3(1-\kappa)} \exp\left(\frac{A}{D}\right) \qquad (4.1)$$

where $A = 2.1\text{x}10^{-9}$ m is a constant evaluated for a surface tension of 0.072 J m^{-2} (pure water) and temperature of 298.15 K [*Petters and Kreidenweis*, 2007]. κ describes a particle's water activity and typical values range from 1.4 (hygroscopic soluble salt; NaCl) to about 0 (insoluble but wettable; fresh soot) for atmospherically relevant systems. The CCN activation diameter (D_{act}) of atmospheric aerosols was estimated using the measured size distributions, CN, and CCN concentrations from

$$1-\frac{CCN}{CN}=\frac{\int_{D_0}^{D_{act}} n(D)dD}{N_{total}} \qquad (4.2)$$

where N_{total} is the cumulative concentration obtained by integrating the observed size distribution of $n(D)$ obtained from the SMPS measurements, D is the electric mobility diameter selected by the SMPS and D_o the smallest size measured by the SMPS (~11 nm). The CCN/CN ratio represents the fraction of the CCN-active aerosol (fCCN). Eqn. (2) assumes that all chemical compositions are internally mixed (i.e. homogeneous particle composition). This approach was taken to simplify the data analysis yet still reflects how much the relative degree of variation in the chemical composition affects CCN activity, as the size resolved chemistry was simultaneously measured [*Furutani et al.*, 2008]. In the estimation of D_{act}, contributions from particles larger than the range of the SMPS (upper range = 600 nm for our settings) were not considered and should be minimal.

The CCN and CPC data were filtered to eliminate any instrumental noise from the data. The instantaneous CCN/CPC ratio, or fCCN, was then calculated every second and used to determine the instantaneous activation diameter from the cumulative SMPS size distribution as mentioned previously. Hygroscopicity parameter, κ was calculated from the instantaneous estimated activation diameter and the corresponding mCCNc supersaturation values using a version of Petters' interactive data language (IDL) script (http://www4.ncsu.edu/~mdpetter/findkappa.pro) based on [*Petters and Kreidenweis*, 2007] modified to run in the R programming language (http://www.r-project.org/) and can be found on the Prather group website (http://atofms.ucsd.edu/content/code). Due to the high volume of data, CCN concentrations and hygroscopicity parameter κ were binned by supersaturation.

4.4 Results

4.4.1 Particle mass and meteorology overview

$PM_{2.5}$ and PM_{10} particle mass, temperature, relative humidity (RH), wind speed, wind direction and APS size distribution are shown in Figure 4.1. The two dust events are shown clearly by the increase in both $PM_{2.5}$ and PM_{10} particle mass, the first on Nov. 11-12th and the second November 20-21st (Figure 4.1, top). During the second event, PM_{10} and $PM_{2.5}$ were just below 2000 and 200 μg/m^3, respectively (Figure 4.1, top). During these events, wind speeds gusted up to 20 m/s, with hourly-averaged wind speeds of ~ 10-14 m/s, predominantly from the south (Figure 4.1, 2nd from bottom). During these high wind periods, there was a clear increase in particles with sizes between 0.5-4 μm (Figure 4.1, bottom). HYSPLIT air mass back trajectories during the first dust event indicate air mass histories were first from the south and then the west of the regional area, while during the second event the air masses were in a local/regional spiral pattern (Figure 4.2).

Relative changes in particle chemistry during the dust events (described below) can most likely be explained by the predominating wind direction. The sampling site was located at the south end of the lake, and the local wind direction during both dust events was from the south. Therefore, the main dust being sampled during the events was mostly from desert areas south of the lake and not the actual lakebed.

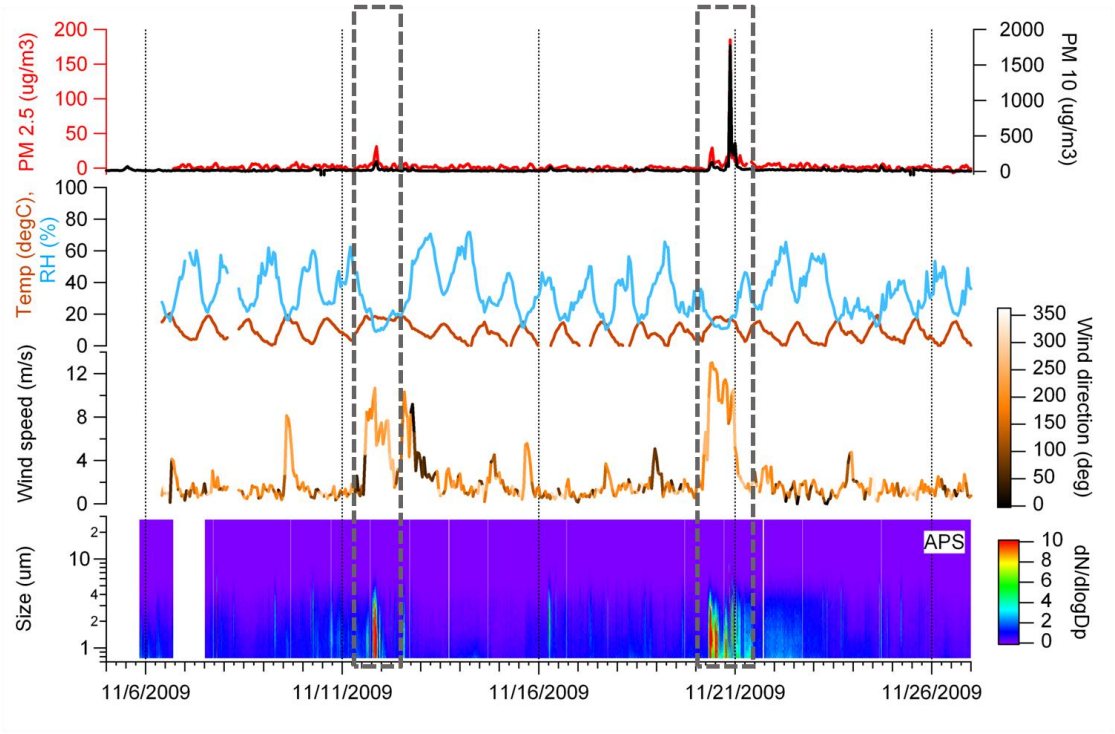

Figure 4.1. Temporal behavior of hourly-averaged particle mass (top), hourly-averaged temperature and relative humidity (RH) (2nd from top), hourly-averaged wind speed and direction (2nd from bottom), and APS size distribution (bottom). Dashed boxes indicate the approximate times of the dust events.

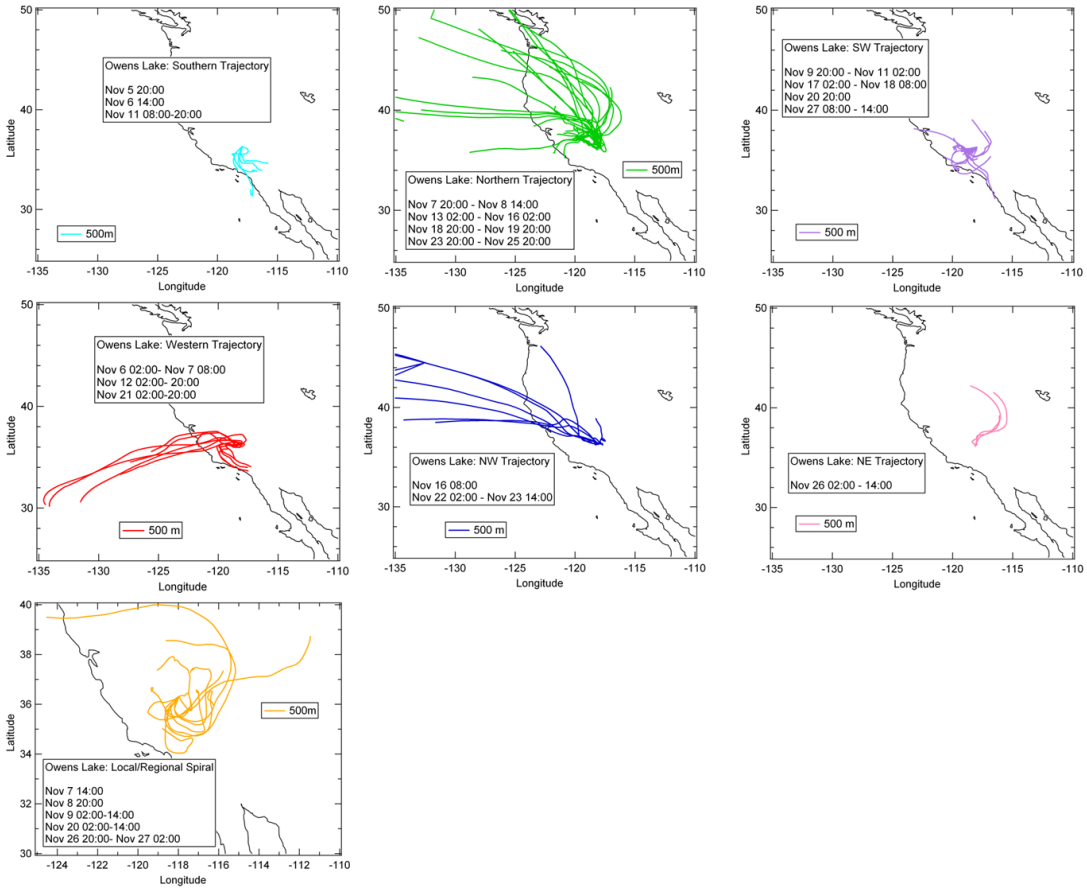

Figure 4.2. HYSPLIT air mass back trajectories for different time periods during the Owens Lake study.

4.4.2 Ambient particle chemistry overview

Mineral dust made up a large fraction of the particles analyzed; approximately 10-80% of submicron and 40-90% of supermicron particles were classified as mineral dust, at various times throughout the study. Within this general classification of mineral dust, there were many different dust particle types based on distinct mineralogy that are unique to Owens Lake that have not been described previously. The mass spectra signatures of the main dust types are shown in detail in Figure 4.3. The most abundant supermicron dust particle type, AlNaK I (Figure4.3, top left), has a mass spectral signature with intense sodium (m/z +23), aluminum (m/z +27) and potassium (+39) ions, with minor contributions from lithium (m/z

+7) and potassium hydroxide (m/z +56) ions in the positive mass spectra; the negative mass spectra of this particle type were dominated by oxygen (m/z -16) and nitrite (m/z -46) with minor contributions from alumina-silicates AlO^-, SiO_2^-, SiO_3^- (m/z -43, -60, -76, -77), nitrogen-containing organics CN^-, CNO^- (m/z -26,-42) and chloride (m/z -35). The AlNaK II and III types (not shown) are very similar to the AlNaK I type with increased prevalence of carbonaceous species and sulfate; C^- (m/z -12), C_2^- (m/z -24), C_3^- (m/z -36), sugar marker $C_3H_6O_2^-$ (m/z -73) and sulfate (m/z -97). The K I type (Figure 4.3, 2nd from top right) is another variant of the AlNaK I type, but while both aluminum and sodium are present, the potassium peak dominates. Additionally, for the negative ions there is increased prevalence of nitrate (m/z -62). The K II and K III types (not shown) are very similar to the K I type with an increase in the occurrence of titanium (m/z +48) and titanium dioxide (m/z +64). The CaMg I type (Figure 4.3, 2nd from top left) is characterized by an intense calcium (m/z +40) peak with smaller contributions from sodium, magnesium (m/z +24), aluminum, calcium oxide (m/z +56) and Ca_2O^+ (m/z +96) in the positive ions; the negative ions are dominated by oxygen and nitrite with smaller contributions from alumina-silicates, nitrogen-containing organics and chloride. The CaMg II type (not shown) is a variant of the CaMg I type with a more intense magnesium peak and a less intense calcium peak and less prevalence of alumina-silicate peaks. The KNa type (Figure 4.3, 2nd from top right) is characterized by intense sodium and potassium peaks with minor contributions from lithium, aluminum, and potassium hydroxide in the positive ions; the negative ions were dominated by alumina-silicates, nitrogen-containing organics, chloride, nitrite, nitrate and a minor contribution of phosphate. The Fresh Salt type (Figure 4.3, 2nd from bottom left) is characterized by an intense sodium peak, followed by medium intensity potassium with minor contributions from Na_2^+ (m/z +46), Na_2O^+ (m/z +62, 63) and Na_2Cl^+ (m/z +81,83); the negative ions are dominated by chloride, alumina-silicates and nitrogen-containing organics similar to other dust types with the

exception of minor contributions from $NaCl_2^-$ (m/z -93, 95) and has a striking similarity to sea salt particles from marine environments [*Noble and Prather*, 1997]. The Aged Salt type (Figure 4.3, 2nd from bottom right) is very similar to the Fresh Salt type but does not have the sodium chloride clusters and instead has a much higher prevalence of nitrite and nitrate. The Fe type (Figure 4.3, bottom left) is characterized by an intense iron peak (m/z +56) as well as its lower abundant isotope (m/z +54) and iron oxide, FeOH (m/z +73) in addition to other smaller contributions from sodium, aluminum, potassium and titanium in the positive ions; the negative ions were very similar to the Aged Salt type with an additional inclusion of phosphate (m/z -79). The Ti type (Figure 4.3, 2nd from bottom right) is characterized by intense potassium, titanium and titanium oxide peaks with minor contributions from sodium and aluminum in the positive ions; the negative ions are very similar to the Aged Salt type. The biogenic type (not shown) is identified as such because of its similarities to vegetative detritus types that have been previous analyzed [*Holecek et al.*, 2007; *Silva*, 2000] and is most likely associated with algal/biological growth observed in the small puddles nearby the sampling site. Overall, there were many different dust particle types observed during this study. These special types are based on distinct mineralogies that are unique to the Owens (dry) Lakebed area that have not been described previously with ATOFMS.

The temporal behavior of these dust particle types and the other non-dust particle types previously described for both sub- and supermicron are shown in Figure 4.4. The plot of fractional submicron temporal particle chemistry (Figure 4.4, top) shows that the submicron mode is dominated by biomass burning and ECOC particle types for the majority of the study. The remaining fraction is dust, consisting mainly of the K I dust type, with smaller contributions from the Aged Salt type. During the dust storm events on Nov. 11th and Nov. 20th and 21st, there is a notable increase in the fraction of submicron K II particle type and a notable absence of the submicron Aged Salt type. The plot of fractional supermicron particle

chemistry (Figure 4.4, bottom) shows that the temporal behavior is dominated by mineral dust with minor contributions from biomass burning and OC particle types.

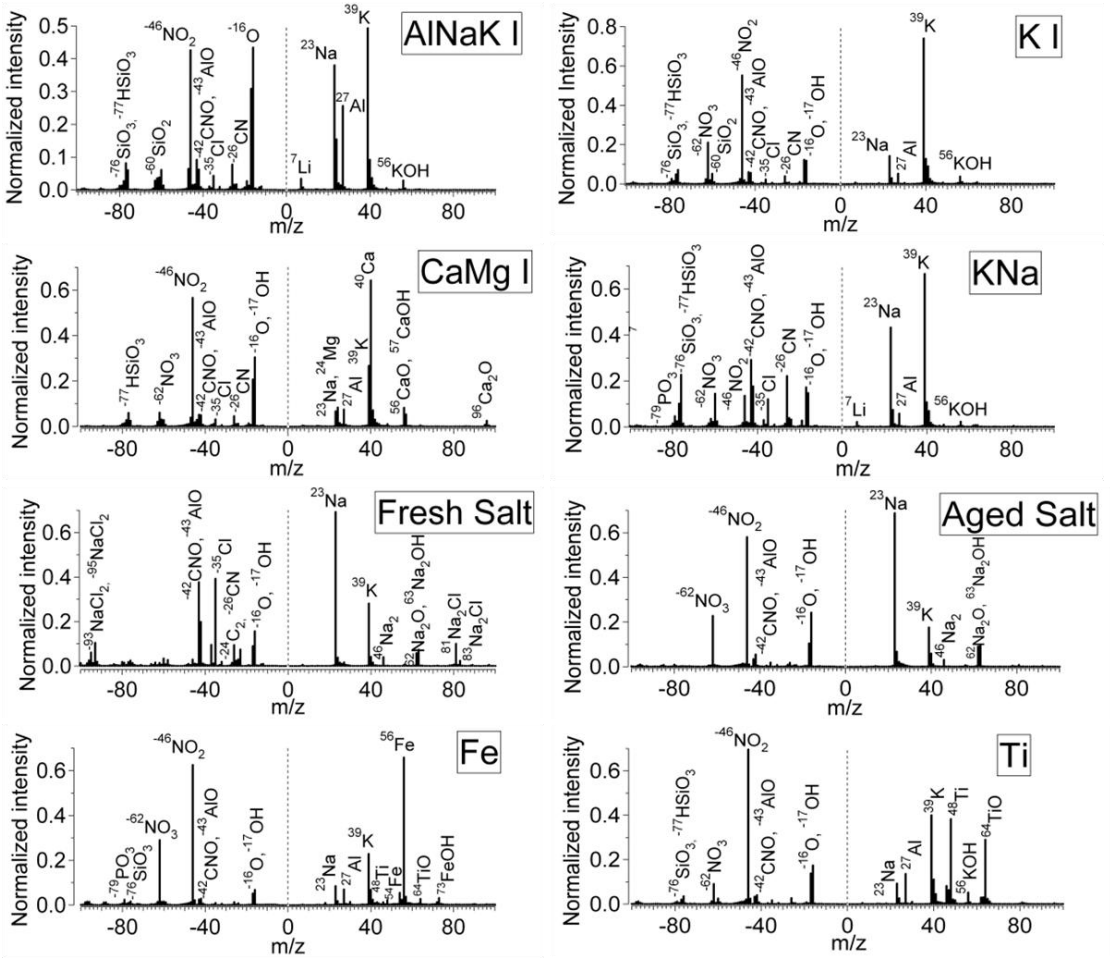

Figure 4.3. Mass spectra of main dust particle types observed during the study.

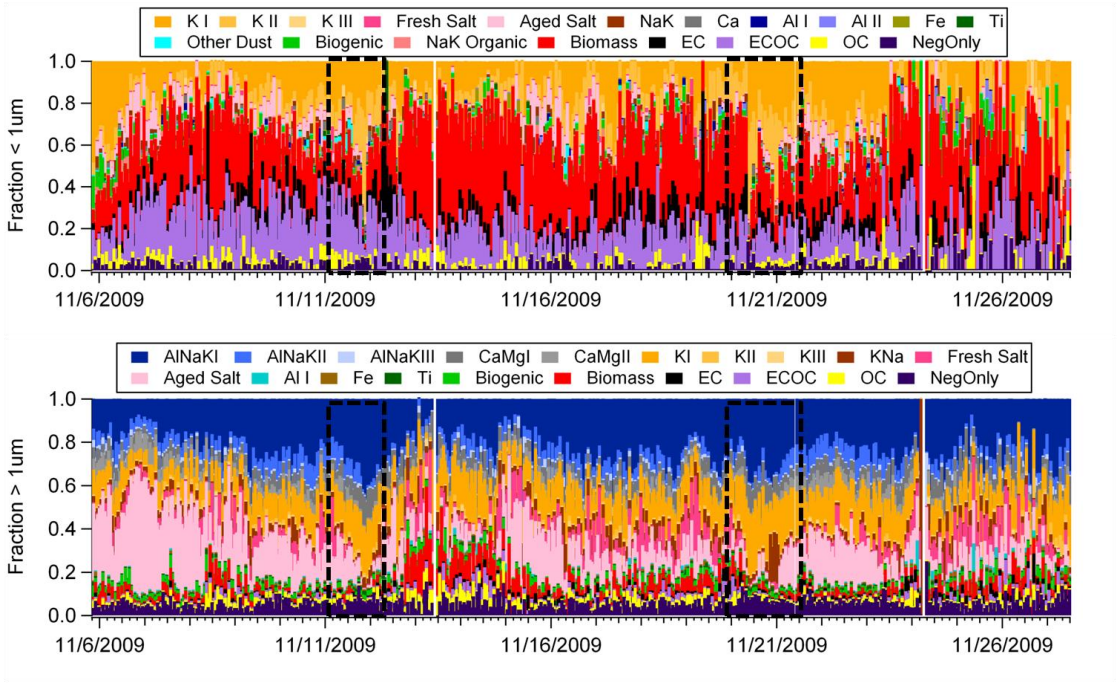

Figure 4.4. Submicron (top) and supermicron (bottom) fraction temporal chemistry. Dashed boxes indicate the approximate times of the dust events.

The supermicron dust is largely the AlNaK I, K I and Aged Salt types with minor contributions from KNa, Fresh Salt, CaMg I, CaMg II and AlNaK II types. There was a notable absence of supermicron Fresh Salt and Aged Salt during the dust events and therefore an increase in the relative contribution of the other dust types, most notably the AlNaK I type. Particle mixing state shows a very high prevalence of nitrate was observed on just about every type of dust (Figure 4.3), indicating that there was significant atmospheric processing of the ambient dust particles before sampling. There was no clear enhancement on any particular particle type or size range.

The size-resolved chemistry of the particle types is shown in Figure 4.5. The smallest sizes are dominated by biomass burning and ECOC, and the contribution of dust increases with increasing particle size. Most interesting is the large contribution of the NaK dust type to

the smallest size bin around 0.2 µm. The remainder of the dust types do not seem to show any size-dependent behavior.

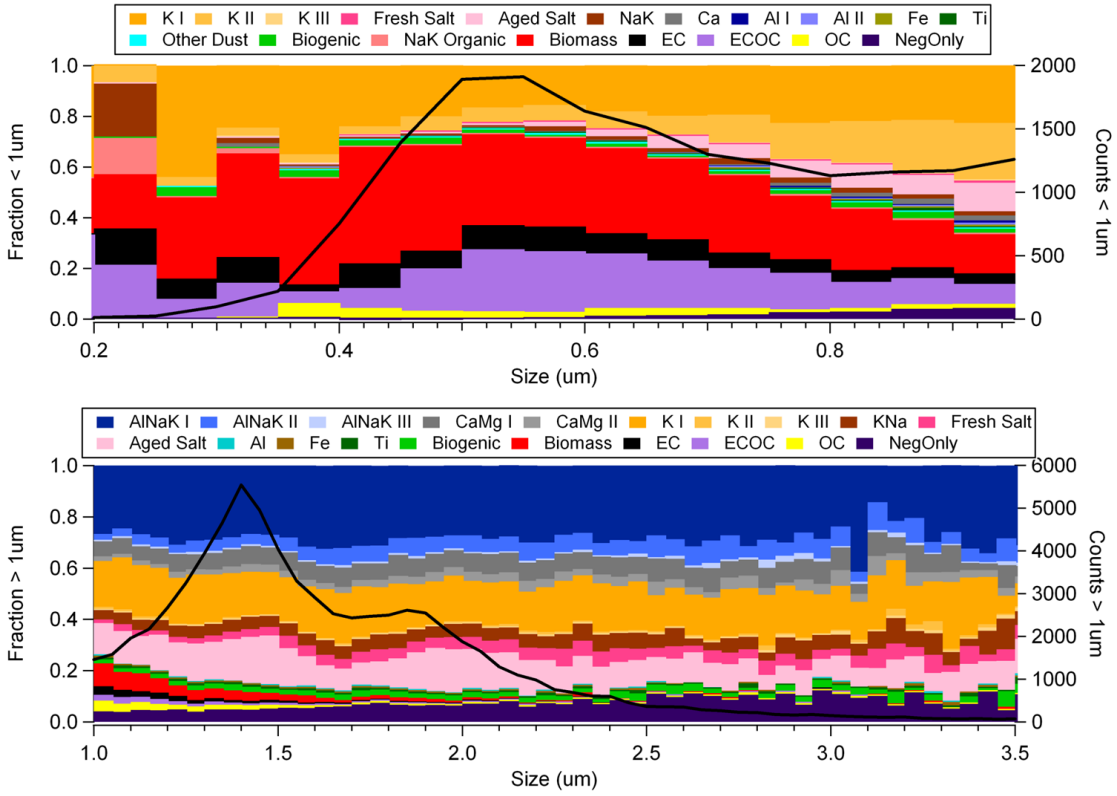

Figure 4.5. Submicron (top) and supermicron (bottom) fraction size-resolved chemistry.

Overall, the submicron temporal behavior is dominated by biomass burning and ECOC particle types, with the remaining fraction consisting of K dust types, with smaller contributions from the Aged Salt type. The supermicron temporal particle chemistry is dominated by the AlNaK, K and Aged Salt types with more minor contributions from KNa, Fresh Salt, and CaMg types. During both dust storm events (Nov. 11-12, Nov. 20-21), single particle chemistry showed a small shift in both sub- and supermicron particle types from a salt-like dust to an alumina-silicate type dust. We hypothesize that the absence of the salt-like

dust during the dust events is because the salt-like dust is associated with the dry-lake bed only and the prevailing winds sent it away from the sampling site.

4.4.3 Ambient CCN overview

CCN concentrations for the entire study range from $CCN_{0.1}$ 0.21 to 356 cm^{-3} (CCN concentration at 0.1% supersaturation) and $CCN_{0.9}$ = 466 to 1829 cm^{-3} (CCN concentration at 0.9% supersaturation) with median concentrations of $CCN_{0.1}$ 8.3 cm^{-3} and $CCN_{0.9}$ = 708 cm^{-3} (Figure 4.6, Table 4.2).

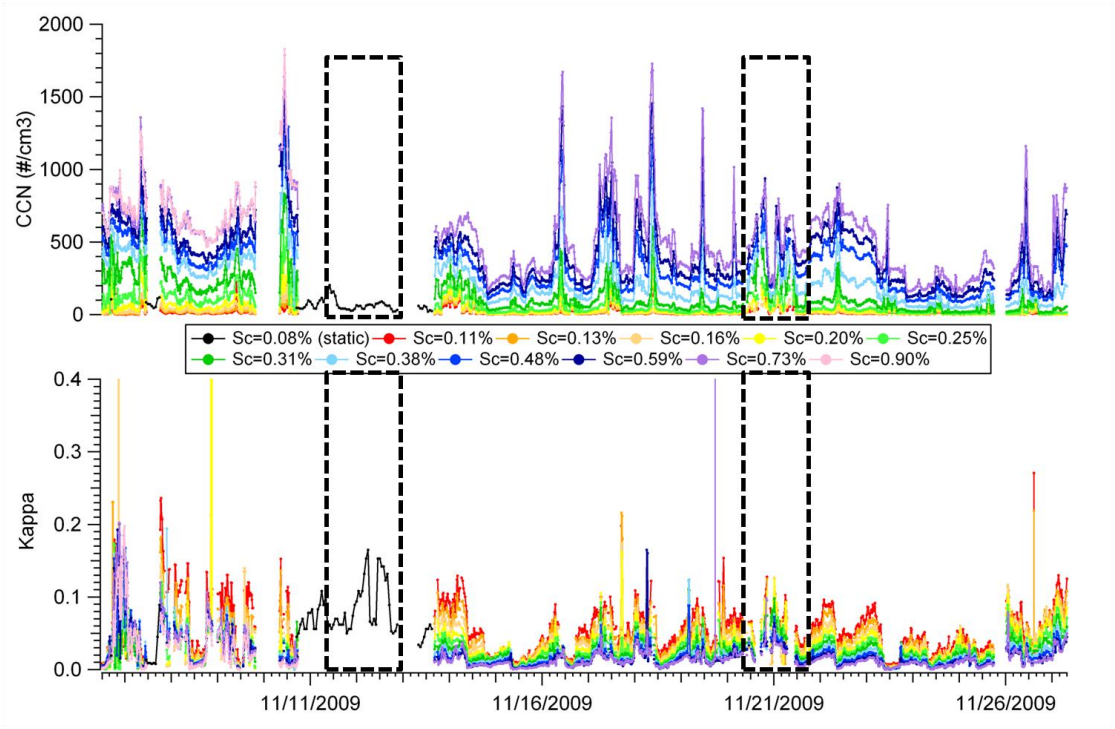

Figure 4.6. CCN concentration as a function of supersaturation(top) and kappa as a function of supersaturation (bottom). Dashed boxes indicate the approximate times of the dust events.

Table 4.2. CCN and Kappa statistics. The median values for the CCN and kappa for the entire study are shown as a function of supersaturation. Below the median values are the minimum/maximum values.
*CCN was in static mode (SS=0.08%) during dust event 1 and therefore is slightly different than lowest bin

	Sc 0.11	Sc 0.13	Sc 0.16	Sc 0.20	Sc 0.25	Sc 0.31	Sc 0.38	Sc 0.48	Sc 0.59	Sc 0.73	Sc 0.90
CCN whole study	8.3 0.21/356	11 0.64/422	16 0.79/460	29 1.1/510	57 2.9/586	102 10/847	213 45/1292	332 84/1429	419 120/1563	552 157/1787	708 466/1829
Kappa whole study	0.05 0.005/6.7	0.04 0.003/7.9	0.03 0.002/5.7	0.03 0.0009/2.3	0.03 0.0005/0.17	0.02 0.0001/0.16	0.02 0.0001/0.19	0.02 0/0.18	0.01 0.0004/0.20	0.01 0.0002/1.2	0.03 0/0.20
CCN dust event 1	62 19.8/202*										
Kappa dust event 1	0.07 0.05/0.17*										
CCN dust event 2	15 2.3/134	20 2.5/130	20 5.3/138	28 9.1/216	65 16/253	122 40/470	219 104/644	362 186/721	459 199/937	485 191/1016	
Kappa dust event 2	0.06 0.03/0.13	0.05 0.007/0.12	0.04 0.007/0.13	0.04 0.008/0.12	0.03 0.01/0.1	0.03 0.009/0.1	0.02 0.006/0.08	0.02 0.003/0.07	0.02 0.002/0.06	0.01 0.001/0.1	

The behavior of the quantitative hygroscopicity parameter (κ) as a function of supersaturation (S_c) is shown in Figure 4.6. Median κ values for the entire study are $\kappa_{0.1}$ = 0.05 and $\kappa_{0.9}$ = 0.03. A summary of κ and CCN statistics by supersaturation can be found in Table 4.2. A key observation to note is that as supersaturation increases, κ values decrease, indicating that particle hygroscopicity is higher at larger sizes, which is consistent with previous observations that larger particles are more atmospherically processed and contain more soluble material [*Gunthe et al.*, 2009; *Roberts et al.*, 2010]. κ values plateau at ~0.01 around S_c =0.3-0.4%, with the exception of the largest S_c bin, suggesting that there was no atmospheric processing on these particles; a particle having a κ value of 0.01 at S_c=0.35% would be 210 nm, indicating particles ~200 nm or less were not significantly processed.

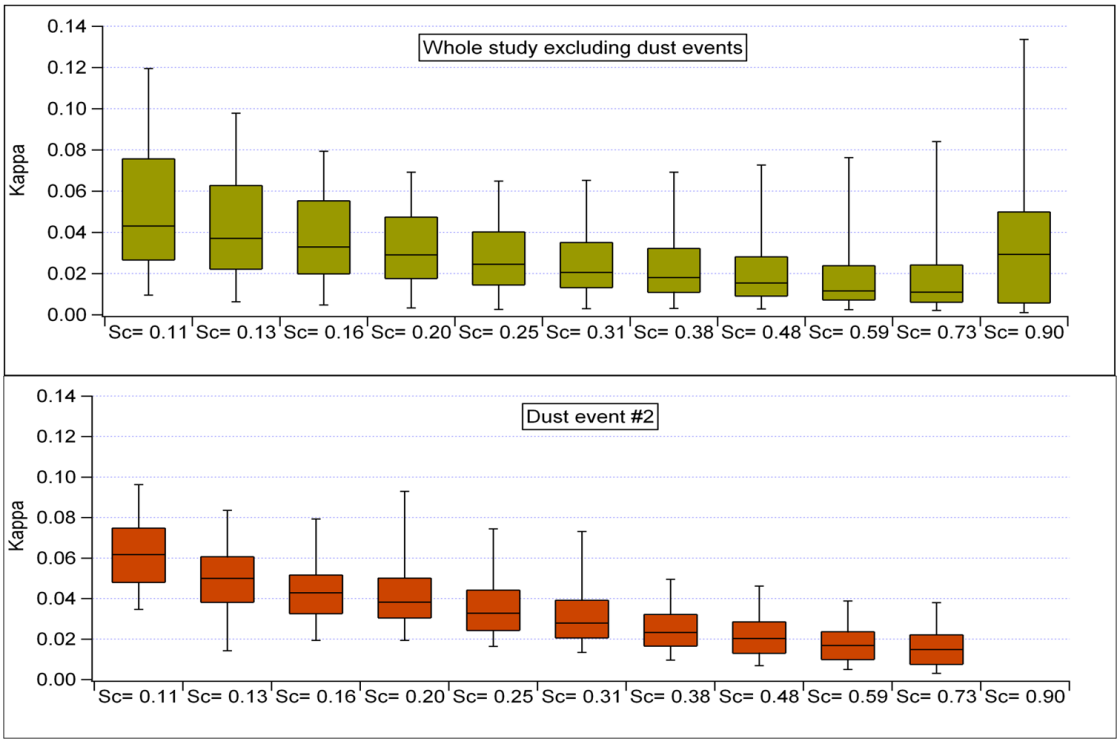

Figure 4.7. Kappa as a function of supersaturation for the entire study excluding dust events (top) and for dust event #2 (bottom). Median value for each bin is shown in middle of boxes, top and bottom of boxes are 25th and 75th percentile values. Whiskers represent 5th and 9th percentiles.

During the dust events, there was no significant shift in κ values for both the static CCN measurements (1st dust event, Nov. 11-12) and the scanning CCN measurements (2nd dust event, Nov. 20-21) compared with the median values and uncertainty for the entire study (Figure 4.7, bottom; Figure 4.8). For the first dust event, the median $\kappa_{0.08}$ value (static) was 0.07, compared to the median value of $\kappa_{0.1}$= 0.05 for the entire study (Figure 4.8, Table 4.2) and is within the uncertainty of the entire study. During the second dust event, the median $\kappa_{0.1}$ value was 0.06, compared to the median value of $\kappa_{0.1}$= 0.05 for the entire study; and the median $\kappa_{0.7}$ was 0.01, similar to the entire study, $\kappa_{0.7}$ =0.01. Particles with κ=0.03 in a cloud of 0.1% S_c would activate at 350 nm or larger.

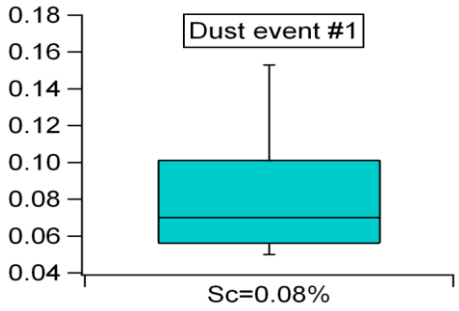

Figure 4.8. Kappa for dust event #1 (CCN in static mode). Median value is shown in middle of box, top and bottom of box is 25th and 75th percentile values. Whiskers represent 5th and 95th percentiles.

A comparison of the SMPS and APS size distributions, cumulative number size distributions, and CCN concentrations (NCCN) at different supersaturations is shown in Figure 4.9 for both a non-dust event (Nov. 15th 2009 at 12 pm) and during the 2nd dust event (Nov. 20th 2009 at 12pm). The disagreement between the SMPS and APS cumulative concentrations for the non-dust event is due to the high concentration of smaller particles measured with the scanning SMPS measurement technique when compared to the non-

scanning nature of the APS measurements [*Shields et al.*, 2008]. For the non-dust event, the cumulative SMPS concentration (0.011- 0.6 µm) was 1569 particles/cm^3 and cumulative APS concentration (0.542 -20 µm) was 2 particles/cm^3. NCCN was 69 cm^{-3} at 0.1% S_c (D_{act}= 427 nm) for the non-dust event. During the 2nd dust event, the cumulative SMPS concentration was 766 particles/cm^{-3} and the APS cumulative concentration was 23 particles/cm^{-3}, while NCCN at 0.1% S_c (D_{act}= 355 nm) was 11 cm^{-3}. While the larger particles from the APS size distributions do not contribute significantly to the overall total particle concentrations (<1% during non-dust events, <3% during the 2nd dust event), they had a larger contribution to NCCN, as the activation diameters at 0.1% S_c were 355 – 427 nm. During the non-dust event, 3% of NCCN were from the larger APS particle sizes, while they were < 1% of the total particle concentrations. During the 2nd dust event, 100% of NCCN were from the larger APS particle sizes, while they were <3% of the total particle concentrations. As most of the particles > 500 nm were dust and most CCN were > 500 nm, the dust needs to be CCN active to explain the NCCN observed.

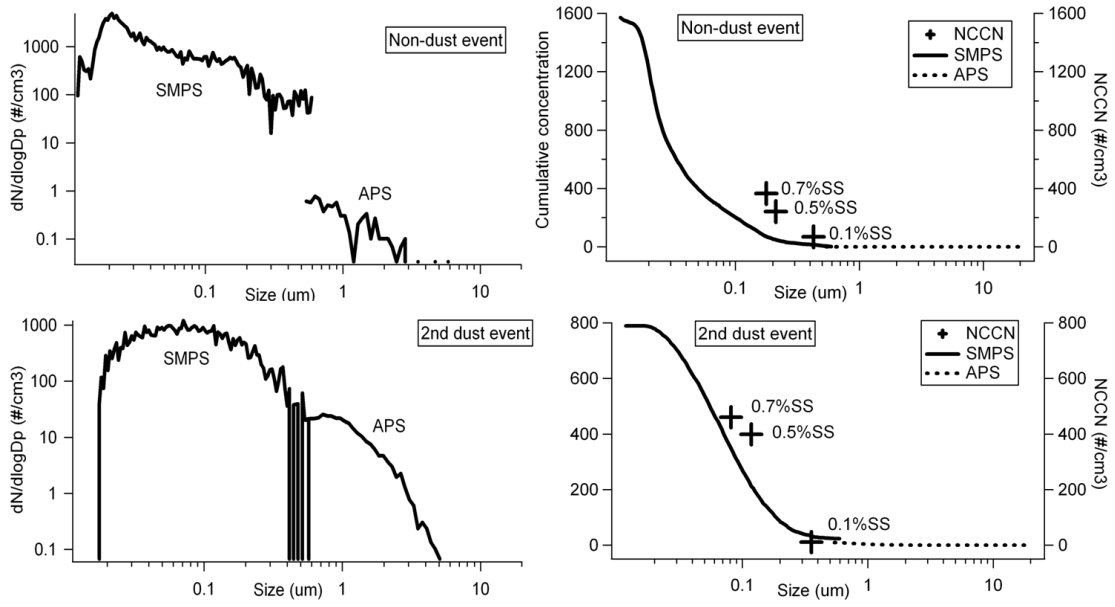

Figure 4.9 Scanning mobility particle sizer (SMPS) and aerodynamic particle sizer (APS) size distributions of ambient particles for a non-dust period (top left) and during the 2nd dust event (bottom left). Cumulative particle concentrations for both the SMPS and the APS for a non-dust period (top right) and the 2nd dust event (top right). Cross markers indicate the NCCN at the activation diameter for the corresponding supersaturation as labeled. SMPS measurements were converted to aerodynamic diameter assuming spherical particles with a density of 1.0 g/cm^3.

A comparison of the SMPS size distribution, κ as a function of supersaturation and dCCN/dlogSc are shown in Figure 4.10. The SMPS size distribution shows a diurnal pattern for most of the study, with a distinct ultrafine mode ~20 nm appearing midday on most days (Figure 4.10, top). Notably, the only days with no apparent ultrafine mode occurred during the two dust storm events, Nov. 11-12 and Nov. 20-21. The κ values are lowest during midday (Figure 4.10, middle; Figure 4.6, bottom) while the CCN is the highest (Figure 4.10 bottom; Figure 4.6, top), corresponding to the peak of the ultrafine particles (Figure 4.10, top). However, the high end of the supersaturation (1%) in the CCNc would not activate these particles regardless of their composition due to their small size. We speculate that the ultrafine particles are from a local biogenic source on the lakebed associated with algal/biological

growth observed in the small puddles nearby the sampling site. A more detailed analysis of the ultrafine particle events will be discussed in a different manuscript [*Fitzgerald et al.*, 2010].

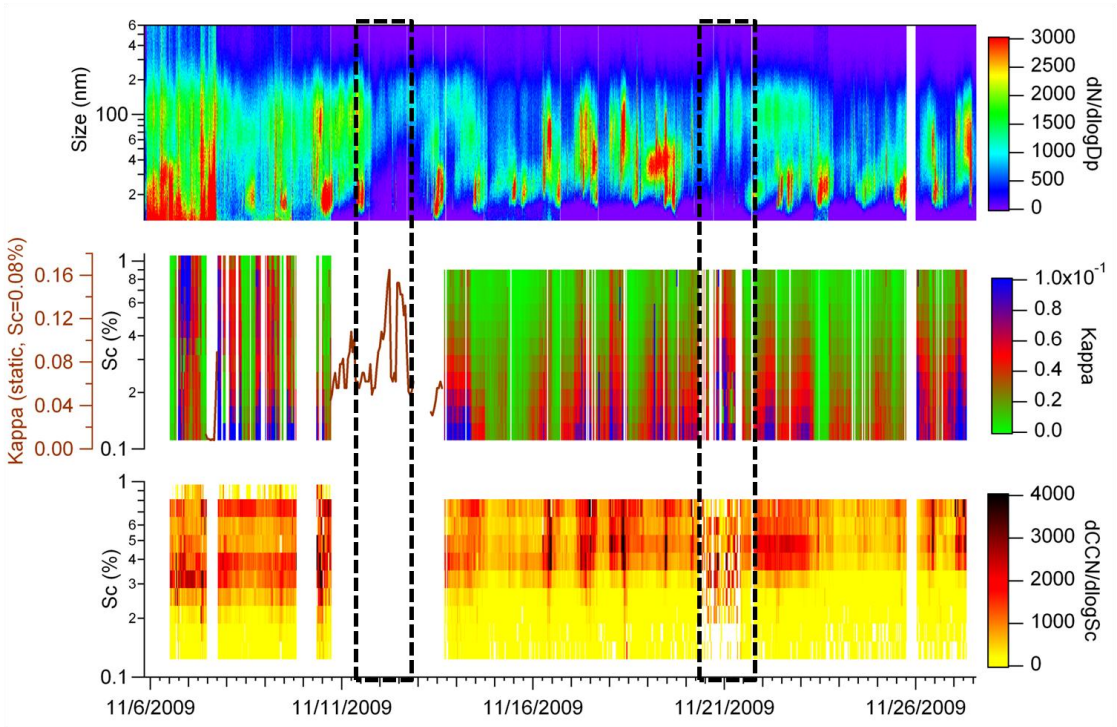

Figure 4.10. SMPS dN/dlogDp size distribution (top) kappa as a function of supersaturation (middle) and dCCN/dlogSc CCN distribution (bottom). Dashed boxes indicate the approximate times of the dust events.

The activation diameters at 0.1%-0.7% S_c were 129-300 nm for the whole study excluding dust events and 129-280 during the 2nd dust event. Hygroscopicity parameter κ ranges were 0.01 (0.7% S_c) – 0.05 (0.1% S_c) during the whole study excluding dust events and were similar for the 2nd dust event, 0.01 (0.7% S_c) – 0.06 (0.1% S_c). Changes in κ ± 50% resulted in changes in CCN concentrations within <1% at 0.1% S_c and < 7% at 0.7 % S_c during the entire study excluding dust events. Changes in κ ± 50% during the 2nd dust event resulted in changes in CCN concentrations <2% at 0.1% S_c and < 16% at 0.7% S_c. The difference in CCN concentrations for the entire study excluding dust events and the 2nd dust

event reflects the large differences in the particle size distributions and influence of ultrafine and dust particles. During the non-dust events, there were strong influences of ultrafine particles that produced high particle number concentrations ~20 nm which were not present during the dust events. Changes in hygroscopicity during the non-dust event periods does not result in large changes in CCN concentrations, as the majority of the particles were ~20 nm and would not activate regardless of the supersaturation due to their small size. However, during the dust events, the main particle size mode is instead ~100 nm due to a decrease in ultrafine particles and an increase in submicron dust 100-300 nm, bringing the size mode closer to the activation diameter range, and therefore changes in hygroscopicity had a larger effect on CCN concentrations.

4.4.4 Soil and suspended dust samples particle chemistry and hygroscopicity

Soil and dust samples that were collected during the study were analyzed afterwards by atomization of aqueous solutions of the samples. This was done to obtain a steady and constant flow of relatively high concentrations of submicron particles that was needed to study CCN activation as well as particle composition via ATOFMS. However, due to the heterogeneous nature of the dust samples, the original size-dependent particle composition will become altered when the bulk samples are suspended in water and then atomized, mainly the soluble compounds can become redistributed across all particles; some particles that were not originally associated with soluble material may have become transformed into an internally mixed particle [*Sullivan et al.*, 2010]. It has been shown that dry generation of samples is more representative of the original soil and dust samples [*Koehler et al.*, 2007; *Sullivan et al.*, 2010], but due to the wet and bulky nature of the samples collected, a steady and constant flow of relatively high concentrations of submicron particles would not be possible to produce using this method. Nevertheless, the formation process of the Owens Lake salt crust involved hydration and recrystallization of the crustal layers, therefore to some

extent the wet particle generation method may also be producing particles via a similar process to those that occur naturally [*Koehler et al.*, 2007], but some of the original mixing of the particles will be lost.

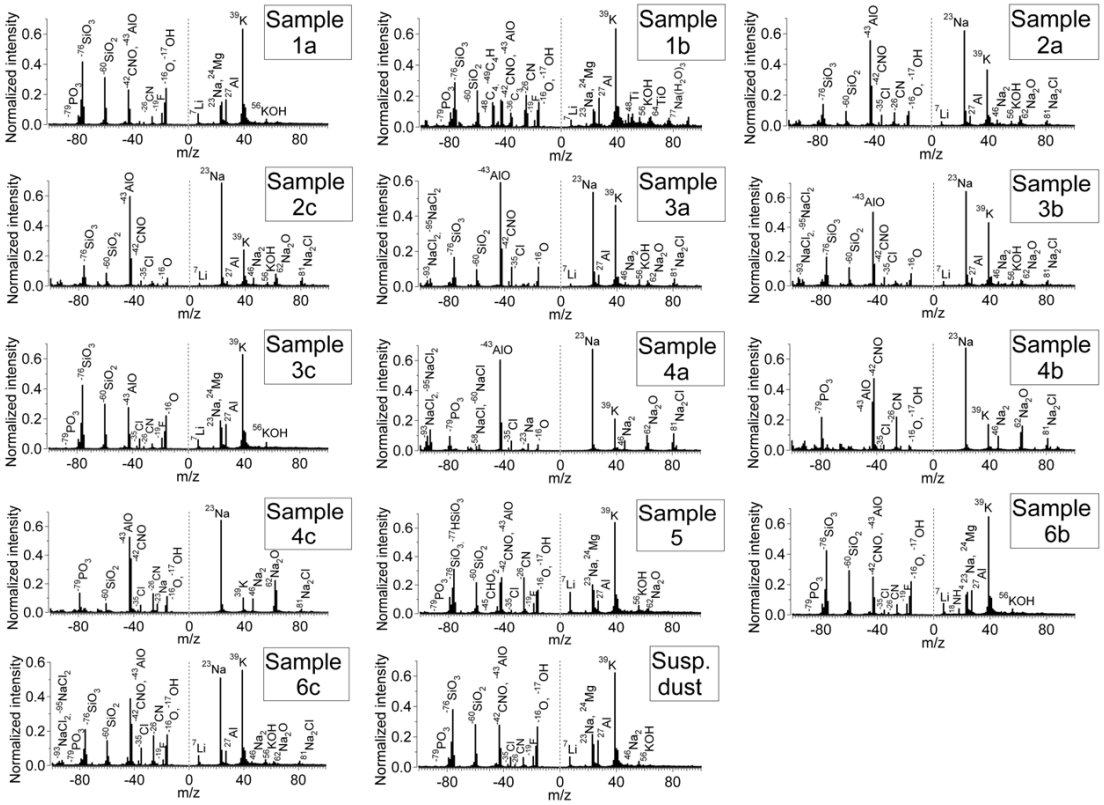

Figure 4.11. Mass spectra of various dust particle types from soil samples.

Mass spectral fingerprints of the various samples compare closely with the sodium-potassium alumina-silicate ambient dust particle types, with the large exceptions being the notable absence of nitrite and nitrate (m/z -46,-62) in the soil samples, and no Fresh or Aged Salt types (see Figure 4.11). In general the samples all have distinct alumina-silicate markers present, including the suspended dust sample. The salt-like dust samples (Sample 2a, 3a; see Table 4.1, Figure 4.11) have an intense sodium peak and sodium chloride clusters, however, other more crustal samples (Sample 2c, 3b, 4a, 4b, 4c, 6c; see Table 4.1, Figure 4.11) also

have sodium chloride clusters in addition to intense sodium peaks. This indicates that due to the wet generation process, the soluble compounds were redistributed across all particles; some particles which were not originally associated with soluble material may have become transformed into an internally mixed particle.

The range of κ values obtained from the CCN experiments on the soil and dust samples are shown in Figure 4.12. While there were many different types of samples analyzed, the overall range of κ values obtained for each sample were similar to each other and ranged from ~0.04-0.8, similar to previous Owens Lake samples , ~0.05-1 [*Koehler et al.*, 2007]. The least hygroscopic sample was 3c (Figure 4.12), the hard brown crust nearby the grass farm area which did not have any sodium chloride clusters in its chemical fingerprint (Figure 4.10). The most hygroscopic sample was 4a (Figure 4.12), the brown/orange crust from the "C" shaped lake which had a clear signature of sodium chloride clusters (Figure 4.11). Smaller particles had higher κ values than larger particles, similar to what has been previously seen with wet-generated Owens lake dust samples [*Koehler et al.*, 2007]. The fact that different sizes of the same sample had different hygroscopicities indicates that the samples were heterogeneous in nature, as previously shown for Owens Lake dust samples [*Koehler et al.*, 2007], but could also be due to differences in surface tension which are not taken into account by the κ estimates. Additionally, hygroscopicities at different sizes of the same sample do not fall along the same κ line, but rather had a shallower slope than the κ lines, could indicate water adsorption effects due to the insoluble nature of some of the dust inclusions, which has been shown previously [*Kumar et al.*, 2009a; *Kumar et al.*, 2009b].

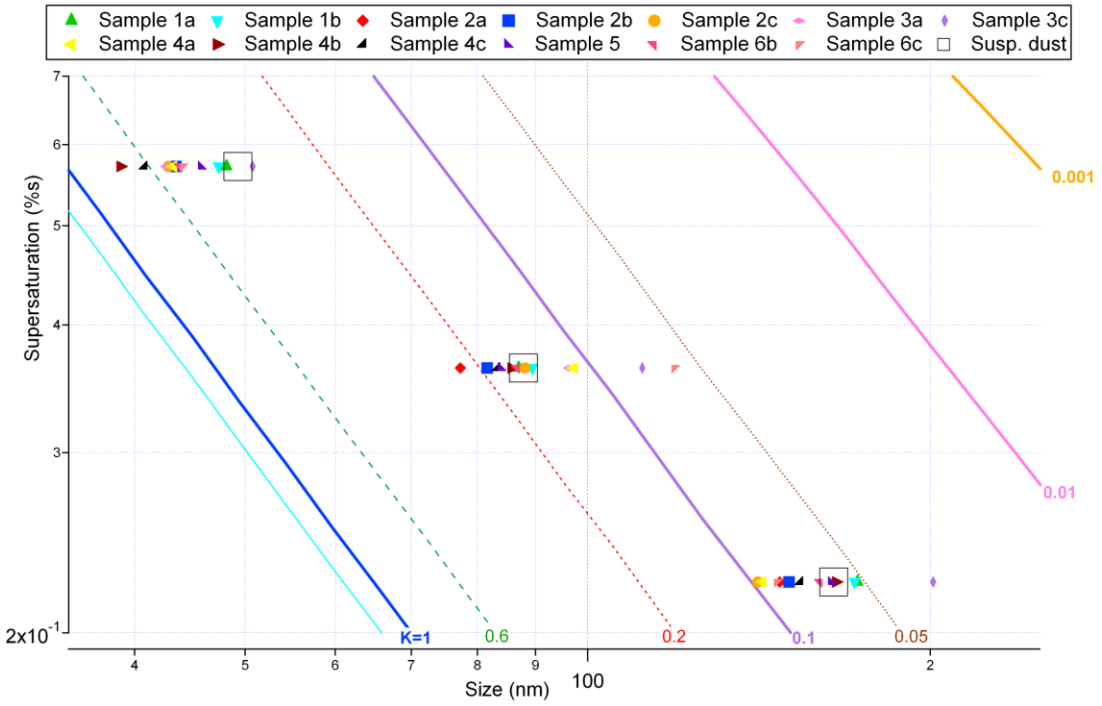

Figure 4.12. Hygroscopicity parameter kappa plot of Owens Lake soil samples run offline (see Table 1 for details on specific samples). Each point is the corresponding activation diameter of that sample for a particular supersaturation (SS=0.22, 0.36, 0.57%). The isolines represent different kappa values and are labeled with the value.

Soil and suspended dust samples collected from the lake and run offline show similar chemistry and hygroscopicity to the ambient field measurements, as well as previous offline measurements. Smaller particles had higher κ values than larger particles. Even though the different samples were very diverse, the differences in particle chemistry and overall spread in κ values was moderate.

4.4.5 Ambient particle chemistry and hygroscopicity comparison

As the lake bed dries out, the most soluble species are the last to dry and partition to the top layer. This surface layer will be most hygroscopic and will show up in wind storms. The method used to estimate κ assumes a completely internally mixed aerosol, which is not the case here. Therefore, the changes in κ represent the overall changes in both the fractions of particle types and the changes in temporal chemistry on each of those particle types, including

particles below the limit of detection of chemical measurements (< 200 nm). During the dust events, the salt-dust from the top surface of the lake was transported north of the sampling site; air masses south of the sampling site from the nearby desert were sampled instead. An increase in detected dust particles was measured during the dust events ~100-4000 nm, with changes in particle chemistry compared to the non-events and an increase in submicron particles 100-500 nm (Figures 4.9, 4.10), within the range of activation diameters, 129-300 nm. Size-resolved particle composition measurements (Figure 4.5) indicate that particles 250-500 nm were significantly impacted by dust, as 25-40% of the particles of those sizes were K-rich dust. However, there was no significant change in particle hygroscopicity within the uncertainty of the measurements observed during the dust events. Median values of the hygroscopicity parameter were $\kappa_{0.1}$ 0.05 and $\kappa_{0.9}$ 0.03 and plateaued at ~0.01 around S_c =0.3-0.4%. A κ value of 0.01 at S_c=0.35% corresponds to a particle diameter of 210 nm; most of the dust particles observed during the event were ~ 100-4000 nm (Figure 4.1). Therefore, a majority of the dust particles are large enough and would activate to become CCN (or GCCN) regardless of their hygroscopicity; as it has been shown that particles ~ 300 nm and larger would activate in laboratory studies of Owens Lake dust [*Koehler et al.*, 2007]. Particles with κ=0.03 in a cloud of 0.1% S_c would activate at 350 nm or larger. During the 2nd dust event, 100% of NCCN were ~500 nm and larger, while they were only <3% of the total particle concentrations, showing that the dust is an important contributor to NCCN at low supersaturations during the dust events.

As the ambient dust showed large peaks of nitrite and nitrate (Figure 4.3) while the collected dust samples showed no nitrite/nitrate (Figure 4.11), this indicates that there was significant atmospheric processing of nitrite/nitrate on the dust particles. Previous single particle mixing state measurements of ambient mineral dust off the coast of Asia showed a segregation of nitrate on Ca-rich dust and sulfate on Al-rich dust [*Sullivan et al.*, 2007], which

was not observed here. Other studies in coastal environments have shown dust largely mixed with sulfate [*Guazzotti et al.*, 2001; *Zhang et al.*, 2003], and some mixed with nitrate [*Zhang et al.*, 2003]. Gas phase measurements of NO and NO_2 (NO_x) were very close to zero (not shown) and will be discussed in a forthcoming manuscript [*Fitzgerald et al.*, 2010]. With NO_x levels very low over the course of the study, the high prevalence of nitrate on the particles was due to uptake of other nitrogen-containing species such as HNO_3 or N_2O_5 elsewhere. However, this would require photochemical production of these gas phase species and/or their precursors [*Mashburn et al.*, 2006; *Sullivan et al.*, 2009a; *Vlasenko et al.*, 2006; *Wagner et al.*, 2009], and the nitrate on the dust would show strong diurnal behavior which was not observed. Therefore, the dust particles could have been atmospherically processed elsewhere and then transported to the region where they were observed to be highly aged.

Heterogeneous processing of the dust can significantly influence the hygroscopicity, as has been shown in previous laboratory studies of the uptake of nitric acid on fresh dust particles [*Sullivan et al.*, 2009a]. For Owens lake dust particles, it is likely that there is enough soluble material already on them, that additional nitrate from atmospheric processing will not greatly increase the hygroscopicity. While 100% of submicron dust and 95% of supermicron dust contained nitrate; over 30% of submicron dust and over 80% of supermicron dust contained chloride. Additionally, over 50% of submicron and 1% of supermicron dust contained sulfate. Because the dust particles already have significant amounts of soluble species, it is most likely the smaller particles around the activation threshold (129-300 nm, some of which are below the chemical detection limit), that are dictating fCCN, and therefore the average hygroscopicity.

4.5 Atmospheric Implications and Conclusions

Sub- and supermicron particle mixing state was measured at Owens Lake in November 2009. The submicron particles were dominated by biomass burning and ECOC particle types, with the remaining fraction consisting of the K dust types, with smaller contributions from the Aged Salt type. The supermicron temporal particle chemistry is dominated by the AlNaK, K and Aged Salt types with minor contributions from KNa, Fresh Salt, and CaMg types. During both dust storm events (Nov. 11-12, Nov. 20-21), there was a shift in both sub- and supermicron particle types from a salt-like dust to a alumina-silicate type dust and an increase in particles 100-4000 nm, including those within the range of activation diameters, 129-300 nm. The absence of the more salt-like dust during the dust events is because the salt-like dust is associated with the dry-lake bed only and the prevailing winds from the south sent it away from the sampling site. Size-resolved particle composition measurements close to the activation threshold indicate that particles 250-500 nm were significantly impacted by dust, as 25-40% of the particles of those sizes were K-rich dust. However, there was no significant change in particle hygroscopicity observed during the dust events. The first real-time ambient CCN measurements at Owens Lake show a median $\kappa_{0.1}$ value of 0.05 and a $\kappa_{0.9}$ value of 0.03, indicating the dust is moderately hygroscopic. Most of the dust particles observed during the events were ~ 100-4000 nm and the dust > 200 nm was observed to have soluble nitrate, chloride and sulfate. Therefore, a majority of the dust particles are large enough and would activate to become CCN (or GCCN). During the 2nd dust event, 100% of NCCN were ~500 nm and larger at 0.1% S_c, while they were only <3% of the total particle concentrations, showing that the dust is an important contributor to NCCN at low supersaturations during dust events. Due to the large contribution of the large dust to CCN concentrations at low supersaturations during the dust events, the dust storms should enhance CCN and possibly ice nuclei (IN) in the regional clouds, however it remains to be seen how

the dust affects the radiative properties of the clouds. Measurements on the radiative cloud properties before, during, and after Owens Lake dust events will be studied in the future.

4.6 Acknowledgements

We would like to thank Dr. Satoshi Takahama, Manuel Ruidiaz and Dr. Alberto Cazorla, UCSD, for their help with CCN data analysis. We acknowledge Prof. Markus Petters (North Carolina State University) and Prof. Sonia Kreidenweis (Colorado State University) for sharing their code in estimating ambient hygroscopicity parameter kappa. The authors are very grateful to the Great Basin Unified Air Pollution Control District (GBU APCD) and its staff for making it possible to use their Dirty Socks sampling site for this study as well as for sharing their PM_{10} data from Dirty Socks. We are also grateful to NOAA for the use of the HYSPLIT back trajectory model. We would like to acknowledge NSF for funding, grant ATM0625526.

Publication Acknowledgement

The contents of Chapter 4 are part of a manuscript in preparation, Moore, M.J.K., Fitzgerald, E.M.M., Zauscher, M.D., Roberts, G.C., Prather, K.A., Real-time Single Particle Composition and Cloud Condensation Nuclei (CCN) Activity at Owens (dry) Lake Bed, to be submitted to Journal of Geophysical Research. The dissertation author was the primary investigator and author of this paper.

4.7 References

(IPCC), I.P.o.C.C., *Climate Change 2007: The Physical Science Basis*, Cambridge University Press, New York, 2007.

Abuduwaili, J., M.V. Gabchenko, and X. Junrong, Eolian transport of salts--A case study in the area of Lake Ebinur (Xinjiang, northwest China), *J. Arid Environ.*, *72* (10), 1843-1852, 2008.

Andreae, M.O., and D. Rosenfeld, Aerosol-cloud-precipitation interactions. Part 1. The nature and sources of cloud-active aerosols, *Earth Science Reviews, 89*, 13-41, 2008.

Blackwelder, E., The lowering of plays by deflation, *Am. J. Sci., 21* (122), 140-144, 1931.

Blank, R.R., J.A. Young, and F.L. Allen, Aeolian dust in a saline playa environment, Nevada, USA, *J. Arid Environ., 41* (4), 365-381, 1999.

Cahill, T.A., T.E. Gill, J.S. Reid, E.A. Gearhart, and D.A. Gillette, Saltating particles, playa crusts and dust aerosols at Owens (dry) Lake, California, *Earth Surf. Processes Landforms, 21* (7), 621-639, 1996.

Fitzgerald, E.M.M., M.J.K. Moore, and K.A. Prather, Observations of new particle formation events at Owens (dry) Lake, *in preparation*, 2010.

Furutani, H.F., M. Dall'osto, G.C. Roberts, and K.A. Prather, Assessment of the relative importance of atmospheric aging on CCN activity derived from field observations, *Atmospheric Environment, 42*, 3130-3142, 2008.

Gard, E., J.E. Mayer, B.D. Morrical, T. Dienes, D.P. Fergenson, and K.A. Prather, Real-Time Analysis of Individual Atmospheric Aerosol Particles: Design and Performance of a Portable ATOFMS, *Analytical Chemistry, 69*, 4083-4091, 1997.

Gill, T.E., and D.A. Gillette, Owens Lake: A natural laboratory for aridification, playa desiccation and desert dust, *Geol. Soc. Am. Abstr. Programs, 23* (5), 462, 1991.

Guazzotti, S.A., K.R. Coffee, and K.A. Prather, Continuous measurements of size-resolved particle chemistry during INDOEX-Intensive Field Phase 99, *Journal of Geophysical Research, 106* (D22), 28,607-28,627, 2001.

Guazzotti, S.A., D.T. Suess, K.R. Coffee, P.K. Quinn, T.S. Bates, A. Wisthaler, A. Hansel, W.P. Ball, R.R. Dickerson, C. Neusuess, P.J. Crutzen, and K.A. Prather, Characterization of carbonaceous aerosols outflow from India and Arabia: Biomass/biofuel burning and fossil fuel combustion, *Journal of Geophysical Research, 108* (D15), 4485, doi:10.1029/2002JD003277, 2003.

Gunthe, S.S., S.M. King, D. Rose, Q. Chen, P. Roldin, D.K. Farmer, J.L. Jimenez, P. Artaxo, M.O. Andreae, S.T. Martin, and U. Poeschl, Cloud condensation nuclei in pristine tropical rainforest air of Amazonia: size-resolved measurements and modeling of atmospheric aerosol composition and CCN activity, *Atmospheric Chemistry and Physics, 9* (19), 7551-7575, 2009.

Holecek, J.C., M.T. Spencer, and K.A. Prather, Analysis of rainwater samples: Comparison of single particle residues with ambient particle chemistry from the northeast Pacific and Indian oceans, *Journal of Geophysical Research, 112* (D22S24), doi:10.1029/2006JD008269, 2007.

Koehler, K., S.M. Kreidenweis, P.J. DeMott, A.J. Prenni, and M.D. Petters, Potential impact of Owens (dry) Lake dust on warm and cold cloud formation, *Journal of Geophysical Research, 112* (D12210), doi:10.1029/2007JD008413, 2007.

Kumar, P., A. Nenes, and I.N. Sokolik, Importance of adsorption for CCN activity and hygroscopic properties of mineral dust aerosol, *Geophysical Research Letters*, *36* (L24804), doi:10.1029/2009GL040827, 2009a.

Kumar, P., I.N. Sokolik, and A. Nenes, Parameterization of cloud droplet formation for global and regional models: including adsorption activation from insoluble CCN, *Atmospheric Chemistry and Physics*, *9*, 2517-2532, 2009b.

Levin, Z., E. Ganor, and V. Gladstein, The effects of desert particles coated with sulfate on rain formation in the eastern Mediterranean, *J. Appl. Meteorol.*, *35* (9), 1511-1523, 1996.

Liu, X., J.E. Penner, and M. Herzog, Global modeling of aerosol dynamics: Model description, evaluation, and interactions between sulfate and nonsulfate aerosols, *Journal of Geophysical Research*, *110* (D18206), doi:10.1029/2004JD005674, 2005.

Lowenstein, T.K., and L.A. Hardie, Criteria for the recognition of salt-pan evaporites, *Sedimentology*, *32* (5), 627-644, 1985.

Mashburn, C.D., E.K. Frinak, and M.A. Tolbert, Heterogeneous uptake of nitric acid on Na-montmorillonite clay as a function of relative humidity, *Journal of Geophysical Research*, *111* (D15213), doi:10.1029/2005JD006525, 2006.

Moffet, R.C., B. de Foy, L.T. Molina, M.J. Molina, and K.A. Prather, Measurement of ambient aerosols in northern Mexico City by single particle mass spectrometry, *Atmospheric Chemistry and Physics*, *8*, 4499-4516, 2008.

Niemeyer, T.C., D.A. Gillette, J.J. Deluisi, Y.J. Kim, W.F. Niemeyer, T. Ley, T.E. Gill, and D. Ono, Optical depth, size distribution and flux of dust from Owens Lake, California, *Earth Surf. Processes Landforms*, *24* (5), 463-479, 1999.

Noble, C.A., and K.A. Prather, Real-time single particle monitoring of a relative increase in marine aerosol concentration during winter rainstorms, *Geophysical Research Letters*, *24* (22), 2753-2756, 1997.

Petters, M.D., and S.M. Kreidenweis, A single parameter representation of hygroscopic growth and cloud condensation nucleus activity, *Atmospheric Chemistry and Physics*, *7* (8), 1961-1971, 2007.

Pratt, K.A., P.J. DeMott, J.R. French, Z. Wang, D.L. Westphal, A.J. Heymsfield, C.H. Twohy, A.J. Prenni, and K.A. Prather, In situ detection of biological particles in cloud ice-crystals, *Nature Geoscience*, *2*, 398-401, 2009.

Pratt, K.A., C.H. Twohy, S.M. Murphy, R.C. Moffet, A.J. Heymsfield, C.J. Gaston, P.J. DeMott, P.R. Field, T.R. Henn, D.C. Rogers, M.K. Gilles, J.H. Seinfeld, and K.A. Prather, Observation of playa salts as nuclei in orographic wave clouds, *Journal of Geophysical Research*, *115* (D15301), doi:10.1029/2009JD013606, 2010.

Rebotier, T.P., and K.A. Prather, Aerosol time-of-flight mass spectrometry data analysis: A benchmark of clustering algorithms., *Analytica Chimica Acta*, *585* (1), 38-54, 2007.

Reheis, M.C., Dust deposition downwind of Owens (dry) Lake, 1991-1994: Preliminary findings, *Journal of Geophysical Research*, *102* (D22), 25,999-26,008, doi:10.1029/97JD01967, 1997.

Reid, J.S., R.G. Flocchini, T.A. Cahill, and R.S. Ruth, Local meteorological, transport, and source aerosol characteristics of late autumn Owens Lake (dry) dust storms, *Atmospheric Environment*, *28* (9), 1699-1706, 1994.

Reynolds, R.L., J.C. Yount, M.C. Reheis, P. Goldstein, R. Chavez, J. Fulton, C. Whitney, C. Fuller, and R.M. Forester, Dust emission from wet and dry playas in the Mojave desert, USA, *Earth Surf. Processes Landforms*, *32* (12), 1811-1827, 2007.

Roberts, G.C., D.A. Day, L.M. Russell, E.J. Dunlea, J.L. Jimenenez, J.M. Tomlinson, D.R. Collins, Y. Shinozuka, and A.D. Clarke, Characterization of particle cloud droplet activity and composition in the free troposphere and the boundary layer during INTEX-B, *Atmospheric Chemistry and Physics*, *10*, 6627-6644, 2010.

Roberts, G.C., and A. Nenes, A Continuous-Flow Streamwise Thermal-Gradient CCN Chamber for Atmospheric Measurements, *Aerosol Science and Technology*, *39*, 206-221, 2005.

Rose, D., G.P. Frank, U. Dusek, S.S. Gunthe, M.O. Andreae, and U. Poschl, Calibration and measurement uncertainties of a continuous-flow cloud condensation nuclei counter (DMT-CCNC): CCN activation of ammonium sulfate and sodium chloride aerosol particles in theory and experiment, *Atmospheric Chemistry and Physics*, *8*, 1153-1179, 2008.

Rosenfeld, D., Y. Rudich, and R. Lahav, Desert dust suppressing precipitation: A possible desertification feedback loop, *Proceedings of the National Academy of Sciences of the United States of America*, *98* (11), 5975-5980, 2001.

Rudich, Y., O. Khersonsky, and D. Rosenfeld, Treating clouds with a grain of salt, *Geophysical Research Letters*, *29* (22), 2060, 2002.

Satheesh, S.K., and K.K. Moorthy, Radiative effects of natural aerosols: A review, *Atmospheric Environment*, *39*, 2089-2110, 2005.

Shields, L.G., X. Qin, S.M. Toner, and K.A. Prather, Detection of Ambient Ultrafine Aerosols by Single Particle Techniques During the SOAR 2005 Campaign, *Aerosol Science and Technology*, *42*, 674-684, 2008.

Silva, P.J., Source Profiling and Apportionment of Airborne Particles: A New Approach Using Aerosol Time-of-Flight Mass Spectrometry, University of California Riverside, 2000.

Silva, P.J., D. Liu, C.A. Noble, and K.A. Prather, Size and Chemical Characterization of Individual Particles Resulting from Biomass Burning of Local Southern California Species, *Environmental Science and Technology*, *33* (18), 3068-3076, 1999.

Singer, A., T. Zobeck, L. Poberezsky, and E. Argaman, The PM10 and PM2.5 dust generation potential of soils/sediments in the Southern Aral Sea Basin, Uzbekistan, *J. Arid Environ.*, *54* (4), 705-728, 2003.

Song, X.-H., and P.K. Hopke, Classification of Single Particles Analyzed by ATOFMS Using an Artificial Neural Network, ART-2A, *Analytical Chemistry*, *71* (4), 860-865, 1999.

Sullivan, R.C., S.A. Guazzotti, D.A. Sodeman, and K.A. Prather, Direct observations of the atmospheric processing of Asian mineral dust, *Atmospheric Chemistry and Physics*, *7* (5), 1213-1236, 2007.

Sullivan, R.C., M.J.K. Moore, M.D. Petters, S.M. Kreidenweis, G. Roberts, and K.A. Prather, Timescale for hygroscopic conversion of calcite mineral particles through heterogeneous reaction with nitric acid, *Physical Chemistry Chemical Physics*, *11*, 7826, 2009a.

Sullivan, R.C., M.J.K. Moore, M.D. Petters, S.M. Kreidenweis, G. Roberts, and K.A. Prather, Increased hygroscopicity of atomized insoluble mineral particles due to metastable hydrate formation, *Aerosol Science and Technology*, *44* (10), 830-846, 2010.

Sullivan, R.C., M.J.K. Moore, M.D. Petters, S.M. Kreidenweis, G.C. Roberts, and K.A. Prather, Effect of chemical mixing state on hygroscopicity and cloud nucleation properties of calcium mineral dust particles, *Atmospheric Chemistry and Physics*, *9*, 3303-3316, 2009b.

Vlasenko, A., S. Sjogren, E. Weingartner, K. Stemmler, H.W. Gaeggler, and M. Ammann, Effect of humidity on nitric acid uptake to mineral dust aerosol particles, *Atmospheric Chemistry and Physics*, *6*, 2147-2160, 2006.

Wagner, C., G. Schuster, and J.N. Crowley, An aerosol flow tube study of the interaction of N2O5 with calcite, Arizona dust and quartz, *Atmospheric Environment*, *43*, 5001-5008, 2009.

Wexler, A.S., and S.L. Clegg, Atmospheric aerosol models for systems including ions H+, NH4+, Na+, SO42-, NO3-, Cl-, Br- and H2O, *Journal of Geophysical Research*, *107* (D14), 4207, 2002.

Yin, Y., S. Wurzler, Z. Levin, and T.G. Reisin, Interactions of mineral dust particles and clouds: Effects on precipitation and cloud optical properties, *Journal of Geophysical Research*, *107* (D23), 4724, doi:10.1029/2001JD001544, 2002.

Zhang, D., Y. Iwasaka, G.Y. Shi, J. Zang, and A. Matsuki, Mixture state and size of Asian dust particles collected at southwestern Japan in spring 2000, *Journal of Geophysical Research*, *108* (D24), 4760, doi:10.1029/2003JD003869, 2003.

Chapter 5

Real-time Single Particle Composition, Absorption, Scattering and Cloud Condensation Nuclei (CCN) Activity at Trinidad Head, CA during the Cloud Indirect Forcing Experiment (CIFEX)

5.1 Synopsis

Individual particle size and composition as well as condensation nuclei (CN), cloud condensation nuclei (CCN) concentrations, particle absorption, and scattering were measured in April 2004 as part of the Cloud Indirect Forcing Experiment (CIFEX) at Trinidad Head, California to better understand the impacts aerosol chemistry on climate relevant properties. Aerosol hygroscopicity was estimated from CCN measurements and compared to simultaneous aerosol chemistry and size distribution measurements. The ambient aerosol was dominated by sub- and super-micron sea salt particle types, with over half of the sea salt particles showing evidence of atmospheric processing. In the sub-micrometer size range, there were significant fractional contributions from organic carbon, elemental carbon with organic carbon, and biomass burning particles with a notable increase in biomass burning on April 13th. The absorption and scattering coefficients underwent large increases on April 12th-13th. During this event, back trajectories indicate an air mass origin from the northwest over the ocean. These findings highlight the importance of mixing state in influencing optical properties, as throughout the study non-aromatic containing BB and dust particles had little to no influence on the particle optical behavior, however, upon association with aromatic compounds caused a considerable increase in total particle absorption. A large increase in aromatic-containing particle number concentrations and aromatic marker ions on biomass

burning and dust particles was observed on April 13th, coinciding with an increase in the absorption and scattering coefficients. Most interestingly, a brown carbon or HULIS particle type, indentified by the presence of high mass organic carbon, had a very strong correlation with all aromatic-containing particles, indicating high mass aromatic compounds had a large effect on absorption. The median aerosol hygroscopicity parameter (κ) observed of 0.49 falls between the average continental value of 0.27 and average marine value of 0.72, indicating influences from both continental and marine air masses observed during the study.

5.2 Introduction

Aerosols play an important role in climate forcing because of their ability to scatter and absorb solar and terrestrial radiation in addition to nucleating cloud droplets. Aerosols remain the largest uncertainty when estimating overall radiative forcing [*(IPCC)*, 2007; *McFiggans et al.*, 2006]. In order to reduce these uncertainties, measurements of aerosol optical, physical and chemical properties are needed. Optical properties such as refractive index(RI) are intrinsically coupled with chemical composition [*Moffet et al.*, 2008b]. Chemical composition also determines aerosol hygroscopicity which in turn affects the size, RI and CCN activity of aerosol particles. Understanding how hygroscopicity and RI evolve over time in the atmosphere is essential for understanding the direct and indirect effects of aerosols on the global radiation budget which strongly depends on particle size and chemistry [*(IPCC)*, 2007; *Andreae and Rosenfeld*, 2008; *McFiggans et al.*, 2006].

The dependence of particle absorption of solar radiation on aerosol chemistry is needed for climate models [*(IPCC)*, 2007; *Habib et al.*, 2008]. Absorption of light by particles generally increases with increasing black carbon content [*Habib et al.*, 2008], but is also strongly influenced by other carbonaceous species such as polycyclic aromatic hydrocarbons

(PAHs)[*Habib et al.*, 2008], aromatic compounds, or brown carbon [*Andreae and Gelencser*, 2006]. Previous field measurements have shown that particle size, single scattering albedo and real RI of aerosols impacted by smoke are dependent on particle hygroscopicity and the amount of black carbon [*Kreidenweis et al.*, 2001]. In addition to aerosol chemistry, the mixing state of the aerosol is very important for determining optical properties. When black carbon is internally mixed with a high refractive index material such as sulfate or sodium chloride, the absorption is greatly enhanced [*Fuller*, 1999; *Zhang et al.*, 2008]. However, there are exceptions: hygroscopic biomass burning aerosol can decrease absorption with increasing relative humidity (thought to be caused by particle collapse with water uptake [*Lewis et al.*, 2009]), and when black carbon mixes with mineral dust, the single scattering albedo of the dust is not largely affected [*Quinn and Bates*, 2005].

Atmospheric scattering, and to a smaller degree, atmospheric absorption depend strongly on the amount of water associated with the aerosol particles [*Malm et al.*, 2005]. The uptake of water on inorganic aerosols is very well understood [*Malm et al.*, 2005; *Wexler and Clegg*, 2002], however, the influence of organics on aerosol hygroscopicity is much less understood [*Malm et al.*, 2005]. It has been shown that the assumption of externally mixed inorganic and organic aerosol is invalid for even very pristine regions [*McFiggans et al.*, 2006], therefore measurements of the detailed mixing state of inorganic and organic compounds in parallel with their hygroscopic properties will help improve global climate models. Even small amounts of ionic material can activate organic particles [*Abdul-Razzak and Ghan*, 2005; *Ervens et al.*, 2005; *Lohmann et al.*, 2004], however, depending on the amount and specific nature of the organics, the aerosol water content and droplet growth kinetics will both be affected [*Chuang*, 2003; *McFiggans et al.*, 2006; *Medina and Nenes*, 2004].

The Cloud Indirect Forcing Experiment (CIFEX) took place from April 1 – 21 at Trinidad Head, a coastal site in northern California representing clean marine air with periodic long-range transport of aerosols from the Asian continent across the Pacific. A primary goal of CIFEX was to study the influence of aerosols on cloud properties [*Roberts et al.,* 2006; *Wilcox et al.,* 2006]. This study was the first to use single particle mass spectrometry for a direct comparison of ambient aerosol chemistry with rainwater sample chemistry [*Holecek et al.*, 2007]. Of special note was the high prevalence of aromatic-containing particle types in rainwater samples compared with low prevalence in ambient samples. This was hypothesized to be because the aromatic compounds consisted largely of humic-like substances (HULIS) or water soluble organic compounds that dissolved from the biomass particles in the rainwater, highlighting the important role of aromatic biomass species in cloud formation [*Andreae et al.*, 2004; *Holecek et al.*, 2007; *Li et al.*, 2003; *Roberts et al.*, 2002]. Airborne measurements during CIFEX showed influence from long-range transport from Asia, clean marine boundary layer and North American emissions [*Roberts et al.,* 2006]. Most of the long-range transport was observed above 2 km [*Hadley et al.,* 2007], as been shown in previous studies on transport of Asian air masses to the western U.S. [*De Gouw et al.,* 2004; *Heald et al.*, 2006], with a significant contribution of Asian aerosols observed at the ground level only during strong frontal passages [*VanCuren et al.*, 2005]. A CCN closure study indicates that cloud-processed aerosol had very similar CCN activity to that of ammonium sulfate, while other aerosol such as regional and long-range transport were less CCN active; highlighting the importance of aerosol chemistry on CCN activity [*Roberts et al.*, 2006; *Roberts et al.,* 2010].

Here we present single particle measurements taken at Trinidad Head, CA (at ground level) during CIFEX from April 1 – 23, 2004. We focus on the comparison of concurrently sampled ambient aerosol chemistry, aerosol optical and cloud property measurements to better understand the impacts aerosol chemistry on climate relevant properties.

5.3 Materials and Methods

5.3.1 Sampling location

The Cloud Indirect Forcing Experiment (CIFEX) took place at Trinidad Head, CA (41.05N, 124.15W, 107m above sea level) from April 1- 21, 2004. Trinidad Head is a clean marine monitoring site that is periodically influenced by long-range transport from Asia across the Pacific. The aerosol was sampled from the summit at Trinidad Head through a 10m sampling stack run by NOAA's Global Monitoring Division (GMD, formerly Climate Monitoring and Diagnostics Lab). The sampling line was relative humidity (RH) controlled to 55% by heating. The flow from the RH conditioner was then sent into a stainless steel sampling manifold and split off to the various instruments. During the study, there were two significant precipitation events; one from April 14 -16 and a second from April 20- 22.

5.3.2 Instrumentation

5.3.2.1 Single particle mass spectrometry

Single particle aerodynamic size and chemical composition were measured in real-time using an aerosol time-of-flight mass spectrometer (ATOFMS) equipped with a nozzle based inlet that transmits particles with an aerodynamic diameter (D_a) between 200 to 3000 nm. Single particle size is determined from the particle's velocity which is measured using the time-of-flight between two 532 nm CW lasers. The particle velocity is then used to time the ablation and ionization of the particle using a Q-switched 266 nm Nd:YAG laser at moment the particle enters the source region of a dual ion time-of-flight mass spectrometer. The resulting positive and negative ions are then analyzed. A detailed description of the ATOFMS instrument design and operation are described elsewhere [*Gard et al.*, 1997].

5.3.2.2 Size distributions

The particle size distributions and number concentrations were measured concurrently by a scanning mobility particle sizer (SMPS, TSI Model 3936) with sheath flow of 6.0 lpm and aerosol flow of 0.6 lpm. SMPS cumulative particle concentrations were scaled to the NOAA Global Monitoring Division's condensation particle counter (CPC, TSI model 3760). An aerosol particle sizer (APS, TSI Model 3321) was also used.

5.3.2.3 Optical properties

The absorption coefficient was determined using a filter absorption photometer (Magee Aethalometer Model AE-31). The absorption coefficient was measured at seven wavelengths, two of which are presented here: 370 and 880 nm. Total aerosol particle scattering for two size cuts (D_p<10 μm and D_p<1 μm) was measured with a 3 wavelength integrating nephelometer (TSI Inc. Model 3563) provided by NOAA's Global Monitoring Division. Here we only use the scattering measured at 550 nm for the 1 μm size cut. The nephelometer sample line was further dried to RH <40%.

5.3.2.4 Cloud condensation nuclei

CCN concentrations were measured with a streamwise thermal-gradient CCN counter (CCNc) at a supersaturation of 0.6% [*Roberts and Nenes*, 2005]. Total particle condensation nuclei (CN) concentrations were measured with a condensation particle counter (CPC, TSI model 3760) from NOAA's Global Monitoring Division. The fraction of CCN active particles, or fCCN, was obtained from the CCN/CN ratio. Due to the lower size limit of the CPC, CN is more precisely CN_{14}, and therefore fCCN is more precisely $fCCN_{14}$. For simplicity, we will refer to $fCCN_{14}$ as fCCN for the remainder of the paper.

5.3.2.5 Other measurements

Wind speed and wind direction were measured using a R.M. Young windbird model #05603 provided by NOAA's Global Monitoring Division. Relative humidity (RH) was

measured using a Campbell model HMP-50 sensor provided by NOAA's Global Monitoring Division. Surface ozone concentrations were measured with a ultraviolet absorption photometer provided by NOAA's Global Monitoring Division [*Oltmans et al.*, 2008]. The NOAA HYSPLIT software versions 4.9 (updated February of 2009) was used to calculate air mass back trajectories.

5.3.3 Data analysis

5.3.3.1 ATOFMS data analysis

A total of 598,515 single particle mass spectra were collected over the course of the study. Analysis based on particular mass spectral features within the data set was performed with a Matlab-based (ver. 6.5.1) toolset, YAADA (ver. 1.2) (http://www.yaada.org). The single particle data was automatically sorted and grouped into clusters of particles with similar mass spectral characteristics using the adaptive resonance theory neural network algorithm, ART-2a [*Song et al.*, 1999]. The main user-defined parameters for ART-2a are the learning rate, number of iterations, and vigilance factor, which were set to 0.05, 20, and 0.80, respectively [*Rebotier and Prather*, 2007]. The resulting clusters were then analyzed manually and classified into distinct particle types based on their mass spectral features [*Furutani et al.*, 2008; *Guazzotti et al.*, 2003; *Moffet et al.*, 2008a; *Silva et al.*, 1999; *Sullivan et al.*, 2007]. The most abundant 50 particle clusters, representing over 95% of the total particles were classified as mineral dust, biomass burning, aged sea salt, fresh sea salt, organic carbon (OC), elemental carbon with organic carbon (ECOC), vegetative detritus, magnesium-rich, sea salt-EC and amine [*Holecek et al.*, 2007]. Sea salt-EC (SSEC) has been hypothesized to be coagulated sea salt and EC particles formed via in-cloud processing [*Holecek et al.*, 2007; *Spencer et al.*, 2008]. The appearance or nonexistence of secondary aerosol species like nitrate, sulfate and ammonium was not used as part of the previous classifications except for sea salt particles. As has been done previously, the differentiation between aged and fresh sea salt is determined by

the presence of large sulfate and/or nitrate peaks in the average mass spectrum for a particular cluster [*Sullivan et al.*, 2007; *Sullivan and Prather*, 2007].

5.3.3.2 Single hygroscopicity parameter

To summarize the hygroscopicity measurements made with the CCNc, a single parameter for particle hygroscopicity (κ) is used [*Petters and Kreidenweis*, 2007]. The following equation defines the relationship between a growing particle's equilibrium water saturation ratio, S, droplet diameter, D, dry diameter, D_{dry}, and hygroscopicity, κ:

$$S(D) = \frac{D^3 - D_{dry}^3}{D^3 - D_{dry}^3(1-\kappa)} \exp\left(\frac{A}{D}\right) \qquad (5.1)$$

where $A = 2.1\text{x}10^{-9}$ m is a constant evaluated for a surface tension of 0.072 J m^{-2} (pure water) and temperature of 298.15 K [*Petters and Kreidenweis*, 2007]. κ describes a particle's water activity and typical values range from 1.4 (hygroscopic soluble salt; NaCl) to about 0 (insoluble but wettable) for atmospherically relevant systems. The CCN activation diameter (D_{act}) of atmospheric aerosols was estimated using the measured size distributions, CN, and CCN concentrations from

$$1 - \frac{CCN}{CN} = \frac{\int_{D_0}^{D_{act}} n(D)dD}{N_{total}} \qquad (5.2)$$

where N_{total} is the cumulative concentration obtained by integrating the observed size distribution of $n(D)$, D is the electric mobility diameter selected by the SMPS and D_{o} the smallest size measured by the SMPS (~11 nm). The CCN/CN ratio represents the fraction of the CCN-active aerosol (fCCN). Eqn. (2) assumes that the particles are internally mixed (i.e. homogeneous particle composition). This approach was taken to simplify the data analysis, yet still reflects how much the relative degree of variation in the chemical composition affects CCN activity, as the size resolved chemistry was simultaneously measured [*Furutani et al.*,

2008]. We have used the previously estimated approximate relationship $D_{act} \sim \kappa^{-1/3}$ [*Shinozuka et al.*, 2009]. In the estimation of D_{act}, contributions from particles larger than the range of the SMPS (upper range = 400 nm for our settings) were not considered.

5.3.3.3 Total particle absorption

Absorption coefficients (m^{-1}) were calculated from the original data ($\mu g/m^3$) using the method by Arnott et al. (2005) [*Arnott et al.*, 2005] using modified parameters as described in Corrigan et al. (2006) [*Corrigan et al.*, 2006].

5.4 Results

5.4.1 Overall particle chemistry

Figure 5.1 shows the fraction of particle classes of both sub- and super-micrometer particles analyzed by the ATOFMS for the study. All times are reported in UTC. The composition of sub-micrometer particles (Figure 5.1, top) is varied and consists of biomass burning (BB), mineral dust, organic carbon (OC), elemental carbon with organic carbon (ECOC), and aged, fresh and positive-only sea salt (SS). Of special note is the large increase in the number fraction of sub-micrometer biomass burning particles on April 13th. The composition of super-micrometer particles (Figure 5.1, bottom) consists largely of aged, fresh and positive-only sea salt (SS). Both the sub-micrometer (48% of total SS, 65% of dual-polarity SS) and super-micrometer (36% of total SS, 41% of dual-polarity SS) have high number fractions of sea salt consisting of aged SS. This shows the large influence of long-range transported pollution and regional pollution on the relatively remote sampling site. Figure 5.2 shows the fractional size-resolved chemistry from the ATOFMS for the entire study. Overall, the particle chemistry was dominated by sea salt, both in the sub- and super-micrometer size ranges with a large fraction of the sea salt being aged. In the sub-micrometer

size range there was a large fraction of OC, ECOC and BB, with a notable increase in the fraction of BB on April 13th.

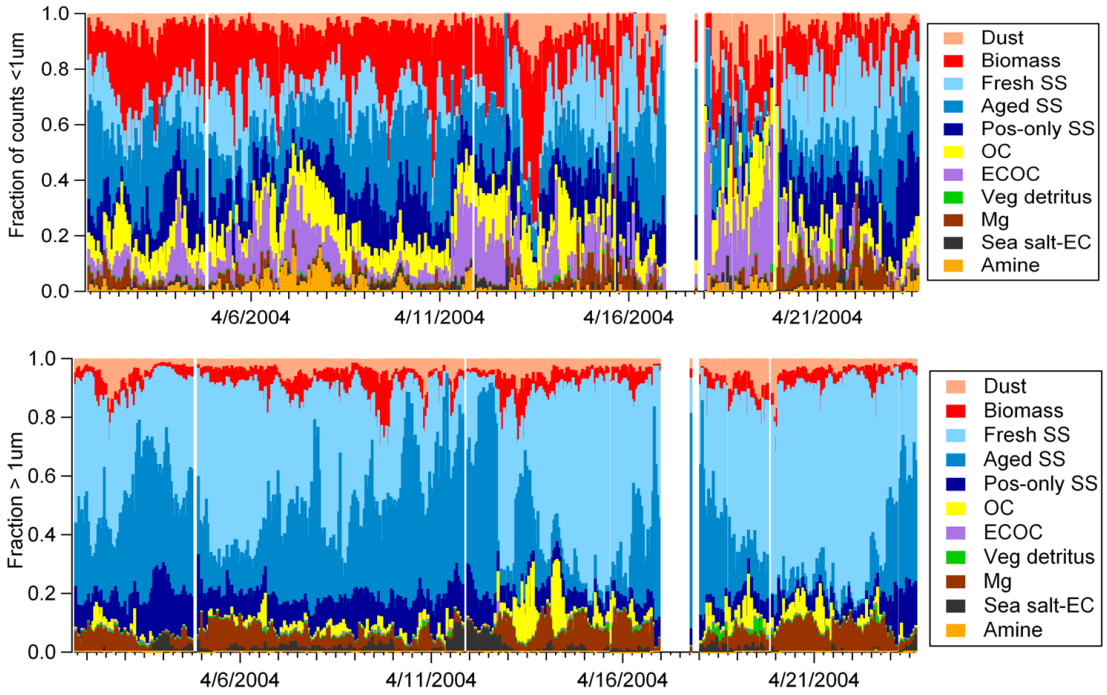

Figure 5.1. Overview of submicron (top) and supermicron (bottom) size ranges showing the ATOFMS fractions of total particle types over the course of the study.

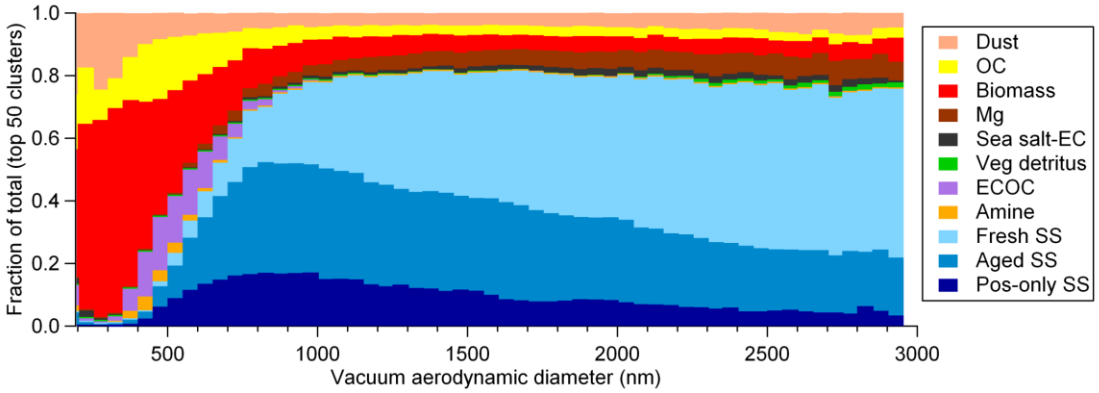

Figure 5.2. Overview of ATOFMS particle types as size-resolved number fraction.

5.4.2 Size distributions

Figure 5.3 shows the 0.011- 0.4 µm (SMPS) and 0.542 – 20 µm (APS) size distributions between these sizes for the course of the study. The SMPS distributions (Figure 5.3, top) shows distinct sub-micrometer particle events, with a mode around 0.1 µm on April 3rd – 6th, April 9th-11th, April 11th-12th and April 13th. There were other sub-micrometer events with a size mode centered around 0.03-0.04 µm on April 1st-2nd and April 15th-19th. On April 22nd-23rd there was a high concentration of particles around 0.05-0.06 µm. The APS distributions (Figure 5.3, bottom) show particle events that generally correspond with the SMPS events with the exception of April 15-19th when there were large concentrations of particles at about ~0.04 µm but very low concentrations of particles > 0.542 µm.

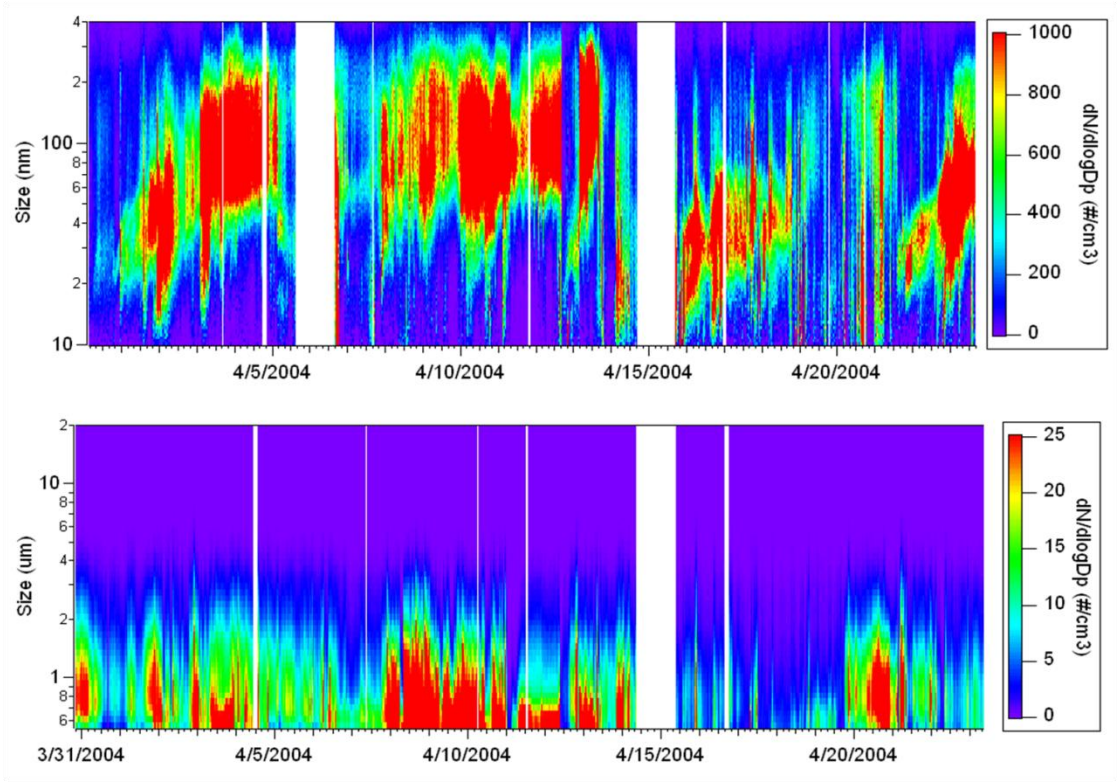

Figure 5.3. Overview of SMPS (top) and APS (bottom) size distributions.

5.4.3 Optical properties

Figure 5.4 shows the hourly-averaged absorption and scattering coefficients. The absorption coefficients (1/m) at 370 and 880 nm (Figure 5.4, top) are fairly constant and low throughout the study with a large increase at 370 nm on April 12th-13th. The scattering coefficient (1/m) (D_p<1 µm) at 550 nm (Figure 5.4, bottom) has a large increase on April 12th-13th, similar to the particle absorption. Total particle scattering indicates other smaller events leading up to and after the April 12th-13th event. The large increase in total particle absorption and scattering coincides with an increase in submicron particles (Figure 5.3) and the large increase in the fraction submicron particles from biomass burning (Figure 5.1, top).

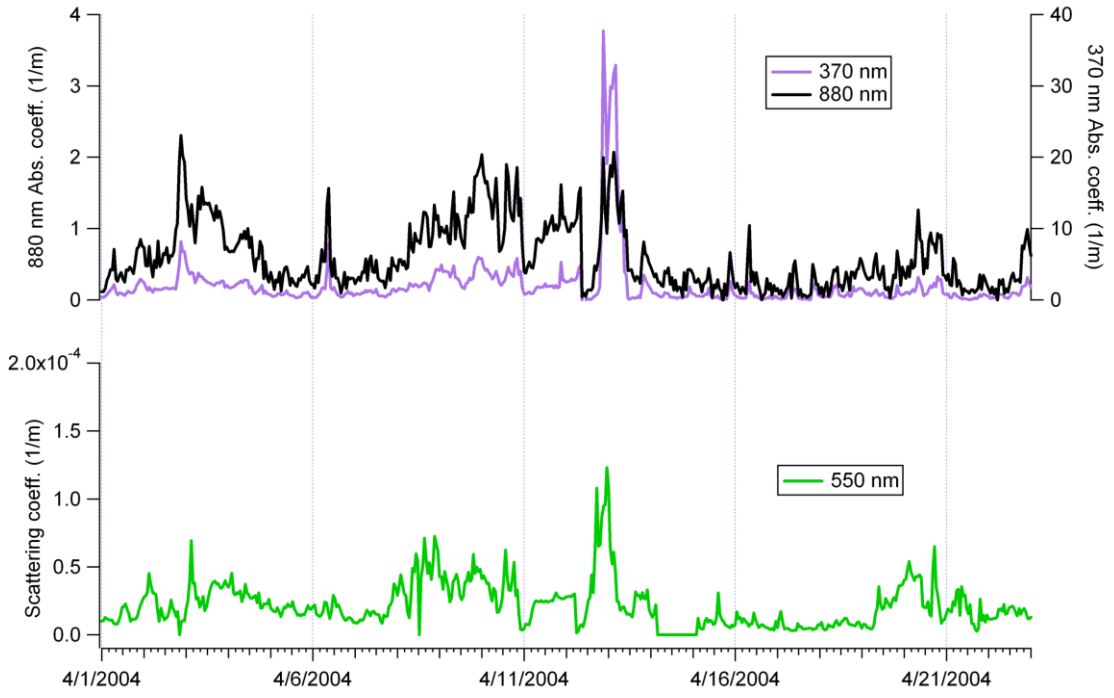

Figure 5.4. Overview of absorption coefficient (top) and scattering coefficient (bottom) during the course of the study.

5.4.4 Meteorological and ozone measurements

Figure 5.5 shows ozone concentrations (top), relative humidity (middle) and wind speed and wind direction (bottom). The ozone follows a very distinct diurnal pattern, and ranges from ~ 10 ppb on April 9th to ~ 55 ppb on April 13th, during the sub-micrometer biomass burning and total particle absorption and scattering event. The concentrations (10-55 ppb) observed over the course of the study are within the expected range for a rural coastal site, as typical ozone concentrations are 20-40 ppb for marine, 20-40 ppb for remote, and 50-120 ppb for rural environments [*Seinfeld and Pandis*, 1998].

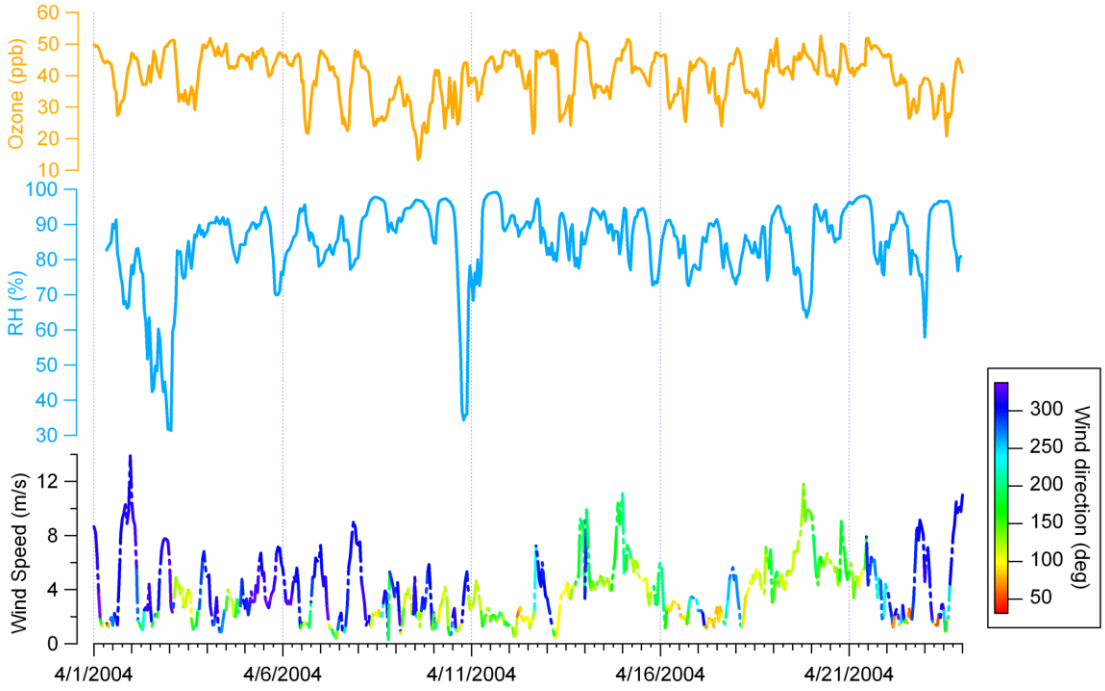

Figure 5.5. Overview of ozone (top), relative humidity (middle) and meteorological data (bottom) during the course of the study. The color on the wind speed indicates the wind direction.

The relative humidity (RH), similar to the ozone, follows a distinct diurnal pattern and ranges from ~70% up to ~95% with the exception of a few events. The time leading up to the

April 12-13th submicron biomass and total particle absorption and scattering event was characterized by a relatively distinct diurnal pattern similar to most of the rest of the study.

The wind speed, similar to the ozone and RH, also follows a distinct diurnal pattern, ranging from ~ 0 m/s on April 13th up to ~14 m/s April 1st-2nd. Wind direction was predominantly from the NW April 1st -11th, after which it was primarily from the SE April 11th-21st and then shifted back to the NW April 21st- 23rd. The time leading up to the April 12-13th submicron biomass and total particle absorption and scattering event was fairly stagnated with wind from the SE, after which the wind picked back up and fluctuated from the SE to NW and back to the SE again. Over the course of the study there was not a typical on-shore off-shore diurnal cycle in wind direction, but rather a swirling pattern around the site, making trajectory analysis the best way to determine source contributions.

HYSPLIT 48 hour air mass back trajectories showed wide-ranging influences from five major regions: long-range transport, from the north, south, a regional spiral from the north, and a regional spiral from the south. An overview of the different back trajectories for the entirety of the study can be found in Figure 5.6. The air mass back trajectory for the April 12th-13th event was from the north, along the coast and over Oregon and Washington (Figure 5.6). Flights on April 12th and 13th indicated the influence of cloud processed aerosol only, with no long range transport [*Roberts et al.*, 2006]. Most of the long-range transport observed during CIFEX occurred above 2 km [*Hadley et al.*, 2007]. However, as shown in Moore et al. (2011) [*Moore et al.*, 2011] and describe in Chapter 6, the air masses were passing close to 3000 m; indicating possible infiltration of the boundary layer and clouds.

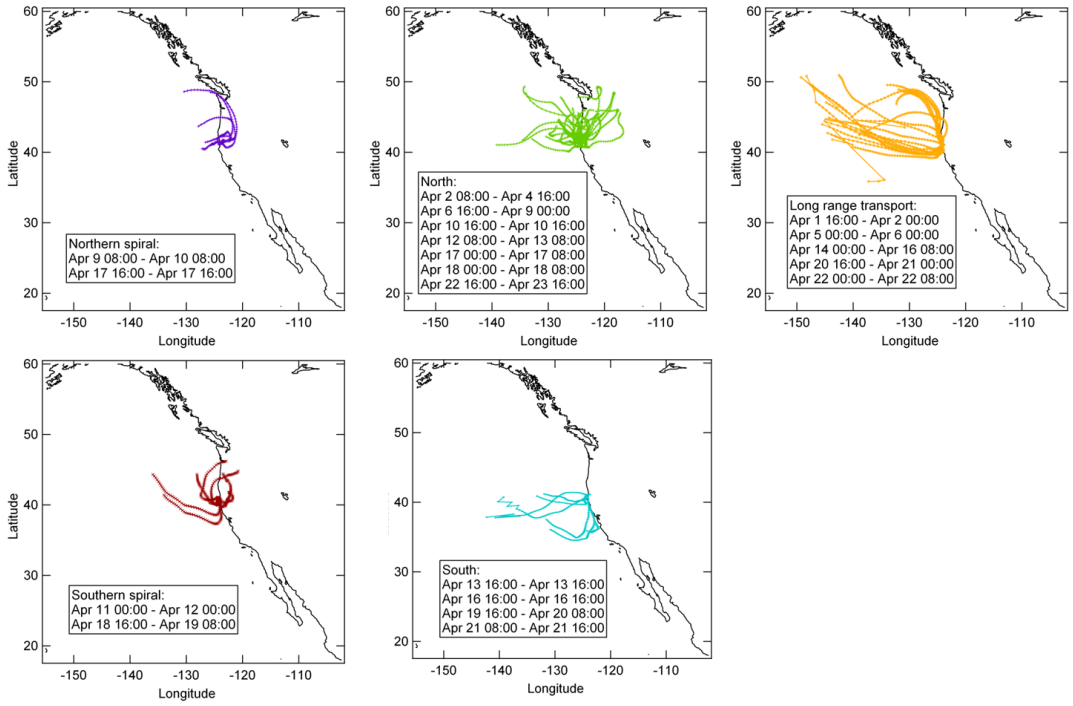

Figure 5.6. Overview of HYSPLIT back trajectories during CIFEX. Each back trajectory is for 48 hours at 500 m.

5.4.5 Cloud condensation nuclei (CCN)

Figure 5.7 shows an overview of CCN, CN, fCCN and κ for the entire study. Total CCN (SS=0.6%) and CN concentrations (Figure 5.7, top) are highly correlated (R^2=0.5). CCN concentrations ranged from ~40 cm^{-3} on April 20th to ~2100 cm^{-3} on April 4th with a median concentration of ~300 cm^{-3} for the whole study, slightly higher than typical marine CCN concentrations (20-40 cm^{-3}), closer to nonurban continental concentrations (100-200 cm^{-3}) [*Hudson*, 1991; *Seinfeld and Pandis*, 1998]. CN concentrations ranged from ~80 cm^{-3} on March 31st to ~4000 cm^{-3} on April 12th-13th with a median concentration of ~600 cm^{-3} for the whole study, within the range of typical marine CN concentrations [*Jaenicke*, 1993; *Seinfeld and Pandis*, 1998]. The maximum CN concentration corresponds to the submicron biomass and total particle absorption and scattering event on April 12th-13th. fCCN, or the ratio of CCN/CN (Figure 5.7, middle), had a median value of ~0.67 for the whole study. The lowest

fCCN values corresponds to the first rain event, while the highest fCCN values correspond to the period immediately preceding the submicron biomass and total particle absorption and scattering event April 12th-13th. For portions of the study, fCCN was close to unity, indicating that the aerosol was fully activated and all particles would become CCN at SS=0.6% during these periods. Due to the method of estimating κ previously mentioned, hygroscopicity cannot be estimated during these fully activated periods. The overall median κ value for the study is 0.49 and ranged from 0.021-5.8 (Figure 5.7, bottom). The higher end of this range reflects the error of the estimation method; however, the relative changes in κ are still indicative of changes in aerosol chemistry. The median κ value falls between the average continental value of 0.27 and average marine value of 0.72, indicating a mix of both continental and marine influences during the course of this study [*Petters and Kreidenweis*, 2007; *Pringle et al.*, 2010], as supported by ATOFMS particle chemistry measurements (Figure 5.1).

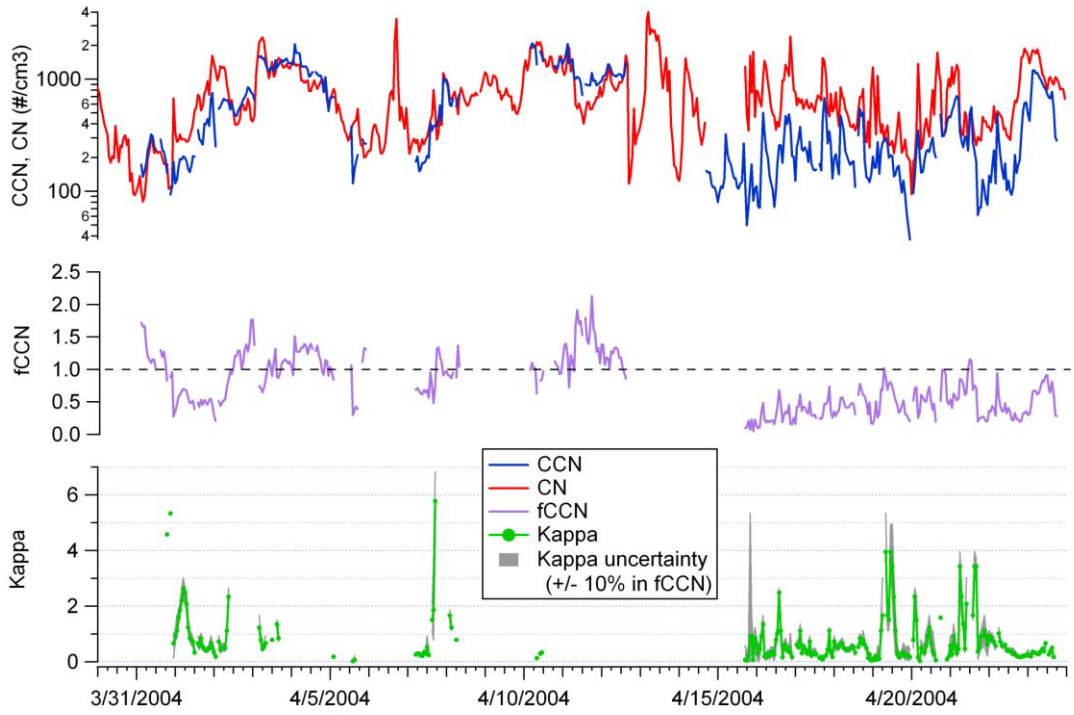

Figure 5.7. Overview of CCN (s=0.6), CN, fCCN and Kappa. The dashed line on the fCCN graph indicates where particles were fully activated. During these periods, no kappa values were able to be estimated. The gray areas on the kappa graph indicates the confidence within 10% of fCCN.

5.4.6 Comparison of particle chemistry with optical properties

Organic carbon that absorbs in the UV and visible range, otherwise known as brown carbon is a significant source of particle absorption [*Andreae and Gelencser*, 2006; *Moosmueller et al.*, 2009], and forms in clouds via aqueous phase chemistry [*Andreae et al.*, 2004; *Holecek et al.*, 2007; *Li et al.*, 2003; *Roberts et al.*, 2002]. Polycyclic aromatic hydrocarbons (PAHs), other aromatic compounds, and HULIS also strongly absorb UV and visible radiation [*Andreae and Gelencser*, 2006; *Jacobson*, 1999]. HULIS is formed from aqueous phase free radical oligmerization of monomeric units that are often times (but not always) aromatic [*Gelencser et al.*, 2002; *Hoffer et al.*, 2004; *Kiss et al.*, 2002]. On April 13th, there was a large increase in light absorption by the particles (Figure 5.4), especially at the

shorter wavelength of 370 nm, which can be explained by the presence of absorbing organic species in the particles. Searches were performed for aromatic-containing particles by querying aromatic ion markers peak areas > 100 for m/z +51 ($C_4H_3^+$), +63 ($C_5H_3^+$), +77 ($C_6H_5^+$), +91 ($C_7H_7^+$), and +115 ($C_9H_7^+$) [*Holecek et al.*, 2007], which correspond to low mass ions of the "low" and "high" aromatic series of peaks identified by McLafferty and Turecek (1993) [*McLafferty and Turecek*, 1993; *Silva and Prather*, 2000]. The particle types with the highest percentage of aromatic-containing particles were biomass burning (8%), OC (8%) and dust (4%). Therefore, aromatic-containing particles consisted of biomass burning (42%), OC (27%) and dust (18%) particle types with much smaller contributions from the remaining particle types.

During CIFEX, there was a high prevalence of aromatic-containing particle types in rainwater samples compared with a low abundance in ambient samples. This suggests that the aromatic compounds consisting largely of HULIS or hygroscopic organic compounds were scavenged by rain or clouds [*Andreae et al.*, 2004; *Holecek et al.*, 2007; *Li et al.*, 2003; *Roberts et al.*, 2002], as PAHs have been previously shown in cloud droplets [*Russell et al.*, 2000]. An important source of HULIS and brown carbon are organic carbon particles produced during smoldering biomass burning combustion [*Chakrabarty et al.*, 2010], and have been identified by single particle mass spectrometry as a subset of the OC particles with many peaks at high m/z in the positive spectrum, or high mass OC (HMOC) [*Qin and Prather*, 2006]. The larger size of the OC, ~ 0.5-1 μm suggested that these were cloud processed (Figure 5.2). HMOC particle counts showed a very strong correlation with all aromatic-containing particle counts (R^2=0.9, Figure 5.8). All aromatic-containing particles and biomass burning (R^2=0.5), dust (R^2=0.5) and all OC (R^2=0.3) particle counts are also correlated (See Figure 5.8). Temporal correlations of aromatic markers m/z +51, +63, +77, +91 and +115 on BB (R^2=0.4, 0.3, 0.3, 0.05, 0.2), dust (R^2=0.4, 0.4, 0.2, 0.3, 0.2), and OC (R^2=0.2, 0.3, 0.2,

0.07, 0.1) particle types and aromatic-containing particle counts indicate a strong link between all aromatic-containing particles, temporal aromatic ion marker behavior and BB, dust and OC particle types. There are low correlations of aromatic markers on HMOC particles with all aromatic-containing particles (R^2=0.01, 0.01, 0.002, 0.001, 0.0003), even though HMOC particle counts are very highly correlated with all aromatic-containing particles. The fact that HMOC particles are correlated with aromatic particles but do not have similar aromatic marker behavior signifies the presence of other absorbing compounds in the HMOC. However, there were no other significant correlations between any other non-aromatic markers, aromatic-containing particles, and particle optical properties on any of the particle types (not shown). The correlations for aromatic ion marker peak areas on the BB and dust particle types vs. total aromatic-containing particle counts are shown in Figure 5.9. There is a large increase in aromatic counts and aromatic ion markers on April 13th, coinciding with the large increase in absorption and scattering coefficients (Figure 5.4), increase in submicron particles (Figure 5.3) and a large increase in the fraction of submicron particles from biomass (Figure 5.1, top). This indicates that the influx of submicron BB and dust particles contained aromatic compounds that strongly increased the local particle absorption and scattering. While there was a fairly constant background fraction of BB and dust particles (Figure 5.1) leading up to the April 13th event, there was not a large increase in aromatic-containing particles until this date (Figure 5.9), highlighting that the mixing state of particles strongly influences their absorption and scattering properties. Throughout the study non-aromatic containing BB and dust particles had little to no influence on the particle optical behavior, however, upon association with aromatic compounds caused a considerable increase in total particle absorption, showing the specific effect of the aromatic chemistry of the BB and dust. There were no other significant correlations between any other non-aromatic markers and aromatic-containing particles and particle optical properties on any of the particle types (not shown).

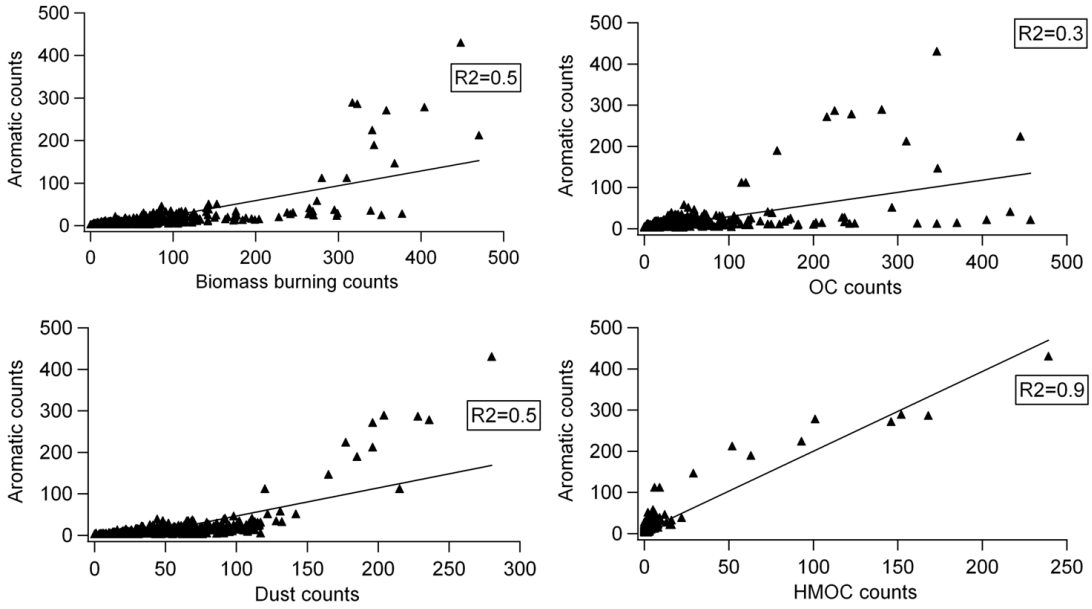

Figure5.8. Comparison of total aromatic counts (all particle types) to biomass burning, dust, OC and HMOC particle counts.

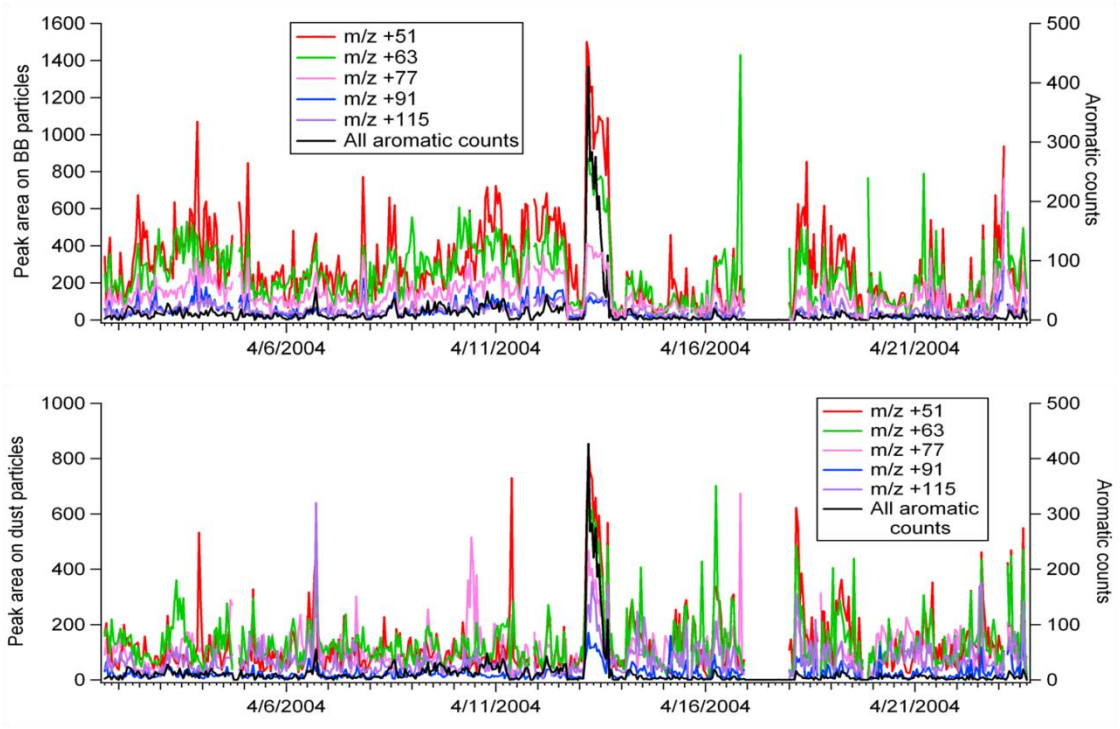

Figure 5.9. Comparison of aromatic ion marker peak areas on the biomass burning (BB) particle type to total aromatic counts (top) and dust particle type (bottom).

5.4.7 Comparison of particle chemistry with aerosol hygroscopicity

As shown on Figure 5.7, there are two different periods of CCN activity (at 0.6% SS). The first period, April 1- 12 consisted largely of almost fully activated or completely activated aerosol with fCCN > 1. The second period, April 15-23 consisted almost entirely of non-fully activated aerosol with fCCN <1. During period 1, the main SMPS size mode was around ~100 nm, while during period 2, the main SMPS size mode was ~40 nm; this shift points to more aged aerosol in period 1 and fresher aerosol in period 2, and had a large effect on fCCN (Figure 5.7). This is also shown with the ATOFMS data in Figure 5.1, with a much higher fraction of aged SS in period 1 than in period 2. For a given composition and supersaturation, the determining factor whether a particle activates or not is its dry diameter. Assuming similar hygroscopicities between the two periods, fCCN should be higher in period 1 due to the larger size of the particles, as observations support. One observation during period 1 is the prolonged period of fully activated aerosol between April 10-12. This coincides with an increase in particle scattering due to the large modes in the SMPS size distribution (Figure 5.4), and an increase in the fraction of sea-salt EC particles in the super-micrometer (Figure 5.1, bottom). While super-micrometer particles are large enough to activate regardless of their composition, sea salt-EC particles are most likely indicative of in-cloud processing [*Holecek et al.*, 2007; *Spencer et al.*, 2008], and meteorological data indicate that local wind speed was mostly stagnant (Figure 5.5), therefore, this increase in fully activated particles is due to increased aerosol hygroscopicity from in-cloud processing. Indeed, single-particle mixing state indicates that particles during April 13 show evidence of in-cloud processing, and is the subject of a different chapter (Chapter 6) [*Moore et al.*, 2011]. CIFEX aircraft findings show that cloud-processed aerosol having similar CCN activity to that of ammonium sulfate [*Roberts et al.*, 2006; *Roberts et al.*, 2010]. This cloud processing caused the particles to increase their hygroscopicity due to aqueous phase oxidation and uptake of additional soluble species. Water

uptake caused an increase in particle scattering, as shown by the correlation between the SMPS size distributions and total scattering (Figures 5.3 and 5.4). The median κ during the study was 0.49, between the marine boundary layer and continental boundary layer values (0.21-0.25) and the free troposphere value of 0.98 [*Roberts et al.*, 2010].

Due to the nature of our estimations of κ described previously, we were not able to estimate κ during the majority of period 1. We therefore focus our comparison between the hygroscopicity parameter and particle chemistry almost entirely on period 2, to better understand the impacts aerosol chemistry on cloud formation. The method used to estimate κ assumes a completely internally mixed aerosol, which is not the case here, as shown by Figure 5.1. Therefore, the changes in κ represent the overall changes in both the fractions of particle types and the changes in temporal chemistry on each of those particle types. Correlations to a given chemical marker will be low if they do not contribute to the soluble fraction or if there is already a substantial fraction of water-soluble ions on the particles. During period 2, there were two noticeable increases in κ, the first on April 19 and the second on April 21, concurrent with an increase in the size of the SMPS mode diameter. The increase in particle size mode and continued presence of the sea salt-EC particle type concurrent with increases in particle hygroscopicity indicates that there was cloud processing of the particles in period 2 and that it significantly increased the hygroscopicity. However, due to the larger particle sizes observed with the ATOFMS, these particles would most likely all be activated as CCN. The evidence of cloud processing in the larger particles suggests that the air mass was processed. Assuming that the larger particle composition measurements could be a proxy for chemical changes in the smaller particles below the detection limit of the ATOFMS (<200 nm), the smaller particles that determine the average hygroscopicity are most likely processed since it is rare to have large amounts of small fresh particles in the same air mass as larger aged particles.

5.5 Conclusions and Atmospheric Implications

Aerosol size, composition, light absorption and scattering and particle hygroscopicity estimated from CCN measurements were measured in real-time and during the 2004 CIFEX study to better understand the impacts aerosol chemistry on climate relevant properties. While previous studies have shown significant atmospheric processing of sea salt aerosol by mass [*Huebert et al.*, 1996; *Sievering et al.*, 2004; *Sievering et al.*, 1999], we looked at the number fraction that are processed for the first time and show that over half of the sea salt particle number fraction were aged in a remote marine environment. In the sub-micrometer mode, a significant fraction of particles contained organic carbon, elemental carbon with organic carbon and biomass burning with a notable increase in the number fraction of biomass burning on April 13th. A large increase in aromatic-containing particle counts and aromatic markers on the biomass burning and dust particles on April 13th coincided with a large increase in total particle absorption and scattering, increase in sub-micrometer particles and a large increase in the total submicron particles from biomass burning. The particle types with the highest percentage of aromatic-containing particles were biomass burning, organic carbon, and dust. Most interestingly, a subset of the organic carbon particles, high mass organic carbon, had a very strong correlation with all aromatic-containing particle counts, indicating that HULIS or brown carbon associated with biomass burning is a significant source of particle absorption, as has been suggested previously. Throughout the study biomass burning and dust particles had little to no influence on the particle optical behavior, however, upon association with aromatic compounds caused a considerable increase in total particle absorption, highlighting the importance of changes in the intrinsic particle mixing state and chemistry on aerosol optical properties.

CCN concentrations ranged from 40-2100 cm^{-3} with a median concentration of 300 cm^{-3}, slightly higher than typical marine CCN concentrations and close to those of nonurban

continental concentrations. CN concentrations ranged from 80-4000 cm^{-3} with a median concentration of 600 cm^{-3}, which were within typical marine particle concentrations. fCCN ranged from 0.05 -2.1 with a median value of 0.67. For portions of the study, fCCN was close to unity, indicating that the aerosol was fully activated at 0.6% SS. Periods of fully activated aerosol and increases in hygroscopicity parameter κ coincided with increases in the fraction of sea salt-EC particle type, most likely indicating increased aerosol hygroscopicity due to in-cloud processing, highlighting the importance of how hygroscopic and soluble marine particles in addition to atmospherically and cloud processed aerosols could be influencing particle hygroscopicity. However, due to the larger particle sizes observed with the ATOFMS, these particles would most likely all be activated as CCN. Therefore, the differences observed in sub- and supermicron particle types were most likely a proxy for chemical changes in the smaller particles below the detection limit of the ATOFMS (<200 nm). Aerosol hygroscopicity parameter (κ) had a median value of 0.49, between the average continental value of 0.27 and average marine value of 0.72, indicating a mix of both continental and marine influences during the course of this study, as was shown by particle composition.

5.6 Acknowledgments

We would like to thank John Holecek and Dr. Odelle Hadley (UCSD) for their help with data collection and analysis. We are grateful to V. Ramanathan (UCSD) for the use of the aethalometer data. The authors are very grateful to NOAA for the use of their HYSPLIT back trajectory program and NOAA/ESRL/GMD, especially John Ogren, Betsy Andrews and Samuel Oltmans, for use of the nephelometer, meteorological, condensation particle counter, relative humidity, and ozone data. We acknowledge the National Oceanic and Atmospheric Administration (NOAA) grant NOAA/NA17RJ1231, and V. Ramanathan (UCSD) for the support of this research.

Publication acknowledgment

The contents of Chapter 5 are part of a manuscript in preparation, Moore, M.J.K., Spencer, M.T., Roberts, G.C., Corrigan, C., Prather, K.A., Real-time Single Particle Composition, Absorption, Scattering and Cloud Condensation Nuclei (CCN) Activity at Trinidad Head, CA during Cloud Indirect Forcing Experiment (CIFEX), to be submitted to Journal of Geophysical Research. The dissertation author was the primary investigator and author of this paper.

5.7 References

(IPCC), I.P.o.C.C., *Climate Change 2007: The Physical Science Basis*, Cambridge University Press, New York, 2007.

Abdul-Razzak, H., and S.J. Ghan, Influence of slightly soluble organics on aerosol activation, *Journal of Geophysical Research*, *110* (D06206), doi:10.1029/2004JD005324, 2005.

Andreae, M.O., and A. Gelencser, Black carbon or brown carbon? The nature of light-absorbing carbonaceous aerosols, *Atmospheric Chemistry and Physics*, *6*, 3131-3148, 2006.

Andreae, M.O., and D. Rosenfeld, Aerosol-cloud-precipitation interactions. Part 1. The nature and sources of cloud-active aerosols, *Earth Science Reviews*, *89*, 13-41, 2008.

Andreae, M.O., D. Rosenfeld, P. Artaxo, A.A. Costa, G.P. Frank, K.M. Longo, and M.A.F. Silva Dias, Smoking Rain Clouds over the Amazon, *Science*, *303* (5662), 1337-1342, 2004.

Arnott, W.P., K. Hamasha, H. Moosmueller, P. Sheridan, and J.A. Ogren, Towards aerosol light-absorption measurements with a 7-wavelength aethalometer: Evaluation with a photoacoustic instrument and 3-wavelength nephelometer, *Aerosol Science and Technology*, *39* (1), 17-29, 2005.

Chakrabarty, R.K., H. Moosmueller, L.-W.A. Chen, K. Lewis, W.P. Arnott, C. Mazzoleni, M.K. Dubey, C.E. Wold, W.M. Hao, and S.M. Kreidenweis, Brown carbon in tar balls from smoldering biomass combustion, *Atmospheric Chemistry and Physics*, *10* (6363-6370), 2010.

Chuang, P.Y., Measurement of the timescale of hygroscopic growth for atmospheric aerosols, *Journal of Geophysical Research*, *108* (D9), 4282, 2003.

Corrigan, C.E., V. Ramanathan, and J.J. Schauer, Impact of monsoon transitions on the physical and optical properties of aerosols, *Journal of Geophysical Research*, *111* (D18208), doi:10.1029/2005JD006370, 2006.

De Gouw, J.A., O.R. Cooper, C. Warneke, P.K. Hudson, F.C. Fehsenfeld, J.S. Holloway, G. Huebler, D.K. Nicks Jr., J.B. Nowak, D.D. Parrish, T.B. Ryerson, E.L. Atlas, S.G. Donnelly, S.M. Schauffler, V. Stroud, K. Johnson, G.R. Carmichael, and D.G. Streets, Chemical composition of air masses transported from Asia to the U.S. West Coast during ITCT 2K2: Fossil fuel combustion versus biomass-burning signatures, *Journal of Geophysical Research*, *109* (D23S20), doi:10.1029/2003JD004202, 2004.

Ervens, B., G. Feingold, and S.M. Kreidenweis, The influence of water-soluble organic carbon on cloud drop number concentration, *Journal of Geophysical Research*, *110* (D18211), doi:10.1029/2004JD005634, 2005.

Fuller, K.A., Effect of mixing on extinction by carbonaceous particles, *Journal of Geophysical Research*, *104*, 15,941-15,954, 1999.

Furutani, H.F., M. Dall'osto, G.C. Roberts, and K.A. Prather, Assessment of the relative importance of atmospheric aging on CCN activity derived from field observations, *Atmospheric Environment*, *42*, 3130-3142, 2008.

Gard, E., J.E. Mayer, B.D. Morrical, T. Dienes, D.P. Fergenson, and K.A. Prather, Real-Time Analysis of Individual Atmospheric Aerosol Particles: Design and Performance of a Portable ATOFMS, *Analytical Chemistry*, *69*, 4083-4091, 1997.

Gelencser, A., A. Hoffer, Z. Krivacsy, G. Kiss, A. Molnar, and E. Meszaros, On the possible origin of humic matter in fine continental aerosol, *Journal of Geophysical Research*, *107* (D12), 4137, 10.1029/2001JD001299, 2002.

Guazzotti, S.A., D.T. Suess, K.R. Coffee, P.K. Quinn, T.S. Bates, A. Wisthaler, A. Hansel, W.P. Ball, R.R. Dickerson, C. Neusuess, P.J. Crutzen, and K.A. Prather, Characterization of carbonaceous aerosols outflow from India and Arabia: Biomass/biofuel burning and fossil fuel combustion, *Journal of Geophysical Research*, *108* (D15), 4485, doi:10.1029/2002JD003277, 2003.

Habib, G., C. Venkataraman, T.C. Bond, and J.J. Schauer, Chemical, Microphysical and Optical Properties of Primary Particles from the Combustion of Biomass Fuels, *Environmental Science and Technology*, *42*, 8829-8834, 2008.

Hadley, O.L., V. Ramanathan, G.R. Carmichael, Y. Tang, C.E. Corrigan, G.C. Roberts, and G. Mauger, Trans-Pacific transport of black carbon and fine aerosols (D<2.5 um) into North America, *Journal of Geophysical Research*, *112* (D05309), doi:10.1029/2006JD007632, 2007.

Heald, C.L., D.J. Jacob, R.J. Park, B. Alexander, T.D. Fairlie, R.M. Yantosca, and D.A. Chu, Transpacific transport of Asian anthropogenic aerosols and its impact on surface air quality in the United States, *Journal of Geophysical Research*, *111* (D14310), doi:10.1029/2005JD006847, 2006.

Hoffer, A., G. Kiss, M. Blazso, and A. Gelencser, Chemical characterization of humic-like substances (HULIS) formed from a lignin-type precursor in model cloud water, *Geophysical Research Letters*, *31* (L06115), doi:10.1029/2003GL018962, 2004.

Holecek, J.C., M.T. Spencer, and K.A. Prather, Analysis of rainwater samples: Comparison of single particle residues with ambient particle chemistry from the northeast Pacific and Indian oceans, *Journal of Geophysical Research*, *112* (D22S24), doi:10.1029/2006JD008269, 2007.

Hudson, J.G., Observations of anthropogenic cloud condensation nuclei, *Atmospheric Environment*, *25A* (11), 2449-2455, 1991.

Huebert, B.J., D.J. Wylie, L. Zhuang, and J.A. Heath, Production and loss of methanesulfonate and non-sea salt sulfate in the equatorial Pacific marine boundary layer, *Geophysical Research Letters*, *23* (7), 737-740, 1996.

Jacobson, M.Z., Isolating nitrated and aromatic aerosols and nitrated aromatic gases as sources of ultraviolet light absorption, *Journal of Geophysical Research*, *104* (D3), 3527-3542, 1999.

Jaenicke, R., Tropospheric Aerosols, in *Aerosol-Cloud-Climate Interactions*, edited by P.V. Hobbs, pp. 1-31, Academic Press, San Diego, 1993.

Kiss, G., B. Varga, Z. Galambos, and I. Ganszky, Characterization of water-soluble organic matter isolated from atmospheric fine aerosol, *Journal of Geophysical Research*, *107* (D21), 8339, doi:10.1029/2001JD000603, 2002.

Kreidenweis, S.M., L.A. Remer, R. Bruintjes, and O. Dubovik, Smoke aerosol from biomass burning in Mexico: Hygroscopic smoke optical model, *Journal of Geophysical Research*, *106* (D5), 4831-4844, 2001.

Lewis, K.A., W.P. Arnott, H. Moosmueller, R.K. Chakrabarty, C.M. Carrico, S.M. Kreidenweis, D.E. Day, W.C. Malm, A. Laskin, J.L. Jimenenez, I.M. Ulbrich, J.A. Huffman, T.B. Onasch, A. Trimborn, L. Liu, and M.I. Mischenko, Reduction in biomass burning aerosol light absorption upon humidification: roles of inorganically-induced hygroscopicity, particle collapse, and photoacoustic heat and mass transfer, *Atmospheric Chemistry and Physics*, *9*, 8949-8966, 2009.

Li, J., M. Posfai, P.V. Hobbs, and P.R. Buseck, Individual aerosol particles from biomass burning in southern Africa: 2. Compositions and aging of inorganic particles, *Journal of Geophysical Research*, *108(D13)* (8484), doi:10.1029/2002JD002310, 2003.

Lohmann, U., K. Broekhuizen, R. Leaitch, N. Shantz, and J. Abbatt, How efficient is cloud droplet formation of organic aerosols? *Geophysical Research Letters, 31* (L05 108), doi:10.1029/2003GL018999, 2004.

Malm, W.C., D.E. Day, S.M. Kreidenweis, J.L. Collett, C. Carrico, G. McMeeking, and T. Lee, Hygroscopic properties of an organic-laden aerosol, *Atmospheric Environment*, *39*, 4969-4982, 2005.

McFiggans, G., P. Artaxo, U. Baltensperger, H. Coe, M.C. Facchini, G. Feingold, S. Fuzzi, M. Gysel, A. Laaksonen, U. Lohmann, T.F. Mentel, D.M. Murphy, C.D. O'Dowd, J.R. Snider, and E. Weingartner, The effect of physical and chemical aerosol properties on warm cloud droplet activation, *Atmospheric Chemistry and Physics, 6*, 2593-2649, 2006.

McLafferty, F.W., and F. Turecek, *Interpretation of Mass Spectra*, University Science Books, Sausalito, CA, 1993.

Medina, J., and A. Nenes, Effects of film-forming compounds on the growth of giant cloud condensation nuclei: Implications for cloud microphysics and the aerosol indirect effect, *Journal of Geophysical Research*, *109* (D20207), doi:10.1029/2004JD004666, 2004.

Moffet, R.C., B. De Foy, L.T. Molina, M.J. Molina, and K.A. Prather, Measurement of ambient aerosols in northern Mexico City by single particle mass spectrometry, *Atmospheric Chemistry and Physics*, *8*, 4499-4516, 2008a.

Moffet, R.C., X. Qin, T.P. Rebotier, H.F. Furutani, and K.A. Prather, Chemically segregated optical and microphysical properties of ambient aerosols measured in a single-particle mass spectrometer, *Journal of Geophysical Research*, *113* (D12213), doi:10.1029/2007JD009393, 2008b.

Moore, M.J.K., M.T. Spencer, and K.A. Prather, Evidence for two distinct sources of oxalate during the Cloud Indirect Forcing Experiment (CIFEX), *in preparation*, 2011.

Moosmueller, H., R.K. Chakrabarty, and W.P. Arnott, Aerosol light absorbtion and its measurement: A review, *J. Quant. Spectrosc. Rad. Trans.*, *110*, 844-878, 2009.

Oltmans, S.J., A.S. Lefohn, J.M. Harris, and D.S. Shadwick, Background ozone levels of air entering the west coast of the US and assessment of longer-term changes, *Atmospheric Environment*, *42* (24), 6020-6038, 2008.

Petters, M.D., and S.M. Kreidenweis, A single parameter representation of hygroscopic growth and cloud condensation nucleus activity, *Atmospheric Chemistry and Physics*, *7* (8), 1961-1971, 2007.

Pringle, K.J., H. Tost, A. Pozzer, U. Poeschl, and J. Lelieveld, Global distribution of the effective aerosol hygroscopicity parameter for CCN activation, *Atmospheric Chemistry and Physics*, *10*, 5241-5255, 2010.

Qin, X., and K.A. Prather, Impact of biomass emissions on particle chemistry during the California Regional Particulate Air Quality Study, *International Journal of Mass Spectrometry*, *258*, 142-150, 2006.

Quinn, P.K., and T.S. Bates, Regional aerosol properties: Comparisons of boundary layer measurements from ACE 1, ACE 2, Aerosols99, INDOEX, ACE Asia, TARFOX, and NEAQS, *Journal of Geophysical Research*, *110* (D14202), doi:10.1029/2004JD004755, 2005.

Rebotier, T.P., and K.A. Prather, Aerosol time-of-flight mass spectrometry data analysis: A benchmark of clustering algorithms., *Analytica Chimica Acta, 585* (1), 38-54, 2007.

Roberts, G., G. Mauger, O. Hadley, and V. Ramanathan, North American and Asian aerosols over the eastern Pacific Ocean and their role in regulating cloud condensation nuclei, *Journal of Geophysical Research*, *111* (D13205), doi:10.1029/2005JD006661, 2006.

Roberts, G.C., P. Artaxo, J. Zhou, E. Swietlicki, and M.O. Andreae, Sensitivity of CCN spectra on chemical and physical properties of aerosol: A case study from the Amazon Basin, *Journal of Geophysical Research*, *107* (D20), 8070, doi:10.1029/2001JD000583, 2002.

Roberts, G.C., D.A. Day, L.M. Russell, E.J. Dunlea, J.L. Jimenenez, J.M. Tomlinson, D.R. Collins, Y. Shinozuka, and A.D. Clarke, Characterization of particle cloud droplet activity and composition in the free troposphere and the boundary layer during INTEX-B, *Atmospheric Chemistry and Physics*, *10*, 6627-6644, 2010.

Roberts, G.C., and A. Nenes, A Continuous-Flow Streamwise Thermal-Gradient CCN Chamber for Atmospheric Measurements, *Aerosol Science and Technology*, *39*, 206-221, 2005.

Russell, L.M., K.J. Noone, R.J. Ferek, R.A. Pockalny, R.C. Flagan, and J.H. Seinfeld, Combustion Organic Aerosol as Cloud Condensation Nuclei in Ship Tracks, *Journal of Aerosol Science*, *57*, 2591-2606, 2000.

Seinfeld, J.H., and S.N. Pandis, *Atmospheric Chemistry and Physics*, John Wiley & Sons, New York, 1998.

Shinozuka, Y., A.D. Clarke, P.F. DeCarlo, J.L. Jimenez, E.J. Dunlea, G.C. Roberts, J.M. Tomlinson, D.R. Collins, S.G. Howell, V.N. Kapustin, C.S. McNaughton, and J. Zhou, Aerosol optical properties relevant to regional remote sensing of CCN activity and links to their organic mass fraction: airborne observations over Central Mexico and the US West Coast during MILAGRO/INTEX-B, *Atmospheric Chemistry and Physics Discussions*, *9*, 12519-12558, 2009.

Sievering, H., J. Cainey, M. Harvey, J. McGregor, S. Nichol, and P.K. Quinn, Aerosol non-sea-salt sulfate in the remote marine boundary layer under clear-sky and normal cloudiness conditions: Ocean-derived biogenic alkalinity enhances sea-salt sulfate production by ozone oxidation, *Journal of Geophysical Research*, *109* (D19317), doi:10.1029/2003JD004315, 2004.

Sievering, H., B. Lerner, J. Slavich, J. Anderson, M. Posfai, and J. Cainey, O3 oxidation of SO2 in sea-salt aerosol water: Size distribution of non-sea-salt sulfate during the First Aerosol Characterization Experiment (ACE 1), *Journal of Geophysical Research*, *104* (D17), 21,707-21,717, 1999.

Silva, P.J., D. Liu, C.A. Noble, and K.A. Prather, Size and Chemical Characterization of Individual Particles Resulting from Biomass Burning of Local Southern California Species, *Environmental Science and Technology*, *33* (18), 3068-3076, 1999.

Silva, P.J., and K.A. Prather, Interpretation of mass spectra from organic compounds in aerosol time-of-flight mass spectrometry, *Analytical Chemistry*, *72* (15), 3553-3562, 2000.

Song, X.H., P.K. Hopke, D.P. Fergenson, and K.A. Prather, Classification of single particles analyzed by ATOFMS using an artificial neural network, ART-2A, *Analytical Chemistry*, *71* (4), 860-865, 1999.

Spencer, M.T., J.C. Holecek, C.E. Corrigan, V. Ramanathan, and K.A. Prather, Size-resolved chemical composition of aerosol particles during a monsoonal transition period over the Indian Ocean, *Journal of Geophysical Research*, *113* (D16305), doi:10.1029/2007JD008657, 2008.

Sullivan, R.C., S.A. Guazzotti, D.A. Sodeman, and K.A. Prather, Direct observations of the atmospheric processing of Asian mineral dust, *Atmospheric Chemistry and Physics*, *7* (5), 1213-1236, 2007.

Sullivan, R.C., and K.A. Prather, Investigations of the Diurnal Cycle and Mixing State of Oxalic Acid in Individual Particles in Asian Aerosol Outflow, *Environmental Science and Technology*, *41*, 8062-8069, 2007.

VanCuren, R.A., S.S. Cliff, K.D. Perry, and M. Jimenez-Cruz, Asian continentail aerosol persistence above the marine boundary layer over the eastern North Pacific: Continuous aerosol measurements from Intercontinental Transport and Chemical Transformation 2002 (ITCT 2K2), *Journal of Geophysical Research*, *110* (D09S90), doi:10.1029/2004JD004973, 2005.

Wexler, A.S., and S.L. Clegg, Atmospheric aerosol models for systems including ions H+, NH4+, Na+, SO42-, NO3-, Cl-, Br- and H2O, *Journal of Geophysical Research*, *107* (D14), 4207, 2002.

Wilcox, E.M., G. Roberts, and V. Ramanathan, Influence of aerosols on the shortwave cloud radiative forcing from North Pacific oceanic clouds: Results from the Cloud Indirect Forcing Experiment (CIFEX), *Geophysical Research Letters*, *33* (L21804), doi:10.1029/2006GL027150, 2006.

Zhang, R., A.F. Khalizov, J. Pagels, D. Zhang, X. Huaxin, and P.H. McMurry, Variability in morphology, hygroscopicity, and optical properties of soot aerosols during atmospheric processing, *Proceedings of the National Academy of Sciences of the United States of America*, *105* (30), 10291-10296, 2008.

Chapter 6

Evidence for two distinct sources of oxalate during the Cloud Indirect Forcing Experiment (CIFEX)

6.1 Synopsis

The mixing state of oxalate-containing particles was measured at a remote marine environment during CIFEX by direct ground-based measurements using an ATOFMS single-particle mass spectrometer to gain insight into formation processes in the atmosphere. There were two distinct oxalate periods; during the 1st period, supermicron oxalate was predominantly mixed with aged sea salt particles, whereas during the 2nd period oxalate was found to be internally mixed with sulfate in the submicron size range mainly on biomass burning and organic carbon particles. Enrichment of oxalate on the aged sea salt type during the 1st period and similar diurnal behavior of nitrate and oxalate on the aged sea salt particles indicate a photochemical source of oxalate during this period. During the 2nd period, the preferential enrichment of oxalate and sulfate on biomass burning and carbonaceous particles, and both temporal and size-resolved correlations between oxalate and other cloud or aqueous markers on these particle types, suggest in-cloud processing as the source of oxalate for this period. These findings provide insight into the mechanisms involved in forming the most abundant atmospheric diacid by showing two distinct sources in a remote marine atmosphere, which can directly affect hygroscopicity and CCN activity as the particles age in the atmosphere.

6.2 Introduction

Oxalic acid is the most abundant atmospheric dicarboxylic acid (DCA) [*Crahan et al.*, 2004; *Kawamura and Yasui*, 2005; *Warneck*, 2003; *Yu et al.*, 2005; *Yu*, 2000]. The prevalence of oxalic acid in aerosol particles in many different environments [*Ervens et al.*, 2004b; *Falkovich et al.*, 2005; *Kundu et al.*, 2010; *Sorooshian et al.*, 2006; *Yu et al.*, 2005] including remote marine regions [*Narukawa et al.*, 2003; *Turekian et al.*, 2003; *Warneck*, 2003] highlights the large range of the sources and atmospheric processes involved globally. Oxalic acid can be produced primarily from fossil fuel combustion [*Crahan et al.*, 2004; *Sorooshian et al.*, 2006; *Yang et al.*, 2009; *Yu et al.*, 2005] and biomass burning [*Saarikoski et al.*, 2007; *Sorooshian et al.*, 2006; *Yang et al.*, 2009; *Yu et al.*, 2005]. Additionally, oxalic acid can be produced through secondary processes such as photo-oxidation during long-range transport [*Saarikoski et al.*, 2007; *Turekian et al.*, 2003; *Yang et al.*, 2009; *Yu et al.*, 2005] or from the degradation of particulate organic carbon(POC) precursors from biogenic activity over the oceans [*Sorooshian et al.*, 2006; *Turekian et al.*, 2003]. Formation mechanisms of oxalic acid include in-cloud processing [*Sorooshian et al.*, 2006; *Yang et al.*, 2009; *Yu et al.*, 2005], gas-phase photo-oxidation followed by condensation [*Sorooshian et al.*, 2006; *Yang et al.*, 2009; *Yu et al.*, 2005], and heterogeneous reactions on aerosol particle surfaces [*Sorooshian et al.*, 2006; *Yang et al.*, 2009; *Yu et al.*, 2005]. However, distinguishing sources of oxalic acid is very difficult due to the complex nature of precursors and different formation processes involved [*Turekian et al.*, 2003]. By looking at what oxalate is associated with, further insight into the most common processes in the atmosphere is possible.

Because 20-90% of aerosol mass is carbonaceous [*Falkovich et al.*, 2005; *Yu*, 2000], and 40-80% of total organic mass is water soluble [*Falkovich et al.*, 2005; *Yu*, 2000], it is necessary to better understand the chemistry of water soluble organic carbon (WSOC) in order to further our understanding of the effects of organic aerosol on cloud condensation nuclei

(CCN) formation and radiative forcing, two important issues for global climate change. DCAs, predominantly oxalic acid, are a large component of WSOC and can have a profound effect on particle deliquescence and hygroscopicity [*Sorooshian et al.*, 2006; *Yu*, 2000]. WSOC DCAs oxalic, malonic and glutaric acids have been shown to have CCN activity comparable to that of pure ammonium sulfate [*Ervens et al.*, 2004a], however, knowing what the oxalic acid is mixed with can completely change whether it is hydrophobic or hydrophilic [*Furukawa and Takahashi*, 2010; *Sullivan et al.*, 2009]. Previous field studies have shown that knowledge of the contribution of WSOC is essential for predicting the hygroscopicity of ambient aerosol [*Chang et al.*, 2007; *Mircea et al.*, 2005; *Rissler et al.*, 2004; *Roberts et al.*, 2002]. Additionally, knowing whether oxalate is on all particles or just certain types yields insight into the sources and mechanisms, and also what fraction of the particles will have changes in their hygroscopicity and CCN activity. A better understanding of condensed phase and in-cloud processing production of WSOC oxalic acid has important implications for understanding the relative importance of the production mechanism leading to secondary organic aerosol (SOA) formation and climate.

In-cloud processing has been shown as the major pathway for secondary sulfate formation [*Yu et al.*, 2005], and oxalic acid has been shown to track particle sulfate, predominantly in the fine mode [*Crahan et al.*, 2004; *Ervens et al.*, 2004b; *Hara et al.*, 2002; *Sorooshian et al.*, 2006; *Warneck*, 2003; *Yu et al.*, 2005]; thus oxalic acid can be a good tracer for in-cloud processing [*Warneck*, 2003; *Yu et al.*, 2005]. Therefore, the main question is trying to understand how significant a source of oxalic acid in-cloud processing is and which conditions lead to this process. Due to similar in-cloud formation mechanisms, oxalic acid and sulfate typically have similar size-resolved chemistry [*Crahan et al.*, 2004; *Sorooshian et al.*, 2006; *Yu et al.*, 2005] and eventually become evenly distributed among different particle types with similar sizes [*Sullivan and Prather*, 2007]. In addition to in-cloud processing, oxalic acid

can be produced in the aqueous phase from oxidation of glycolic and glyoxylic acids [*Sorooshian et al.*, 2006; *Warneck*, 2003], with minor production from the decay of longer chain DCAs [*Sorooshian et al.*, 2006].

Previous single-particle mass spectrometry measurements of oxalate mixing states have shown oxalate to be produced by photochemistry during ACE-Asia [*Sullivan and Prather*, 2007], and a mixture of primary emissions, cloud processing, and photochemical sources in Shanghai [*Yang et al.*, 2009]. During ACE Asia, oxalate was predominantly mixed with mineral dust and aged sea salt, showing a consistent diurnal cycle. The diurnal behavior and preference of dust and sea salt over carbonaceous particle classes suggested that oxalate was produced by heterogeneous and photochemical processing. Oxalate-containing dust particles were only detected simultaneously with elevated nitrate and sulfate dust, indicating heterogeneous processing. The size-resolved chemistry of oxalate and nitrate were on the same particles and very similar, peaking in the supermicron mode. A lack of even-distribution of oxalate among particle classes of a similar size was observed, indicating in-cloud processing was not the major source of oxalate during ACE-Asia. Further evidence of lack of in-cloud processing was shown by lack of similarity of size chemistry of oxalate and sulfate, in addition to lack of significant ion signals from other cloud processing markers [*Sullivan and Prather*, 2007]. In Shanghai, oxalate was predominantly mixed with the biomass burning (BB) particle class. While it was suggested that the oxalate on the BB may be more primary in nature, there was also evidence of cloud processing. The size-resolved chemistry of oxalate and sulfate was very similar. 83% of particles that contained oxalate also contained sulfate, and air mass back trajectories suggested that the particles penetrated the cloud boundary layer. Oxalate was also found on dust and sea salt with a diurnal behavior, suggesting heterogeneous photochemical processing as the source of oxalate on these particle types [*Yang et al.*, 2009].

Here we build on our current understanding of oxalic acid chemistry using single particle ground-based measurements taken at Trinidad Head, CA during the Cloud Indirect Forcing Experiment (CIFEX) from April 1 – 23, 2004. We focus on the size-resolved and hourly temporal distribution of oxalate in single particles classified by type (mixing state) during two distinctly different oxalate events to better understand the sources and processing of oxalate in the remote marine atmosphere.

6.3 Materials and Methods

6.3.1 Sampling location

The Cloud Indirect Forcing Experiment (CIFEX) took place at Trinidad Head, CA (41.05N, 124.15W, 107m above sea level) from April 1- 21, 2004. This site is a clean marine monitoring site, with periodic intrusions from long-range transport from Asia across the Pacific. The aerosol was sampled from the summit at Trinidad Head through a 10 m sampling stack run by NOAA's Climate Monitoring and Diagnostics Lab. The relative humidity within the sampling line was controlled to 55% by heating. The flow from the RH conditioner was then sent into a stainless steel sampling manifold and split off to the various instruments.

6.3.2 Single particle mass spectrometry

Single particle aerodynamic size and chemical composition were measured in real-time using an aerosol time-of-flight mass spectrometer (ATOFMS) equipped with a nozzle-based inlet that transmits particles with an aerodynamic diameter (D_a) between 200 and 3000 nm [*Gard et al.*, 1997]. Single particle size is determined from the particle's velocity which is measured using the time of flight between two 532 nm continuous wave lasers. The particle velocity is then used to time the ablation and ionization of the particle using a Q-switched 266 nm Nd:YAG laser at moment the particle enters the source region of a dual ion time-of-flight mass spectrometer. The resulting positive and negative ions are then analyzed. A more

detailed description of the ATOFMS instrument design and operation are described elsewhere [*Gard et al.*, 1997].

6.3.3 ATOFMS data analysis

A total of 598,515 single particle mass spectra were collected over the course of the study. Analysis based on particular mass spectral features within the data set was performed with a Matlab-based (ver. 6.5.1) toolset, YAADA (ver. 1.2) (http://www.yaada.org). The single particle data was automatically sorted and grouped into clusters of particles with similar mass spectral characteristics using the adaptive resonance theory neural network algorithm, ART-2a [*Song and Hopke*, 1999]. The main user-defined parameters for ART-2a are the learning rate, number of iterations, and vigilance factor, which were set to 0.05, 20, and 0.80, respectively [*Rebotier and Prather*, 2007]. The resulting clusters were then analyzed manually and classified into distinct particle types based on their mass spectral features [*Furutani et al.*, 2008; *Guazzotti et al.*, 2003; *Moffet et al.*, 2008; *Silva et al.*, 1999; *Sullivan et al.*, 2007].

The 50 most populated particle clusters, representing over 95% over the total particles, were classified as mineral dust, biomass burning, aged sea salt, fresh sea salt, organic carbon (OC), elemental carbon (or soot) mixed with organic carbon (ECOC), vegetative detritus, magnesium-rich, sea salt-EC and amine. Sea salt-EC (SSEC) has been hypothesized to be coagulated sea salt and EC particles formed via in-cloud processing [*Holecek et al.*, 2007]. A subset of the OC particles was characterized by high mass hydrocarbon envelopes with ions up to m/z 250, hereafter referred to as high mass OC, or HMOC, which have been seen in other biomass burning rich and foggy environments [*Qin and Prather*, 2006]. For the particle classes presented herein, analysis was on calibrated, dual polarity particles only. For all particle types except ECOC, these mass spectra represent 85-100% of the particles. For the ECOC type (<1% of total particles), all spectra were positive ion only spectra or miscalibrated spectra, and therefore are not used in the presented analysis.

The presence of secondary aerosol species like nitrate, sulfate and ammonium was not used as part of the particle classifications except for sea salt particles. The differentiation between aged and fresh sea salt is determined by the presence of large sulfate and/or nitrate peaks in the average mass spectrum for a particular cluster. Particles containing oxalic acid were searched for by the conjugate anion $[M-H]^-$, oxalate (m/z -89)[*Sullivan and Prather*, 2007]. While it is possible that oxalate is preferentially detected on certain particle types, the ATOFMS has detected oxalate on a variety of different particles including biomass burning, sea salt and mineral dust [*Moffet et al.*, 2008; *Sullivan and Prather*, 2007]. The relative concentrations of oxalate on the various particle classes provides a semi-quantitative picture of the relative atmospheric quantities of oxalate on each particle type.

6.4 Results and Discussion

6.4.1 Detection of oxalate and sulfate in single particles

Oxalate was frequently detected in single particle spectra at Trinidad Head; 22% of submicron and 3% of supermicron particles contained oxalate. 15% of submicron particles contained oxalate and sulfate, meaning 65% of oxalate-containing submicron particles also had sulfate. Oxalate-and sulfate containing supermicron particles represented only 1% of supermicron, while 26% of oxalate-containing supermicron particles also contained sulfate. Oxalate-containing particles were isolated by querying the mass spectra for a peak at m/z – 89 with an area greater than 300. Sulfate-containing particles were defined by querying the particle mass spectra for particles containing a peak at m/z – 97 with an area greater than 5000. Oxalate- and sulfate-containing particles were defined as particles which contained both a peak at m/z – 89 with an area greater than 300 and a peak at m/z – 97 with an area greater than 5000. The particles were then separated into those with D_a less than or greater than 1 μm to eliminate the bias of the ATOFMS nozzle inlet toward supermicron particles, which causes

the submicron particles to be under sampled. Each size range represents the relative fraction or number of each particle type, not ambient concentrations of oxalate-containing particles.

The hourly counts of oxalate-containing, sulfate-containing and both oxalate- and sulfate-containing sub- and supermicron particles are shown in Figure 6.1. Also shown are the hourly counts of HMOC particles and sea salt-EC particles of all sizes. Figure 6.1 shows a large increase in the counts of submicron oxalate- and oxalate-and sulfate-containing particles on April 13th. On April 11-12th, there is a large increase in the counts of supermicron oxalate-containing particles (Figure 6.1). The increase in submicron oxalate-containing particles is concurrent with a large increase in HMOC particles; while the increase in supermicron oxalate-containing particles is concurrent with a large increase in sea salt-EC particles (Figure 6.1, bottom). Figure 6.1 (top) highlights two distinctly different oxalate periods. The 1st period was from April 11-12th and dominated by supermicron oxalate-containing particles. April 13th, the 2nd oxalate period, is dominated by both oxalate and oxalate-and-sulfate containing particles in the submicron. The large spike in sea salt-EC (SSEC) during the 1st oxalate period (April 11-12) (Figure 6.1, bottom) supports an in-cloud formation mechanism for oxalate, as the SS-EC particles were produced via in-cloud processing as described previously [*Holecek et al.*, 2007; *Spencer et al.*, 2008]. The large spike in HMOC counts during the 2nd oxalate period (April 13) supports an in-cloud formation mechanism for oxalate, as the HMOC particles were produced via aqueous-phase oxidation of organic precursors as described previously for a winter study in Fresno, which was also a biomass burning rich environment [*Qin and Prather*, 2006]. It is also possible the oxalate could have been formed via the oxidation or degradation of the HMOC [*Sorooshian et al.*, 2006]. These two distinct oxalate periods show two very different influences which warrant further analysis. Overall, during the 2nd period, the majority of submicron particles that have oxalate also contain sulfate, supporting an in-cloud formation mechanism for submicron oxalate; while during the 1st

period most oxalate-containing supermicron particles do not also contain sulfate, suggesting another formation mechanism for supermicron oxalate.

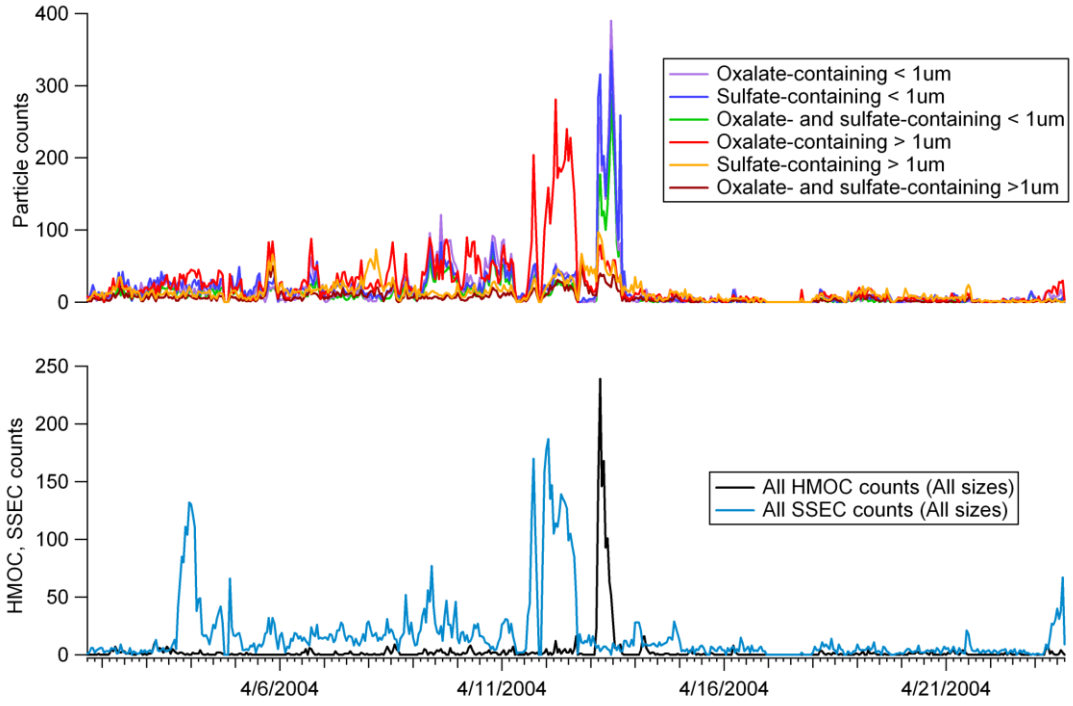

Figure 6.1. Comparison of oxalate –containing, sulfate-containing and oxalate-and sulfate – containing submicron and supermicron particles (top) and high mass organic carbon (HMOC) and sea salt – elemental carbon (SSEC) particles (bottom).

As the presence of oxalate on many different particle types could indicate in-cloud processing [*Sullivan and Prather*, 2007], it is important to determine which particle class(es) are associated with oxalate and sulfate to better understand the sources and formation mechanisms of particulate oxalate and its implications for the atmosphere during these two periods. The hourly counts of the different particle classes that contain oxalate in the sub- and supermicron for the entire study are shown in Figure 6.2. Figure 6.2 (top) shows that submicron oxalate during the 2nd oxalate period is found primarily on the biomass burning (BB) and organic carbon (OC) particle classes; and supermicron oxalate is mainly on aged sea salt particle class during the 1st oxalate period (Figure 6.2, bottom). To better understand the

preferential enrichment of oxalate on certain particle classes in more detail, as well as the possible sources of particulate oxalate during these different oxalate periods, it is necessary to determine which other species are present on oxalate-containing particles. In particular, sulfate is of interest because the presence of sulfate and oxalate on the same particle most likely indicates in-cloud processing as the source of oxalate. The hourly counts of the different particle classes that contain oxalate and sulfate for the entire study show that sub- and supermicron oxalate and sulfate for both periods 1 and 2 are found primarily on the biomass burning (BB) and organic carbon (OC) particle classes (Figure 6.3).

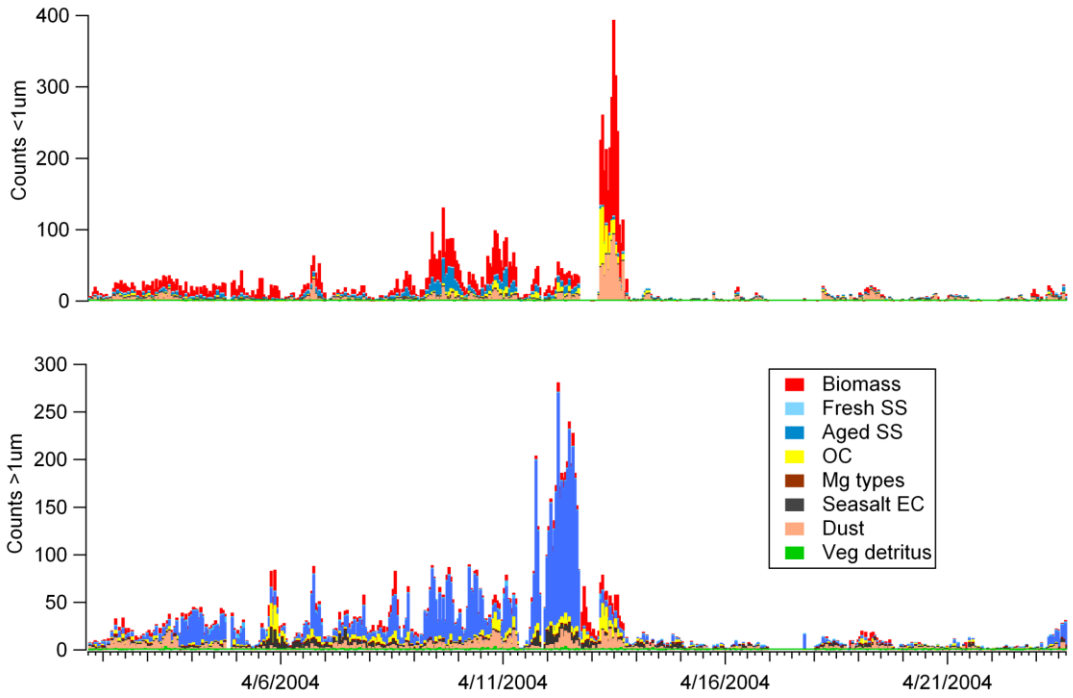

Figure 6.2. Comparison of oxalate-containing particles by class: submicron (top) and supermicron (bottom).

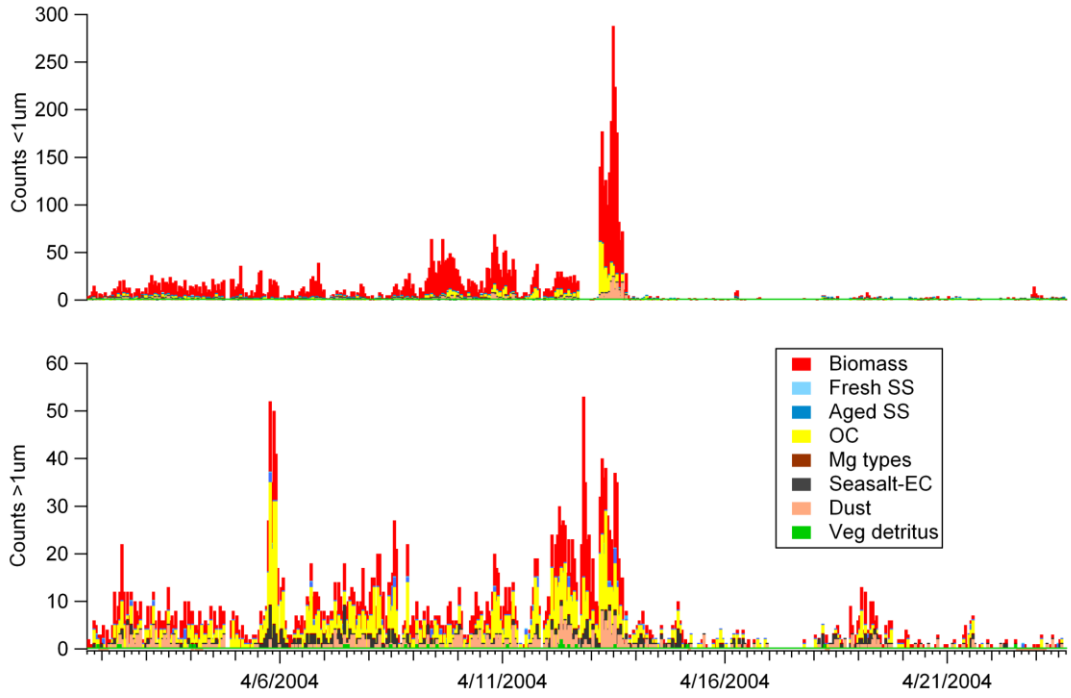

Figure 6.3. Comparison of oxalate-and sulfate- containing particles by type: submicron (top) and supermicron (bottom).

Figure 6.4 shows a breakdown of particle types for all sub- and super-micron particles as well as for sub- and supermicron oxalate- and oxalate- and sulfate-containing particles for the 1st and 2nd oxalate periods. Figure 6.4a (top left) shows that composition of the submicron particles was varied during the 1st period (2900 particles), with the majority (>80%) collectively coming from the aged SS, biomass burning, and OC particle classes. Oxalate-containing submicron particles during the 1st period (Figure 6.4a, top middle) (797 particles, 27% period 1 submicron) largely consist of BB (51%), followed by aged SS (18%), OC (17%), and dust (13%). The 1st period oxalate- and sulfate-containing submicron particles (Figure 6.4a, top right) (511 particles, 18% event 1 submicron, 64% period 1 oxalate-containing submicron) are mainly BB (72%) and OC (23%). This highlights the large enrichment of oxalate-and sulfate-containing submicron particles on the BB particle class, as the biomass burning class is only 27% of period 1 submicron particles and makes up 72% of

oxalate-and sulfate-containing submicron particles. Supermicron particles during period 1 (33,814 particles) show less variations in composition than the submicron particles, and consist mainly of aged (62%) and fresh sea salt (18%) (Figure 6.4a, bottom left). Oxalate-containing supermicron particles during the 1st period (Figure 6.4a, bottom middle) (3944 particles, 12% period 1 supermicron) are largely aged sea salt (75%), followed by BB (8%), OC (6%), and dust (5%). The first period oxalate- and sulfate-containing supermicron particles are largely BB (44%) and OC (35%) (Figure 6.4a, bottom right) (601 particles, 2% period 1 supermicron, 15% period 1 oxalate-containing supermicron). This once again highlights the large enrichment of oxalate-and sulfate-containing particles on the BB and OC particle classes, this time on the supermicron particles, as the BB type is 3% of supermicron particles during period 1 and makes up 44% of oxalate-and sulfate-containing supermicron particles. The OC type is 1% of period 1 supermicron particles and makes up 35% of oxalate-and sulfate-containing supermicron particles. Figure 6.4b (top left) shows that composition of the submicron particles during period 2 showed less variations than event 1 (6000 particles), with the majority (>60%) collectively coming from the BB and dust particle classes. Oxalate-containing submicron particles during period 2 largely consist of BB (60%), followed by dust (25%), and OC (14%) (Figure 6.4b, top middle) (2863 particles, 48% period 2 submicron). 2nd period oxalate- and sulfate-containing submicron particles (Figure 6.4b, top right) (1948 particles, 32% period 2 submicron, 68% period 2 oxalate-containing submicron) are mainly BB (79%) and OC (14%); highlighting the enrichment of oxalate-and sulfate-containing submicron particles on the BB particle class, as the BB class is 48% of period 2 submicron particles and makes up 79% of oxalate-and sulfate-containing submicron particles. Supermicron particles (24,730 particles) show more compositional variations than the period 2 submicron particles and supermicron particles in period 1; and consist mainly of fresh (39%) and aged sea salt (26%) (Figure 6.4b, bottom left). Oxalate-containing event 2 supermicron

particles (Figure 6.4b, bottom middle) (794 particles, 3% period 2 supermicron) are varied and consist of BB (27%), followed by OC (25%) and dust (23%). Oxalate- and sulfate-containing period 2 supermicron particles (Figure 6.4b, bottom right) (435 particles, 2% period 2 supermicron, 55% oxalate-containing supermicron) are largely BB (44%) and OC (34%), highlighting the enrichment of oxalate-and sulfate-containing particles on the BB and OC particle classes during period 2, as the BB type is 9% of supermicron particles and makes up 44% of oxalate-and sulfate-containing supermicron particles. The OC type is 12% of total supermicron particles and makes up 34% of oxalate-and sulfate-containing supermicron particles.

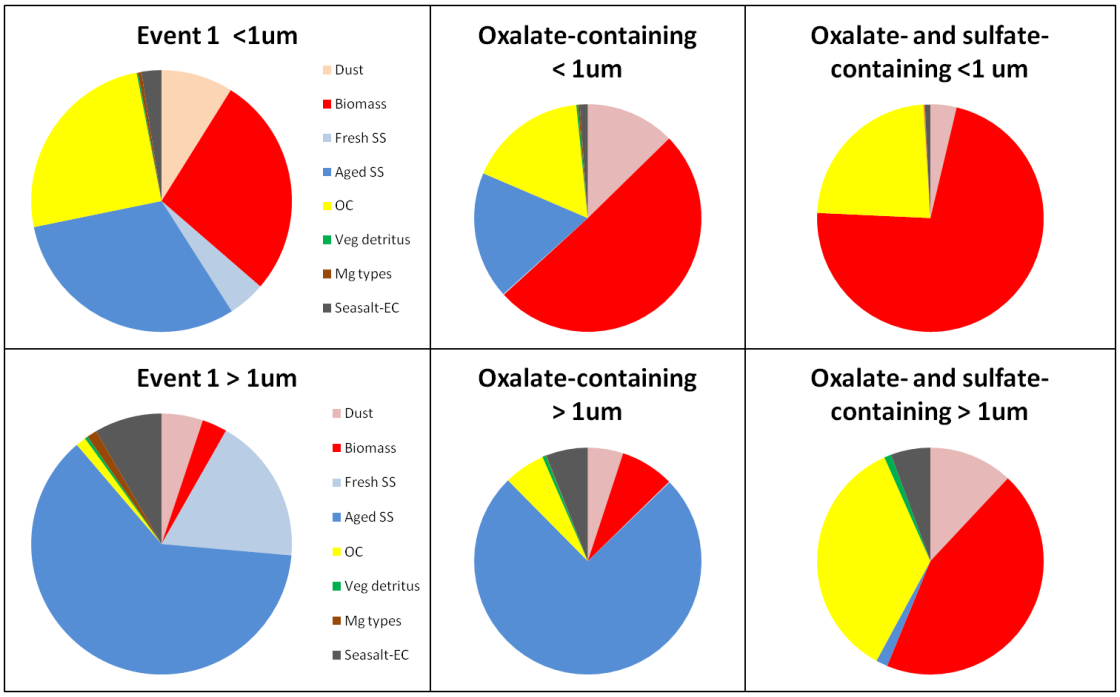

Figure 6.4a. Particle class fractions of submicron total particles (top left), oxalate-containing particles (top center), oxalate and sulfate containing particles (top right) during the 1st period on April 11-12th . Particle class fractions of supermicron total particles (bottom left), oxalate-containing particles (bottom center), oxalate and sulfate containing particles (bottom right) during the 1st period on April 11-12th.

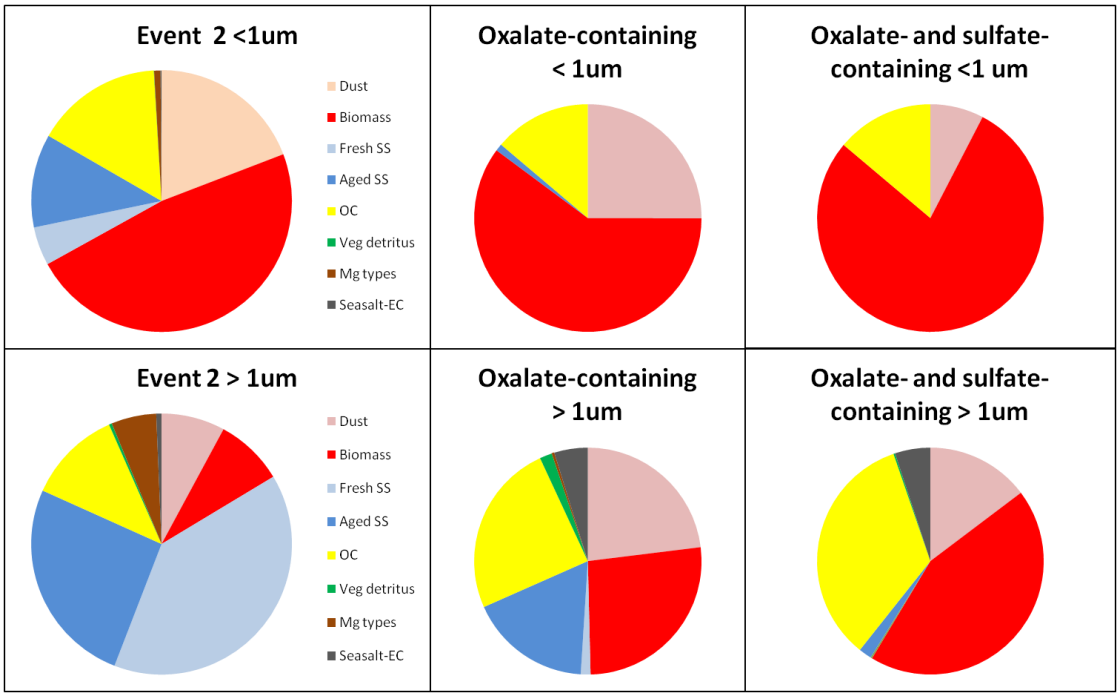

Figure 6.4b. Particle class fractions of submicron total particles (top left), oxalate-containing particles (top center), oxalate and sulfate containing particles (top right) during the 2nd period on April 13th. Particle class fractions of supermicron total particles (bottom left), oxalate-containing particles (bottom center), oxalate and sulfate containing particles (bottom right) during the 2nd period on April 13th.

Figure 6.4c (top left) shows a varied composition of the submicron particles during the entire study with large contributions of fresh and aged sea salt (43,414 particles), with the majority (>80%) collectively coming from the BB, OC, and fresh and aged sea salt particle classes. Oxalate-containing submicron particles (Figure 6.4c, top middle) (9659 particles, 22% total submicron) largely consist of BB (61%), followed by dust (19%), OC (12%), and aged sea salt (12%). Oxalate- and sulfate-containing submicron particles (Figure 6.4c, top right) (6300 particles, 15% total submicron, 65% oxalate-containing submicron) are mainly BB (80%) and OC (13%). This highlights the large enrichment of oxalate-and sulfate-containing submicron particles on the BB particle class, as the biomass burning class is only 29% of total submicron particles and makes up 80% of oxalate-and sulfate-containing submicron particles.

Supermicron particles (427,487 particles) are less varied in composition than the submicron particles, and consist mainly of fresh (47%) and aged sea salt (32%) (Figure 6.4c, bottom left). Oxalate-containing supermicron particles (Figure 6.4c, bottom middle) (13,054 particles, 3% supermicron) are largely aged sea salt (52%), followed by BB (13%), dust (13%), and OC (11%). Oxalate- and sulfate-containing supermicron particles (Figure 6.4c, bottom right) (3372 particles, 1% supermicron, 26% oxalate-containing supermicron) are largely BB (42%) and OC (36%).This once again highlights the large enrichment of oxalate-and sulfate-containing particles on the BB and OC particle classes, this time on the supermicron, as the BB type is 5% of supermicron particles and makes up 42% of oxalate-and sulfate-containing supermicron particles. The OC type is 4% of total supermicron particles and makes up 36% of oxalate-and sulfate-containing supermicron particles. For oxalate-containing particles that also contain sulfate, there is a large enrichment on the BB and OC particle classes for both the sub- and supermicron. This enrichment is especially noticeable in the supermicron as the majority of supermicron particles were sea salt, but the majority of supermicron oxalate- and sulfate-containing particles were BB and OC.

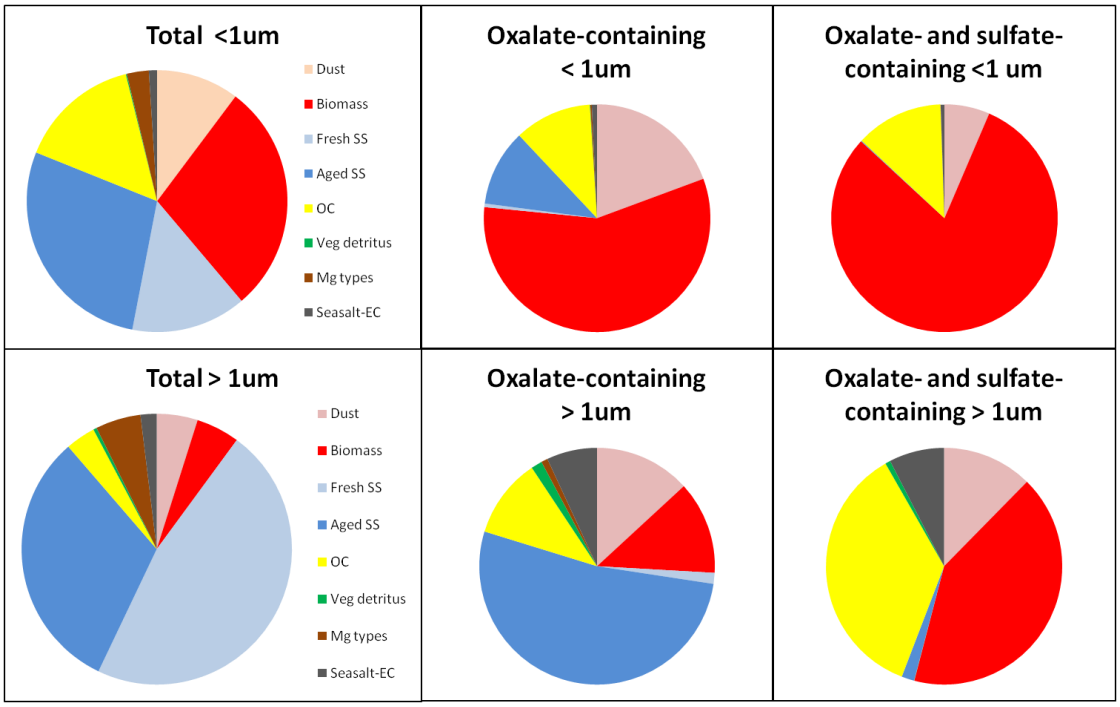

Figure 6.4c. Particle class fractions of submicron total particles (top left), oxalate-containing particles (top center), oxalate and sulfate containing particles (top right) for the whole study. Particle class fractions of supermicron total particles (bottom left), oxalate-containing particles (bottom center), oxalate and sulfate containing particles (bottom right) for the whole study.

For oxalate-containing particles that also contain sulfate during period 1, there is a large enrichment on the BB and OC particle classes for both the sub- and supermicron. This enrichment is especially noticeable in the supermicron as the majority of supermicron particles were largely aged SS, but the majority of supermicron oxalate- and sulfate-containing particles were BB and OC. Again during period 2, for oxalate-containing particles that also contain sulfate, there is a large enrichment on the BB and OC particle classes for both the sub- and supermicron. Interestingly, for oxalate-containing particles, there is enrichment on the aged SS particle type, especially in the supermicron during period 1, but not during period 2, which shows enrichment in OC, BB and dust instead. In summary, there are two separate oxalate-containing events that occur at different times; period 1 is dominated by supermicron aged SS (Figs 6.1, 6.2, 6.4a) while period 2 is dominated by an oxalate source predominantly

submicron in nature that is strongly associated with sulfate on the BB and OC particle types (Figs 6.1, 6.2, 6.3,6.4b).

6.4.2 Temporal chemistry of oxalate

The relationship between oxalate-containing particle counts and oxalate-and sulfate-containing particle counts for both submicron and supermicron particles are shown in Figure 6.5. If the oxalate was formed via in-cloud processing, then it should correlate with sulfate and the other aqueous processing markers. The strong correlation of submicron oxalate-containing particles, largely found on BB and OC particles (74% period 2) during period 2, with submicron oxalate-and sulfate-containing particles (R^2=0.98) indicates that the source of oxalate in the submicron particles is the same as the sulfate, and most likely from cloud processing (Figure 6.5, top). Additionally, there are strong correlations between sulfate-containing submicron with oxalate-containing submicron particles (R^2=0.90) and oxalate and sulfate-containing submicron (R^2=0.92) (Figure 6.5 top, color). Supermicron oxalate, predominantly found on aged sea salt (75%, period 1) during period 1, has a much lower correlation with oxalate-and sulfate-containing particles (R^2=0.40), suggesting that supermicron oxalate and sulfate are mostly from different sources, therefore most likely not in-cloud processing (Figure 6.5, bottom). Additionally, there are correlations between sulfate-containing submicron with oxalate-containing submicron particles (R^2=0.26) and oxalate and sulfate-containing submicron (R^2=0.77) (Figure 6.5 top, color). The very strong correlations ($R^2 \geq 0.90$) between submicron oxalate, sulfate, and oxalate-and-sulfate containing particle counts suggest a similar source of sulfate and oxalate, most likely in-cloud processing, implying similar sources of SO_2 and oxalate precursors such as glyoxylate, acetate, glycolate, or pyruvate. The low correlation between supermicron oxalate-containing and sulfate-containing particle counts (R^2=0.26) implies a lack of similar source of the oxalate and sulfate.

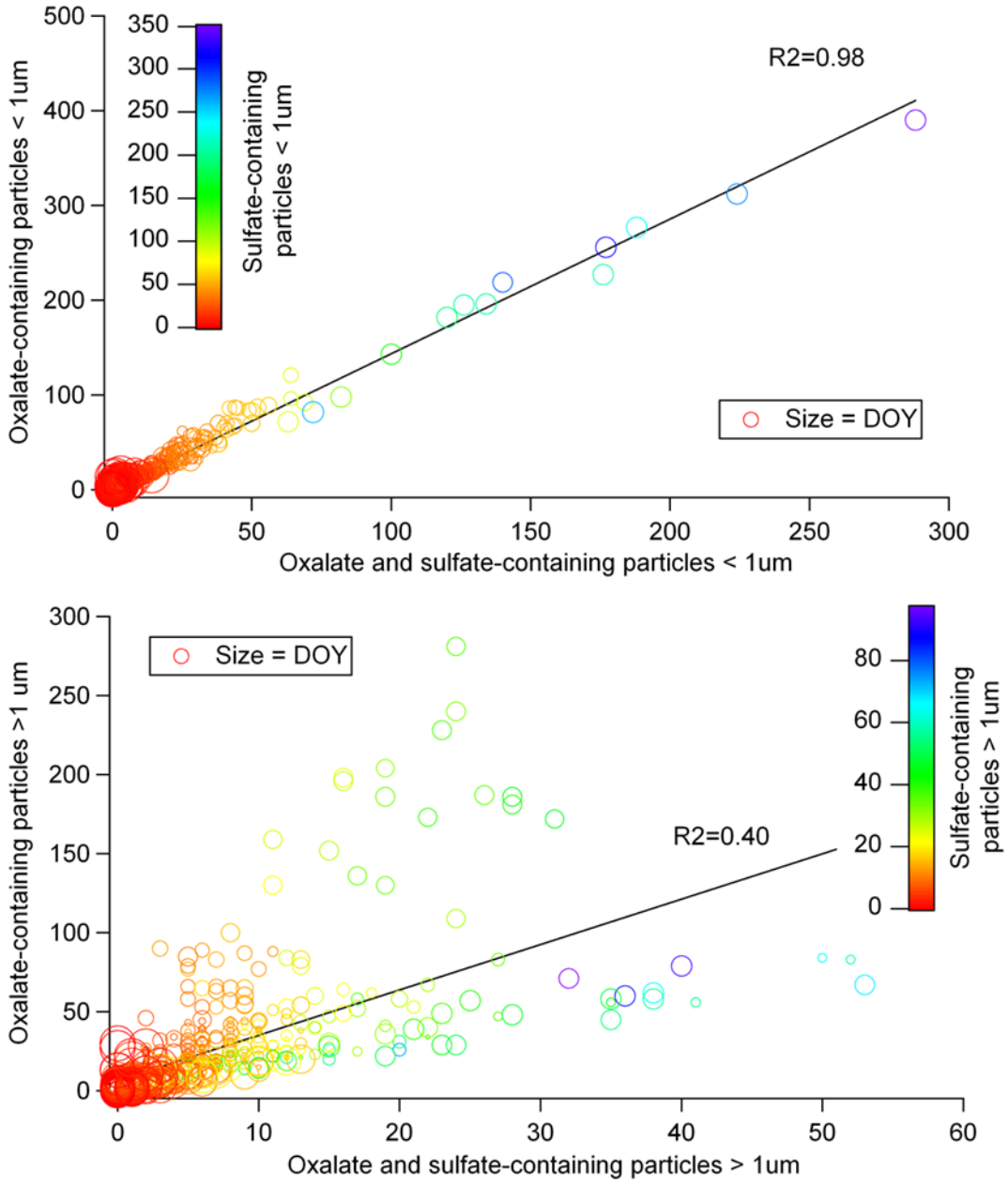

Figure 6.5. Oxalate-containing particle counts vs. oxalate- and sulfate-containing particle counts for submicron (top) and supermicron (bottom). Color of markers is sulfate-containing particle counts and marker size is day of year (DOY).

To further understand the temporal correlations of oxalate, peak areas of oxalate and other chemical markers on the different particle types of interest may lend significant insight into the sources of oxalate. Figure 6.6 shows the temporal behavior of hourly-averaged nitrate

and oxalate peak areas on the aged SS. There is a distinct diurnal pattern of both the oxalate and nitrate, with a correlation of R^2=0.24. The similar diurnal behavior of the oxalate and nitrate on the aged SS particle type shows that both the oxalate and nitrate could be from the same source, most likely photochemical due to the diurnal pattern [*Kawamura and Yasui*, 2005; *Sullivan and Prather*, 2007].

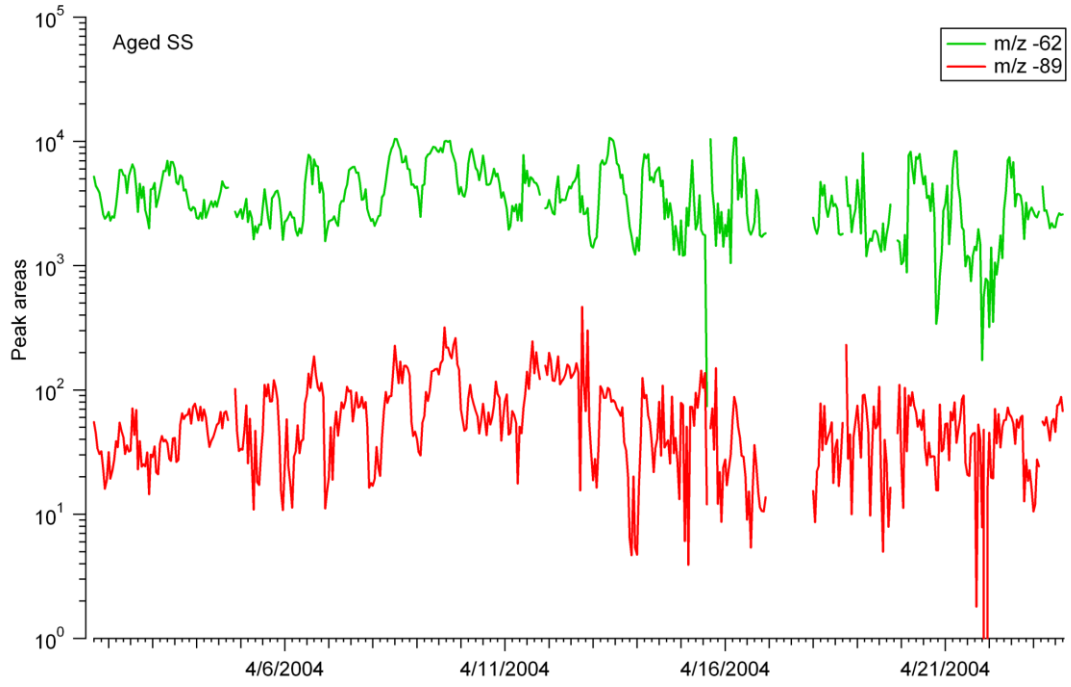

Figure 6.6. Hourly-averaged peak areas of nitrate (m/z -62) and oxalate (m/z -89) on the aged SS particle type for the entire study.

Figure 6.7 shows the temporal behavior of hourly-averaged correlations of oxalate (m/z -89) with sulfate (m/z -97) and cloud or aqueous processing markers glyoxylate (m/z -57), acetate (m/z -59), glycolate (m/z -75), pyruvate (m/z -87), and hydroxymethane sulfonate (m/z -111) [*Sullivan and Prather*, 2007; *Whiteaker and Prather*, 2003] for both the BB and

OC. BB temporal correlations with sulfate (R^2=0.34) and cloud markers (R^2=0.49-0.83) strongly suggest a cloud/aqueous processing source. OC temporal correlations of oxalate with sulfate (R^2=0.34) and aqueous processing markers (R^2=0.54-0.73) also indicate a cloud or aqueous processing source. In addition to correlations between oxalate- and sulfate-containing particle counts demonstrating the key differences between the two distinct oxalate periods; the temporal behavior of oxalate on the main oxalate-containing particle types supports similar findings. Temporal behavior of oxalate on supermicron aged SS showed a diurnal trend and was very similar to that of photochemical marker nitrate. There are also strong correlations between oxalate, sulfate, and cloud or aqueous processing markers on the BB and OC particle types.

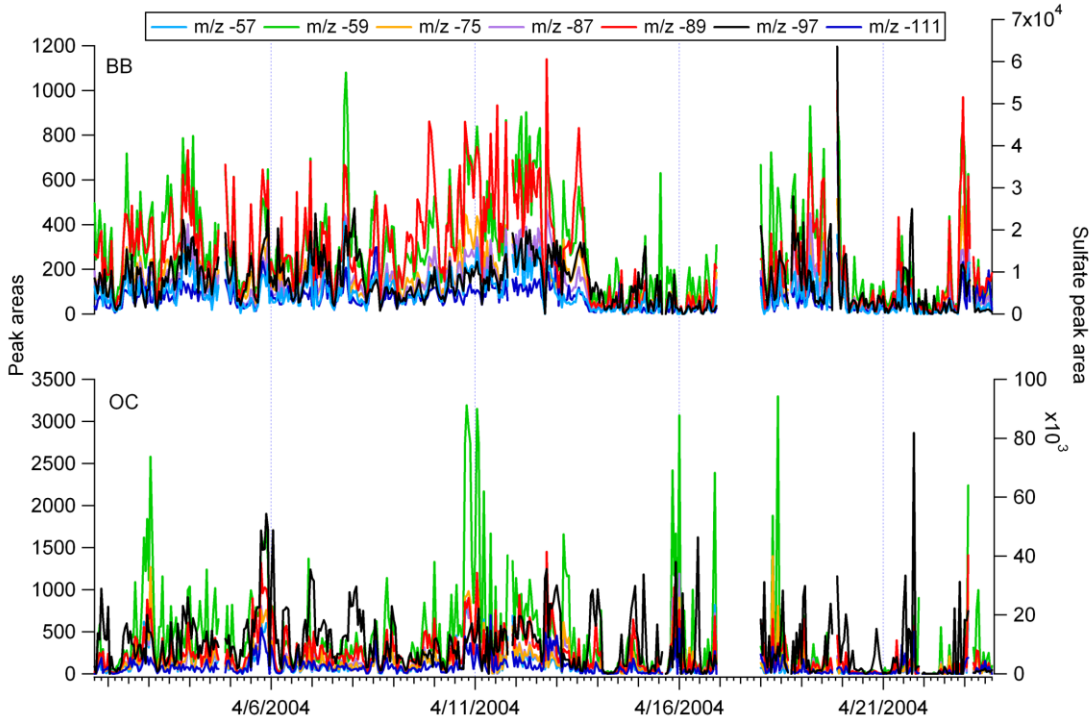

Figure 6.7. Hourly-averaged peak areas of oxalate (m/z -89), sulfate (m/z -97) and cloud or aqueous processing markers glyoxylate (m/z -57), acetate (m/z -59), glycolate (m/z -75), pyruvate (m/z -87), and hydroxymethane sulfonate (m/z -111) on the BB (top) and OC (bottom) particle types for the entire study.

6.4.3 Size-resolved chemistry of oxalate

It has been previously shown that if in-cloud processing has occurred, oxalate and sulfate will have similar size-resolved chemistry [*Crahan et al.*, 2004; *Sorooshian et al.*, 2006; *Yu et al.*, 2005]. Therefore, similarities between the size-resolved chemistry of oxalate and sulfate could indicate a similar in-cloud processing source. Figure 6.8 shows the size-resolved ATOFMS peak areas of oxalate (m/z -89), sulfate (m/z -97) and cloud or aqueous processing markers glyoxylate (m/z -57), acetate (m/z -59), glycolate (m/z -75), pyruvate (m/z -87), and hydroxymethane sulfonate (m/z -111) on the BB (top) and OC (bottom) particle types during period 2. Both the BB and OC particle classes have nearly identical size-resolved chemistry of oxalate and sulfate (R^2=0.71 BB, R^2=0.64 OC), peaking in the submicron mode. Additional size-resolved chemistry of oxalate and aqueous processing markers glyoxylate (R^2=0.25 BB, R^2=0.39 OC), acetate (R^2=0.47 BB, R^2=0.50 OC), glycolate (R^2 =0.60 BB, R^2=0.60 OC), pyruvate (R^2=0.42 BB, R^2=0.60 OC), and hydroxymethane sulfonate (R^2=0.008 BB, R^2=0.49 OC) indicate that the oxalate on BB and OC particles is most likely from in-cloud processing. The correlations for BB and OC particle classes during non-oxalate periods (not shown) are similar to during period 2, with slightly worse correlations between oxalate and sulfate (R^2=0.61 BB, R^2=0.50 OC); and slightly better correlations between oxalate and aqueous processing markers glyoxylate (R^2=0.77 BB, R^2=0.38 OC), acetate (R^2=0.77 BB, R^2=0.55 OC), glycolate (R^2 =0.81 BB, R^2=0.72 OC), pyruvate (R^2=0.87 BB, R^2=0.59 OC), and hydroxymethane sulfonate (R^2=0.65 BB, R^2=0.71 OC) indicating that in-cloud processing could have also been the source of the oxalate outside of period 2 as well.

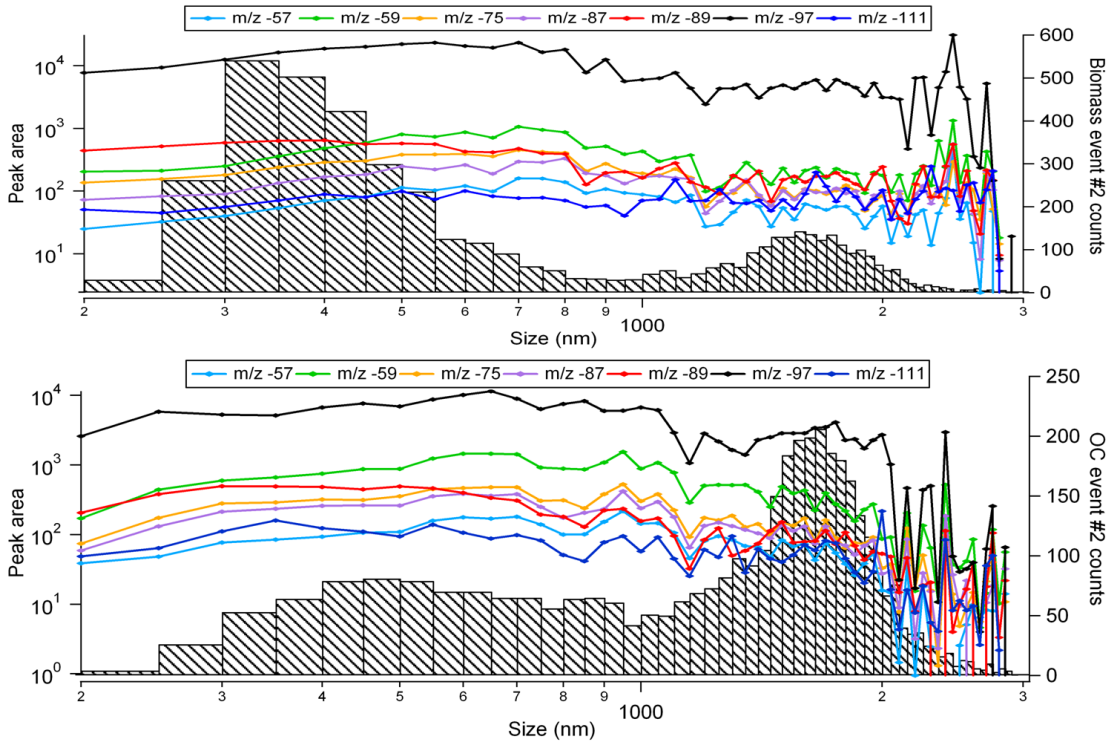

Figure 6.8. Size-resolved peak areas of oxalate (m/z -89), sulfate (m/z -97) and cloud or aqueous processing markers glyoxylate (m/z -57), acetate (m/z -59), glycolate (m/z -75), pyruvate (m/z -87), and hydroxymethane sulfonate (m/z -111) on the BB (top) and OC (bottom) particle types during period 2.

6.4.4 Air mass back trajectories

Airborne measurements during CIFEX showed an influence from long-range transport from Asia, clean marine boundary layer, and North American emissions [*Roberts et al.*, 2006]. The air mass back trajectory during the 1st and 2nd oxalate periods was from the north, along the coast and over Oregon and Washington (Figure 6.9). Flights during these days indicated the influence of cloud processed aerosol only, no long range transport [*Roberts et al.*, 2006]. Ground-based air masses were passing close to 3000 m (Figure 6.9); indicating possible infiltration of the boundary layer and clouds. As both period 1 and period 2 had similar air mass back trajectories, there must be other explanations for the differences in these events. Because the air masses could have infiltrated the boundary layer and clouds, and there are

high correlations between oxalate and sulfate; in-cloud processing as the main source of oxalate on the BB and OC particles is highly probable during period 2 [*Yang et al.*, 2009]. The diurnal behavior of the oxalate, similar to photochemical marker nitrate in addition to the low correlation with sulfate suggests a regional or local photochemical source of the oxalate, most likely due to heterogeneous reactions, as nitrate on sea salt is usually an indication that a heterogeneous reaction has taken place [*Sullivan and Prather*, 2007].

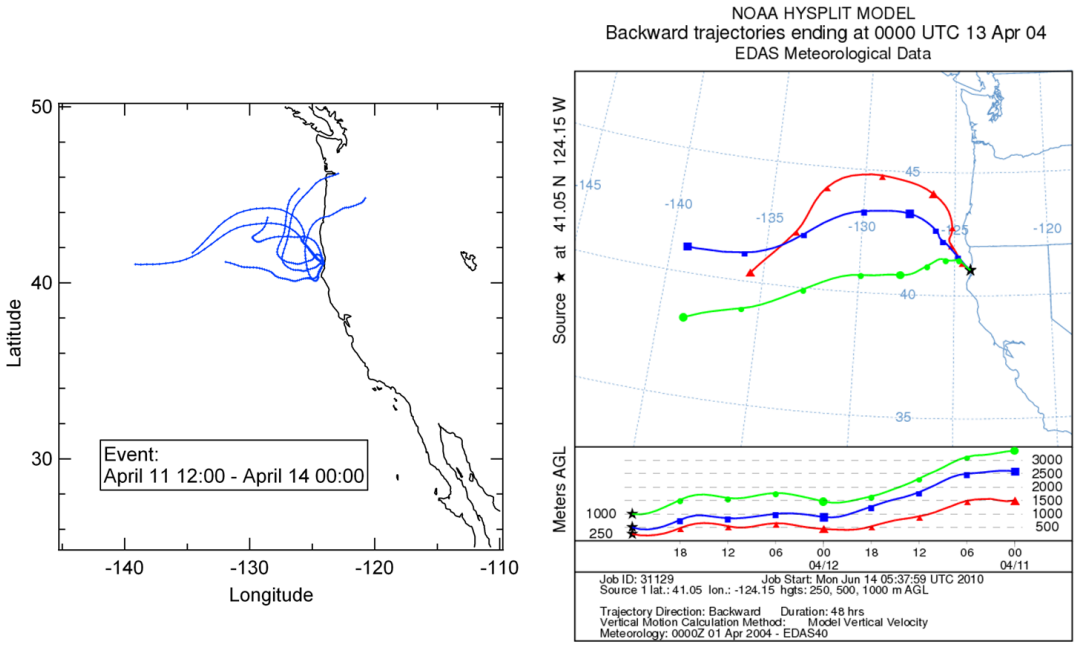

Figure 6.9. HYPLIT back trajectories during the April 11 – 13 event (left). Each trajectory is at 500 m for 48 hours. One particular back trajectory is highlighted (upper right) showing the time lapsed altitude of the 250, 500, and 1000 m back trajectories (bottom right).

6.5 Atmospheric Implications

During CIFEX, the mixing state of oxalate-containing particles was measured at a remote marine environment by direct ground-based measurements using an ATOFMS single-particle mass spectrometer. Oxalate was frequently detected in single particle spectra with

22% of submicron and 3% of supermicron particles containing oxalate. There were two distinct oxalate events; during the 1st period, supermicron oxalate was predominantly mixed with the aged sea salt particle class, while during the 2nd period oxalate was found to be internally mixed with sulfate in the submicron size range, and found mainly on the biomass burning and organic carbon particle classes. Enrichment of oxalate on the aged sea salt type during the 1st period and similar diurnal behavior of nitrate and oxalate on the aged sea salt particle type indicate a photochemical source of oxalate for this period. During the 2nd period the preferential enrichment of oxalate and sulfate on biomass burning and carbonaceous particles, and correlations between oxalate and other cloud or aqueous markers on these particle types, both temporally and size-resolved, suggests an in-cloud processing source of oxalate for this period. Evidence of air masses possibly infiltrating the boundary layer and clouds, further supports in-cloud processing as the main source of oxalate on the BB and OC during period 2.

While it can be very difficult to distinguish between the sources of oxalate, particles that undergo long-range transport most likely undergo in-cloud or aqueous processing. However, the extent to which the in-cloud processing contributes to particulate oxalate, which strongly depends on the original particle hygroscopicity, and other sources of oxalate, is still not well understood. Further investigation is needed to determine the factors that control the main oxalate production mechanisms in different environments. Better understanding of the production of oxalate in the condensed phase via in-cloud processing has important implications for understanding the mechanism of a major source of secondary organic aerosols (SOA). Oxalic acid is a very soluble organic acid that can changes the ability of a particle to act as CCN, thereby affecting particle lifetime, aerosol-cloud interactions, and radiative forcing, and thus understanding its sources and partitioning in the atmosphere is important to provide insight into the mechanisms involved.

6.6 Acknowledgments

The authors are grateful to John Holecek (UCSD) for his help with data collection and analysis. We acknowledge Elizabeth Fitzgerald (UCSD) for editing this paper. The authors thank the National Oceanic and Atmospheric Administration (NOAA), grant NOAA/NA17RJ1231, and V. Ramanathan for the support of this research. We would like to thank NOAA for the use of their HYSPLIT back trajectory program.

Publication acknowledgment

The contents of Chapter 6 are part of a manuscript in preparation, Moore, M.J.K., Spencer, M.T., Prather, K.A., Evidence for two distinct sources of oxalate during the Cloud Indirect Forcing Experiment (CIFEX), to be submitted to Environmental Science and Technology. The dissertation author was the primary investigator and author of this paper.

6.7 References

Chang, R.Y.-W., P.S.K. Liu, W.R. Leaitch, and J.P.D. Abbatt, Comparison between measured and predicted CCN concentrations at Egbert, Ontario: Focus on the organic aerosol fraction at a semi-rural site, *Atmospheric Environment, 41*, 8172-8182, 2007.

Crahan, K.K., D. Hegg, D.S. Covert, and H. Jonsson, An exploration of aqueous oxalic acid production in the coastal marine atmosphere, *Atmospheric Environment*, *38*, 3757-3764, 2004.

Ervens, B., G. Feingold, S.L. Clegg, and S.M. Kreidenweis, A modeling study of aqueous production of dicarboxylic acids: 2. Implications for cloud microphysics, *Journal of Geophysical Research*, *109* (D15206), doi:10.1029/2004JD004575, 2004a.

Ervens, B., G. Feingold, G.J. Frost, and S.M. Kreidenweis, A modeling study of aqueous production of dicarboxylic acids: 1. Chemical pathways and speciated organic mass production, *Journal of Geophysical Research*, *109* (D15205), doi:10.1029/2003JD004387, 2004b.

Falkovich, A.H., E.R. Graber, G. Schkolnik, Y. Rudich, W. Maenhaut, and P. Artaxo, Low molecular weight organic acids in aerosol particles from Rondonia, Brazil, during the biomass-burning, transition and wet periods, *Atmospheric Chemistry and Physics*, *5*, 781-797, 2005.

Furukawa, T., and S. Takahashi, Metal complexation inhibits the effect of oxalic acid in aerosols as cloud condensation nuclei, *Atmospheric Chemistry and Physics Discussions*, *10*, 27099-27134, 2010.

Furutani, H.F., M. Dall'osto, G.C. Roberts, and K.A. Prather, Assessment of the relative importance of atmospheric aging on CCN activity derived from field observations, *Atmospheric Environment*, *42*, 3130-3142, 2008.

Gard, E., J.E. Mayer, B.D. Morrical, T. Dienes, D.P. Fergenson, and K.A. Prather, Real-Time Analysis of Individual Atmospheric Aerosol Particles: Design and Performance of a Portable ATOFMS, *Analytical Chemistry*, *69*, 4083-4091, 1997.

Guazzotti, S.A., D.T. Suess, K.R. Coffee, P.K. Quinn, T.S. Bates, A. Wisthaler, A. Hansel, W.P. Ball, R.R. Dickerson, C. Neususess, P.J. Crutzen, and K.A. Prather, Characterization of carbonaceous aerosols outflow from India and Arabia: Biomass/biofuel burning and fossil fuel combustion, *Journal of Geophysical Research*, *108* (D15), 4485, doi:10.1029/2002JD003277, 2003.

Hara, K., K. Osada, K. Matsunaga, T. Sakai, Y. Iwasaka, and K. Furuya, Concentration trends and mixing states of particulate oxalate in Artic boundary layer in winter/spring, *Journal of Geophysical Research*, *107* (D19), 4399, doi:10.1029/2001JD001584, 2002.

Holecek, J.C., M.T. Spencer, and K.A. Prather, Analysis of rainwater samples: Comparison of single particle residues with ambient particle chemistry from the northeast Pacific and Indian oceans, *Journal of Geophysical Research*, *112* (D22S24), doi:10.1029/2006JD008269, 2007.

Kawamura, K., and O. Yasui, Diurnal changes in the distribution of dicarboxylic acids, ketocarboxylic acids and dicarbonyls in the urban Tokyo atmosphere, *Atmospheric Environment*, *39*, 1945-1960, 2005.

Kundu, S., K. Kawamura, T.W. Andreae, A. Hoffer, and M.O. Andreae, Molecular distribution of dicarboxylic acids, ketocarboxylic acids and alpha-dicarbonyls in biomass burning aerosols: implications for photochemical production and degradation in smoke layers, *Atmospheric Chemistry and Physics*, *10*, 2209-2225, 2010.

Mircea, M., M.C. Facchini, S. Decesari, F. Cavalli, L. Emblico, S. Fuzzi, A. Vestin, J. Rissler, E. Swietlicki, G. Frank, M.O. Andreae, W. Maenhaut, Y. Rudich, and P. Artaxo, Importance of the organic aerosol fraction for modeling aerosol hygroscopic growth and activation: a case study in the Amazon Basin, *Atmospheric Chemistry and Physics*, *5*, 3111-3126, 2005.

Moffet, R.C., B. De Foy, L.T. Molina, M.J. Molina, and K.A. Prather, Measurement of ambient aerosols in northern Mexico City by single particle mass spectrometry, *Atmospheric Chemistry and Physics*, *8*, 4499-4516, 2008.

Narukawa, M., K. Kawamura, K. Okada, Y. Zaizen, and Y. Makino, Aircraft measurement of dicarboxylic acids in the free tropospheric aerosols over the western to central North Pacific, *Tellus*, *55B*, 777-786, 2003.

Qin, X., and K.A. Prather, Impact of biomass emissions on particle chemistry during the California Regional Particulate Air Quality Study, *International Journal of Mass Spectrometry*, *258*, 142-150, 2006.

Rebotier, T.P., and K.A. Prather, Aerosol time-of-flight mass spectrometry data analysis: A benchmark of clustering algorithms., *Analytica Chimica Acta*, *585* (1), 38-54, 2007.

Rissler, J., E. Swietlicki, J. Zhou, G. Roberts, M.O. Andreae, L.V. Gatti, and P. Artaxo, Physical properties of the sub-micrometer aerosol over the Amazon rain forest during the wet-to-dry season transition- comparison of modeled and measured CCN concentrations, *Atmospheric Chemistry and Physics*, *4*, 2119-2143, 2004.

Roberts, G., G. Mauger, O. Hadley, and V. Ramanathan, North American and Asian aerosols over the eastern Pacific Ocean and their role in regulating cloud condensation nuclei, *Journal of Geophysical Research*, *111* (D13205), doi:10.1029/2005JD006661, 2006.

Roberts, G.C., P. Artaxo, J. Zhou, E. Swietlicki, and M.O. Andreae, Sensitivity of CCN spectra on chemical and physical properties of aerosol: A case study from the Amazon Basin, *Journal of Geophysical Research*, *107* (D20), 8070, doi:10.1029/2001JD000583, 2002.

Saarikoski, S., M. Sillanpaa, M. Sofiev, H. Timonen, K. Saarnio, K. Teinila, A. Karppinen, J. Kukkonen, and R. Hillamo, Chemical composition of aerosols during a major biomass burning episode over northern Europe in spring 2006: Experimental and modelling assessments, *Atmospheric Environment*, *41*, 3577-3589, 2007.

Silva, P.J., D. Liu, C.A. Noble, and K.A. Prather, Size and Chemical Characterization of Individual Particles Resulting from Biomass Burning of Local Southern California Species, *Environmental Science and Technology*, *33* (18), 3068-3076, 1999.

Song, X.-H., and P.K. Hopke, Classification of Single Particles Analyzed by ATOFMS Using an Artificial Neural Network, ART-2A, *Analytical Chemistry*, *71* (4), 860-865, 1999.

Sorooshian, A., V. Varutbangkul, F.J. Brechtel, B. Ervens, G. Feingold, R. Bahreini, S.M. Murphy, J.S. Holloway, E.L. Atlas, G. Buzorius, H. Jonsson, R.C. Flagan, and J.H. Seinfeld, Oxalic acid in clear and cloudy atmospheres: Analysis of data from International Consortium for Atmospheric Research on Transport and Transformation 2004, *Journal of Geophysical Research*, *111* (D23S45), doi:10.1029/2005JD006880, 2006.

Spencer, M.T., J.C. Holecek, C.E. Corrigan, V. Ramanathan, and K.A. Prather, Size-resolved chemical composition of aerosol particles during a monsoonal transition period over the Indian Ocean, *Journal of Geophysical Research*, *113* (D16305), doi:10.1029/2007JD008657, 2008.

Sullivan, R.C., S.A. Guazzotti, D.A. Sodeman, and K.A. Prather, Direct observations of the atmospheric processing of Asian mineral dust, *Atmospheric Chemistry and Physics*, *7* (5), 1213-1236, 2007.

Sullivan, R.C., M.J.K. Moore, M.D. Petters, S.M. Kreidenweis, G.C. Roberts, and K.A. Prather, Effect of chemical mixing state on hygroscopicity and cloud nucleation properties of calcium mineral dust particles, *Atmospheric Chemistry and Physics*, *9*, 3303-3316, 2009.

Sullivan, R.C., and K.A. Prather, Investigations of the Diurnal Cycle and Mixing State of Oxalic Acid in Individual Particles in Asian Aerosol Outflow, *Environmental Science and Technology*, *41*, 8062-8069, 2007.

Turekian, V.C., S. Macko, and W.C. Keene, Concentrations, isotopic compositions, and sources of size-resolved, particulate organic carbon and oxalate in near-surface marine air at Bermuda during spring, *Journal of Geophysical Research*, *108* (D5), 4157, 2003.

Warneck, P., In-cloud chemistry opens pathway to the formation of oxalic acid in the marine atmosphere, *Atmospheric Environment*, *37*, 2423-2427, 2003.

Whiteaker, J.R., and K.A. Prather, Hydroxymethanesulfonate as a tracer for fog processing of individual aerosol particles, *Atmospheric Environment*, *37*, 1033-1043, 2003.

Yang, F., H. Chen, X. Wang, X. Yang, J. Du, and J. Chen, Single particle mass spectrometry of oxalic acid in ambient aerosols in Shanghai: Mixings state and formation mechanism, *Atmospheric Environment*, *43* (3876-3882), 2009.

Yu, J.Z., X.-F. Huang, J. Xu, and M. Hu, When Aerosol Sulfate Goes Up, So Does Oxalate: Implication for the Formation Mechanisms of Oxalate, *Environmental Science and Technology*, *39*, 128-133, 2005.

Yu, S., Role of organic acids (formic, acetic, pyruvic and oxalic) in the formation of cloud condensation nuclei (CCN): a review, *Atmospheric Research*, *53*, 185-217, 2000.

Chapter 7

Conclusions

7.1 Synopsis

The research in this dissertation focuses on the chemistry of atmospheric aerosol particles, relating how chemistry impacts cloud properties. Chapter 2 describes the effect of organics on the CCN activity of sea spray aerosols. Chapter 3 compares the particle mixing state, CCN activity and estimated hygroscopicity of particles produced during the wildfire events in San Diego County in 2007 and 2008. Chapter 4 investigates particle mixing state and estimates the hygroscopicity of mineral dust at Owens Lake. Chapters 5 & 6 explore particle mixing state, optical properties, and estimated hygroscopicity during the Cloud Indirect Forcing Experiment (CIFEX).

7.2 Conclusions

7.2.1 Sea spray aerosol conclusions

The effect of organics on the CCN activity of sea spray aerosol produced by bubbling artificial seawater (ASW) and NaCl solutions was investigated. The organic materials range from simplistic model systems to more complex mixtures produced by representative marine microorganisms. Mixtures of aqueous NaCl with a single surface-active organic, oleic acid or sodium dodecyl sulfate, in solution showed a small increase in CCN activity by a decrease in activation diameter. However, no significant shift in CCN activity was observed for sea spray aerosols produced from ASW-complex organic solutions produced by biological activity

from microorganisms *Synechococcus* and *Ostreococcus*. These observations suggest the formation of a neat film could occur on the top layer of the seawater when using the pure surfactants, causing a decrease in surface tension and therefore causing the increase in CCN activity observed. For the more complex organic mixtures, the microorganisms most likely produced many different types of organic species with a broad range of properties. While there was a large fraction of carbon in the particles (~27%) for this case, there was no net change in CCN activity. This was due to the decreased surface tension of the particle being offset by the decrease in solute from the displaced salt [*Asa-Awuku et al.*, 2009; *Asa-Awuku et al.*, 2007; *Asa-Awuku et al.*, 2010]. These findings indicate that organic matter from primary production in the ocean, when incorporated into sea spray aerosol particles, can cause a change in sea salt aerosol CCN activity. However, this is strongly dependent on the type and complex mixture of the organic compounds. These changes in CCN activity for both the NaCl and ASW experiments mixed with surfactants and microorganisms account for < 3% of a change in CCN number concentrations over the remote marine boundary layer and did not result in a change in the size distributions of particles produced. This shows that under "bloom" conditions, changes in CCN concentrations due to chemical changes from inclusion of marine biological organic material from these two specific microorganisms would have a negligible effect on cloud formation from their resulting sea spray aerosol. These experiments cannot comprehensively address the role of organics from other microorganisms for the entire SSA. Another recent study showed a decrease in CCN activity of sea spray aerosol due to organics produced by 4 different microorganisms, highlighting the importance of the particular type of microorganism and biological activity in the ocean on the CCN activity[*Fuentes et al.*, 2010]. While primary production from the ocean may add significant amounts of organic material to sea spray aerosols, this study shows how, as least for the specific microorganisms investigated, the net effect on CCN activity is relatively small. This can most likely be

accounted for by the existing large fraction of water-soluble salts having the largest effect on CCN activation.

7.2.2 Biomass burning aerosol conclusions

Aerosol size and composition were measured in real-time and particle hygroscopicity estimated from CCN measurements during the 2007 and 2008 wildfire events in San Diego. The contribution of wildfire emissions were much larger and played a more significant role in affecting CCN and CN concentrations in 2007 than in 2008. During both of these studies, chemical measurements showed that biomass burning was the dominant particle type for sizes 100-300 nm. Particle size distributions indicate that 2007 was dominated by biomass burning emissions with size modes (~125-190 nm), while in 2008 emissions were dominated by local pollution sources with much smaller particle size modes (~35-95 nm). Hygroscopicity parameter κ ranges were 0.018-0.089 in 2007 and 0.01-0.2 in 2008. The overall particle hygroscopicity (κ) during the BBA dominant periods (periods 1-3 in 2007; period 1 in 2008) was very similar (~0.04), however in 2008, the particle hygroscopicity was dominated by local sources rather than biomass burning, due to the much smaller particle size mode. In 2007, the two main BBA types were BB nitr-sulf and BB sulf-nitr; while in 2008 BB sulf-nitr and Aged BB were the main types. Even though the BBA chemical signatures were different between the years, they had similar hygroscopicities. However, due to the larger sizes and soluble material on the BBA, they were mostly CCN active. Hygroscopicity parameter values were within previously measured values from various BBA sources (0.01-0.7), and close to that of soot-rich biomass (0.01), ponderosa pine (0.04) and fresh anthropogenic emissions (0.05). Activation diameters at 0.3% SS were 117 – 195 nm for 2007 and 90-235 nm in 2008. By varying the hygroscopicity parameter κ by ± 50% resulted in changes in CCN number concentrations within 15% for 2007, while in 2008 resulted in a <3% change in CCN number concentrations for the main biomass burning dominated

periods. The difference in CCN concentration changes in 2007 and 2008 reflects the large differences in particle size distributions and biomass burning influence. The activation diameters in 2007 were around the main particle size mode (~100-200 nm), which was attributed to the large impact of biomass emissions that year. In 2008, the activation diameters were much larger (90-235 nm) than the particle size mode (~40-60 nm) and varying the hygroscopicity did not have as large an effect as most of the particles were too small to activate regardless. This reflects the much lower influence of larger-sized biomass burning and the much larger impact of the smaller-sized local emissions that year.

7.2.3 Mineral dust aerosol conclusions

Aerosol size and composition were measured in real-time and particle hygroscopicity was estimated from CCN measurements at Owens Lake in November of 2009, during two dust storm events. During both dust storm events, single particle chemistry showed a small shift in both sub- and supermicron particle types from a salt-like dust to an alumina-silicate type dust. The absence of the more salt-like dust during the dust events is because the salt-like dust is associated with the dry-lake bed only and the prevailing winds from the south transported it away from the sampling site. The first real-time ambient CCN measurements at Owens Lake show a median $\kappa_{0.1}$ value of 0.05 and a $\kappa_{0.9}$ value of 0.03. The activation diameters at 0.1%-0.7% SS were 129-300 nm for the whole study excluding dust events, 310 nm for the 1st dust event (0.08%SS static only) and 129-280 during the 2nd dust event. Hygroscopicity parameter κ ranges were 0.01 (0.7%SS) – 0.05 (0.1%SS) during the whole study excluding dust events and were similar to the 2nd dust event, 0.01 (0.7% SS) – 0.06 (0.1% SS). Changes in $\kappa \pm 50\%$ resulted in changes in CCN concentrations within <1% at 0.1% SS and < 7% SS during the entire study excluding dust events. Changes in $\kappa \pm 50\%$ during the 2nd dust event resulted in changes in CCN concentrations <2% at 0.1% SS and < 16% at 0.7 SS. The difference in CCN concentrations for the entire study excluding dust

events and the 2nd dust event reflects the large differences in the particle size distributions and influence of ultrafine and dust particles. During the non-dust events, there were strong influences of ultrafine particles that produced a large particle mode ~20 nm which was not present during the dust events. Changes in hygroscopicity during the non-dust event periods do not result in large changes in CCN concentrations, as the majority of the particles were ~20 nm and would not activate regardless of the supersaturation due to their small size. However, during the dust events, the main particle size mode is instead ~100 nm, closer to the activation diameter range, and therefore changes in hygroscopicity had a larger effect on CCN concentrations. Most of the dust particles observed during the events were ~ 100-4000 nm and the dust > 200 nm was observed to have soluble nitrate, chloride and sulfate. Therefore, a majority of the dust particles are large enough and would activate to become CCN (or GCCN). As most of the particles > 500 nm were dust and most CCN were > 500 nm at 0.1% S_c, the dust needs to be CCN active to explain the NCCN observed.

Soil and suspended dust samples collected from the lake and run offline show similar chemistry and hygroscopicity (κ ~0.04-0.8) to the field measurements, as well as previous to offline measurements (~0.05-1) [*Koehler et al.,* 2007]. Even though the different samples were observed to be heterogeneous and collected from various locations on the lake bed, the differences in particle chemistry and overall spread in κ values was moderate. No significant change within the uncertainty of the study in particle hygroscopicity or CCN activity occurred concurrently with the change in mixing of particle classes during both dust events, indicating that the large dust particles were completely CCN active; and the smaller, fresher particles, most of which are below the chemical detection limit, are dictating the hygroscopicity. While there were very high amounts of nitrate on just about every type of dust with no clear enhancement on any particle type or size range; we suggest that because the dust particles already have significant amounts of soluble species, and therefore the additional nitrate from

atmospheric processing would not significantly affect the hygroscopicity. Most of the dust particles are large enough and would activate to become CCN regardless of their hygroscopicity. Due to the large contribution of the large dust to CCN concentrations at low supersaturations during the dust events, the dust storms should enhance CCN and possibly ice nuclei (IN) in the regional clouds, however it remains to be seen how the dust affects the radiative properties of the clouds.

7.2.4 CIFEX measurements conclusions

Aerosol size, composition, light absorption and scattering and particle hygroscopicity estimated from CCN measurements were measured in real-time during the 2004 CIFEX study. Sub- and super-micron sea salt particles made up the largest fraction of all observed particle types; with over half of the sea salt being aged. In the sub-micrometer mode, a significant fraction of particles contained organic carbon, elemental carbon with organic carbon and biomass burning with a notable increase in biomass burning on April 13th. A large increase in aromatic-containing particle counts and aromatic markers on the biomass burning and dust particles on April 13th coincided with a large increase in total particle absorption and scattering, increase in sub-micrometer particles, and a large increase in total submicron particles from biomass burning. The particle types with the highest percentage of aromatic-containing particles were biomass burning, organic carbon, and dust. Most interestingly, a subset of the organic carbon particles, high mass organic carbon representative of humic-like substances (HULIS), had a very strong correlation with all aromatic-containing particle counts, indicating that HULIS or brown carbon associated with biomass burning is a significant source of particle absorption, as has been shown previously. Throughout the study biomass burning and dust particles had little to no correlation with the particle optical behavior, however, upon association with aromatic compounds a considerable increase in total particle absorption occurred, highlighting the importance of particle mixing state on aerosol

optical properties. Aerosol hygroscopicity parameter (κ) had a median value of 0.49, between the average continental value of 0.27 and average marine value of 0.72, indicating a mix of both continental and marine influences during the course of this study, as was supported by particle composition measurements.

During CIFEX, oxalate was frequently detected in single particle spectra with 22% of submicron and 3% of supermicron particles containing oxalate. There were two distinct oxalate events; during the 1st event, supermicron oxalate was predominantly mixed with the aged sea salt particle class, while during the 2nd event oxalate was found to be internally mixed with sulfate in the submicron size range, and found mainly on the biomass burning and organic carbon particle classes. Enrichment of oxalate on the aged sea salt type during the 1st event and similar diurnal behavior of nitrate and oxalate on the aged sea salt particle type indicate a photochemical source of oxalate for this event. During the 2nd event, the preferential enrichment of oxalate and sulfate on biomass burning and carbonaceous particles, and both temporal and size-resolved correlations between oxalate and other cloud and aqueous markers on these particle types suggests in-cloud processing as the source of oxalate for this event.

7.2.5 Overall mixing state and hygroscopicity conclusions

Overall particle hygroscopicity and mixing state are most important in determining CCN concentrations when the main particle size mode of the aerosol is close to the activation threshold of the aerosol. For sea spray aerosol, the CCN activity of the particles depends on the particular source of biological activity, indicating the importance of the particular type of microorganism on the CCN activity of sea spray aerosol. During the wildfire studies, simultaneous measurements of particle mixing state and hygroscopicity were measured for the first time in San Diego and indicate that varying the hygroscopicity of the biomass burning aerosol strongly influenced the CCN concentrations in 2007 when the biomass burning

dominated the chemistry of the activation threshold. However, in 2008, varying the hygroscopicity of the biomass burning did not significantly influence the CCN concentrations due to the domination of the activation threshold by local emissions much smaller in size. During the Owens Lake study, first time particle mixing state measurements simultaneous with hygroscopicity indicate that the mineral dust contributes significantly to CCN concentrations during dust events at low supersaturations ~0.1%. The mineral dust was completely CCN active because it was large and moderately hygroscopic, therefore CCN concentrations were dominated by the changes in hygroscopicity around the activation threshold. Care needs to be taken in oversimplification of the effects of both particle size and chemistry [*Dusek et al.,* 2006], as simultaneous particle chemistry changes with size and cannot be separated. An average hygroscopicity does not explain all of the effects on CCN concentration, especially if the chemistry is significantly changing around the activation diameter threshold.

7.3 Remaining questions and future work

While the research described in this dissertation has helped to strengthen the understanding of the relationship between aerosol particle chemistry and its effect on cloud condensation nuclei activity, further research in this field is required to more fully understand the interactions between particle chemistry, atmospheric chemistry, cloud nucleation, and climate change. A brief list of some of the major outstanding questions and suggested future work are covered in the following sections.

7.3.1 Overall future work

Although single particle chemical mixing state measurements were compared to particle hygroscopicity, the hygroscopicity measurements were made for the entire particle size range, while the chemical measurements had a lower size limit of 100-200 nm. Therefore,

the chemical measurements were used as a proxy to understand how the chemistry of the particles below the size detection limit could be affecting hygroscopicity. As the activation threshold in the atmosphere is ~40-200 nm, future measurements need to include single particle mixing state measurements down to 40 nm. Such a method has been developed, which couples a growth tube (GT) to an ultrafine aerosol time of flight mass spectrometer (UF-ATOFMS) to allow measurements of the composition of individual particles as small as 38 nm by using water to grow particles to larger sizes so they can be optically detected by the UF-ATOFMS [*Zauscher et al.*, 2011]. As particles are varied in composition around the activation threshold, an additional chemical effect on CCN activity is expected with chemical measurements of smaller particle sizes. The GT-UF-ATOFMS was deployed in parallel to a CCN in the field, and future single particle mixing state measurements will be able to compare hygroscopicity to the chemical composition of a much larger size range of particles, further improving our understanding of aerosol cloud interactions. Additionally, size-selected CCN spectra measurements will further improve the ability to compare the single particle measurements to hygroscopicity. Having hygroscopicity estimates over many discrete size ranges will improve the ability of a direct comparison of mixing state to CCN activity without needing to assume an internal mixture for all particles of all sizes. Size-selection before the CCN will allow a direct comparison of particle chemistry and hygroscopicity over specific size ranges, and the range of activation diameters measured will be further expanded by collection of CCN spectra (CCN concentration as a function of supersaturation), improving the range of chemical sensitivities measured.

7.3.2 Sea spray aerosol further questions and future work

What is the effect of organic matter from many different microorganisms on the CCN activity of sea spray aerosol? What effect could this have on the climate?

Recent experiments relating the CCN activity of primary sea spray aerosol and phytoplankton-derived organic matter show a decrease in hygroscopic growth and CCN activity associated with the addition of organics [*Fuentes et al.*, 2010]. Additionally, there were notable differences in CCN activity and hygroscopic growth between different types of organisms; diatomaceous associated organic matter was more hydrophobic than nanoplankton associated organic matter [*Fuentes et al.*, 2010]. This clearly illustrates the need for further experiments involving increasing numbers of different marine microorganisms, including detailed analysis of the organic material associated with these microorganisms, to better understand the effect of marine organic matter from different sources of primary production on the CCN activity and hygroscopic growth of sea spray aerosols.

7.3.3 Biomass burning aerosol further questions and future work

What is the net effect of biomass burning aerosol on climate? How does the mixing state and chemistry of the biomass burning aerosol influence its effect on climate?

While biomass burning aerosol can contribute a large amount of CCN which can increase cloud reflectivity and therefore have a cooling effect [*Lewis et al.*, 2009; *Ramanathan et al.*, 2001; *Wilcox*, 2010]; the black carbon produced during the biomass combustion process has high absorption, which has a warming effect [*Hopkins et al.*, 2007; *Lewis et al.*, 2009; *Ramanathan et al.*, 2001; *Wilcox*, 2010], therefore the net effect on climate is highly uncertain [*Ramaswamy et al.*, 2001; *Solomon et al.*, 2007]. The balance of the warming and cooling effects depend on the quantity and optical properties of the absorbing smoke aerosol, in addition to the optical thickness and fractional coverage of the clouds [*Wilcox*, 2010]. Organic carbon that absorbs in the UV range, or brown carbon, is also a significant source of particle absorption [*Andreae and Gelencser*, 2006; *Moosmueller et al.*, 2009]. A recent study highlights that spherical organic carbon particles, or tar balls, produced during smoldering biomass burning combustion are an important source of brown carbon [*Chakrabarty et al.*,

2010]. Their sensitivity calculations show that accounting for the absorption from brown carbon during smoldering biomass burning may cause an increase in additional atmospheric absorption and warming [*Chakrabarty et al.*, 2010]. As smoldering combustion produces close to three quarters of the global total carbonaceous aerosol mass [*Einfeld et al.*, 1991], this should have a significant impact on the Earth's radiation balance. In addition to continued studies such as those presented in this dissertation and other manuscripts [*Carrico et al.*, 2008; *Carrico et al.*, 2010; *Petters et al.*, 2009] that examine the relationship between biomass burning aerosol composition, burning conditions and CCN activity; additional measurements of aerosol absorption and scattering of biomass burning aerosol, such as [*Hand et al.*, 2010; *Hopkins et al.*, 2007; *Levin et al.*, 2010; *Lewis et al.*, 2009], are also needed to help understand the net effect of biomass burning on the climate.

7.3.4 Mineral dust aerosol further questions and future work

How does Owens Lake mineral dust affect cloud properties in the region? Does it enhance or suppress precipitation? How does fresh Owens Lake mineral dust react with gas phase nitrogen-containing compounds and how does this affect their hygroscopicity?

Studies have suggested that mineral dust suppresses precipitation [*Klueser and Holtzer-Popp*, 2010; *Li and Min*, 2010; *Min et al.*, 2009; *Rosenfeld et al.*, 2001], while other studies show that mineral dust can also can enhance precipitation [*Rudich et al.*, 2002; *Teller and Levin*, 2006; *van den Heever et al.*, 2006]. Due to the large sizes and moderate hygroscopic nature of Owens (dry) Lake dust, it appears that the dust would most likely enhance precipitation. Further studies on the radiative cloud properties before, during, and after Owens Lake dust events are needed to confirm this hypothesis and to gain insight into the regional climate impacts.

Additionally, mineral dust is a reactive surface for heterogeneous reactions with trace gas phase species in the atmosphere. These reactions can alter the physiochemical properties

of the dust particles as well as modify the chemical composition of the troposphere [*Navea et al.*, 2010]. The reactivity of mineral dust aerosol to heterogeneous reaction is highly dependent on their mineralogy and composition [*Krueger et al.*, 2004; *Mogili et al.*, 2006; *Navea et al.*, 2010; *Sullivan et al.*, 2007; *Usher et al.*, 2003], as well as the relative humidity of the atmosphere [*Al-Abadleh et al.*, 2005; *Gibson et al.*, 2006; *Goodman et al.*, 2001; *Goodman et al.*, 2000; *Liu et al.*, 2008; *Mashburn et al.*, 2006; *Sullivan et al.*, 2009a; *Vlasenko et al.*, 2006; *Wagner et al.*, 2009]. Owens lake ambient mineral dust showed a high prevalence of nitrate on all types of dust, for the entirely of the study with no apparent dependence on relative humidity. The presence of nitrate on the dust particles most likely increased the hygroscopicity, as has been previously shown [*Gibson et al.*, 2006; *Sullivan et al.*, 2009a; *Sullivan et al.*, 2009b]. The actual increase in hygroscopicity of the source dust once reacted with nitric acid was not able to be determined from the results; therefore further laboratory experiments examining the uptake of nitrogen-containing gases on the different unreacted Owens Lake source dust samples and the resulting changes in particle hygroscopicity and CCN activity over a range of relative humidity are needed.

7.3.5 Oxalic acid/oxalate further questions and future work

How do changes in hygroscopicity and optical properties evolve over time in the atmosphere as a function of particle chemistry and the mixing state of the aerosol? What are the factors that control which oxalate production mechanism dominates in specific environments? What effect does aqueous phase production of oxalate have on SOA and what implications does this have for climate?

In addition to being a marker for in-cloud processing, oxalic acid has also been shown to be hygroscopic and CCN active [*Ervens et al.*, 2004; *Sorooshian et al.*, 2006; *Yu*, 2000]. The extent to which the in-cloud processing contributes to particulate oxalate, which strongly depends on the original particle hygroscopicity, and when other sources of oxalate are

involved, is still not well understood. Further investigation is needed to determine the factors that control which oxalate production mechanism dominates in specific environments.

Additionally, a recent study shows that most of the oxalic acid present in the aerosols is in the form of metal-oxalate complexes which are not hygroscopic and do not make good CCN [*Furukawa and Takahashi*, 2010], as has been shown previously [*Sullivan et al.*, 2009b]. As knowledge of the contribution of WSOC is essential for predicting the hygroscopicity of ambient aerosol [*Chang et al.*, 2007; *Mircea et al.*, 2005; *Rissler et al.*, 2004; *Roberts et al.*, 2002]; further study is needed into the mixing state of oxalate in different types of ambient aerosol in different environments to determine the possible effects on CCN activity and hygroscopicity.

7.4 References

Al-Abadleh, H.A., H.A. Al-Hosney, and V.H. Grassian, Oxide and carbonate surfaces as environmental interfaces: the importance of water in surface composition and surface reactivity, *Journal of Molecular Catalysis A: Chemical*, *228*, 47-54, 2005.

Andreae, M.O., and A. Gelencser, Black carbon or brown carbon? The nature of light-absorbing carbonaceous aerosols, *Atmospheric Chemistry and Physics*, *6*, 3131-3148, 2006.

Asa-Awuku, A., G.J. Engelhart, B.H. Lee, S.N. Pandis, and A. Nenes, Relating CCN activity, volatility, and droplet growth kinetics of Beta-caryophyllene secondary organic aerosol, *Atmospheric Chemistry and Physics*, *9*, 795-812, 2009.

Asa-Awuku, A., A. Nenes, S. Gao, R.C. Flagan, and J.H. Seinfeld, Alkene ozonolysis SOA: inferences of composition and droplet growth kinetics from Köhler theory analysis, *Atmospheric Chemistry and Physics Discussions*, *7*, 8983-9011, 2007.

Asa-Awuku, A., A. Nenes, S. Gao, R.C. Flagan, and J.H. Seinfeld, Alkene ozonolysis SOA: inferences of composition and droplet growth kinetics from Köhler theory analysis, *Atmospheric Chemistry and Physics*, *10*, 1585-1597, 2010.

Carrico, C.M., M.D. Petters, S.M. Kreidenweis, J.L. Collett, G. Engling, and W.C. Malm, Aerosol hygroscopicity and cloud droplet activation of extracts of filters from biomass burning experiments, *Journal of Geophysical Research*, *113* (D08206), doi:10.1029/2007JD009274, 2008.

Carrico, C.M., M.D. Petters, S.M. Kreidenweis, A.P. Sullivan, G.R. McMeeking, E.J.T. Levin, G. Engling, W.C. Malm, and J.L. Collett, Water uptake and chemical composition of fresh aerosols generated in open burning of biomass, *Atmospheric Chemistry and Physics*, *10*, 5165-5178, 2010.

Chakrabarty, R.K., H. Moosmueller, L.-W.A. Chen, K. Lewis, W.P. Arnott, C. Mazzoleni, M.K. Dubey, C.E. Wold, W.M. Hao, and S.M. Kreidenweis, Brown carbon in tar balls from smoldering biomass combustion, *Atmospheric Chemistry and Physics*, *10* (6363-6370), 2010.

Chang, R.Y.-W., P.S.K. Liu, W.R. Leaitch, and J.P.D. Abbatt, Comparison between measured and predicted CCN concentrations at Egbert, Ontario: Focus on the organic aerosol fraction at a semi-rural site, *Atmospheric Environment*, *41*, 8172-8182, 2007.

Dusek, U., G.P. Frank, L. Hildebrant, J. Curtius, J. Schneider, S. Walter, D. Chand, F. Drewnick, S.S. Hings, D. Jung, S. Borrmann, and M.O. Andreae, Size Matters More Than Chemistry for Cloud-Nucleating Ability of Aerosol Particles, *Science*, *312* (5778), 1375-1378, 2006.

Einfeld, W., D.E. Ward, and C. Hardy, Effects of fire behavior on prescribed fire smoke characteristics: A case study in: Global biomass burning: Atmospheric, climatic, and biospheric implications, *MIT Press, Cambridge, MA* (USA), 412-419, 1991.

Ervens, B., G. Feingold, S.L. Clegg, and S.M. Kreidenweis, A modeling study of aqueous production of dicarboxylic acids: 2. Implications for cloud microphysics, *Journal of Geophysical Research*, *109* (D15206), doi:10.1029/2004JD004575, 2004.

Fuentes, E., H. Coe, D. Green, and G. McFiggans, On the impacts of phytoplankton-derived organic matter on the properties of the primary marine aerosol - Part 2: Composition, hygroscopicity and cloud condensation activity, *Atmospheric Chemistry and Physics Discussions*, *10*, 26157-26205, 2010.

Furukawa, T., and S. Takahashi, Metal complexation inhibits the effect of oxalic acid in aerosols as cloud condensation nuclei, *Atmospheric Chemistry and Physics Discussions*, *10*, 27099-27134, 2010.

Gibson, E.R., P.K. Hudson, and V.H. Grassian, Physicochemical Properties of Nitrate Aerosols: Implications for the Atmosphere, *Journal of Physical Chemistry A*, *110*, 11785-11799, 2006.

Goodman, A.L., E.T. Bernard, and V.H. Grassian, Spectroscopic Study of Nitric Acid and Water Adsorption on Oxide Particles: Enhanced Nitric Acid Uptake Kinetics in the Presence of Adsorbed Water, *Journal of Physical Chemistry A*, *105*, 6443-6457, 2001.

Goodman, A.L., G.M. Underwood, and V.H. Grassian, A laboratory study of the heterogeneous reaction of nitric acid on calcium carbonate particles, *Journal of Geophysical Research*, *105* (D23), 29,053-29,064, 2000.

Hand, J.L., D.E. Day, G.M. McMeeking, E.J.T. Levin, C.M. Carrico, S.M. Kreidenweis, W.C. Malm, A. Laskin, and Y. Desyaterik, Measured and modeled humidification factors of

fresh smoke particles from biomass burning: role of inorganic constituents, *Atmospheric Chemistry and Physics*, *10*, 6179-6194, 2010.

Hopkins, R.J., K. Lewis, Y. Desyaterik, Z. Wang, A.V. Tivanski, W.P. Arnott, A. Laskin, and M.K. Giles, Correlations between optical, chemical and physical properties of biomass burn aerosols, *Geophysical Research Letters*, *34* (L18806), doi:10.1029/2007GL030502, 2007.

Klueser, L., and T. Holtzer-Popp, Relationships between mineral dust and cloud properties in the West African Sahel, *Atmospheric Chemistry and Physics*, *10*, 6901-6915, 2010.

Koehler, K., S.M. Kreidenweis, P.J. DeMott, A.J. Prenni, and M.D. Petters, Potential impact of Owens (dry) Lake dust on warm and cold cloud formation, *Journal of Geophysical Research*, *112* (D12210), doi:10.1029/2007JD008413, 2007.

Krueger, B.J., V.H. Grassian, J.P. Cowin, and A. Laskin, Heterogeneous chemistry of individual mineral dust particles from different dust source regions: the importance of particle minerology, *Atmospheric Environment*, *38*, 6253-6261, 2004.

Levin, E.J.T., G.R. McMeeking, C.M. Carrico, L.E. Mack, S.M. Kreidenweis, C.E. Wold, H. Moosmueller, W.P. Arnott, W.M. Hao, J.L. Collett, and W.C. Malm, Biomass burning smoke aerosol propertie measured during Fire Laboratory at Missoula Experiments (FLAME), *Journal of Geophysical Research*, *115* (D18210), doi:10.1029/2009JD013601, 2010.

Lewis, K.A., W.P. Arnott, H. Moosmueller, R.K. Chakrabarty, C.M. Carrico, S.M. Kreidenweis, D.E. Day, W.C. Malm, A. Laskin, J.L. Jimenenez, I.M. Ulbrich, J.A. Huffman, T.B. Onasch, A. Trimborn, L. Liu, and M.I. Mischenko, Reduction in biomass burning aerosol light absorption upon humidification: roles of inorganically-induced hygroscopicity, particle collapse, and photoacoustic heat and mass transfer, *Atmospheric Chemistry and Physics*, *9*, 8949-8966, 2009.

Li, R., and Q.-L. Min, Impacts of mineral dust on the vertical structure of precipitation, *Journal of Geophysical Research*, *115* (D09203), doi:10.1029/2009JD011925, 2010.

Liu, Y., E.R. Gibson, J.P. Cain, H. Wang, V.H. Grassian, and A. Laskin, Kinetics of heterogeneous reaction of CaCO3 particles with gaseous HNO3 over a wide range of humidity, *Journal of Physical Chemistry A*, *112* (7), 1561-1571, 2008.

Mashburn, C.D., E.K. Frinak, and M.A. Tolbert, Heterogeneous uptake of nitric acid on Na-montmorillonite clay as a function of relative humidity, *Journal of Geophysical Research*, *111* (D15213), doi:10.1029/2005JD006525, 2006.

Min, Q.-L., R. Li, B. Lin, E. Joseph, S. Wang, Y. Hu, V. Morris, and F. Chang, Evidence of mineral dust altering cloud microphysics and precipitation, *Atmospheric Chemistry and Physics*, *9*, 3223-3231, 2009.

Mircea, M., M.C. Facchini, S. Decesari, F. Cavalli, L. Emblico, S. Fuzzi, A. Vestin, J. Rissler, E. Swietlicki, G. Frank, M.O. Andreae, W. Maenhaut, Y. Rudich, and P. Artaxo, Importance of the organic aerosol fraction for modeling aerosol hygroscopic growth

and activation: a case study in the Amazon Basin, *Atmospheric Chemistry and Physics, 5*, 3111-3126, 2005.

Mogili, P.K., P.D. Kleiber, J.A. Young, and V.H. Grassian, N2O5 hydrolysis on the components of mineral dust and sea salt aerosol: Comparison study in an environmental aerosol reaction chamber, *Atmospheric Environment, 40*, 7401-7408, 2006.

Moosmueller, H., R.K. Chakrabarty, and W.P. Arnott, Aerosol light absorbtion and its measurement: A review, *J. Quant. Spectrosc. Rad. Trans., 110*, 844-878, 2009.

Navea, J.C., H. Chen, M. Huang, G.R. Carmichael, and V.H. Grassian, A comparative evaluation of water uptake on several mineral dust sources, *Environ. Chem., 7*, 162-170, 2010.

Petters, M.D., C.M. Carrico, S.M. Kreidenweis, A.J. Prenni, P.J. DeMott, J.L. Collett, and H. Moosmueller, Cloud Condensation Nuclei Activity of Biomass Burning Aerosol, *Journal of Geophysical Research, 114* (D22205), doi:10.1029/2009JD012353, 2009.

Ramanathan, V., P.J. Crutzen, J. Lelieveld, A.P. Mitra, D. Althausen, J. Anderson, M.O. Andreae, W. Cantrell, G.R. Cass, C.E. Chung, A.D. Clarke, J.A. Coakley, W.D. Collins, W.C. Conant, F. Dulac, J. Heintzenberg, A.J. Heymsfield, B. Holben, S. Howell, J. Hudson, A. Jayaraman, J.T. Kiehl, T.N. Krishnamurti, D. Lubin, G. McFarquhar, T. Novakov, J.A. Ogren, I.A. Podgorny, K.A. Prather, K. Priestley, J.M. Prospero, P.K. Quinn, E. Rajeev, P. Rasch, S. Rupert, R. Sadourny, S.K. Satheesh, G.E. Shaw, P. Sheridan, and F.P.J. Valero, Indian Ocean Experiment: An integrated analysis of the climate forcing and effects of the great Indo-Asian haze, *Journal of Geophysical Research, 106* (D22), 28,371-28,398, 2001.

Ramaswamy, V., O. Boucher, J. Haigh, D. Hauglustaine, J. Haywood, G. Myhre, T. Nakajima, G.Y. Shi, and S. Solomon, Climate Change 2001: The Scientific Basis, Contribution of working group I to the Third Assessment Report of the Intergovernmental Panel on Climate Change, 2001.

Rissler, J., E. Swietlicki, J. Zhou, G. Roberts, M.O. Andreae, L.V. Gatti, and P. Artaxo, Physical properties of the sub-micrometer aerosol over the Amazon rain forest during the wet-to-dry season transition- comparison of modeled and measured CCN concentrations, *Atmospheric Chemistry and Physics*, *4*, 2119-2143, 2004.

Roberts, G.C., P. Artaxo, J. Zhou, E. Swietlicki, and M.O. Andreae, Sensitivity of CCN spectra on chemical and physical properties of aerosol: A case study from the Amazon Basin, *Journal of Geophysical Research*, *107* (D20), 8070, doi:10.1029/2001JD000583, 2002.

Rosenfeld, D., Y. Rudich, and R. Lahav, Desert dust suppressing precipitation: A possible desertification feedback loop, *Proceedings of the National Academy of Sciences of the United States of America*, *98* (11), 5975-5980, 2001.

Rudich, Y., O. Khersonsky, and D. Rosenfeld, Treating clouds with a grain of salt, *Geophysical Research Letters*, *29* (22), 2060, 2002.

Solomon, S., D. Qin, M. Manning, Z. Chen, M. Marquis, K.B. Averyt, M. Tignor, and H.L. Miller, Climate Change 2007: The Physical Science Basis, Contribution of Working Group I to the Fourth Assessment Report of the Intergovernmental Panel on Climate Change, 2007.

Sorooshian, A., V. Varutbangkul, F.J. Brechtel, B. Ervens, G. Feingold, R. Bahreini, S.M. Murphy, J.S. Holloway, E.L. Atlas, G. Buzorius, H. Jonsson, R.C. Flagan, and J.H. Seinfeld, Oxalic acid in clear and cloudy atmospheres: Analysis of data from International Consortium for Atmospheric Research on Transport and Transformation 2004, *Journal of Geophysical Research*, *111* (D23S45), doi:10.1029/2005JD006880, 2006.

Sullivan, R.C., S.A. Guazzotti, D.A. Sodeman, and K.A. Prather, Direct observations of the atmospheric processing of Asian mineral dust, *Atmospheric Chemistry and Physics*, *7* (5), 1213-1236, 2007.

Sullivan, R.C., M.J.K. Moore, M.D. Petters, S.M. Kreidenweis, G. Roberts, and K.A. Prather, Timescale for hygroscopic conversion of calcite mineral particles through heterogeneous reaction with nitric acid, *Physical Chemistry Chemical Physics*, *11*, 7826, 2009a.

Sullivan, R.C., M.J.K. Moore, M.D. Petters, S.M. Kreidenweis, G.C. Roberts, and K.A. Prather, Effect of chemical mixing state on hygroscopicity and cloud nucleation properties of calcium mineral dust particles, *Atmospheric Chemistry and Physics*, *9*, 3303-3316, 2009b.

Teller, A., and Z. Levin, The effects of aerosols on precipitation and dimensions of subtropical clouds: a sensitivity study using a numerical cloud model, *Atmospheric Chemistry and Physics*, *6* (67-80), 2006.

Usher, C.R., A.E. Michel, and V.H. Grassian, Reactions on Mineral Dust, *Chem. Rev.*, *103*, 4883-4939, 2003.

van den Heever, S.C., G.C. Carrio, W.R. Cotton, P.J. DeMott, and A.J. Prenni, Impacts of Nucleating Aerosol on Florida Storms. Part I: Mesoscale Simulations, *J. Atmos. Sci.*, *63*, 1752-1775, 2006.

Vlasenko, A., S. Sjogren, E. Weingartner, K. Stemmler, H.W. Gaeggler, and M. Ammann, Effect of humidity on nitric acid uptake to mineral dust aerosol particles, *Atmospheric Chemistry and Physics*, *6*, 2147-2160, 2006.

Wagner, C., G. Schuster, and J.N. Crowley, An aerosol flow tube study of the interaction of N2O5 with calcite, Arizona dust and quartz, *Atmospheric Environment*, *43*, 5001-5008, 2009.

Wilcox, E.M., Stratocumulus cloud thickening beneath layers of absorbing smoke aerosol, *Atmospheric Chemistry and Physics*, *10*, 11769-11777, 2010.

Yu, S., Role of organic acids (formic, acetic, pyruvic and oxalic) in the formation of cloud condensation nuclei (CCN): a review, *Atmospheric Research*, *53*, 185-217, 2000.

Zauscher, M.D., M.J.K. Moore, G.S. Lewis, S.V. Hering, and K.A. Prather, A new approach for measuring the chemistry of individual particles in the size range critical for cloud formation, *submitted to Analytical Chemistry*, 2011.

Appendix 1

Preliminary Bubbling Experiments

A1.1 Objective

To observe the effect of surfactant on the morphology of sea spray aerosol (SSA) produced from air bubble bursting. These experiments were preliminary to those of Chapter 2, "Effect of Organic Compounds on Cloud Condensation Nuclei (CCN) Activity of Sea Spray Aerosol Produced by Bubble Bursting."

A1.2 Methods and materials

A1.2.1 Laboratory generation of sea salt aerosol

The bubble bursting apparatus that was used to generate particles in these experiments is an L-shaped sintered glass filter with porosity "C" rated at 25-50 μm (Ace Glass Vineland, NJ) was immersed 2 cm below each of the 100mL sample solutions in a 32oz Mason jar (approximately 3" D x 7"H). The glass filter was attached to a 1/8" stainless steel tube that protruded from a hole in a stainless steel cap on the jar. Another hole in the cap allowed for an additional 1/8" stainless steel tube to supply the sheath air. This sheath tube did not go below the surface of the water, it was approximately 1 cm from the surface and was bent in a spiral motion to have the flow almost perpendicular to the surface and towards a 3rd hole, the exit port of the cap. All holes were sealed with o-rings and ferrules to prevent contamination with outside air. The glass was combusted for 4 hours at 450 °C to help prevent organic contamination. The stainless steel components were cleaned by sonicating in water for 72 hours total prior to use; 24 hours with tap water, 24 hours with distilled water and 24 hours

with ultra pure deionized water to remove contamination. A flow of 30 cm^3/min dry filtered nitrogen flowed through the glass filter to produce bubbles. Approximately 1 cm above the solution, a sheath flow ("surface wind") flowed perpendicular to the solution surface with a flow of 1500 cm^3/min dry filtered nitrogen to take ejected and suspended seawater droplets away from the bubbling chamber. The wet seawater droplets from the bubbling chamber were then sent through a glass flow tube where they were diluted with 6000 cm^3/min dry filtered nitrogen, letting the droplets dry up and form solid SSA with RH < 25%. The RH and temperature were measured by a hygrometer (Vaisala, HMP45AC, accuracy ±1.5% RH). The flow tube had an inner diameter of 6.1 cm and was 120 cm long. At a flow rate of 6000 cm^3/min, the Reynolds's number was 136, corresponding to a laminar flow regime.

A1.2.2 SEM collection

To collect sea spray aerosols generated in the laboratory bubble bursting experiments for off-line single particle analysis via, 12 mm OD carbon conductive tab substrates, 12mm OD (PELCO Tabs™, Ted Pella Inc.) were used. Substrates were attached to a Micro-orifice uniform deposit impactor (MOUDI) foil and placed on stage 2 (>5.6μm) and 9 (<0.1μm). All other stages in the MOUDI used foil only. The aerosol output of the bubbler was sent through a glass flow tube and diluted with 6000 cm^3/min dry filtered nitrogen (RH < 25%). After the flow tube, the aerosol was then diluted with dry nitrogen ~25 lpm into the MOUDI, with a HEPA vent on the MOUDI inlet having an excess flow of approximately 1 lpm. A Phillips XL30 field emission scanning electron microscope (SEM) was used to take the images. Energy dispersive x-rays (EDX) were used to determine the elemental composition whenever possible. Due to the presence of carbon in the substrate, EDX was not able to distinguish between carbon in the samples and carbon from the substrate.

A1.2.3 Model seawater solution and seawater collection

Salt solutions, either 3.5% by weight NaCl (99.999% Sigma), $MgCl_2$ (98%,Aldrich) or 3.5% sea salts (No purity stated, Sigma) in Mill-Q water were used as model seawater in the experiments. Fresh seawater was collected from the Scripps Institution of Oceanography (SIO) Pier (32° 51'47.232"N, 117° 15'21.6"W) 400 meters over the water from the beach by extending a weighted Nalgene jar (rinsed 3x with seawater before collection) into the ocean from 12 meters above sea level and placed in a combusted 32 oz Mason jar (rinsed 3x with seawater before collection).

A1.2.4 Addition of organic surfactant to salt solutions

1000 µl of a concentrated solution of 0.025 mg/ml 4-dodecyloxyphthalonitrile (99+%, TCI America) in hexanes (99.95%, EMD OmniSolv) was then added to the surface of the sea water solution that was to be bubbled. After adding the surfactant, only the sheath air flowed to allow the hexane to evaporate for 15-20 min, leaving only the surfactant on the surface. After the 15-20 min pre-preparation, both sheath and bubbling air were turned on and generation of sea spray aerosol was initiated. The surfactant added to the solution surface with an automated pipet.

A1.2.5. Laboratory preparation of large crystal droplets from bulk salt solution mixtures

A drop of salt solution was applied directly to the surface of the SEM grid via pipet. To add surfactant, an additional drop of concentrated surfactant solution was applied directly to the salt solution droplet on the SEM grid. Grids were stored under dry nitrogen until they were viewed by the SEM to ensure that the drops had crystallized (at least 24 hours).

A1.3 Results

A1.3.1 Effect of surfactant on large crystal droplets from bulk salt solution mixtures

A1.3.1.1 SIO Seawater without and with surfactant

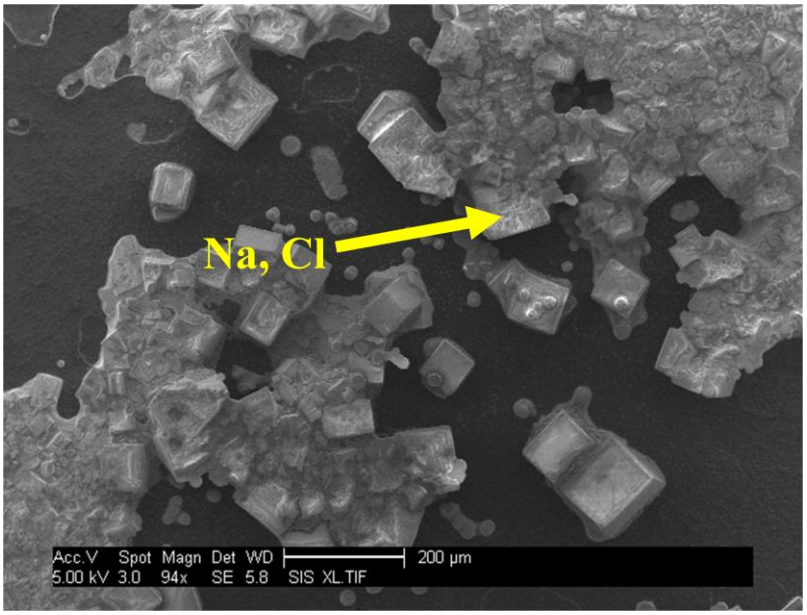

Figure A1.1. SIO Sea water bulk crystal droplet on SEM substrate. EDX shows the predominant composition of the large square crystals is Na and Cl.

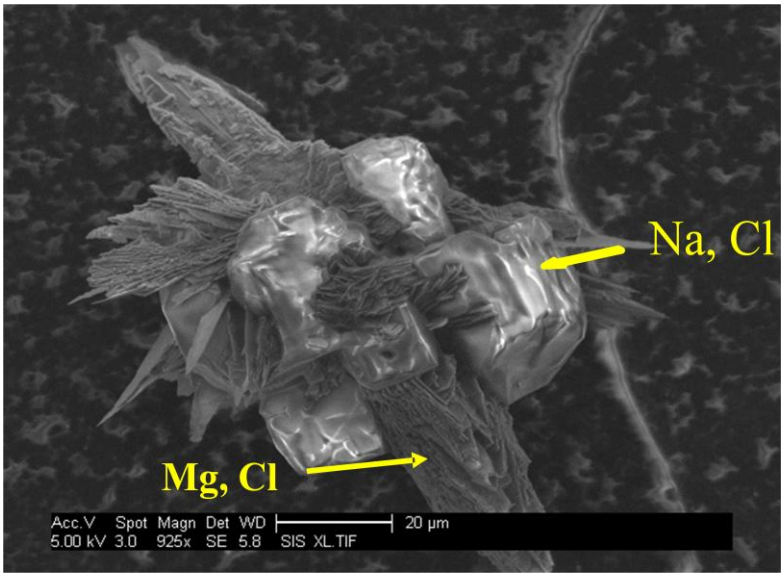

Figure A1.2 SIO Sea water bulk crystal droplet with surfactant on SEM substrate. Presence of surfactant caused separate domains of Mg-rich (spiked parks) and Na-rich (smooth square parts).

A1.3.1.2 NaCl and $MgCl_2$ (1:1) with and without surfactant

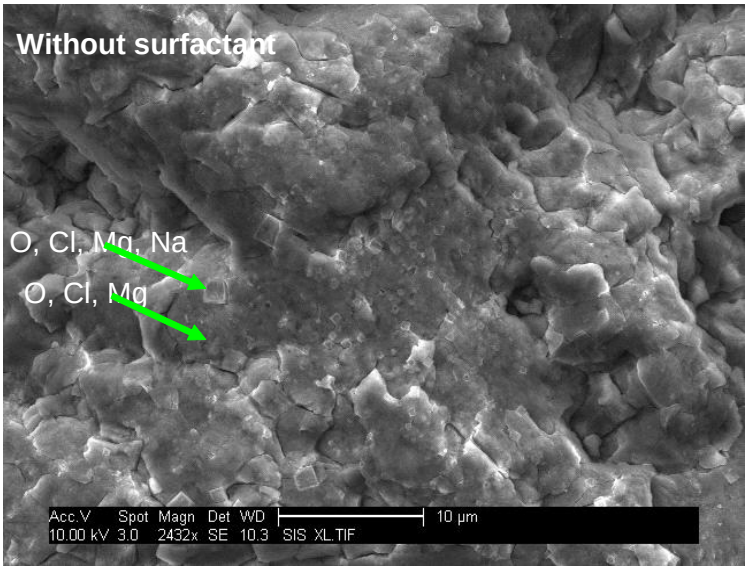

Figure A1.3. NaCl:$MgCl_2$ (1:1) bulk crystal droplet on SEM substrate. EDX shows the predominant composition of the crystal is Na,Mg,Cl and O.

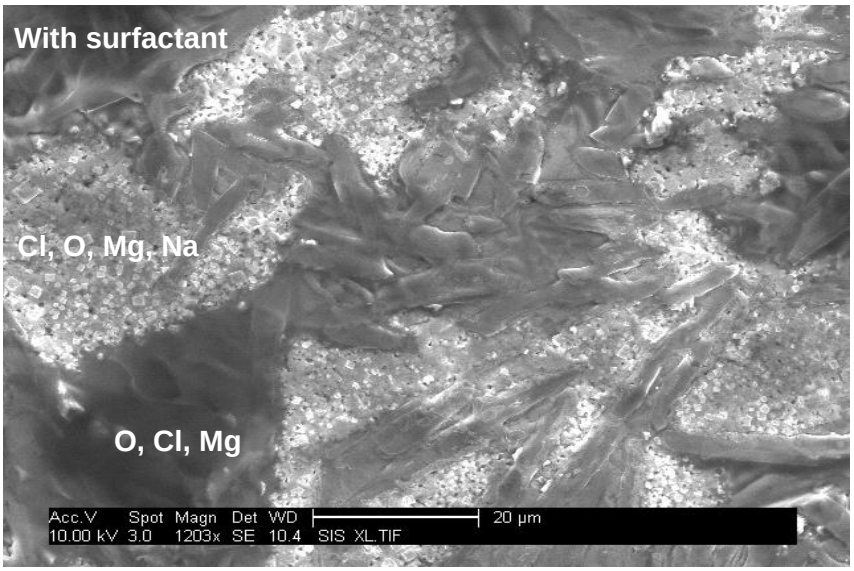

Figure A1.4. NaCl:$MgCl_2$ (1:1) bulk crystal droplet with surfactant on SEM substrate. Presence of surfactant caused separate domains of Mg-rich (smoother, darker parks) and Na-rich (lighter parts made up of many small squares).

A1.3.1.3 Summary of effect of surfactant on large crystal droplets from bulk salt solution mixtures

The morphology of the salt drops change with surfactant if Mg^{2+} cations are present. Surfactant can lead to a segregation into separate Mg-rich and Na-rich domains. These large crystals show a large effect of surfactant in presence of Mg^{2+}.

A1.3.2 Effect of surfactant on aerosol morphology

A1.3.2.1 Effect of surfactant on NaCl aerosol

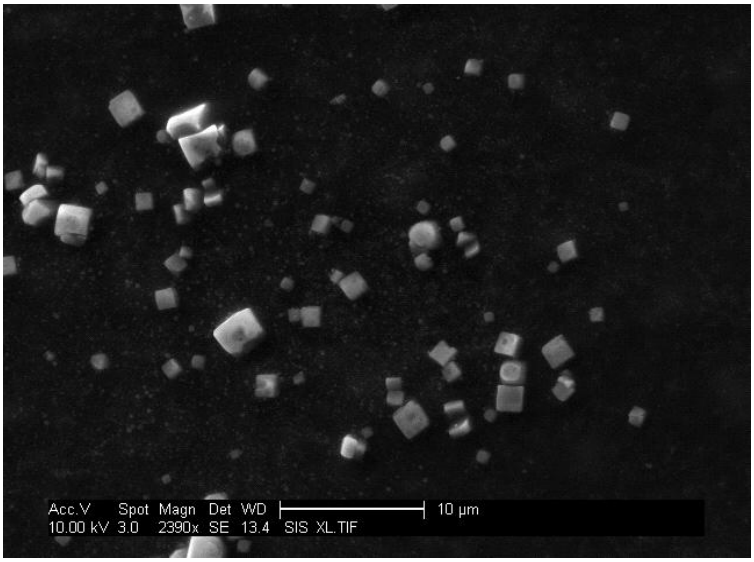

Figure A1.5. NaCl aerosol particles on SEM substrate.

Figure A1.6. NaCl aerosol particles with surfactant on SEM substrate.

A1.3.2.2 Effect of surfactant on NaCl and $MgCl_2$ (8:1)

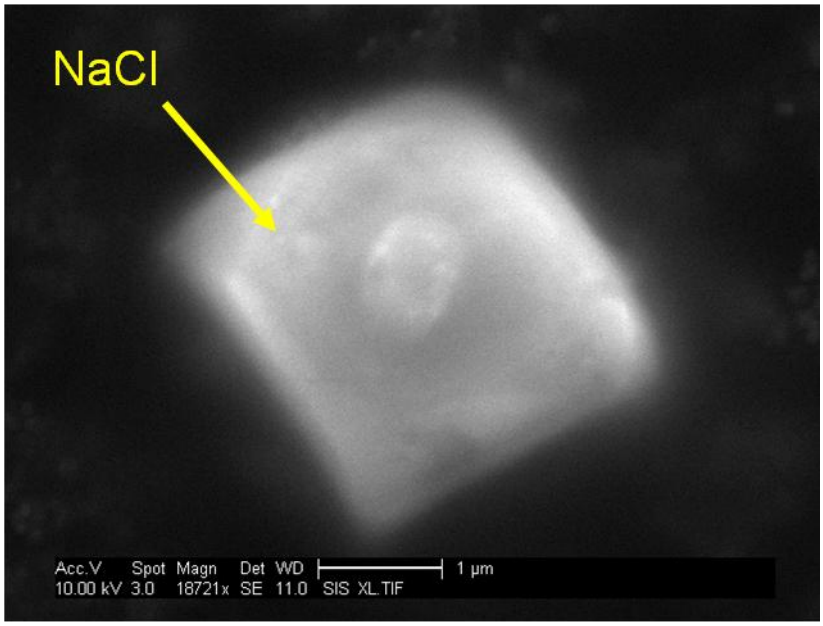

Figure A1.7. NaCl:$MgCl_2$ (8:1) aerosol particles on SEM substrate.

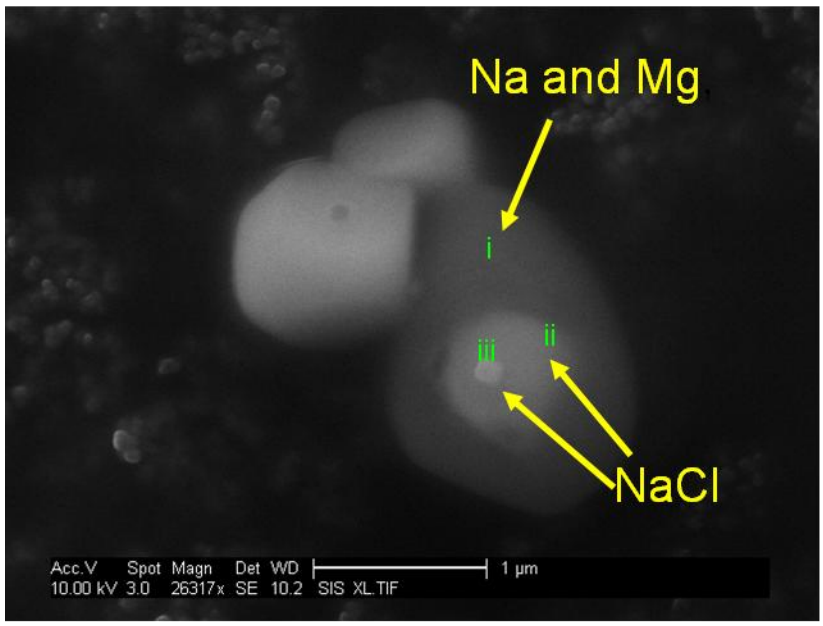

Figure A1.8. NaCl:$MgCl_2$ (8:1) aerosol particles with surfactant on SEM substrate. It is observed that with a negligible amount of surfactant, one can see morphology changes in the aerosol phase.

A1.3.2.3 Summary of effect of surfactant on aerosol morphology

The morphology of the aerosol particles change with surfactant if Mg^{2+} cations are present. Surfactant can lead to segregation into separate Mg-rich and Na-rich domains. These sea salt aerosol particle experiments show a large effect of surfactant in presence of Mg^{2+}.

A1.4 Acknowledgments

I am grateful to Jessie Charrier and Dr. Hiroshi Furutani, Department of Chemistry at UCSD, for helpful discussions on experimental techniques and data interpretation. I am grateful to the Lihini Aluware laboratory, Scripps Institution of Oceanography, for use of their oven for combustion of glassware and use of their seawater collection apparatus.

Appendix 2

CIFEX mineral dust mixing state analysis

A2.1 Objective

Previous studies have shown that the uptake of secondary acids depended on the individual dust particle mineralogy. During ACE-Asia, high amounts of nitrate accumulated on calcium-rich dust while high amounts of sulfate accumulated on aluminosilicate-rich dust [*Sullivan et al.*, 2007]. These results have implications for dust particle hygroscopicity, as mineralogy dictates solubility. Aged dust particles, such as calcium sulfate and calcium oxalate have been shown to not be significantly more hygroscopic than a fresh dust proxy, calcium carbonate; while calcium nitrate and calcium chloride are significantly more hygroscopic [*Sullivan et al.*, 2009].

A detailed analysis of the mixing state of the mineral dust particle type during CIFEX showed that once the dust particles became internally mixed with sea salt that the original mineralogy of the dust no longer seemed to influence the uptake of secondary acids.

A2.2 Methods and materials

A2.2.1 Sampling location

The Cloud Indirect Forcing Experiment (CIFEX) took place at Trinidad Head, CA (41.05N, 124.15W, 107m above sea level) from April 1- 21, 2004. Trinidad Head is a clean marine monitoring site that is periodically influenced by long-range transport from Asia across the Pacific. The aerosol was sampled from the summit at Trinidad Head through a 10m sampling stack run by NOAA's Global Monitoring Division (GMD, formerly Climate

Monitoring and Diagnostics Lab). The sampling line was relative humidity (RH) controlled to 55% by heating. The flow from the RH conditioner was then sent into a stainless steel sampling manifold and split off to the various instruments. During the study, there were two significant precipitation events; one from April 14 -16 and a second from April 20- 22.

A2.2.2 ATOFMS data analysis

A total of 598,515 single particle mass spectra were collected over the course of the study. Analysis based on particular mass spectral features within the data set was performed with a Matlab-based (ver. 6.5.1) toolset, YAADA (ver. 1.2) (http://www.yaada.org). The single particle data was automatically sorted and grouped into clusters of particles with similar mass spectral characteristics using the adaptive resonance theory neural network algorithm, ART-2a [*Song and Hopke*, 1999]. The main user-defined parameters for ART-2a are the learning rate, number of iterations, and vigilance factor, which were set to 0.05, 20, and 0.80, respectively [*Rebotier and Prather*, 2007]. The 50 largest particle clusters, representing over 95% over the total particles were classified as mineral dust, biomass burning, aged sea salt, fresh sea salt, organic carbon (OC), elemental carbon with organic carbon (ECOC), vegetative detritus, magnesium-rich, sea salt-EC and amine [*Holecek et al.*, 2007]. The appearance or nonexistence of secondary aerosol species like nitrate, sulfate and ammonium was not used as part of the previous classifications except for sea salt particles. The differentiation between aged and fresh sea salt is determined by the presence of large sulfate and/or nitrate peaks in the average mass spectrum for a particular cluster. “Aged” (other than for sea salt) means that the particles had peak areas of sulfate (m/z -97), nitrate (m/z -62) or chloride (m/z -35) > 5000.

A2.3 Results

Figure A2.1 shows ternary plots of mixing state of single particle "filtered" mineral dust with secondary species for the whole study (5% of total mineral dust particles). "Filtered" dust is not internally mixed with sea salt (SS) or mistaken for biomass by requiring the peak areas of $^{81}Na_2Cl^+$ <100 and $^{27}Al^+$ >5000 [*Sullivan et al.*, 2007].

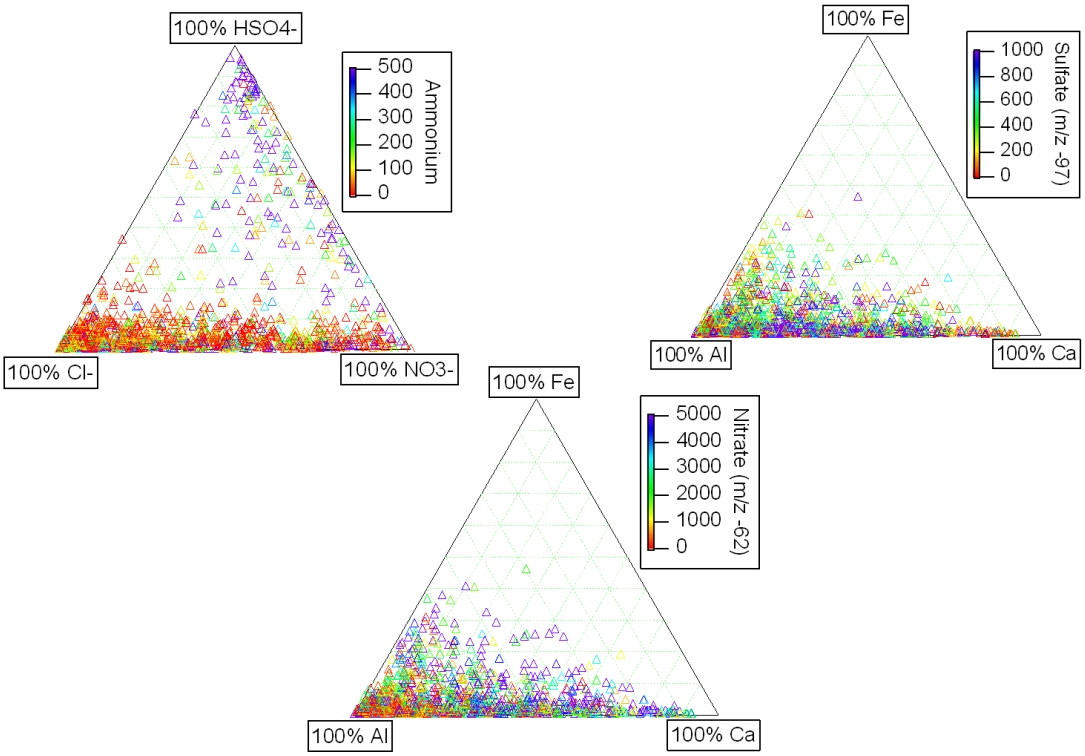

Figure A2.1. Comparison of secondary markers on all filtered dust particles. Each marker is one single particle and shows the mixing between different dust markers. Top left is ammonium vs chloride, nitrate and sulfate. Top right and bottom center are sulfate and nitrate vs aluminum, iron and calcium.

Figure A2.1a (top left) shows that sulfate-rich dust particles are externally mixed from nitrate- and chloride-rich particles. Ammonium is preferentially mixed with sulfate-rich over nitrate- and chloride-rich dust, most likely indicating that the particles were not fully neutralized and ammonium first reacted with the strongest acid, sulfuric acid. Figure A2.1b

and c (top right, bottom) show the mixing of nitrate and sulfate, respectively, between calcium-, aluminum- and iron-rich dust. Nitrate is more associated with the calcium-rich dust while sulfate is more associated with aluminum-rich dust. This difference in uptake of secondary acids being dependent on individual dust mineralogy has been shown previously [*Sullivan et al.*, 2007].

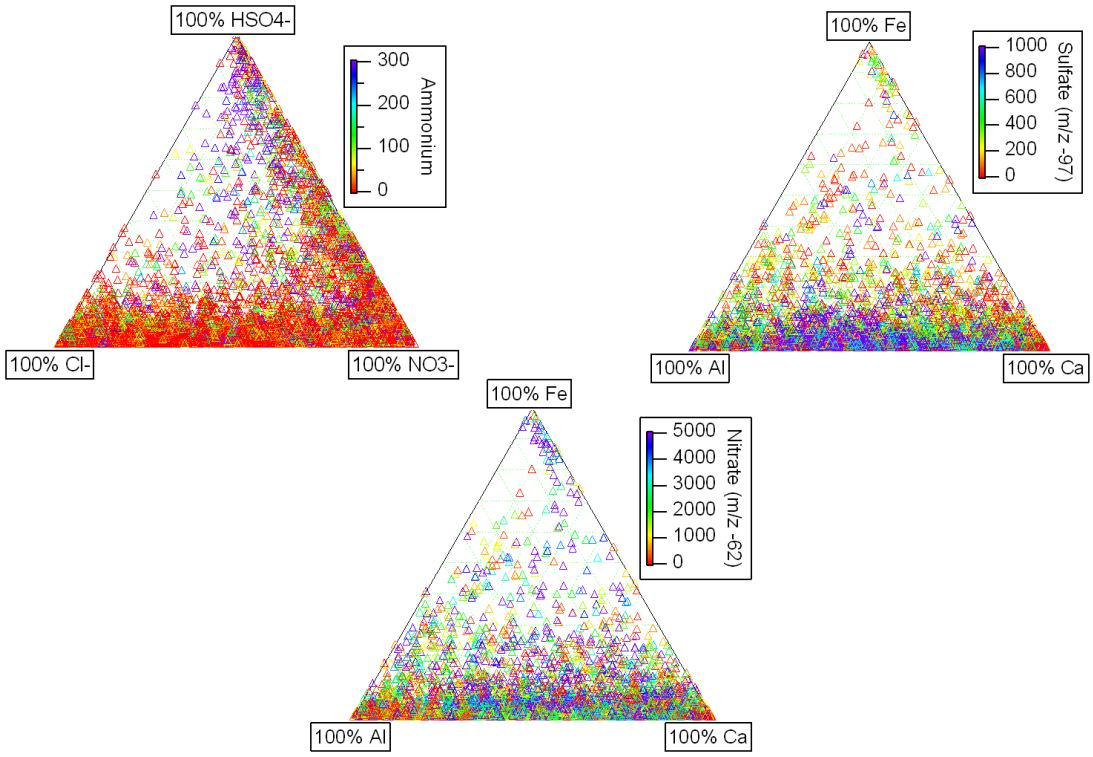

Figure A2.2. Comparison of secondary markers on all dust particles not internally mixed with SS. Each marker is one single particle and shows the mixing between different dust markers. Top left is ammonium vs chloride, nitrate and sulfate. Top right and bottom center are sulfate and nitrate vs aluminum, iron and calcium.

Figure A2.2 shows ternary plots of mixing state of single particle non-sea salt dust ($^{81}Na_2Cl^+$ <100 only, 33% total dust), with secondary species for the whole study. Figure A2.2a (top left) shows that sulfate-rich dust particles are not completely externally mixed from nitrate- and chloride-rich particles. Ammonium is preferentially mixed with sulfate-rich

particles, most likely indicating that the particles were not completely neutralized. Figure A2.2b and c (top right, bottom) show the mixing of nitrate and sulfate, respectively, between calcium-, aluminum- and iron-rich dust. Nitrate and sulfate do not indicate a preference of Ca- or Al-rich dust.

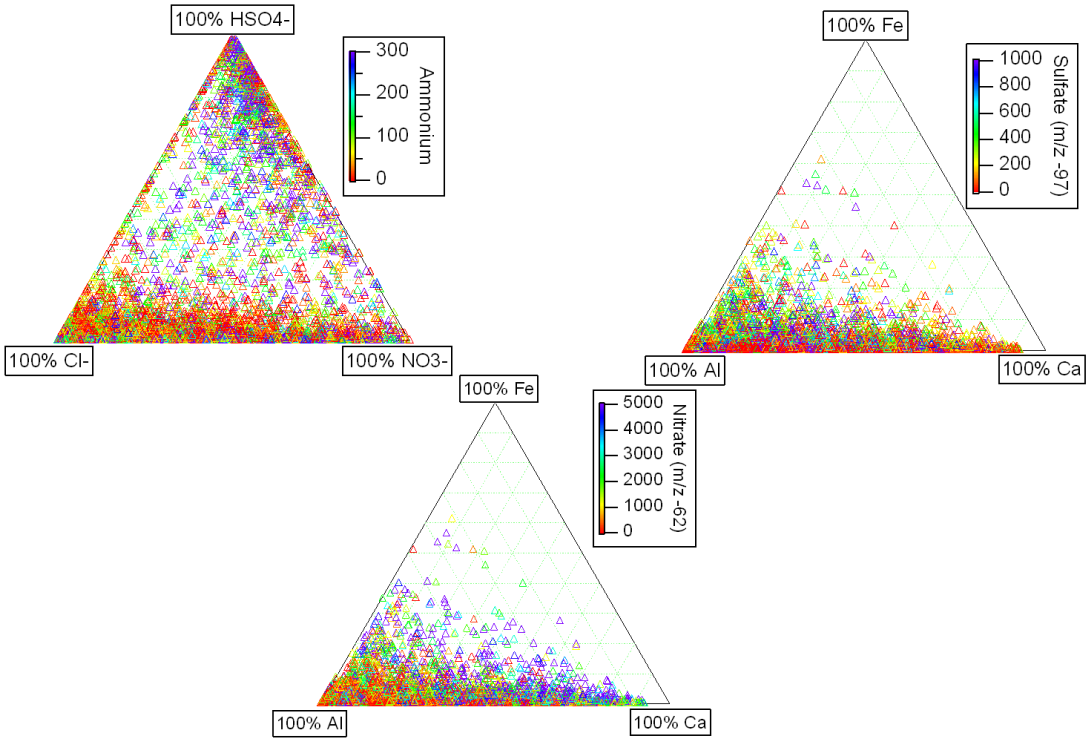

Figure A2.3. Comparison of secondary markers on all Al-rich dust particles. Each marker is one single particle and shows the mixing between different dust markers. Top left is ammonium vs chloride, nitrate and sulfate. Top right and bottom center are sulfate and nitrate vs aluminum, iron and calcium.

Figure A2.3 shows ternary plots of mixing state of single particle Al-rich dust ($^{27}Al^{+}$ >5000 only, 34% total dust), with secondary species for the whole study. Figure A2.3a (top left) shows that sulfate-rich dust particles are not completely externally mixed from nitrate- and chloride-rich particles. Ammonium is preferentially mixed with sulfate-rich particles, most likely indicating that the particles were not completely neutralized. Figure A2.3b and c

(top right, bottom) show the mixing of nitrate and sulfate, respectively, between calcium-, aluminum- and iron-rich dust. Nitrate and sulfate do not indicate a preference of Ca- or Al-rich dust.

The differences in the observed mixing state of the dust under different filtration parameters indicate that once the mineral dust particles become internally mixed with sea salt, or are not strongly associated with aluminum/alumina-silicates, that the original mineralogy of the dust no longer seems to influence the uptake of secondary acids. Additionally, Al-rich dust particles tend to have increased external mixing of nitrate and sulfate compared to non-Al-rich dust. The segregation of the sulfate from the nitrate and the chloride indicates that sulfate accumulated on the dust first [*Sullivan et al.*, 2007]. These findings have important implications for CCN activity, as it has been shown previously that the mixing state of mineral dust is very important in determining its hygroscopicity [*Sullivan et al.*, 2009]. Not all atmospherically processed mineral dust becomes more hygroscopic with atmospheric processing, as calcium sulfate and calcium oxalate, two examples of aged mineral dust, are non- hygroscopic; while calcium nitrate and calcium chloride, two additional examples of aged mineral dust, are very soluble and have hygroscopicities similar to that of ammonium sulfate [*Sullivan et al.*, 2009]. The fact that the calcium in the filtered mineral dust was more strongly associated with nitrate over sulfate shows that the Ca-rich mineral dust particles could be quite soluble and hygroscopic. This could have increased the likelihood that these particles would become cloud processed, where they most likely became internally mixed with sea salt. After the dust is associated with highly soluble and hygroscopic sea salt, the original mineralogy and mixing of secondary acids is of decreased importance in determining the new hygroscopicity of the dust, as it is now highly soluble and hygroscopic due to the sea salt inclusion; and additionally, as we show here, it changes how the particle continues to react heterogeneously with secondary acids in the atmosphere.

A2.4 Summary

A detailed analysis of the mixing state of the mineral dust particle type showed that once the dust particles become internally mixed with sea salt that the original mineralogy of the dust no longer seems to influence the uptake of secondary acids. The fact that the calcium in the non-internally mixed with sea salt mineral dust was more strongly associated with nitrate over sulfate shows that the Ca-rich mineral dust particles could be quite soluble and hygroscopic. This could have increased the likelihood that these particles would become cloud processed, where they most likely became internally mixed with sea salt. After the dust is associated with highly soluble and hygroscopic sea salt, the original mineralogy and mixing of secondary acids is of decreased importance in determining the new hygroscopicity of the dust, as it is now highly soluble and hygroscopic due to the sea salt inclusion; and additionally, as we show here, it changes how the particle continues to react heterogeneously with secondary acids in the atmosphere.

A2.5 Acknowledgements

I am grateful to John Holecek (UCSD) for his help with data collection and analysis. I thank the National Oceanic and Atmospheric Administration (NOAA), grant NOAA/NA17RJ1231, and V. Ramanathan for the support of this research.

A2.6 References

Rebotier, T.P., and K.A. Prather, Aerosol time-of-flight mass spectrometry data analysis: A benchmark of clustering algorithms., *Analytica Chimica Acta*, *585* (1), 38-54, 2007.

Sullivan, R.C., S.A. Guazzotti, D.A. Sodeman, and K.A. Prather, Direct observations of the atmospheric processing of Asian mineral dust, *Atmospheric Chemistry and Physics*, *7* (5), 1213-1236, 2007.

Sullivan, R.C., M.J.K. Moore, M.D. Petters, S.M. Kreidenweis, G.C. Roberts, and K.A. Prather, Effect of chemical mixing state on hygroscopicity and cloud nucleation properties of calcium mineral dust particles, *Atmospheric Chemistry and Physics*, *9*, 3303-3316, 2009.

Appendix 3

Pre-CIFEX analysis

A3.1 Objective

To observe the mixing state of oxalate during the pre-CIFEX measurements. These experiments were preliminary and not included with those of Chapter 6, "Evidence for two distinct sources of oxalate during the Cloud Indirect Forcing Experiment (CIFEX)."

A3.2 Methods and materials

A3.2.1 Sampling location

The pre-Cloud Indirect Forcing Experiment (CIFEX) took place at Trinidad Head, CA (41.05N, 124.15W, 107m above sea level) from March 27- April 1, 2004. The aerosol was sampled from the summit at Trinidad Head through a 10m sampling stack run by NOAA's Climate Monitoring and Diagnostics Lab. The sampling line was relative humidity (RH) controlled to 55% by heating.

A3.2.2 ATOFMS data analysis

A total of 121,547 single particle mass spectra were collected over the course of the pre-study. The single particle data was automatically sorted and grouped into clusters of particles with similar mass spectral characteristics using the adaptive resonance theory neural network algorithm, ART-2a. The main user-defined parameters for ART-2a are the learning rate, number of iterations, and vigilance factor, which were set to 0.05, 20, and 0.80, respectively.

The 50 largest particle clusters, representing over 95% over the total particles, were classified as mineral dust, biomass burning, aged sea salt, fresh sea salt, organic carbon (OC), elemental carbon with organic carbon (ECOC), vegetative detritus, magnesium-rich, sea salt-EC, dust-EC and amine. A subset of the OC particles were characterized by high mass hydrocarbon envelopes with ions up to m/z 250, hereafter referred to as high mass OC, or HMOC. For the particle classes presented herein, analysis was on non-miscalibrated, dual polarity particles only.

The appearance or nonexistence of secondary aerosol species like nitrate, sulfate and ammonium was not used as part of the previous classifications except for sea salt particles. The differentiation between aged and fresh sea salt is determined by the presence of large sulfate and/or nitrate peaks in the average mass spectrum for a particular cluster. Oxalate-containing particles were defined by querying the particle mass spectra for particles containing a peak at m/z – 89 with an area greater than 300. Sulfate-containing particles were defined by querying the particle mass spectra for particles containing a peak at m/z – 97 with an area greater than 5000. Oxalate- and sulfate-containing particles were defined as particles which contained both a peak at m/z – 89 with an area greater than 300 and a peak at m/z – 97 with an area greater than 5000.

A3.3 Results

A3.3.1 Detection of oxalate and sulfate in single particles

The hourly counts of oxalate-containing, sulfate-containing and both oxalate- and sulfate-containing sub- and supermicron particles are shown in Figure A3.1. Also shown is the fraction of sub- and supermicron oxalate particles which also contain sulfate, and hourly counts of HMOC particles, sea salt-EC particles and dust-EC particles of all sizes.

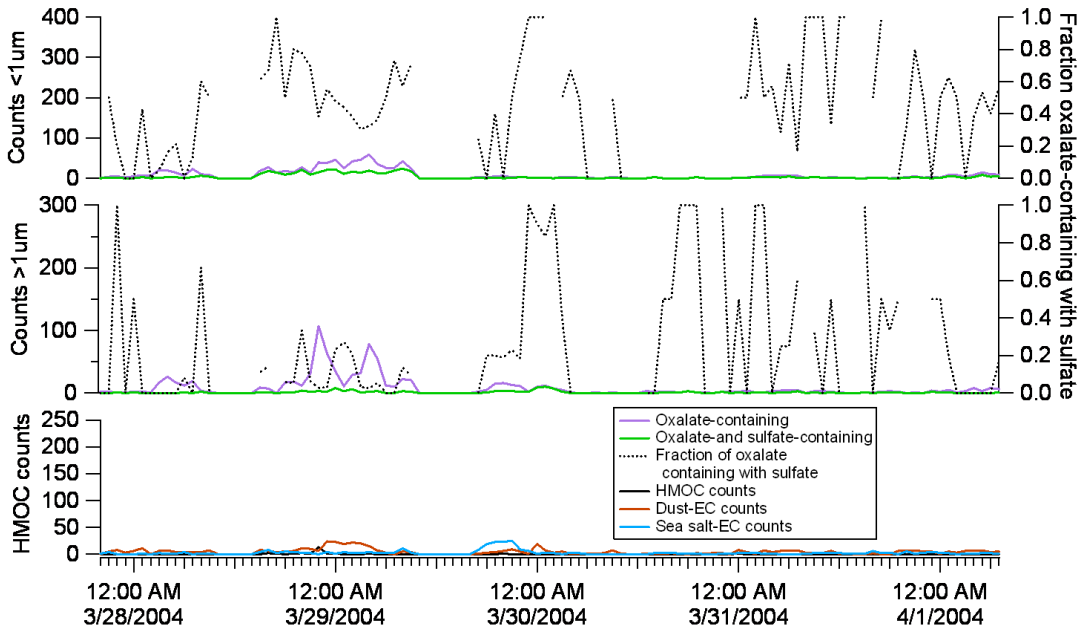

Figure A3.1. Comparison of oxalate -containing and sulfate –containing submicron (top) and supermicron (middle) particles and high mass organic carbon (HMOC), sea salt-EC and dust-EC particles (bottom).

Figure A3.1 shows that there was a very limited presence of oxalate-containing particles in both the sub- (top) and supermicron (middle). HMOC, sea-salt EC and dust-EC particle counts are also very low. The hourly counts of the different particle classes that contain oxalate in the sub- and supermicron for the entire study are shown in Figure A3.2.

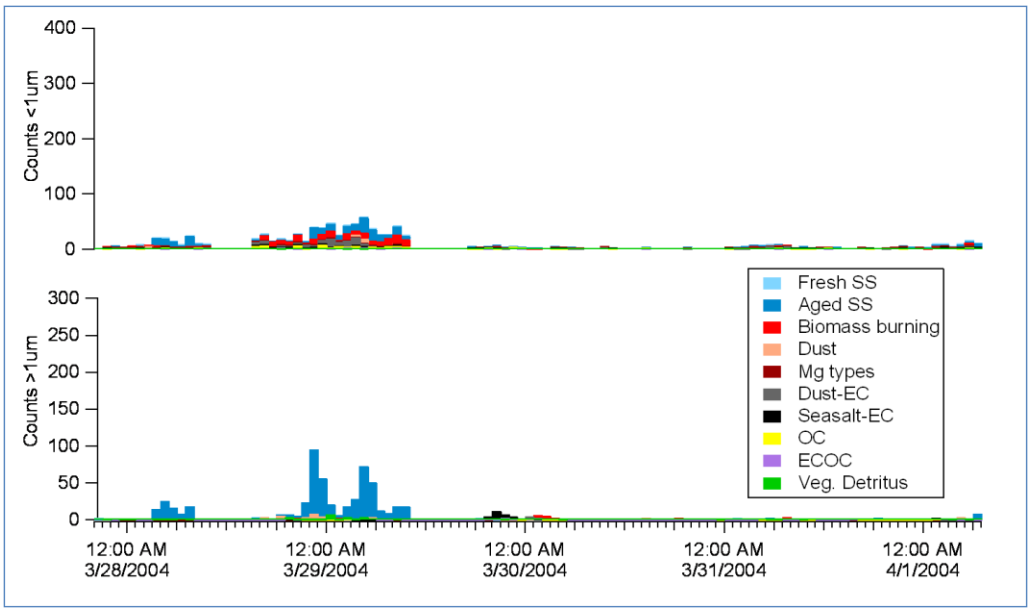

Figure A3.2. Comparison of oxalate-containing particles by type: submicron (top) and supermicron (bottom) [same scale as during rest of CIFEX].

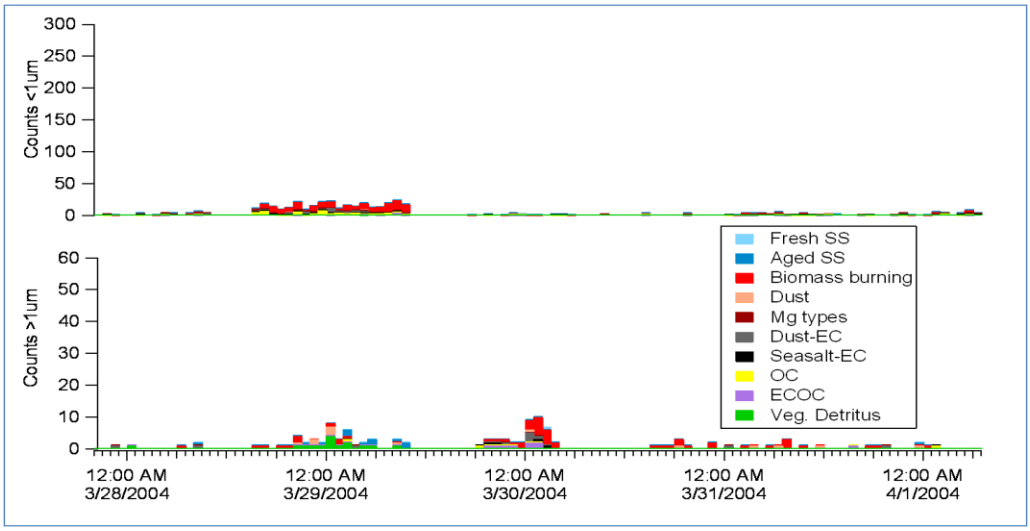

Figure A3.2. Comparison of oxalate-and sulfate-containing particles by type: submicron (top) and supermicron (bottom) [same scale as during rest of CIFEX].

Figure A3.2 (top) shows that submicron oxalate-containing particles consist primarily of aged sea salt, biomass burning and dust-EC. Figure A3.2 (bottom) shows that supermicron oxalate-containing particles consist primarily of aged sea salt. Figure A3.3 (top) shows that submicron oxalate-and sulfate-containing particles consist primarily of biomass burning. Figure A3.2 (bottom) shows that supermicron oxalate-containing particles consist primarily of biomass burning and vegetative detritus.

Figure A3.4 shows a breakdown of particle types for all sub- and super-micron particles as well as for sub- and supermicron oxalate- and oxalate- and sulfate-containing particles for the entire pre-study.

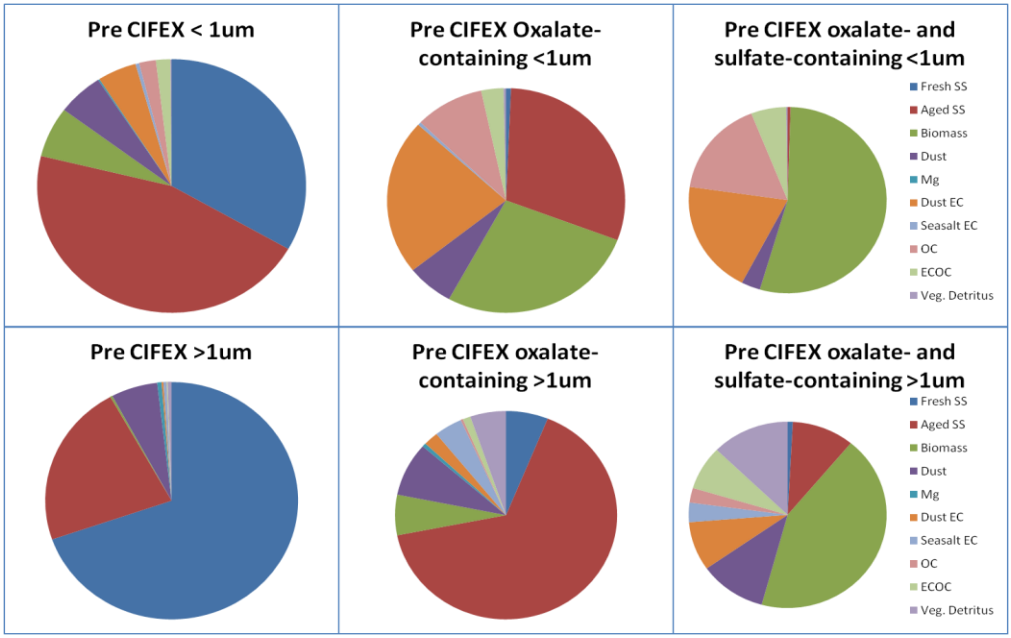

Figure A3.4. Particle class fractions of submicron total particles (top left), oxalate-containing particles (top center), oxalate and sulfate containing particles (top right) during preCIFEX. Particle class fractions of supermicron total particles (bottom left), oxalate-containing particles (bottom center), oxalate and sulfate containing particles (bottom right).

Figure A3.4 (top left) shows that composition of the submicron particles was varied during the study (7576 counts), with the majority (>70%) collectively coming from the fresh

and aged sea salt particle classes. Oxalate-containing submicron particles (Figure A3.4, top middle) (894 counts, 12% total submicron) largely consist of aged sea salt (30%), followed by BB (27%), and dust-EC (22%). Oxalate- and sulfate-containing submicron particles (Figure A3.4, top right) (418 counts, 6% total submicron, 47% oxalate-containing submicron) are mainly BB (54%), dust- EC (20%) and OC (18%). This highlights the large enrichment of oxalate-and sulfate-containing submicron particles on the BB particle class, as the biomass burning class is only 6% of total submicron particles and makes up 54% of oxalate-and sulfate-containing submicron particles. Supermicron particles (55,727 counts) are less varied in composition then the submicron particles, and consist mainly of fresh (70%) and aged sea salt (22%) (Figure 4, bottom left). Oxalate-containing supermicron particles (Figure A3.4, bottom middle) (879 counts, 2% supermicron) are largely aged sea salt (66%), followed by dust (8%), BB (6%), and fresh sea salt (6%). Oxalate- and sulfate-containing supermicron particles (Figure A3.4, bottom right) (118 counts, <1% supermicron, 13% oxalate-containing supermicron) are largely BB (43%), vegetative detritus (13%), aged SS (10%) and dust EC (9%).This once again highlights the large enrichment of oxalate-and sulfate-containing particles on the BB particle class, this time on the supermicron, as the BB type is <1% of supermicron particles and makes up 43% of oxalate-and sulfate-containing supermicron particles. For oxalate-containing particles that also contain sulfate, there is a large enrichment on the BB particle class for both the sub- and supermicron. This enrichment is especially noticeable in the supermicron as the majority of supermicron particles were sea salt, but the majority of supermicron oxalate- and sulfate-containing particles were BB.

A3.4 Acknowledgements

I am grateful to John Holecek (UCSD) for his help with data collection and analysis. I thank the National Oceanic and Atmospheric Administration (NOAA), grant NOAA/NA17RJ1231, and V. Ramanathan for the support of this research.